CENTRO DE INVESTIGACIÓN Y DE ESTUDIOS AVANZADOS
DEL INSTITUTO POLITÉCNICO NACIONAL

UNIDAD ZACATENCO
DEPARTAMENTO DE FÍSICA

"Explorando nueva física con leptones usando teorías efectivas"

Tesis que presenta

Juan Manuel Márquez Morales

para obtener el Grado de

Doctor en Ciencias

en la Especialidad de

Física

Director de la tesis:
Dr. Pablo Roig Garcés

Ciudad de México Noviembre, 2025

CENTER FOR RESEARCH AND ADVANCED STUDIES OF THE NATIONAL POLYTECHNIC INSTITUTE

UNIT ZACATENCO
PHYSICS DEPARTMENT

"Exploring new physics with leptons using EFTs"

by

Juan Manuel Márquez Morales

In order to obtain the

Doctor of Science

degree, speciality in

Physics

Advisor:
Ph. D. Pablo Roig Garcés

Mexico City November, 2025

Exploring new physics with leptons using EFTs

A thesis submitted for the degree of

Doctor of Science

Juan Manuel Márquez Morales

Advisor: Dr. Pablo Roig Garcés

Centro de Investigación y de Estudios Avanzados

del Instituto Politécnico Nacional

Acknowledgments

Me gustaría agradecer a todas aquellas personas que hicieron del doctorado una experiencia mucho más llevadera, por su apoyo incondicional y por todos los buenos momentos que ayudaron a aliviar los días de estrés, las clases, tareas, exposiciones y artículos, que en ocasiones pueden llegar a saturarte. Gracias a ellos, nunca faltaron las risas. Son amistades que perdurarán toda la vida. En especial, quiero agradecer a mis hermanos, conocidos por sus apodos en español: Liz, Cesarín, Potrillo, Celestial, Johanson y Evercín.

De igual manera, quiero agradecer y reconocer el gran apoyo que me brindó Pablo. Él ha sido mi asesor desde la maestría y, sin duda, un pilar fundamental para poder culminar mi doctorado. Gracias, Pablo, por estar siempre disponible, por los consejos, las pláticas, la motivación, por compartir lo que sabes conmigo y por todas las oportunidades que me brindaste durante estos años. Eres un gran asesor y amigo.

Agradezco también a mis sinodales, quienes se tomaron el tiempo de evaluar esta tesis, por sus comentarios y el apoyo brindado a lo largo del doctorado; cada uno de ellos fue una motivación para culminar este proceso.

Finalmente, agradezco el apoyo de la Secretaría de Ciencia, Humanidades, Tecnología e Innovación (SECIHTI) durante estos cuatro años de doctorado.

Este trabajo está dedicado a mis padres, Paulina y Juan Manuel. No existen palabras suficientes para expresar todo mi agradecimiento hacia ellos. Los amo profundamente.

Abstract

This thesis has centered on applying Effective Field Theory (EFT) frameworks to study neutrino phenomenology across various processes, as well as exploring the implications of new physics (NP) for the muon g-2 anomaly. In addition, we have computed high-precision calculations of hadronic light-by-light (HLbL) contributions to the muon g-2 within the Standard Model (SM). The ultimate goal of this work is to identify alternative processes and potential measurements that could complement or extend existing efforts, such as neutrinoless double beta decay, in the search for NP and the answer of some intriguing problems as the nature of neutrinos. In the following, I will provide a general overview of the works [1], [2], [3], [4], [5] and discuss the direction of future research.

Keywords – Effective field theories, Michel parameters, neutrino interactions and nature, muon g-2.

Resumen

Esta tesis se ha centrado en aplicar formalismos de teorías cuánticas de campo efectivas (EFT, por sus siglas en inglés) para estudiar fenomenología de neutrinos mediante diversos procesos, así como en explorar las implicaciones de nueva física (NP, íd.) de la anomalía en el g-2 del muón. Además, hemos calculado contribuciones de alta precisión a la dispersión luz por luz hadrónica (HLbL, íd.) al g-2 del muón dentro del Modelo Estándar (SM, íd.). El fin último de este trabajo es identificar procesos alternativos y medidas potenciales que puedan complementar o extender los esfuerzos actuales, como las enfocadas al descubrimiento de desintegraciones doble beta sin neutrinos, en busqueda de NP, y la respuesta a alguno de los problemas abiertos intrigantes, como la naturaleza de los neutrinos. En lo sucesivo, proporcionaré una introducción general a los trabajos producto de esta tesis [1], [2], [3], [4], [5] y discutiré posibles direcciones de investigaciones futuras.

Palabras clave – Teorías efectivas, parámetros de Michel, naturaleza e interacciones de neutrinos, g-2 del muón.

Contents

Chapter 1

Introduction

One of the biggest and more challenging dreams of humans as a species is to understand the laws of nature. Since we were little children, curiosity has been an inherent quality we possess. Questions about everything we see and experience arise spontaneously: Why is the sky blue? Why is the grass green? Or even, why are we not yet able to formulate a complete quantum theory of gravity? (For the more curious).

Thanks to the giant efforts of the scientific community, we have been able to answer some of these questions, but the task is far from complete. From a more fundamental point of view, the Standard Model of Elementary Particles (SM) [6], [7], [8] is the most successful theory describing nature by studying the fundamental particles and their interactions. It has been tested many times, with ever-increasing precision, and remains consistent with experimental data [9]. Nevertheless, the SM does not explain everything, such as gravity interaction, neutrino masses or dark matter, mainly because this phenomena is not encoded in its prescription. All of these motivate the search for new physics (NP) that is beyond the SM.

One of the main experimental strategies in the search for a fundamental description of nature which goes beyond the SM is to perform high precision measurements where an observed discrepancy with the SM would reveal the signature of NP. For this purpose, muon and tau leptons are specially important, where many precision measurements can be made, see e.g. [10], [11], [12].

Investigations involving muon decays not only determine the overall coupling strength but also reveal the Lorentz structure characterizing weak interactions. Additionally, they impose extremely stringent constraints on processes that violate charged lepton flavor (LFV). Furthermore, measurements of the anomalous magnetic moment of the muon provide exceptional sensitivity to potential deviations from the Standard Model and to the predictions of various beyond-the-Standard-Model scenarios. Overall, the remarkable precision and sensitivity achieved in muon-based experiments make this lepton

an outstanding probe for testing the Standard Model with high accuracy.

In contrast, experiments involving the tau lepton lack the same level of precision as those performed with muons. Nevertheless, the tau possesses distinctive properties that make it equally relevant in the search for new physics. In recent years, thorough analyses of higher-order electroweak corrections and QCD effects have elevated tau physics to the realm of precision testing. The purely leptonic and semileptonic nature of tau decays offers an excellent framework for probing the structure of weak currents and verifying the universality of their couplings to gauge bosons. Additionally, since the tau is the only lepton massive enough to decay into hadrons, its semileptonic decay modes serve as an exceptional means to investigate strong interaction phenomena under remarkably clean experimental conditions [10]. Finally, since one naively expects the fermions to be sensitive to the possible NP proportionally to their masses, the large tau mass allows one to investigate NP contributions, through a broad range of kinematically-allowed decay modes, complementing the high-precision searches performed in muon decay.

In this thesis we are specially interested in exploring two main topics: neutrino interactions and the anomalous magnetic moment of the muon, throughout precision tests analysis within the effective field theory (EFT) approach.

Regarding the first topic, a central open question in contemporary particle physics is whether neutrinos are Dirac or Majorana fermions. Resolving this issue is essential not only for understanding the origin of neutrino masses but also for determining which physical processes are permitted or forbidden. Various experimental approaches have been proposed to investigate the fundamental nature of neutrinos, among which the search for neutrinoless double beta decay ($0\nu\beta\beta$) stands out as the most promising [13], [14], [15]. There are alternative possibilities, such as lepton number violating processes [16], [17], [18], [19], [20], [21], [22] or lepton flavor changing decays [23], most of them motivated by the propagation of massive heavy neutral leptons. Moreover, many searches for the neutrino's nature are also conducted within the framework of cosmology, including cosmic neutrino capture via tritium [24], the evaporation of primordial black holes [25], the cosmological effective number of neutrino species [26], [27], and more [28], [29], [30], [31].

It is however extremely challenging to distinguish experimentally between Dirac and Majorana neutrinos, since any observable difference between both neutrinos nature is

always suppressed by some power of m_ν/E in theories with $V-A$ interactions such as the SM. As stated by the "practical Dirac-Majorana confusion theorem" (DMCT) [32], valid when the unobservable neutrinos momenta get fully integrated out.

Then, two main alternatives, which are studied in detailed in this thesis applying an EFT analysis to a broad of muon and tau processes, are possible:

-If neutrinos possess interactions beyond those predicted by the Standard Model, high-precision measurements could provide valuable insights into both their intrinsic nature and potential new physics contributions.

-Given that neutrino momenta cannot be directly measured experimentally, find a method to infer them. Such an approach should preserve the distinctions between Dirac and Majorana neutrinos independently of the exact neutrino mass, provided that the neutrinos are not strictly massless.

Now, for the second topic, the muon's anomalous magnetic moment has garnered considerable interest within particle physics, primarily because of the long-standing tension between its experimentally measured value and the predictions provided by the Standard Model. The latest measurements by the Muon g-2 collaboration at Fermilab [33], [34], when combined with earlier results from the Brookhaven E821 experiment [35], indicate a deviation of 5.1σ from the SM prediction [36]

$$\Delta a_\mu = a_\mu^{\text{exp}} - a_\mu^{\text{SM}} = 249(48) \times 10^{-11}. \tag{1.1}$$

Moreover, theoretical predictions themselves exhibit some tension, particularly in the determination of the Hadronic Vacuum Polarization (HVP), which can be estimated through various approaches. One commonly used method relies on e^+e^- data-driven analyses, leading to the previously noted 5.1σ discrepancy. In contrast, estimates based on τ data-driven approaches [37], [38], [39] or lattice QCD calculations [40] significantly reduce the tension between theoretical and experimental values to 2.0σ and 1.5σ, respectively. The latest CMD-3 measurement of $\sigma(e^+e^- \to \pi^+\pi^-)$ [41], [42] also points in this direction [1].

[1]This trend has been confirmed by publications appeared after those contained in this thesis. The final measurement from FNAL reduced the experimental error to 15×10^{-11}. Slightly before that, the second White Paper by the Muon g-2 Theory Initiative (to which the author belongs) updated the SM prediction [43], in such a way that now it is compatible with the world average within less than a standard deviation, $\Delta a_\mu = a_\mu^{\text{exp}} - a_\mu^{\text{SM}} = 39(64) \times 10^{-11}$.

As the uncertainty in a_μ^{exp} is expected to decrease further in the future,it becomes increasingly important to improve the theoretical calculations in order to clarify whether the observed discrepancy signals new physics. Consequently, efforts are ongoing to refine the various contributions, with particular emphasis on the hadronic components—the Hadronic Vacuum Polarization (HVP) and hadronic light-by-light (HLbL) terms—which constitute the dominant sources of uncertainty. The precision of QED and Electroweak determinations are two and one order of magnitude more accurate than the hadronic ones, respectively. The HVP data-driven computation is directly related to the experimental input from $\sigma(e^+e^- \to \text{hadrons})$ data. HLbL in contrast, requires a decomposition in all possible intermediate states.

To this end, we present two main contributions. First, we perform a high-precision calculation of the HLbL scattering contribution within the SM, focusing specifically on the proton-box diagram. This constitutes the first reported baryonic contribution to a_μ^{HLbL}. Second, we investigate potential new physics (NP) effects in a_μ by analyzing high-energy lepton pair annihilation cross sections within the more general Higgs EFT (HEFT) framework.

The thesis is structured as follows: in Ch. 2 and Ch. 3, we briefly introduce the main concepts about the SM formulation and the EFT framework. Ch. 4 addresses neutrino interactions. The analysis of NP effects, through the inclusion of the most general Lorentz structure within the EFT approach for the processes $\ell \to \ell' \bar{\nu}_{\ell'} \nu_\ell$ and $\nu e \to \nu e$ is presented in detailed in Sub Ch. 4.1 and Sub Ch. 4.2, respectively. In Sub Ch. 4.3, we discuss the alternative method of inferring neutrino momenta in order to distinguish the specific nature of neutrinos within the SM, focusing on the $\ell \to \ell' \bar{\nu}_{\ell'} \nu_\ell \gamma$ decay. The second main topic, concerning the muon $g-2$, is covered in Ch. 5, where the NP contributions within the HEFT framework are analyzed in Sub Ch. 5.1, and the precision calculation of the HLbL proton-box contribution is presented in Sub Ch. 5.2. Finally, a brief comment on the current works in progress are made in Ch. 6, and our conclusions are summarized in Ch. 7. Several appendices complement the main material of the thesis.

Chapter 2

Standard Model

The SM is the most successful theory we have ever had to describe nature, where gauge invariance plays an indispensable role to determine the dynamical forces among the fundamental constituents of matter. Nevertheless, it is far away from the so-called Theory of everything and precision tests are needed for the search of the possible NP that is beyond. In this chapter, we briefly discusse the particle content, structure and symmetries of the SM.

2.1 Introduction to the SM

The SM is a renormalizable quantum field theory (QFT) that is used to describe fundamental particles and their interactions. Specifically, it is a gauge theory, based on the symmetry group $SU(3)_C \otimes SU(2)_L \otimes U(1)_Y$, that describes the interactions via the exchange of the corresponding spin-1 gauge fields. Its Lagrangian also possesses Poincaré and CPT invariance, together with some additional symmetries, not postulated at the outset of its construction, collectivity denoted as accidental symmetries, such as baryon number, lepton number, custodial symmetry, etc.

The gauge group describes strong, weak and electromagnetic interactions with eight massless gluons, three massive bosons ($W^{\pm}$ and Z) and a massless photon as the corresponding gauge boson mediators, respectively. The remaining fermionic matter content will be discussed in more detail in the next section.

Within the framework of quantum field theory, all gauge bosons, as well as fermionic and scalar fields included in the Standard Model, are defined at every point in spacetime. The Standard Model Lagrangian density, $\mathcal{L}_{SM}$, governs the dynamics of these fields, incorporating their kinetic terms and mutual interactions through appropriate coupling terms. When the most general Lagrangian is constructed assuming massless neutrinos, the resulting dynamics depends on 19 parameters, whose numerical values are determined

through experimental measurements. The compact form of the SM Lagrangian is concise enough to fit on a coffee mug -a popular item for science outreach-. However, its full explicit expression, as detailed in [44], is significantly more complex and rarely used in conference presentations to inspire young scientists to pursue research in particle physics.

Within this elegant theoretical framework, we are able to describe the known experimental facts in particle physics with high precision, constituting the SM one of the most successful achievements in modern physics. A detailed treatment of the formal aspects of this construction lies beyond the scope of this brief introduction, but comprehensive explanations can be found in numerous research articles and textbooks, which are specifically designed to provide a clear and technically sound introduction to the Standard Model at both undergraduate and graduate levels, see e.g. [45], [46], [47].

2.1.1 Particle Content

In the current view, all matter is made out of three kinds of elementary particles: leptons, quarks and mediators (gauge bosons), as seen in Fig.2.1. The fermionic matter content

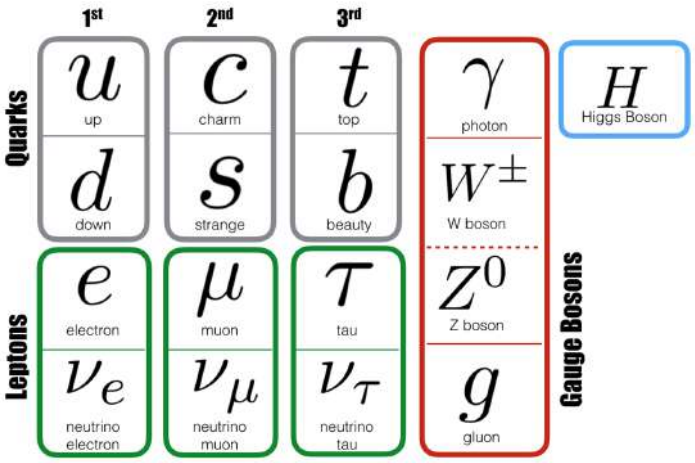

Figure 2.1: SM particle content.

(leptons and quarks), is organized in a three-fold family structure, each quark appearing in three different colours [2]:

$$\begin{bmatrix} \nu_e & u \\ e^- & d' \end{bmatrix}, \quad \begin{bmatrix} \nu_\mu & c \\ \mu^- & s' \end{bmatrix}, \quad \begin{bmatrix} \nu_\tau & t \\ \tau^- & b' \end{bmatrix}, \tag{2.1}$$

[2]The prime below identifies the quark weak/flavor/gauge eigenstate. One could proceed similarly for neutrinos whenever their masses are non-negligible, see 4.

where the notation, following [48] , is

$$\begin{bmatrix} \nu_\ell & q_u \\ \ell^- & q_d \end{bmatrix} \equiv \begin{pmatrix} \nu_\ell \\ \ell^- \end{pmatrix}_L , \quad \begin{pmatrix} q_u \\ q_d \end{pmatrix}_L , \quad \ell_R^-, \quad q_{uR} \quad , q_{dR}, \tag{2.2}$$

together with the corresponding antiparticles. The left-handed fields, denoted by a subindex L, are $SU(2)_L$ doublets, while their right-handed partners, denoted by a subindex R, transform as $SU(2)_L$ singlets. The three fermionic families appear to have identical properties (gauge interactions); they differ only by their mass and their flavour quantum number.

As already discussed, every interaction has its mediators; the photon for the electromagnetic force, two W's and a Z for the weak force and eight gluons for the strong force. Finally, to explain why some particles have mass, the so-called Higgs mechanism [49] was proposed [50], [51], [52], [53], which requires the existence of a spinless particle.

Specifically, the gauge symmetry is broken by the vacuum, which triggers the spontaneous symmetry breaking (SSB) of the electroweak group to the electromagnetic subgroup:

$$SU(3)_C \otimes SU(2)_L \otimes U(1)_Y \xrightarrow{\text{SSB}} SU(3)_C \otimes U(1)_{\text{QED}}. \tag{2.3}$$

Thus, the SSB mechanism generates the masses of the weak gauge bosons, and gives rise to the appearance of a physical scalar particle in the model, the so-called Higgs boson. This particle was was discovered in 2012 by the ATLAS and CMS experiments at the Large Hadron Collider (LHC) at CERN [54], [55].

Including their corresponding antiparticles and accounting for the three color charges of each quark, the Standard Model encompasses 12 leptons, 36 quarks, 12 gauge bosons, and a single Higgs boson, for a total of 61 fundamental particles (see Fig.2.2). Despite this large number, these particles are highly interconnected. For instance, the eight gluons differ only in their color combinations, and the second and third generations of fermions replicate the properties of the first generation.

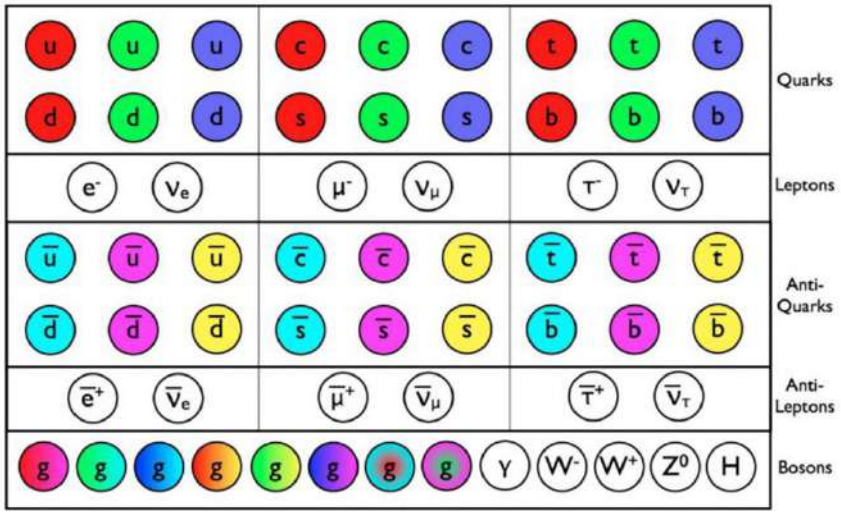

Figure 2.2: Full particle content of the SM.

2.2 Beyond SM

The SM provides a very elegant theoretical framework, which is able to describe the known experimental facts in particle physics with high precision, but it does not explain everything. There are some physical phenomena that motivate the research of new physics that is beyond the SM.

Here we list some of the most important unsolved problems in fundamental physics that lie beyond the SM formulation:

- How to unify all forces, including gravity, in a consistent theory?
- Why do its 19 parameters have the values that we measure?
- Why are there three generations of particles?
- Why is there (much) more matter than antimatter in the universe?
- Does dark matter even consist of new particles? Where does it fit into the SM?
- Are neutrinos Dirac or Majorana fermions? What is the mechanism by which they acquire mass?

The pursuit of a fundamental theory that extends beyond the Standard Model is guided by two complementary experimental strategies. The first involves constructing increasingly powerful colliders, such as the Large Hadron Collider (LHC) at CERN, capable of probing matter at unprecedented energy scales. The second strategy relies on conducting high-

precision measurements, where any observed deviation from Standard Model predictions could provide a clear signal of new physics [11].

In this thesis, we implement the second strategy across various processes, where theoretical analysis of these deviations can be performed using effective field theories (EFTs), which are one of the best tools to test NP, in my opinion. Since EFTs, under certain general assumptions, provide a model-independent framework for studying NP contributions.

Chapter 3

Effective Theories

Effective field theories represent a crucial framework for providing a simplified yet comprehensive description of physical phenomena at specific energy scales. While the basic concept of an effective theory is relatively intuitive, constructing them in a mathematically consistent manner within an interacting quantum field theory is far from straightforward.

In this chapter, we summarize the basic principles of effective theories (EFT's), as well as some examples, specially useful in this thesis: the Fermi theory of weak interactions, the Standard Model EFT (SMEFT) and the Higgs EFT (HEFT).

3.1 Introduction to EFT

The idea behind effective field theories (EFT) is that you can compute observables without knowing the precise fundamental theory. This allows you to calculate an experimentally measurable quantity with some finite uncertainty. That is the reason why you are able to calculate the hydrogen atom energy levels without using the fact that the proton is made up of quarks, the existence of weak interactions or any detailed input from QED or QCD; just taking into account an electron of mass m_e interacting via a Coulomb potential with a proton treated as an infinitely heavy point particle with charge $+1$.

To study a given physical system more effectively, it is important to isolate its most relevant components, achieving a reliable approximation without needing to account for every detail. This approach allows the analysis of low-energy dynamics in problems where energy scales are widely separated, while remaining largely independent of the specific details of high-energy interactions.

Therefore, EFTs provide a suitable framework for describing low-energy phenomena, where "low" is defined relative to a particular energy scale, Λ. The approximation for a given problem can be systematically refined by incorporating corrections arising from the higher energy scales that were initially neglected, treating them as small perturbations. In EFTs

this implies taking explicitly into account the relevant degrees of freedom, i.e. those states with $m << \Lambda$, while the heavier ones with $M >> \Lambda$ are integrated out from the action.[56]

Numerous successful examples of EFTs exist in physics, including Fermi's theory of weak interactions, Heavy Quark Effective Theory (HQET), Non-Relativistic Quantum Chromodynamics (NRQCD), Chiral Perturbation Theory (χPT), Soft-Collinear Effective Theory (SCET), as well as SMEFT and HEFT, among others. [57].

3.2 EFT Lagrangians

The EFT effective Lagrangian is of the following form:[3]

$$\mathcal{L} = \sum_i c_i O_i, \tag{3.1}$$

where O_i are operators constructed with the light fields, and c_i its couplings.

While we mentioned that high-energy dynamics can be neglected when studying low-energy processes, the effects of these heavy or high-energy degrees of freedom are in fact encoded in the couplings c_i, as will be discussed in more detail later.

The Lagrangian density needs to have dimension 4, for the action to be dimensionless. Then, if the dimension of the operators O_i are d_i, then the coefficients dimension are fixed as:

$$[O_i] = d_i \quad \longrightarrow \quad c_i \sim \frac{1}{\Lambda^{d_i-4}}, \tag{3.2}$$

with Λ some characteristic short-distance scale of the system.

The EFT Lagrangian can be seen as an expansion of a more fundamental theory with a small expansion parameter δ, known as the power counting parameter. The calculations are then done in an expansion to some order n in δ, being the error of order δ^{n+1}.

Typically, the expansion parameter is the ratio of a low-energy scale E (the energy at which the observables will be calculated) such as the external momentum p or particle mass m, and the short-distance scale Λ, $\delta = m/\Lambda$.

It is crucial to note that an effective field theory provides reliable predictions only when

[3]From now on we will use natural units.

$E < \Lambda$; for energies $E > \Lambda$, higher-order terms dominate over lower-order ones, rendering the calculations invalid. Another important point is that the behavior of each operator is dictated by its dimensionality. Actually, we can distinguish three types of operators [56]:

- Relevant ($d_i < 4$)
- Marginal ($d_i = 4$)
- Irrelevant ($d_i > 4$)

In the low-energy regime ($E \ll \Lambda$), the *Relevant* operators are amplified by factors of $(\Lambda/E)^{4-d_i}$, becoming increasingly significant at lower energies, whereas the *Irrelevant* operators are suppressed by $(E/\Lambda)^{d_i-4}$ and contribute more weakly—though this does not imply they are negligible. Finally, the *Marginal* operators lead to dimensionless coefficients and maintain comparable importance across all energy scales, although quantum effects can alter their scaling behavior on either side of the energy spectrum.

The EFT Lagrangian is then given by an infinite series of terms of increasing operator dimension, treated as an expansion in powers of (E/Λ),

$$\mathcal{L} = \mathcal{L}_{d\leq 4} + \mathcal{L}_5(E/\Lambda) + \mathcal{L}_6(E/\Lambda)^2 + ... \tag{3.3}$$

Finally, although effective field theories are generally non-renormalizable, this does not pose a significant problem. It has been shown [56], [57] that, by applying standard renormalization schemes along with dimensional analysis, an EFT effectively behaves like a renormalizable theory when calculations are performed up to a fixed order in $1/\Lambda$. This is because only a finite number of terms in the effective Lagrangian $\mathcal{L}$ are allowed at a given order in $1/\Lambda$. Higher-order terms can be safely ignored, as they cannot be enhanced by positive powers of Λ to match the contributions of lower-order terms.

In other words, a non-renormalizable theory is just as good as a renormalizable theory for computations, provided one is satisfied with a finite accuracy. The success of QED in describing low-energy electron–positron scattering is not primarily due to its renormalizability, but rather because the Z boson mass, M_Z, is very large, causing the leading non-renormalizable contributions to be suppressed by factors of $(E/M_Z)^2$.

Summarizing these ideas, we can get the following set of general principles for EFT [56]:

1. Dynamics at low energies (large distances) does not depend on details of dynamics at high energies (short distances).

2. If there are large energy gaps, put to zero (infinity) the light (heavy) scales, i.e.

$$0 \longleftarrow m << E << \Lambda \longrightarrow \infty$$

   Corrections induced by these scales can be incorporated as perturbations.

3. The EFT describes the low–energy physics, to a given accuracy ϵ, in terms of a finite set of parameters:

$$\epsilon \leq (E/\Lambda)^{(d_i-4)}$$

4. The EFT has the same infra-red, but different ultra-violet, behavior than the underlying fundamental theory.

5. The remnants of the high–energy dynamics are in the symmetries of the EFT and in the low–energy couplings.

In the following, we are going to review some examples of EFT's, that will be apply in the works done in this thesis.

3.2.1 Fermi Theory of Weak Interactions

Historically, Fermi developed his theory to describe beta decay, before the Standard Model (SM) existed. He based his intuition from electrodynamics, which is based on a vector current. Today, we understand that Fermi's original vector interaction is replaced by the $V - A$ structure, which accurately accounts for experimental observations, including parity violation [58], [59].

Here, we shall discuss how to obtain the Fermi theory as the low-energy limit of the renormalizable $SU(2) \times U(1)$ electroweak theory at tree level. In the SM, weak decays proceed at lowest order through the exchange of a $W^{\pm}$ boson between two fermionic left–handed currents (except for the heavy quark top which decays into a real W). In the Standard Model (assuming massless neutrinos), the charged current Lagrangian that

governs this process is expressed as:

$$\mathcal{L} = -\frac{g}{2\sqrt{2}} W_\mu^\dagger \left\{ \sum_l \bar{\nu}_l \gamma^\mu (1-\gamma^5) l + \sum_{ij} \bar{u}_i \gamma^\mu (1-\gamma^5) V_{ij} d_j \right\} + h.c \tag{3.4}$$

Where $g/\sqrt{2}$ is the W coupling constant, u_i are the up-type quarks, d_j are down-type quarks and V_{ij} is the CKM mixing matrix, l is a lepton and ν_l the corresponding neutrino.

Focusing on the leptonic sector, the derivation of the quark sector will be almost identical. The tree-level amplitude for the leptonic $l \longrightarrow l^{'} + \bar{\nu}_{l'} + \nu_l$ decay from (3.4) is:

$$\mathcal{M} = \left(\frac{-ig}{2\sqrt{2}}\right)^2 [\bar{u}_4 \gamma^\mu (1-\gamma^5) v_2] \left(\frac{-ig_{\mu\nu}}{p^2 - M_W^2}\right) [\bar{u}_3 \gamma^\nu (1-\gamma^5) u_1], \tag{3.5}$$

where we use the 't Hooft-Feynman gaugethe for the W boson propagator, the momentum transferred by the W is p, and u_1,v_2,u_3 and u_4 are the spinors corresponding to l,$\bar{\nu}_{l'}$,ν_l and $l^{'}$ respectively.

The amplitude given by (3.5) produces a non-local four-fermion interaction, due to the factor $p^2 - M_W^2$ in the denominator. Now, if the momentum transfer p is small compared with M_W, i.e, $p << M_W$, the non-local interaction can be approximated by a local one, using the Taylor series expansion as follows

$$\frac{1}{p^2 - M_W^2} = -\frac{1}{M_W^2}\left(1 + \frac{p^2}{M_W^2} + \frac{p^4}{M_W^4} + ...\right) \tag{3.6}$$

To lowest order, the amplitude is

$$\mathcal{M} = \left(\frac{i}{M_W^2}\right)\left(\frac{ig}{2\sqrt{2}}\right)^2 [\bar{u}_4 \gamma^\mu (1-\gamma^5) v_2][\bar{u}_3 \gamma_\mu (1-\gamma^5) u_1] + \mathcal{O}\left(\frac{1}{M_W^4}\right), \tag{3.7}$$

which is the same amplitude as that produced by the local Lagrangian

$$\mathcal{L} = -\frac{g^2}{8M_W^2} [\bar{l^{'}} \gamma^\mu (1-\gamma^5) \nu_{l'}][\bar{\nu}_l \gamma^\nu (1-\gamma^5) l] + \mathcal{O}\left(\frac{1}{M_W^4}\right). \tag{3.8}$$

Equation (3.8) is the lowest order Lagrangian for leptonic lepton decays (and related processes) in the EFT ($p << M_W$). For historical reasons, it is written in terms of the

so-called Fermi coupling constant G_F:

$$\mathcal{L} = -\frac{G_F}{\sqrt{2}}[\bar{l'}\gamma^\mu(1-\gamma^5)\nu_{l'}][\bar{\nu}_l\gamma^\nu(1-\gamma^5)l] + \mathcal{O}\left(\frac{1}{M_W^4}\right), \tag{3.9}$$

where the relation between G_F and the W coupling g is

$$\frac{G_F}{\sqrt{2}} = \frac{g^2}{8M_W^2}. \tag{3.10}$$

These results can be generalized to the quark sector [4], so weak decays can then be described through an effective local four-fermion interaction

$$\mathcal{L} = -\frac{G_F}{\sqrt{2}}\mathcal{J}_\mu\mathcal{J}^{\mu\dagger}, \tag{3.11}$$

where

$$\mathcal{J}^\mu = \sum_l \bar{\nu}_l\gamma^\mu(1-\gamma^5)l + \sum_{ij}\bar{u}_i\gamma^\mu(1-\gamma^5)V_{ij}d_j. \tag{3.12}$$

Equation (3.11) corresponds to what is known as Fermi's theory of weak interactions. This theory is only valid in the regime where $p << M_W$; which describes to a really good accuracy the weak decays, where p is of the order of the decaying particle mass such as m_b, m_c and m_l; since $m_b, m_c, m_l << M_W$. The theory involves dimension-6 operators, leading to couplings with mass dimension -2. Consequently, the *Irrelevant* ($d > 4$) property of the operators explains why such interactions are weak at low energies ($E << M_W$).

Equation (3.10) is technically called a *matching condition*; and shows explicitly the relation between the effective coupling constant and the underlying electroweak theory parameters (g,M_W). The Fermi Lagrangian, as any other EFT, has the usual expansion form, with the expansion parameter $\delta = p/M_W$. The higher-order corrections $\mathcal{O}\,(1/M_W^4)$ can be neglected, provided we are satisfied with an accuracy not better than (p^2/M_W^2).

As a review; at low energies ($p << M_W$), there is not enough energy to produce a physical W boson. Therefore, the vector-boson propagator shrinks to a point and can be well approximated through a local four-fermion interaction (Fig. 3.1), i.e, for weak decays

[4] Quark masses cannot be generally neglected, which gives rise to the mass eigenstate basis. Its misalignment with the weak basis gives rise to the V_{ij} CKM factor [60], [61]. In the lepton sector, for massive neutrinos, an analogous mixing appears, parametrized in terms of the PMNS matrix [62], [63].

the electroweak theory can be replaced by the Fermi effective theory up to corrections of order $\mathcal{O}\left(1/M_W^4\right)$.

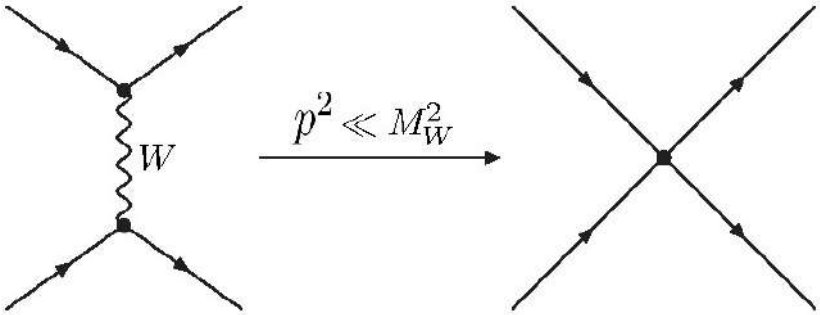

Figure 3.1: Left: Non-local weak interaction by the exchange of a W boson. Right:Local weak interaction described by Fermi's theory.

Fermi theory of weak interactions includes the effect of W exchange via dimension-six four-fermion operators and the higher-energy parameters are hidden in the effective coupling G_F. Notice that the EFT Lagrangian (3.11) has the same chiral symmetry as the fundamental theory, coupling just left-handed particles (right-handed antiparticles) via the V-A Lorentz structure.

At first glance, this may appear straightforward, since the EFT was explicitly derived as a low-energy limit of the fundamental electroweak theory. However, in many cases the underlying high-energy theory is unknown. In such situations, the EFT is constructed by considering the most general framework consistent with the relevant symmetries and the known light particles. Still, the characteristics of the unknown high-energy theory manifest themselves through non-trivial symmetry structures within the EFT.

3.2.2 The SM EFT

In this section, based on [64], [65], [66], [67], [68], a brief introduction of the basic concepts relevant to the construction of the Standard Model Effective Field Theory (SMEFT) are reviewed in a qualitative manner.

For the fundamental point of view of particle physics, we know the low-energy limit of the theory, which is the SM, while we do not know its UV completion. The goal is to find a general description, in terms of higher-dimensional operators, of the effects generated by integrating out heavy degrees of freedom that are a priori unknown, as already discussed in

this chapter. The symmetries we assume are Lorentz invariance, the SM gauge symmetry, and possible additional global symmetries, such as baryon and lepton number. With the known symmetries, it becomes a pure group theory exercise –although a non-trivial one– to construct all the allowed operators.

More formal, the SMEFT is a consistent EFT generalization of the SM constructed out of a series of $\mathrm{SU_c}(3) \times \mathrm{SU_L}(2) \times \mathrm{U_Y}(1)$ invariant higher-dimensional operators, built out of SM fields. The idea of the SMEFT is that extensions to the SM are assumed to involve massive particles heavier than the measured vev, which sets the scale (up to coupling suppression) of the SM states. In addition, it is assumed that any non-perturbative matching effects are characterized by a scale parametrically separated from the EW scale and the observed Higgs-like boson is embedded in the $\mathrm{SU}(2)_\mathrm{L}$ Higgs doublet.

The SMEFT follows from these assumptions and is defined as

$$\mathcal{L}_{SMEFT} = \mathcal{L}_{SM} + \mathcal{L}^{(5)} + \mathcal{L}^{(6)} + \mathcal{L}^{(7)} + ..., \qquad \mathcal{L}^{(d)} = \sum_{i=1}^{n_d} \frac{C_i^{(d)}}{\Lambda^{d-4}} Q_i^{(d)} \quad \text{for } d > 4. \tag{3.13}$$

The operators $Q_i^{(d)}$ are suppressed by $d-4$ powers of the cutoff scale Λ, and the $C_i^{(d)}$ are the Wilson coefficients. The number of non-redundant operators in $\mathcal{L}^{(5)}$, $\mathcal{L}^{(6)}$, $\mathcal{L}^{(7)}$ and $\mathcal{L}^{(8)}$ is known [64], [65], [66], [69], [70], [71], [72].

The dimension-five piece $\mathcal{L}^{(5)}$ consists of a single term, the so-called Weinberg operator [64], the only one consistent with the dimensional requirements, gauge and Lorentz invariance. After electroweak symmetry breaking, the Weinberg operator introduces a Majorana mass for the left-handed neutrinos ν_L that violates total lepton number by two units, as explained in appendix B, that could naturally justify the smallness of neutrino masses.

The operators of $\mathcal{L}^{(6)}$ –and higher– are built analogously, with the same symmetry considerations. A giant effort to obtain a complete SMEFT operator set up to a higher dimension has been done and continuously checked by the scientific community, since a lot of lists contain many redundant operators that need to be eliminated to provide a minimal basis. This goal is achieved with general arguments on how different effective operators can be related and how an independent set can be obtained, see [67], [68] for technical details.

There are many viable choices of basis that can be used to write the complete set of SMEFT operators at certain dimension. The Warsaw basis is the most commonly used for the $d = 6$ SMEFT, although other bases can be advantageous when considering specific sets of observables. A commonly adopted set of dimension-six operators in phenomenological analyses is the so-called strongly-interacting light Higgs (SILH) and the HISZ "basis" [5]. The Green functions' basis is another common set of SMEFT operators, etc. An extensive discussion about the basis choice in the SMEFT can be found in [73].

As a summary, the SMEFT is an enormously powerful consistent field theory useful to characterize the low-energy limit of physics beyond the SM. Even if a full model extension of the SM becomes experimentally supported in the future, the SMEFT can still be a useful and appropriate tool to use to interface with large swaths of experimental data below the characteristic scale(s) Λ of a new physics sector. Considering the current global data set of particle physics, adopting the IR assumptions that define the SMEFT seems to be a very reasonable compromise between utility and generality of the theoretical framework assumed to accommodate the certain fact that the SM is an incomplete description of reality but an extremely successful one in particle physics.

3.2.3 The Higgs EFT

A naive overview of the aspects about the Higgs EFT is given in this section. This is a relevant EFT that is explicitly applied in one of the main works of this thesis [4].

Although the SMEFT framework considers the Higgs as an elementary $SU(2)$ doublet, there exist scenarios in which the Higgs does not strictly reside in this representation. Such possibilities, including Composite Higgs models, remain consistent with current experimental constraints [74], [75], [76], [77], [78]. This makes intriguing to identify observables that can distinguish between these different possibilities.

For SMEFT, one singlet scalar h–coming from the scalar complex $SU(2)_L$ doublet field H–[6], corresponding to the physical Higgs boson, ensures the exact unitarity at all energies of scattering amplitudes with external π^I fields. Nevertheless, this requirement can be relaxed and the EFT can remain self-consistent for lower energies scattering events where

[5] However, although called basis, they do not represent a complete set at dimension six.
[6] We refer to this embedding as the linear realization of the electroweak symmetry breaking mechanism.

the EFT is well-defined. We recall that an EFT does not have to exactly preserve unitarity. It only has to be unitary up to the cut off scale where the Taylor expansion used in its construction breaks down.

The scenarios where the Higgs does not belong to an $SU(2)_L$ doublet are described by the so-called Higgs EFT (HEFT) [79], [80], [81], [82], [83], [84], [85], [86], [87], [88], based on the Callan-Coleman-Wess-Zumino (CCWZ) formalism and offers a parameterization of the scalar sector with minimal infrared assumptions. In this approach, the physical Higgs h is treated as a singlet under the Standard Model gauge group, separate from the three electroweak Goldstone bosons, which in SMEFT are collectively represented by the Higgs doublet. As a result, the number of independent operators at any given order in the expansion is substantially larger than in SMEFT. Furthermore, within HEFT, the dependence on the h field is typically captured by generic functions, $\mathcal{F}_i(h)$, which serve as the fundamental building blocks for constructing effective operators.

The differences between the SMEFT and HEFT approaches can lead to distinct phenomenological outcomes in processes involving the Higgs sector. A large number of interesting discussions, such as those in Refs. [89], [90], have identified signatures that may help distinguish between these two frameworks. Some of these include studies of Dark Matter [91] and the scattering of the longitudinal components of gauge bosons [92], [93]. At the present moment, all observations are compatible with the SM, and the SMEFT extension, but the evidence in favor of this option is still not compelling. For a comprehensive review of both formalisms, we recommend Refs.[68], [94].

In analogy with the formalism employed in chiral perturbation theory (χPT) for the pions of QCD [7], we construct the HEFT with a non-linear realization of the electroweak symmetry breaking mechanism, where the three Goldstone bosons π^I are embedded into a dimensionless unitary matrix

$$U = \exp\left(i\tau^I\pi^I/v\right), \qquad U \mapsto LUR^\dagger, \tag{3.14}$$

where τ denotes the three-vector of Pauli matrices and U transforms as a bi-doublet under global $\mathrm{SU_L}(2) \times \mathrm{SU_R}(2)$ transformations.

[7] In fact, the HEFT used to be called electroweak chiral Lagrangians because of that.

It is convenient to define objects that transform in the adjoint of $\mathrm{SU(2)_L}$, to be employed as building blocks of a $\mathrm{SU(3)_c \times SU(2)_L \times U(1)_Y}$ invariant Lagrangian. It is possible to construct a scalar and a vector as follows:

$$\begin{aligned} T &= U\tau^3 U^\dagger, & T &\mapsto LTL^\dagger, \\ V_\mu &= (D_\mu U)U^\dagger, & V_\mu &\mapsto LV_\mu L^\dagger\,, \end{aligned} \tag{3.15}$$

where the covariant derivative of the U field is

$$D_\mu U = \partial_\mu U + \frac{ig_2}{2} W_\mu^I \tau^I U - \frac{ig_1}{2} B_\mu U \tau^3\,. \tag{3.16}$$

Note that the field T is invariant under hypercharge transformations, but not under the global $\mathrm{SU(2)_R}$ group, so it can be treated as a custodial symmetry-breaking spurion.

The physical Higgs scalar is introduced as a gauge singlet h. This choice ensures the most general approach to the physics of this state and makes the HEFT a versatile tool, which includes the $\mathrm{SU(2)_L}$ doublet case as a particular limit. Specifically, the SM Higgs doublet H can be written as a fixed combination of the fields h and U according to:

$$\begin{pmatrix} \tilde{H} & H \end{pmatrix} = \frac{v+h}{\sqrt{2}}\, U\,. \tag{3.17}$$

Being a singlet, the h field has completely arbitrary couplings, that are customarily encoded in generic functions [83], [84]

$$F_i(h) = 1 + 2a_i \frac{h}{v} + b_i \frac{h^2}{v^2} + \dots \tag{3.18}$$

that constitute another building block for the HEFT Lagrangian. Note that here the polynomial structure should be interpreted as the result of a Taylor expansion in (h/v), which may include an infinite number of terms.

The HEFT Lagrangian is then composed of the gauge and fermion fields of the SM and the scalar fields U, h previously defined. It can be written as

$$\mathcal{L}_{HEFT} = \mathcal{L}_0 + \Delta\mathcal{L} + \dots\,, \tag{3.19}$$

where $\mathcal{L}_0$ contains the leading order terms and $\Delta\mathcal{L}$ includes first order deviations. Unlike

the SMEFT, it is not possible to classify the HEFT invariants based on just the canonical dimension. This is due to the fact that the HEFT is a fusion of χPT (in the scalar sector) with the SMEFT (in the fermions and gauge sector). Because these two theories follow different counting rules, the structure of the joint expansion is complex. A rigorous and self-contained method to determine the expected suppression of a given HEFT invariant represents a non-trivial and subtle task that has been intensely debated in the literature.

The explicit form of the leading and first order deviations Lagrangian can be found in [67], together with discussion of technical points that are out of the scope of this brief introduction.

Chapter 4

Neutrinos Nature and New Interactions

4.1 Michel Parameters: Lorentz Structure of the Charged Current

Based on Ref.[1], we explored the impact of NP on leptonic tau and muon decays ($\ell^- \to \ell'^- \bar{\nu}_{\ell'} \nu_\ell$), within an EFT framework. This analysis allowed us to define general parameters that can be directly extracted from experimental data to constrain NP Wilson coefficients in a model-independent manner. We also incorporated the effects of finite neutrino masses, particularly relevant when considering a possible heavy neutrino sector. Specifically, for tau neutrinos, the current mixing limits with a heavy mode could generate significant distortions in the corresponding energy and angular distributions, as we shall see, motivating their experimental search.

All the basic information about Majorana fermions, including their Feynman rules, together with neutrinos masses and mixings models are given in appendices A and B.

4.1.1 Effective Decay Rate for Dirac Neutrinos

Let us consider the leptonic decays $\ell^- \longrightarrow \ell'^- \bar{\nu}_{\ell'} \nu_\ell$, where the lepton pair (ℓ,ℓ') may be (μ,e), (τ,e) or (τ,μ). The most general, local, derivative-free, lepton-number conserving, four-lepton interaction Hamiltonian, consistent with locality and Lorentz invariance is [10], [95], [96][8]

$$\mathcal{H} = 4\frac{G_{\ell\ell'}}{\sqrt{2}} \sum_{n,\epsilon,\omega} g^n_{\epsilon\omega} \left[\bar{\ell}'_\epsilon \Gamma^n (\nu_{\ell'})_\sigma\right] \left[(\bar{\nu}_\ell)_\lambda \Gamma_n \ell_\omega\right]. \tag{4.1}$$

The subindices $\epsilon, \omega, \sigma, \lambda$ label the chiralities (L, R) –for left- and right-handed, respectively– of the corresponding fermions, and $n = S, V, T$ the type of interaction: scalar ($\Gamma^S = I$), vector ($\Gamma^V = \gamma^\mu$) and tensor ($\Gamma^T = \sigma^{\mu\nu}/\sqrt{2}$). Since tensor interactions can contribute only for opposite chiralities of the charged leptons, this leads to the existence of 10 complex

[8]The relation between different set of Hamiltonians used in the literature are derived in appendix C

coupling constants, related to 4 scalar, 4 vector and 2 tensor interactions.

After removing an unphysical global phase, 19 real parameters remain to be determined experimentally. In addition, the global factor $G_{\ell\ell'}$, obtained from the total decay rate, defines the normalization of the coupling constants as follows:[97]

$$\begin{aligned} 1 = \frac{1}{4}(|g^S_{RR}|^2 + |g^S_{RL}|^2 + |g^S_{LR}|^2 + |g^S_{LL}|^2) + 3(|g^T_{LR}|^2 + |g^T_{RL}|^2) \\ + (|g^V_{RR}|^2 + |g^V_{RL}|^2 + |g^V_{LR}|^2 + |g^V_{LL}|^2). \end{aligned} \tag{4.2}$$

Thus, $|g^S_{\epsilon\omega}| \leq 2$,$|g^V_{\epsilon\omega}| \leq 1$ and $|g^T_{\epsilon\omega}| \leq 1/\sqrt{3}$. The Standard Model predicts $|g^V_{LL}| = 1$ and all others couplings vanishing. In the search for new physics it is important to calculate the final charged-lepton distribution using the Hamiltonian (4.1).

Within the general framework, the charged weak current interaction is expressed in the mass eigenstate basis of the charged leptons ℓ and neutrinos N_j, following the diagonalization of their respective mass matrices. When working in a basis where the charged lepton sector is already diagonal, the flavor neutrino fields ($\nu_{L,R}$) are treated as superpositions of the neutrino mass eigenstates (N_j) with masses m_j, namely:

$$\nu_{lL} = \sum_j U_{lj} N_{jL}, \quad \nu_{lR} = \sum_j V_{lj} N_{jR}, \tag{4.3}$$

where $j = \{1, 2, ..., n\}$ with n the number of mass-eigenstate neutrinos.

As shown by Langacker and London [98], explicit lepton-number nonconservation still leads to a matrix element equivalent to the one derived from eq.(4.1). In the mass basis, the effective Hamiltonian for the $\ell^- \longrightarrow \ell'^- \overline{N}_j N_k$ process is written as:

$$\begin{aligned} \mathcal{H} = 4\frac{G_{\ell\ell'}}{\sqrt{2}} \sum_{j,k} \Big\{ & g^S_{LL} \left[\overline{\ell}'_L V_{\ell' j} N_{jR}\right] \left[\overline{N}_{kR} V^*_{\ell k} \ell_L\right] + g^V_{LL} \left[\overline{\ell}'_L \gamma^\mu U_{\ell' j} N_{jL}\right] \left[\overline{N}_{kL} U^*_{\ell k} \gamma_\mu \ell_L\right] \\ & + g^S_{RR} \left[\overline{\ell}'_R U_{\ell' j} N_{jL}\right] \left[\overline{N}_{kL} U^*_{\ell k} \ell_R\right] + g^V_{RR} \left[\overline{\ell}'_R \gamma^\mu V_{\ell' j} N_{jR}\right] \left[\overline{N}_{kR} V^*_{\ell k} \gamma_\mu \ell_R\right] \\ & + g^S_{LR} \left[\overline{\ell}'_L V_{\ell' j} N_{jR}\right] \left[\overline{N}_{kL} U^*_{\ell k} \ell_R\right] + g^V_{LR} \left[\overline{\ell}'_L \gamma^\mu U_{\ell' j} N_{jL}\right] \left[\overline{N}_{kR} V^*_{\ell k} \gamma_\mu \ell_R\right] \\ & + g^T_{LR} \left[\overline{\ell}'_L \frac{\sigma^{\mu\nu}}{\sqrt{2}} V_{\ell' j} N_{jR}\right] \left[\overline{N}_{kL} U^*_{\ell k} \frac{\sigma_{\mu\nu}}{\sqrt{2}} \ell_R\right] + g^S_{RL} \left[\overline{\ell}'_R U_{\ell' j} N_{jL}\right] \left[\overline{N}_{kR} V^*_{\ell k} \ell_L\right] \\ & + g^V_{RL} \left[\overline{\ell}'_R \gamma^\mu V_{\ell' j} N_{jR}\right] \left[\overline{N}_{kL} U^*_{\ell k} \gamma_\mu \ell_L\right] + g^T_{RL} \left[\overline{\ell}'_R \frac{\sigma^{\mu\nu}}{\sqrt{2}} U_{\ell' j} N_{jL}\right] \left[\overline{N}_{kR} V^*_{\ell k} \frac{\sigma_{\mu\nu}}{\sqrt{2}} \ell_L\right] \Big\}. \end{aligned} \tag{4.4}$$

It is important to note that $\overline{N}$ denotes an antineutrino in the case of Dirac neutrinos, whereas in the Majorana scenario, it is identified with the neutrino itself, satisfying $N = N^c = C\overline{N}^T$. Consequently, for Dirac neutrinos—unlike the Majorana case—only a single first-order Feynman diagram contributes to the process.

The differential decay rate for the process $\ell^- \longrightarrow \ell'^- \overline{N}_j N_k$ is

$$d\Gamma = \sum_{j,k} d\Gamma^{jk}. \tag{4.5}$$

Explicitly:

$$d\Gamma = \sum_{j,k} \frac{(2\pi)^4 \delta^4(p_1 - p_2 - p_3 - p_4)}{2m_\ell} \frac{d^3p_2 d^3p_3 d^3p_4}{(2\pi)^3 2E_2 (2\pi)^3 2E_3 (2\pi)^3 2E_4} |\mathcal{M}_{jk}|^2, \tag{4.6}$$

where we are taking into account all the possible neutrino final states, ni the mass basis, and the sum extends over all energetically allowed neutrino pairs, assuming that the neutrinos are not detected.

It is important to emphasize that, in the phase-space integration, we neglect terms depending on the neutrino masses. This approximation is well justified, as it remains consistent with the observed charged-lepton energy distribution. Such terms enter only quadratically in the phase-space factor, through expressions of the form $r_{jk}^2 = \frac{(m_j+m_k)^2}{2m_\ell \omega}$; which are strongly suppressed—either due to the smallness of light-neutrino masses or to the mixing suppression of heavy neutrinos. Moreover, these effects become relevant only near the endpoint of the energy spectrum, where the experimental statistics are limited. A detailed discussion of these corrections can be found in [99], [100]. In cases where higher precision is required, one must include non-negligible neutrino mass effects in the calculation. For this thesis, we are dealing with neutrino masses effects up to the matrix element calculation. With this consideration, the explicit differential decay rate for Dirac neutrinos is given in section 4.1.3.

4.1.2 Effective Decay Rate for Majorana Neutrinos

Unlike the Dirac case, the properties of Majorana neutrinos have strong consequences in the amplitude. As it has been pointed out in well-known previous works, see the

discussion just before note added of Ref.[101], for Majorana neutrinos the decay modes $\ell^- \longrightarrow \ell'^- \bar{N}_j N_k$ and $\ell^- \longrightarrow \ell'^- \bar{N}_k N_j$ yield the same final states for $j \neq k$ as well as for $j = k$, and hence the amplitudes must be added coherently. Then the possible first order Feynman diagrams for the $\ell^- \longrightarrow \ell'^- N_j N_k$ decay are shown in figure 4.1. The first

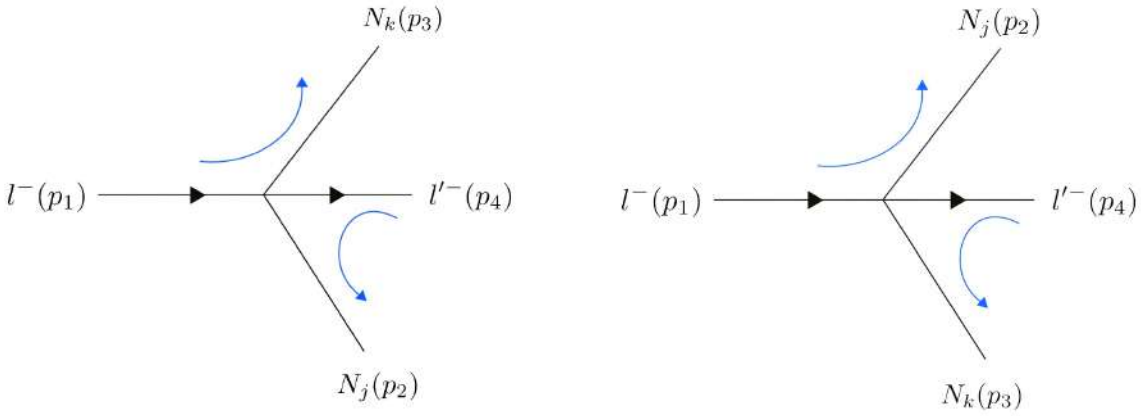

Figure 4.1: Feynman diagrams for the $\ell^- \longrightarrow \ell'^- N_j N_k$ decay. The orientation chosen for the fermion chains is defined by the blue arrows.

diagram leads to the same matrix element as the Dirac case, while the second diagram is only possible in the Majorana neutrino case, where the orientation for each fermion chain is already defined (blue arrows). [9]

In this case, the differential decay rate for the process $\ell^- \longrightarrow \ell'^- N_j N_k$ is

$$d\Gamma = \frac{1}{2} \sum_{j,k} d\Gamma^{jk}. \tag{4.7}$$

Explicitly:

$$d\Gamma = \frac{1}{2} \sum_{j,k} \frac{(2\pi)^4 \delta^4(p_1 - p_2 - p_3 - p_4)}{2m_\ell} \frac{d^3p_2 d^3p_3 d^3p_4}{(2\pi)^3 2E_2 (2\pi)^3 2E_3 (2\pi)^3 2E_4} |\mathcal{M}_{jk}|^2, \tag{4.8}$$

where the $1/2$ factor that appears in the Majorana case arises from two distinct reasons. For the $j = k$ case it is a statistical factor accounting for the presence of indistinguishable fermions in the final state, while for the $j \neq k$ case it arrives because of double counting, since the sum $\sum_{j,k}$ is not restricted to $j \leq k$. The same discussion can be found in section

[9] We select this orientation of the fermion chain in order to apply the spinor completeness relation directly within the matrix element calculation. This choice does not affect any physical observables, provided that the appropriate Feynman rules for Majorana fermions are consistently followed [102].

11.2.2 of Ref.[103].

Then, after integrating over the neutrinos momenta, the decay rate will have the following dependence on the amplitude:[10]

$$\begin{aligned} d\Gamma &\propto \frac{1}{2}\sum_{j,k} |\mathcal{M}^1_{jk} - \mathcal{M}^2_{jk}|^2 \\ &= \frac{1}{2}\sum_{j,k} \left\{ |\mathcal{M}^1_{jk}|^2 + |\mathcal{M}^2_{jk}|^2 - 2\,\mathrm{Re}(\mathcal{M}^1_{jk}\mathcal{M}^{2*}_{jk}) \right\} \\ &= \sum_{j,k} |\mathcal{M}^1_{jk}|^2 - \sum_{j,k} \mathrm{Re}(\mathcal{M}^1_{jk}\mathcal{M}^{2*}_{jk}). \end{aligned} \tag{4.9}$$

Thus the fundamental difference between Dirac and Majorana cases is precisely the last interference term, sometimes called the Majorana term [103].
Using this property, we can write the final differential decay rate for both cases in a single expression, where the Dirac and Majorana nature is distinguishable by the Majorana term. This was done with the implementation of a flag parameter $\epsilon = 0, 1$.

4.1.3 Dirac vs Majorana Distributions

For efficiency, we present our final result using the PDG parametrization, which is currently the most practical. Additionally, we isolate the Majorana contribution by explicitly calculating the corresponding term, introducing a flag parameter $\epsilon = 0, 1$. Finally we rename dummy indices wherever possible in order to make our expressions clearer and more convenient for general applications.

4.1.3.1 Massless neutrino case

Considering massless neutrinos, the differential decay probability to obtain a final charged lepton with (reduced) energy between $x = E_{\ell'}/\omega$ and $x + dx$, emitted in the direction $\hat{z}$ at an angle between θ and $\theta + d\theta$ with respect to the initial lepton polarization vector $\mathcal{P}$, and with its spin parallel to the arbitrary direction $\hat{\zeta}$, neglecting radiative corrections, is

[10] Where $\mathcal{M}^1_{jk}$ and $\mathcal{M}^2_{jk}$ are related by the exchange $j \leftrightarrow k$ once the neutrinos momenta are integrated out.

given by

$$\begin{aligned}\frac{d\Gamma}{dx d\cos\theta} = \frac{m_\ell}{4\pi^3}\omega^4 G^2_{\ell\ell'}\sqrt{x^2-x_0^2}\times\Big(F(x)-\frac{\xi}{3}\mathcal{P}\sqrt{x^2-x_0^2}\cos\theta A(x)\Big)\\ \times\big[1+\hat{\zeta}\cdot\vec{\mathcal{P}}_{\ell'}(x,\theta)\big],\end{aligned} \tag{4.10}$$

where $w \equiv (m_\ell^2 + m_{\ell'}^2)/2m_\ell$, $x_0 \equiv m_{\ell'}/\omega$ and the polarization vector $\vec{\mathcal{P}}_{\ell'}$ in eq.(4.10) is

$$\vec{\mathcal{P}}_{\ell'} = P_{T_1}\,\hat{x} + P_{T_2}\,\hat{y} + P_L\,\hat{z}. \tag{4.11}$$

Here $\hat{x}, \hat{y}$ and $\hat{z}$ are unit vectors defined as:

$$\begin{aligned}\hat{z} &\quad \text{is along the } \ell' \text{ momentum } \vec{p}_{\ell'},\\ \frac{\hat{z}\times\vec{\mathcal{P}}_{\ell'}}{|\hat{z}\times\vec{\mathcal{P}}_{\ell'}|} = \hat{y} &\quad \text{is transverse to } \vec{p}_{\ell'} \text{ and perpendicular to the decay plane,}\\ \hat{y}\times\hat{z} = \hat{x} &\quad \text{is transverse to } \vec{p}_{\ell'} \text{ and in the decay plane,}\end{aligned} \tag{4.12}$$

and the components of $\vec{\mathcal{P}}_{\ell'}$ are, respectively

$$\begin{aligned}P_{T_1} &= \mathcal{P}\sin\theta\cdot F_{T_1}(x)\ /\ \Big\{F(x)-\frac{\xi}{3}\mathcal{P}\sqrt{x^2-x_0^2}\cos\theta A(x)\Big\},\\ P_{T_2} &= \mathcal{P}\sin\theta\cdot F_{T_2}(x)\ /\ \Big\{F(x)-\frac{\xi}{3}\mathcal{P}\sqrt{x^2-x_0^2}\cos\theta A(x)\Big\},\\ P_L &= \frac{-F_{IP}(x)+\mathcal{P}\cos\theta\cdot F_{AP}(x)}{F(x)-\frac{\xi}{3}\mathcal{P}\sqrt{x^2-x_0^2}\cos\theta A(x)},\end{aligned} \tag{4.13}$$

where

$$\begin{aligned}F(x) &= x(1-x)+\frac{2}{9}\rho\left(4x^2-3x-x_0^2\right)+\eta x_0(1-x),\\ A(x) &= 1-x+\frac{2}{3}\delta\left(4x-4+\sqrt{1-x_0^2}\right),\\ F_{T_1}(x) &= \frac{1}{12}\Big[-2\Big(\xi''+12\Big(\rho-\frac{3}{4}\Big)\Big)(1-x)x_0-3\eta(x^2-x_0^2)+\eta''(-3x^2+4x-x_0^2)\Big],\\ F_{T_2}(x) &= \frac{1}{3}\sqrt{x^2-x_0^2}\Big[3\frac{\alpha'}{\mathcal{A}}(1-x)+2\frac{\beta'}{\mathcal{A}}\sqrt{1-x_0^2}\Big],\\ F_{IP}(x) &= \frac{1}{54}\sqrt{x^2-x_0^2}\Big[9\xi'\Big(-2x+2+\sqrt{1-x_0^2}\Big)+4\xi\Big(\delta-\frac{3}{4}\Big)\Big(4x-4+\sqrt{1-x_0^2}\Big)\Big],\\ F_{AP}(x) &= \frac{1}{6}\Big[\xi''(2x^2-x-x_0^2)+4\Big(\rho-\frac{3}{4}\Big)(4x^2-3x-x_0^2)+2\eta''(1-x)x_0\Big],\end{aligned} \tag{4.14}$$

are written in terms of the Michel parameters $\rho, \eta, \delta, \xi, \eta^{''}, \xi^{'}, \xi^{''}, \alpha^{'}, \beta^{'}$, which are bilinear combinations of the $g^n_{e\omega}$ couplings [9], [10], [95], [97], [104]. In the SM, $\rho = \delta = 3/4$, $\eta = \eta^{''} = \alpha^{'} = \beta^{'} = 0$ and $\xi = \xi^{'} = \xi^{''} = 1$. We can obtain the total decay rate integrating over all energy and angular configurations, leading to

$$\Gamma_{\ell\to\ell'} = \frac{\hat{G}^2_{\ell\ell'} m^5_\ell}{192\pi^3} f(m^2_{\ell'}/m^2_\ell)\left(1+\delta^{\ell\ell'}_{RC}\right), \tag{4.15}$$

where

$$\hat{G}_{\ell\ell'} \equiv G_{\ell\ell'}\sqrt{1+4\eta\frac{m_{\ell'}}{m_\ell}\frac{g(m^2_{\ell'}/m^2_\ell)}{f(m^2_{\ell'}/m^2_\ell)}}, \tag{4.16}$$

in which $f(x) = 1-8x+8x^3-x^4-12x^2\log(x)$, $g(x) = 1+9x-9x^2-x^3+6x(1+x)\log(x)$ and the SM radiative correction $\delta^{\ell\ell'}_{RC}$ has been included [105], [106], [107].

The normalization $G_{e\mu}$ corresponds to the Fermi coupling G_F, as determined from μ decay. Unlike the other Michel parameters, the dependence of Eq.(4.15) on η is retained, although it is suppressed by a factor of $(m_{\ell'}/m_\ell)$. Consequently, this contribution is negligible in decays such as $\mu^- \to e^-\nu_\mu\bar{\nu}_e$ or $\tau^- \to e^-\nu_\tau\bar{\nu}_e$ but it can have measurable effects in $\tau^- \to \mu^-\nu_\tau\bar{\nu}_\mu$, potentially distorting the partial decay width, see e.g.[108]. This difference enables a determination of η by comparing the branching ratios of the two τ leptonic decays.

If e/μ universality is assumed[11], the leptonic decay ratio B_μ/B_e implies:

$$\eta = 0.016 \pm 0.013. \tag{4.17}$$

A non-zero value of η would indicate the presence of at least two different couplings with opposite chiralities for the charged leptons. Assuming the V-A coupling g^V_{LL} to be dominant (as supported by data), then the term $\frac{1}{2}\,\mathrm{Re}[g^V_{LL}g^{S*}_{RR}]$ is the only one linear in non-standard couplings in the whole spectrum, thus the measurement of η is of particular interest for the determination of new couplings, specially the scalar coupling g^S_{RR}, which frequently appears in many extensions of the standard model. This coupling is unique in that it involves only left-handed neutrinos and right-handed antineutrinos, as shown in Eq. (4.4).

[11] Assuming lepton universality leads to a more restrictive value for η.

Table 4.1: Michel parameters and their most accurate determinations.

	$\mu^- \to e^-\nu_\mu\bar{\nu}_e$	$\tau^- \to e^-\nu_\tau\bar{\nu}_e$	$\tau^- \to \mu^-\nu_\tau\bar{\nu}_\mu$
ρ	0.74979 ± 0.00026	0.747 ± 0.010	0.763 ± 0.020
η	0.057 ± 0.034	—	0.094 ± 0.073
ξ	$1.0009^{+0.0016}_{-0.0007}$	0.994 ± 0.040	1.030 ± 0.059
$\xi\delta$	$0.7511^{+0.0012}_{-0.0006}$	0.734 ± 0.028	0.778 ± 0.037
ξ'	1.00 ± 0.04	—	0.22 ± 0.94
ξ''	0.65 ± 0.36	—	—

The experimental status on the τ-decay Michel parameters [109], [110], [111], [112], [113], [114], [115] together with the more accurate values measured in μ decay [116], [117], [118], [119] are shown in table 4.1. The parameter ξ' has been measured for the first time in 2023 at Belle [120], while ξ'' has never been measured directly. This has be done measuring the $\bar{\eta}$ and $\xi\kappa$ parameters[12] in the radiative leptonic τ-decay [121], since the distribution of the photons emitted by the daughter lepton is sensitive to the lepton polarization [122]. Nevertheless the experimental precision does not provide a significant impact on the knowledge about the couplings, yet. Michel parameters for the five-lepton muon and tau decays were derived in ref. [123] and are being studied at Belle(-II) [124].

4.1.3.2 Massive neutrino case

The differential decay probability taking into account finite Dirac ($\epsilon = 0$) or Majorana ($\epsilon = 1$) neutrino masses is given by[13]

$$\begin{aligned}\frac{d\Gamma}{dx\,d\cos\theta} = &\sum_{j,k} \frac{m_\ell}{4\pi^3}\omega^4 G^2_{\ell\ell'}\sqrt{x^2 - x_0^2} \\ &\times \Big((F_{IS}(x) + F'_{IS}(x) + F''_{IS}(x)) - \mathcal{P}\cos\theta\big(F_{AS}(x) + F'_{AS}(x) + F''_{AS}(x)\big)\Big) \\ &\times \big[1 + \hat{\zeta}\cdot\vec{\mathcal{P}}_{\ell'}(x,\theta)\big],\end{aligned} \tag{4.18}$$

[12] Where $\xi' = -\xi - 4\xi\kappa + 8\xi\delta/3$ and $\xi'' = 16\rho/3 - 4\bar{\eta} - 3$.

[13] The ϵ parameter appears explicitly in the definition of the functions given in appendix D.

and the components of $\vec{\mathcal{P}}_{\ell'}$ are, respectively,

$$\begin{aligned}
P_{T_1} &= \mathcal{P}\sin\theta\cdot\big(F_{T_1}(x)+F'_{T_1}(x)+F''_{T_1}(x)\big)\ /\ N,\\
P_{T_2} &= \mathcal{P}\sin\theta\cdot\big(F_{T_2}(x)+F'_{T_2}(x)+F''_{T_2}(x)\big)\ /\ N,\\
P_{L} &= \Big(-\big(F_{IP}(x)+F'_{IP}(x)+F''_{IP}(x)\big)+\mathcal{P}\cos\theta\cdot\big(F_{AP}(x)+F'_{AP}(x)+F''_{AP}(x)\big)\Big)\ /\ N\,,
\end{aligned} \tag{4.19}$$

with N the normalization factor $N = \big(F_{IS}(x)+F'_{IS}(x)+F''_{IS}(x)\big) - \mathcal{P}\cos\theta\big(F_{AS}(x)+F'_{AS}(x)+F''_{AS}(x)\big)$.

As it is shown, in the massive case, we have generalized the previous result with the inclusion of new primed and biprimed functions which will depend linearly and quadratically on neutrino masses, respectively. The explicit form of all the new functions and parameters are given in appendix D.

Finally, integrating over all energy and angular configurations we obtained:

$$\Gamma_{\ell\to\ell'} = \sum_{j,k}\frac{m_\ell w^4}{\pi^3}G^2_{\ell\ell'}\int_{x_0}^{1}\sqrt{x^2-x_0^2}\Big(F_{IS}(x)+F'_{IS}(x)+F''_{IS}(x)\Big)dx \tag{4.20}$$

$$\Gamma_{\ell\to\ell'} = \sum_{j,k}\frac{\hat{G}^2_{\ell\ell'}m^5_\ell}{192\pi^3}f(m^2_{\ell'}/m^2_\ell)\left(1+\delta^{\ell\ell'}_{RC}\right), \tag{4.21}$$

where

$$\begin{aligned}
\hat{G}_{\ell\ell'} \equiv G_{\ell\ell'}\Bigg\{&(I)_{jk}+4(\eta)_{jk}\frac{m_{\ell'}}{m_\ell}\frac{g(m^2_{\ell'}/m^2_\ell)}{f(m^2_{\ell'}/m^2_\ell)}-2\frac{m_j}{m_\ell}\left[(\kappa^+_L)_{jk}\frac{f'(m^2_{\ell'}/m^2_\ell)}{f(m^2_{\ell'}/m^2_\ell)}+(\kappa^+_R)_{kj}\frac{m_{\ell'}}{m_\ell}\frac{g'(m^2_{\ell'}/m^2_\ell)}{f(m^2_{\ell'}/m^2_\ell)}\right]\\
&-4\frac{m_jm_k}{m^2_\ell}\left[(C^+)_{jk}\frac{f''(m^2_{\ell'}/m^2_\ell)}{f(m^2_{\ell'}/m^2_\ell)}+3(H^+)_{jk}\frac{m_{\ell'}}{m_\ell}\frac{g''(m^2_{\ell'}/m^2_\ell)}{f(m^2_{\ell'}/m^2_\ell)}\right]\Bigg\}^{1/2},
\end{aligned} \tag{4.22}$$

with the functions defined as:

$$\begin{aligned}
f(x) &= 1 - 8x - 12x^2 \log(x) + 8x^3 - x^4, \\
f'(x) &= -1 + 6x - 2x^3 + 3x^2 \left(4 \operatorname{arctanh}\left(\frac{x-1}{x+1} \right) - 1 \right), \\
f''(x) &= 1 - 3x + 3x^2 - x^3, \\
g(x) &= 1 + 9x - 9x^2 - x^3 + 6x(1+x)\log(x), \\
g'(x) &= 2 - 6x^2 + x^3 + 3x \left(4 \operatorname{arctanh}\left(\frac{x-1}{x+1} \right) + 1 \right), \\
g''(x) &= 1 - x^2 + 2x \log(x).
\end{aligned} \tag{4.23}$$

As we can see, the $(I)_{jk}$ parameter defines the normalization of the $G_{\ell\ell'}$ coupling, while the other parameters entering as suppressed corrections. In addition, there are both linear and quadratic neutrino mass terms, each exhibiting the same behavior as in the massless case: one parameter remains unsuppressed, while the other is suppressed by the factor $m_{\ell'}/m_\ell$ that is usually named as low-energy parameter. This suppression can become more relevant in tau decays. Nevertheless, the neutrino mass suppression makes these contributions to the $G_{\ell\ell'}$ coupling almost negligible.

Now, we shall focus on the suppression due only to the masses and mixings, considering just one extra heavy neutrino for simplicity. Of course there will be other suppression factors such as the specific phase-space structure dependence and the explicit form of the new parameters, but this will not be the main contribution, so we are not taking them into account in this analysis, we will study them later.

• If the production of heavy neutrinos is kinematically forbidden, then only the light neutrinos will be produced as final states resulting in a very strong suppression. Considering the light neutrino masses to be of order $\mathcal{O}(\text{eV})$ and the decaying particle mass of order $\mathcal{O}(10^9\text{eV})$, then the new contributions with neutrino mass dependence will be suppressed by a factor of $\sim 10^{-9}$ for the linear mass terms and $\sim 10^{-18}$ for the quadratic one. Both of them out of the scope of near-future experiments.

• Moreover, the absence of heavy neutrinos affects the unitarity of the mixing matrix, leading to small deviations from unity when the squared mixing matrix elements are summed over all kinematically accessible neutrino states.

• In contrast, if the heavy neutrinos are kinematically accessible, then the suppression of the terms with explicit neutrino mass dependence will change, depending on the heavy neutrino mass and its mixing with the active and sterile sectors.

Considering the experimental constraints on an invisible heavy neutrino ν_4, obtained from different experimental sources and some reasonable phenomenological assumptions (ν_4 decays and its lifetime), see e.g. [125], [126] [14], we can estimate the suppression of the neutrino mass-dependent terms compared with those without this dependence (standard Michel distribution).

We note that one or two heavy neutrinos may appear in the final state, and each corresponding term is suppressed by specific mixing matrix elements, depending on the precise structure of the coupling constants $[f^n_{lm}]_{jk}$. Therefore, for this rough estimation we will consider both cases (one and two final heavy neutrinos) and the mixing suppression as $|U_{\ell 4}|^2$ for one final heavy neutrino and $|U_{\ell 4}|^2|U_{\ell' 4}|^2$ for two heavy final-state neutrinos. With these considerations, the suppression of the neutrino mass–dependent terms can be summarized in 4.2.

The mean life of the muon and tau has been measured to a precision of order 10^{-6} and 10^{-3} respectively [9]. In order to make new precision tests, the most recent and future experiments are working hard to increase this sensitivity. From table 4.2, sadly, almost all of the new contributions are really suppressed and out of reach at the near future experiments, but a few of them are just around the current precision limit and could be measurable in current and forthcoming experiments.

Specifically, in the case of one final heavy neutrino with a mass around $10^2 - 10^3$ MeV[15], the linear term suppression could be low enough to make sizeable distortions in the differential decay rate, specially in tau decays, where the Majorana or Dirac neutrino nature can be tested, as well as the underlying Lorentz structure and possible new physics.

Finally, since the maximum measurable effect of a neutrino mass in the decay rate would be of order 10^{-3} for τ-decay and 10^{-6} for μ-decay, as shown in table 4.2, it is important for the precision electroweak tests to consider all radiative corrections and their sub-leading

[14] In this table we focus on the mass intervals that can be most effectively probed in the Michel decays. See, e. g., Ref. [127] for bounds on sub-eV scale sterile neutrinos and its connection to anomalies in short-baseline neutrino oscillation experiments.

[15] We note that, in this mass range, the limit on $|U_{\ell 4}|^2$ has recently been slightly improved in ref. [128].

Neutrino	Mass (MeV)	Mixing Suppression	Linear Term Suppression (m_ν)	Quadratic Term Suppression (m_ν^2)
Light (2)	1×10^{-6}	—	10^{-9}	10^{-18}
Heavy (1) ($\ell = e$)	0.001 - 0.45	10^{-3}	$10^{-9} - 10^{-7}$	$10^{-18} - 10^{-16}$
	10 - 55	10^{-8}	10^{-10}	10^{-19}
	135 - 350	10^{-6}	10^{-7}	10^{-16}
Heavy (1) ($\ell = \mu$)	10 - 30	10^{-4}	10^{-6}	10^{-15}
	70 - 300	10^{-5}	$10^{-7} - 10^{-6}$	$10^{-16} - 10^{-15}$
	175 - 300	10^{-8}	10^{-9}	10^{-18}
Heavy (1) ($\ell = \tau$)	$100 - 1.2 \times 10^3$	$10^{-7} - 10^{-3}$	$10^{-8} - 10^{-3}$	$10^{-18} - 10^{-12}$
	$1 \times 10^3 - 60 \times 10^3$	$10^{-5} - 10^{-3}$	$10^{-5} - 10^{-3}$	$10^{-14} - 10^{-12}$
Heavy (2) ($\mu \to eNN$)	10 - 30	10^{-12}	10^{-14}	10^{-16}
	175 - 300	$10^{-14} - 10^{-11}$	$10^{-15} - 10^{-12}$	$10^{-16} - 10^{-13}$
Heavy (2) ($\tau \to eNN$)	135 - 350	$10^{-13} - 10^{-9}$	$10^{-14} - 10^{-10}$	$10^{-14} - 10^{-10}$
Heavy (2) ($\tau \to \mu NN$)	100 - 300	$10^{-12} - 10^{-8}$	$10^{-13} - 10^{-9}$	$10^{-14} - 10^{-10}$
	175 - 350	$10^{-15} - 10^{-11}$	$10^{-16} - 10^{-12}$	$10^{-16} - 10^{-12}$

Table 4.2: Estimation of neutrino mass dependent terms suppression.

Radiative Corrections and Finite Mass Effects	Numerical Effect (μ-decay)	Numerical Effect (τ-decay)
Electroweak	$(3/5)(m_\mu^2/M_W^2) \sim 1.0 \times 10^{-6}$	$(3/5)(m_\tau^2/M_W^2) \sim 2.9 \times 10^{-4}$
QED	$\mathcal{O}(\alpha) \sim 10^{-3}$	$\mathcal{O}(\alpha) \sim 10^{-3}$
Hadronic	$\mathcal{O}(\alpha^2/\pi^2) \sim 10^{-5}$	$\mathcal{O}(\alpha^2/\pi^2) \sim 10^{-5}$

Table 4.3: Main numerical effects of radiative corrections.

effects. These effects take into account radiative QED corrections, higher-order electroweak corrections and the non-local structure of the W propagator, all of these within the SM framework, where the corrections to the total decay rate are well-known at this precision level [105], [106], [107].

These corrections can also be analyzed at the level of differential decay rate, specifically the most recent corrections induced by the W-boson propagator to the differential rates of the leptonic decay of a polarized muon and tau lepton and the numerical effect of these corrections are discussed in [129] and analyzed in appendix E for the specific Michel distribution, where we also introduce the result for this correction taking into account a final charged-lepton polarization (for a recent related proposal see [130]).

It is important to emphasize that we can safely employ these radiative corrections, calculated in the SM limit $|f_{LL}^V| = 1$, in order to measure with high precision the Michel parameters, since, to a high degree of accuracy, the current experimental information is consistent with a $V - A$ structure, so possible deviations are expected to be very small and can therefore be treated at the tree level, making the SM radiative corrections the main higher-order contributions. The interested reader is addressed to ref. [131] for a helpful discussion.

We also summarize the main numerical contributions, including hadronic corrections, in table 4.3, where the subleading contributions of these corrections are of order $\mathcal{O}(10^{-11} - 10^{-7})$, which are out of experimental reach in the foreseeable future.

From table 4.3 it is evident that the three main radiative corrections must be taken into account in the muon decay analysis, since the smallest of them is of the same magnitude as the present experimental relative uncertainty of the muon decay rate.

In principle for tau decays, due to the current precision achieved, the QED and electroweak corrections are the most important. The hadronic corrections are not needed, since they would imply a correction up to 1-10% to something that has not yet been measured.

With these results, the presence of a heavy Dirac or Majorana neutrino could make measurable distortions in the differential decay rate, specially in the case of a τ-decay with one heavy final-state neutrino with a mass around $10^2 - 10^3$ MeV and in the $x \approx 1$ phase space zone, i.e., where the final charged lepton reaches its maximum energy, emphasizing again that we are neglecting terms with neutrino mass dependence in the phase space integration, so actually the upper x limit will be less than one unit, even so, for greater x, the neutrinos mass effects are slightly increased.

4.1.3.3 Dirac vs Majorana

As discussed previously, the only distinction between the Dirac and Majorana differential decay rates is the interference term unique to Majorana neutrinos. This additional contribution modifies all Dirac parameters and, depending on the underlying new physics, could produce measurable distortions. Therefore, investigating this interference term offers a potential method to determine the neutrino nature and to probe the presence of new physics.

In our analysis we define this new contribution with the help of the flag parameter ϵ, being $\epsilon = 0$ for the Dirac case and $\epsilon = 1$ for the Majorana one. Since the difference between both cases is precisely this Majorana term, we show the full and explicit dependence on the coupling constant of each parameter due to this Majorana contribution in table 4.4.

From table 4.4, it is evident that the difference between the Dirac and Majorana cases depends in a non-trivial way on the coupling constants, particularly those associated with new physics. This dependence can provide valuable insight into the underlying Lorentz structure of a theory, as illustrated in the examples that follow.

First of all, if no new-physics is present, i.e., in the SM case ($|f^V_{LL}| = 1$), we obtained the results displayed in table 4.5 for the Majorana term. This result shows explicitly the Kaiser Theorem [132], that states: "For massless neutrinos in a world where all weak currents are left-handed, there is no distinction between a two-component Dirac (i.e., Weyl) neutrino and a Majorana neutrino. Once the mass is non-zero, however, then no

Term	Coupling Dependence
No Neutrino Mass Dependence	
$(I)^M_{jk}$	$\frac{1}{8}\Big[12(f^T_{LR})_{jk}(f^S_{LR})^*_{kj} + 12(f^T_{LR})_{jk}(f^T_{LR})^*_{kj} + 8(f^V_{RL})_{jk}(f^V_{RL})^*_{kj} - (f^S_{LR})_{jk}(f^S_{LR})^*_{kj}$ $+8(f^S_{LL})_{jk}(f^V_{LL})^*_{kj} + (L \leftrightarrow R)\Big]$
$(\rho)^M_{jk}$	$\frac{3}{16}\Big[-(f^S_{LR})_{jk}(f^S_{LR})^*_{kj} + 4(f^S_{LR})_{jk}(f^T_{LR})^*_{kj} + 4(f^S_{LL})_{jk}(f^V_{LL})^*_{kj} - 4(f^T_{LR})_{jk}(f^T_{LR})^*_{kj} + (L \leftrightarrow R)\Big]$
$(\xi)^M_{jk}$	$-(f^S_{RR})_{jk}(f^V_{RR})^*_{kj} + \frac{17}{2}(f^T_{LR})_{jk}(f^T_{LR})^*_{kj} + \frac{1}{2}(f^S_{LR})_{jk}(f^T_{LR})^*_{kj} + 3(f^V_{LR})_{jk}(f^V_{LR})^*_{kj}$ $+\frac{5}{8}(f^S_{LR})_{jk}(f^S_{LR})^*_{kj} - (L \leftrightarrow R)$
$(\xi\delta)^M_{jk}$	$\frac{3}{4}\Big[-(f^S_{RR})_{jk}(f^V_{RR})^*_{kj} + (f^T_{LR})_{jk}(f^T_{LR})^*_{kj} - (f^S_{LR})_{jk}(f^T_{LR})^*_{kj} + \frac{1}{4}(f^S_{LR})_{jk}(f^S_{LR})^*_{kj} - (L \leftrightarrow R)\Big]$
$(\eta)^M_{jk}$	$\frac{1}{8}\Big[4(f^S_{LR})_{jk}(f^V_{RL})^*_{kj} + 24(f^T_{LR})_{jk}(f^V_{RL})^*_{kj} + (f^S_{LL})_{jk}(f^S_{RR})^*_{kj} + 4(f^V_{LL})_{jk}(f^V_{RR})^*_{kj} + (L \leftrightarrow R)\Big]$
$(\xi')^M_{jk}$	$(f^S_{LL})_{jk}(f^V_{LL})^*_{kj} + \frac{3}{2}(f^S_{LR})_{jk}(f^T_{LR})^*_{kj} + \frac{3}{2}(f^T_{LR})_{jk}(f^T_{LR})^*_{kj} + (f^V_{LR})_{jk}(f^V_{LR})^*_{kj}$ $-\frac{1}{8}(f^S_{LR})_{jk}(f^S_{LR})^*_{kj} - (L \leftrightarrow R)$
$(\xi'')^M_{jk}$	$\frac{1}{2}(f^S_{LR})_{jk}(f^T_{LR})^*_{kj} + \frac{17}{2}(f^T_{LR})_{jk}(f^T_{LR})^*_{kj} + (f^S_{LL})_{jk}(f^V_{LL})^*_{kj} + \frac{5}{8}(f^S_{RL})_{jk}(f^S_{RL})^*_{kj}$ $+3(f^V_{RL})_{jk}(f^V_{RL})^*_{kj} + (L \leftrightarrow R)$
$(\eta'')^M_{jk}$	$\frac{1}{2}\Big[3(f^S_{LR})_{jk}(f^V_{RL})^*_{kj} + 18(f^T_{LR})_{jk}(f^V_{RL})^*_{kj} - \frac{1}{4}(f^S_{LL})_{jk}(f^S_{RR})^*_{kj} - (f^V_{LL})_{jk}(f^V_{RR})^*_{kj} + (L \leftrightarrow R)\Big]$
$(\frac{\alpha'}{\mathcal{A}})^M_{jk}$	$\frac{1}{2}(f^V_{RL})^*_{jk}((f^S_{LR})_{kj} + 6(f^T_{LR})_{kj}) - (L \leftrightarrow R)$
$(\frac{\beta'}{\mathcal{A}})^M_{jk}$	$-\frac{1}{2}(f^V_{LL})_{jk}(f^V_{RR})^*_{kj} - \frac{1}{8}(f^S_{LL})_{jk}(f^S_{RR})^*_{kj}$
Linear Neutrino Mass Dependence	
$(\kappa^\pm_L)^M_{jk}$	$-2(f^V_{LL})_{kj}(f^V_{LR})^*_{jk} - \frac{1}{2}(f^S_{LL})_{kj}(f^S_{LR})^*_{jk} + 3(f^S_{LL})_{kj}(f^T_{LR})^*_{jk} + 2(f^V_{LL})_{jk}(f^S_{LR})^*_{kj}$ $-(f^S_{LL})_{jk}(f^V_{LR})^*_{kj} \pm (L \leftrightarrow R)$
$(\kappa^\pm_R)^M_{jk}$	$-2(f^V_{RR})_{kj}(f^V_{LR})^*_{jk} - \frac{1}{2}(f^S_{RR})_{kj}(f^S_{LR})^*_{jk} + 3(f^S_{RR})_{kj}(f^T_{LR})^*_{jk} + 2(f^V_{RR})_{jk}(f^S_{LR})^*_{kj}$ $-(f^S_{RR})_{jk}(f^V_{LR})^*_{kj} \pm (L \leftrightarrow R)$
$(\lambda^\pm_L)^M_{jk}$	$-2(f^V_{LL})_{kj}(f^V_{LR})^*_{jk} + \frac{1}{2}(f^S_{LL})_{kj}(f^S_{LR})^*_{jk} + (f^S_{LL})_{kj}(f^T_{LR})^*_{jk} + 4(f^V_{LL})_{jk}(f^T_{LR})^*_{kj}$ $-(f^S_{LL})_{jk}(f^V_{LR})^*_{kj} \pm (L \leftrightarrow R)$
$(\lambda^\pm_R)^M_{jk}$	$-2(f^V_{RR})_{kj}(f^V_{LR})^*_{jk} + \frac{1}{2}(f^S_{RR})_{kj}(f^S_{LR})^*_{jk} + (f^S_{RR})_{kj}(f^T_{LR})^*_{jk} + 4(f^V_{RR})_{jk}(f^T_{LR})^*_{kj}$ $-(f^S_{RR})_{jk}(f^V_{LR})^*_{kj} \pm (L \leftrightarrow R)$
Quadratic Neutrino Mass Dependence	
$(C^\pm)^M_{jk}$	$(f^V_{LL})_{jk}(f^V_{LL})^*_{kj} + \frac{1}{4}(f^S_{LL})_{jk}(f^S_{LL})^*_{kj} + (f^S_{RL})_{jk}(f^V_{RL})^*_{kj} + 6(f^V_{RL})_{jk}(f^T_{RL})^*_{kj} \pm (L \leftrightarrow R)$
$(C'^\pm)^M_{jk}$	$\frac{1}{4}(f^S_{LL})_{jk}(f^S_{LL})^*_{kj} + (f^V_{LL})_{jk}(f^V_{LL})^*_{kj} - (f^S_{RL})_{jk}(f^V_{RL})^*_{kj} - 6(f^V_{RL})_{jk}(f^T_{RL})^*_{kj} \pm (L \leftrightarrow R)$
$(J^+)^M_{jk}$	$\frac{1}{4}(f^S_{LR})_{kj}(f^S_{RL})^*_{jk} + \frac{1}{2}(f^S_{LR})_{kj}(f^T_{RL})^*_{jk} + \frac{1}{2}(f^T_{LR})_{kj}(f^S_{RL})^*_{jk} + 5(f^T_{LR})_{kj}(f^T_{RL})^*_{jk}$ $+2(f^V_{LR})_{jk}(f^V_{RL})^*_{kj}$
$(H^+)^M_{jk}$	$2(f^V_{LL})_{jk}(f^S_{RR})^*_{kj} - \frac{1}{4}(f^S_{LR})_{jk}(f^S_{RL})^*_{kj} + 3(f^T_{LR})_{jk}(f^S_{RL})^*_{kj} + 3(f^T_{LR})_{jk}(f^T_{RL})^*_{kj}$ $+2(f^V_{LR})_{jk}(f^V_{RL})^*_{kj} + (L \leftrightarrow R)$

Table 4.4: Majorana term for the general coupling case.

Term	Coupling Dependence	Term	Coupling Dependence
No Neutrino Mass Dependence		**Linear Neutrino Mass Dependence**	
$(I)^M_{jk}$	0	$(\kappa^{\pm}_L)^M_{jk}$	0
$(\rho)^M_{jk}$	0	$(\kappa^{\pm}_R)^M_{jk}$	0
$(\xi)^M_{jk}$	0	$(\lambda^{\pm}_L)^M_{jk}$	0
$(\xi\delta)^M_{jk}$	0	$(\lambda^{\pm}_R)^M_{jk}$	0
$(\eta)^M_{jk}$	0	**Quadratic Neutrino Mass Dependence**	
$(\xi^{'})^M_{jk}$	0	$(C^{\pm})^M_{jk}$	$(f^V_{LL})_{jk}(f^V_{LL})^*_{kj}$
$(\xi^{''})^M_{jk}$	0	$(C^{'\pm})^M_{jk}$	$(f^V_{LL})_{jk}(f^V_{LL})^*_{kj}$
$(\eta^{''})^M_{jk}$	0	$(J^{+})^M_{jk}$	0
$(\frac{\alpha^{'}}{\mathcal{A}})^M_{jk}$	0	$(H^{+})^M_{jk}$	0
$(\frac{\beta^{'}}{\mathcal{A}})^M_{jk}$	0		

Table 4.5: SM Case $|f^V_{LL}| = 1$.

matter how small it is, a Dirac and a Majorana neutrino are different."

Indeed, from table 4.5, we see that in the SM case, there is no difference between a Dirac and a Majorana neutrino for the terms with no neutrino mass dependence (also for the linear neutrino mass dependence), but –even in the SM case– if neutrino masses are taken into account, we find a substantial difference between the Dirac and Majorana cases, specifically in the quadratic neutrino mass dependence. Unfortunately, these terms are really suppressed, as shown in table 4.2.

Finally, we present a rapid implementation of our results within a well-studied, model-dependent framework that incorporates finite neutrino mass effects. This framework is based on the effective weak interaction Hamiltonian with $(V \pm A)$ currents [99], [103]. For the presence of $V \pm A$ currents, keeping only the leading order terms, the Majorana terms are shown in table 4.6. Then, as an example, if we focus now only on the component of the transverse polarization perpendicular to the decay plane (F_{T_2} and $F^{'}_{T_2}$) up to linear neutrino mass effects, taking into account the Dirac ($\epsilon = 0$) and Majorana ($\epsilon = 1$) cases and considering $x_0 << 1$ we can approximate the result to:

$$\begin{aligned} F_{T_2}(x) + F'_{T_2}(x) = &\frac{x}{3m_\ell}\Big\{\epsilon\Big[m_\ell \,\mathrm{Im}(f^V_{LL})^*_{jk}(f^V_{RR})_{kj} - 3m_j \,\mathrm{Im}(f^V_{LL})^*_{jk}(f^V_{RL})_{kj}\Big] \\ &- 3m_j \,\mathrm{Im}(f^V_{LL})^*_{jk}(f^V_{RL})_{jk}\Big\}. \end{aligned} \tag{4.24}$$

Term	Coupling Dependence	Term	Coupling Dependence
No Neutrino Mass Dependence		**Linear Neutrino Mass Dependence**	
$(I)^M_{jk}$	0	$(\kappa^\pm_L)^M_{jk}$	$-2(f^V_{LL})_{kj}(f^V_{LR})^*_{jk}$
$(\rho)^M_{jk}$	0	$(\kappa^\pm_R)^M_{jk}$	$\mp 2(f^V_{LL})_{kj}(f^V_{RL})^*_{jk}$
$(\xi)^M_{jk}$	0	$(\lambda^\pm_L)^M_{jk}$	$-2(f^V_{LL})_{kj}(f^V_{LR})^*_{jk}$
$(\xi\delta)^M_{jk}$	0	$(\lambda^\pm_R)^M_{jk}$	$\mp 2(f^V_{LL})_{kj}(f^V_{RL})^*_{jk}$
$(\eta)^M_{jk}$	$(f^V_{LL})_{jk}(f^V_{RR})^*_{kj}$	**Quadratic Neutrino Mass Dependence**	
$(\xi')^M_{jk}$	0	$(C^\pm)^M_{jk}$	$(f^V_{LL})_{jk}(f^V_{LL})^*_{kj}$
$(\xi'')^M_{jk}$	0	$(C'^\pm)^M_{jk}$	$(f^V_{LL})_{jk}(f^V_{LL})^*_{kj}$
$(\eta'')^M_{jk}$	$-(f^V_{LL})_{jk}(f^V_{RR})^*_{kj}$	$(J^+)^M_{jk}$	0
$(\frac{\alpha'}{\mathcal{A}})^M_{jk}$	0	$(H^+)^M_{jk}$	0
$(\frac{\beta'}{\mathcal{A}})^M_{jk}$	$-\frac{1}{2}(f^V_{LL})_{jk}(f^V_{RR})^*_{kj}$		

Table 4.6: Majorana term for $V \pm A$ currents.

Finally, if we define the quantity between curly brackets as $T(E)$, we have:

$$T(E) = \epsilon\Big[m_\ell \,\mathrm{Im}(f^V_{LL})^*_{jk}(f^V_{RR})_{kj} - 3m_j \,\mathrm{Im}(f^V_{LL})^*_{jk}(f^V_{RL})_{kj}\Big] - 3m_j \,\mathrm{Im}(f^V_{LL})^*_{jk}(f^V_{RL})_{jk}, \quad (4.25)$$

which is a well-known result [103][16]

From eq.(4.25) we can see that the only Dirac contribution ($\epsilon = 0$) is suppressed by a factor of neutrino mass, while the first Majorana contribution does not have a neutrino mass suppression. Thus, the Majorana term dominates over the Dirac term, so that the Majorana properties of neutrinos can be observed in $T(E)$. Many other discussions and properties of this model can be found in [99].

Therefore, our model-independent results can be used to derive model-dependent expressions efficiently and with high theoretical precision, allowing for a comprehensive discussion of the implications of the new physics within specific frameworks.

As a final motivation, we estimate the possible effects of the heavy neutrino sector using a realistic example. We take the g^V_{LL} coupling to be dominant and consider a non-zero g^S_{RR} coupling, which is one of the most motivated new physics couplings since it would couple the well-known left-handed neutrinos and it naturally appears in many beyond SM theories, also it can be tested in more detail via the η parameter, as we just discussed. Finally, in order to obtain a non-vanishing contribution from the linear neutrino mass

[16] Note that due to our Hamiltonian definition, our results are related by the exchange $f^V_{RL} \leftrightarrow f^V_{LR}$ with respect to those obtained in [103].

terms, we add a g^S_{LR} coupling.

As a realistic approach, for the standard Michel parameters we consider the experimental mean values, while for the new parameters, that appear in the neutrino mass-dependent terms, we work with the current coupling upper limits and assign the following numerical values: $g^V_{LL} = 0.96$, $g^S_{RR} =$ and $g^S_{LR} =$, which agree with the corresponding normalization condition.

Using these values, we can obtain the specific neutrino mass term contribution for Dirac and Majorana cases making the subtraction between the differential rate with neutrino mass effects and the one without this contribution. This result is shown in figure 4.2, where the y-axis corresponds to $\frac{1}{N}\left(\frac{d\Gamma}{dx} - \frac{d\Gamma}{dx}|_{m_\nu=0}\right)$ with $N = m\omega^4 G^2_{\ell\ell'}/(4\pi)$.

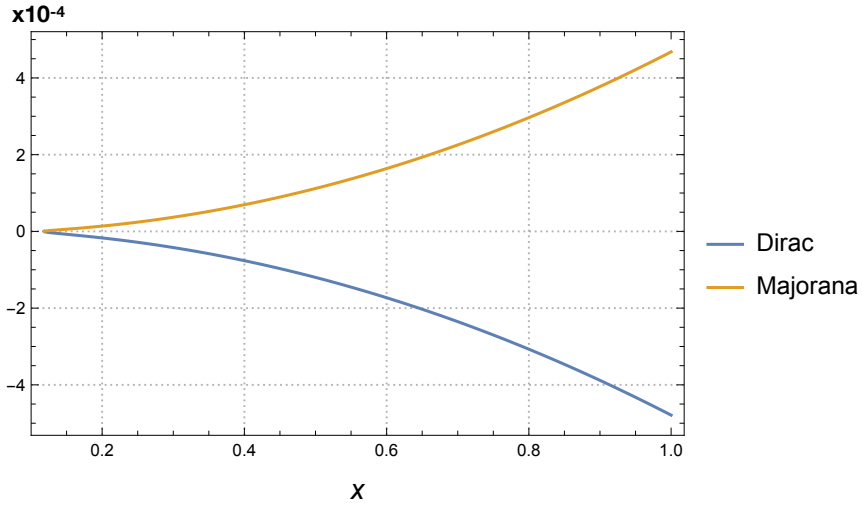

Figure 4.2: Neutrino mass contribution to Dirac and Majorana distributions.

Then, for this realistic example we find that even considering the suppression of the specific new physics couplings and phase space structures, this neutrino mass effect could be as high as 10^{-4} and lead to measurable distortions in the energy spectrum, as seen in figure 4.2. Another interesting feature in this example is that the neutrino mass terms influence the energy distribution differently depending on the neutrino type. For Dirac neutrinos, these terms reduce the differential decay rate, whereas for Majorana neutrinos, they have the opposite effect.

Therefore, potential distortions of the energy spectrum can provide insight not only into the presence of a heavy neutrino sector but also into distinguishing the Dirac or Majorana

nature of neutrinos. Further applications to model-dependent scenarios, as well as a detailed discussion of the angular distribution results, are presented in [1].

4.2 Effective $\nu e \to \nu e$ Scattering Analysis

In Ref. [2], a complementary analysis on elastic neutrino-electron scattering within an EFT framework is carried out. This again allows us to constrain the NP Wilson coefficients in a model-independent manner and incorporate the effects of finite neutrino masses, extending the results previously obtained in [133], in the presence of generic new interactions.

4.2.1 General neutrino-electron scattering interaction

Let us consider the most general Lorentz-invariant interaction between neutrinos and charged lepton pairs at dimension six [133] [17]:

$$\mathcal{L} \supset \frac{G_F}{\sqrt{2}} \sum_{a=S,P,V,A,T} \bar{\nu}\Gamma^a\nu\Big[\bar{l}\,\Gamma^a(C_a + \bar{D}_a i\gamma^5)l\Big], \tag{4.26}$$

where Γ^a, with $a = S, P, V, A, T$; commonly known as scalar, pseudo-scalar, vector, axial-vector, and tensor interactions, respectively, are the different Dirac matrices that can be combined independently,

$$\Gamma^a = \left\{ I, i\gamma^5, \gamma^\mu, \gamma^\mu\gamma^5, \sigma^{\mu\nu} \equiv \frac{i}{2}[\gamma^\mu, \gamma^\nu] \right\}. \tag{4.27}$$

There are two options for contracting the terms in the tensor case, $g_{\mu\mu'}g_{\nu\nu'}\sigma^{\mu\nu}\sigma^{\mu'\nu'}$ and $\varepsilon_{\mu\nu\mu'\nu'}\sigma^{\mu\nu}\sigma^{\mu'\nu'}$. We only make use of the first one since, in accordance with [135], the latter can be turned into the former up to a redefinition of C_T and D_T.

Hermiticity of eq. (4.26) enables us to define

$$\begin{aligned} D_a &\equiv \bar{D}_a, \quad a = S, P, T, \\ D_a &\equiv i\bar{D}_a, \quad a = V, A, \end{aligned} \tag{4.28}$$

thus, each coupling constant C_a and D_a is a real number. Additionally, by imposing the

[17] Ref. [134] discusses its ultraviolet completion, from the effective field theory perspective.

Majorana condition $\nu_j = \nu_j^c = C\bar{\nu}_j^T$, where C is the charge conjugation matrix, some coefficients must vanish ($C_V = D_V = C_T = D_T = 0$). This feature is what allows us to distinguish between Dirac and Majorana neutrinos in the general case.

As an example, the SM scenario is just a specific case of (4.26). Indeed, the Lagrangian that describes the neutral current interaction (NC) in the SM is: [18]

$$\mathcal{L}_{\text{NC}} = \frac{G_F}{\sqrt{2}} 2\Big[\bar{\nu}\gamma^\mu(g_V^\nu - g_A^\nu\gamma^5)\nu\Big]\Big[\bar{l}\gamma^\mu(g_V^l - g_A^l\gamma^5)l\Big], \tag{4.29}$$

$$g_V^\nu = g_A^\nu = \frac{1}{2}, \quad g_V^l = -\frac{1}{2} + 2s_{\text{w}}^2, \quad g_A^l = -\frac{1}{2}. \tag{4.30}$$

By comparing eqs. (4.26) and (4.29), we get

$$\text{Dirac}\begin{cases} C_V^{\text{SM}} = 2g_V^\nu g_V^l, & D_V^{\text{SM}} = -2g_V^\nu g_A^l, \\ C_A^{\text{SM}} = 2g_A^\nu g_A^l, & D_A^{\text{SM}} = -2g_A^\nu g_V^l, \\ C_S^{\text{SM}} = 0, & D_S^{\text{SM}} = 0, \\ C_P^{\text{SM}} = 0, & D_P^{\text{SM}} = 0, \\ C_T^{\text{SM}} = 0, & D_T^{\text{SM}} = 0, \end{cases} \quad \text{Majorana}\begin{cases} C_V^{\text{SM}} = 0, & D_V^{\text{SM}} = 0, \\ C_A^{\text{SM}} = 4g_A^\nu g_A^l, & D_A^{\text{SM}} = -4g_A^\nu g_V^l, \\ C_S^{\text{SM}} = 0, & D_S^{\text{SM}} = 0, \\ C_P^{\text{SM}} = 0, & D_P^{\text{SM}} = 0, \\ C_T^{\text{SM}} = 0, & D_T^{\text{SM}} = 0. \end{cases} \tag{4.31}$$

We emphasize that for Majorana neutrinos $C_V = D_V = C_T = D_T = 0$ and, for the specific SM case, the remaining ones double their values compared to the Dirac case.

4.2.2 Cross Section for Massless Neutrinos

As done in ref. [133], the result for the cross section of elastic scattering of neutrinos (antineutrinos) with massive charged leptons at energies where the local interaction

[18] The charged current (CC) interaction may also contribute if the neutrino and the charged lepton have the same flavor. To include the charged current contribution one simply replaces $g_V^l \to g_V^l + 1$ and $g_A^l \to g_A^l + 1$ after a Fierz transformation.

approximation holds, neglecting neutrino masses, is

$$\frac{d\sigma}{dT}(\nu + e) = \frac{G_F^2 M}{2\pi}\left[A + 2B\left(1 - \frac{T}{E_\nu}\right) + C\left(1 - \frac{T}{E_\nu}\right)^2 + D\frac{MT}{4E_\nu^2}\right], \tag{4.32}$$

$$\frac{d\sigma}{dT}(\bar{\nu} + e) = \frac{G_F^2 M}{2\pi}\left[C + 2B\left(1 - \frac{T}{E_\nu}\right) + A\left(1 - \frac{T}{E_\nu}\right)^2 + D\frac{MT}{4E_\nu^2}\right], \tag{4.33}$$

where E_ν is the incident neutrino energy, T and M are the recoil energy and mass of the charged lepton, respectively, and

$$\begin{aligned} A \equiv & \frac{1}{4}(C_A - D_A + C_V - D_V)^2 + \frac{1}{8}(C_P^2 + C_S^2 + D_P^2 + D_S^2 + 8C_T^2 + 8D_T^2) \\ & + \frac{1}{2}(C_P C_T - C_S C_T + D_P D_T - D_S D_T), \end{aligned} \tag{4.34}$$

$$B \equiv -\frac{1}{8}(C_P^2 + C_S^2 + D_P^2 + D_S^2 - 8C_T^2 - 8D_T^2), \tag{4.35}$$

$$\begin{aligned} C \equiv & \frac{1}{4}(C_A + D_A - C_V - D_V)^2 + \frac{1}{8}(C_P^2 + C_S^2 + D_P^2 + D_S^2 + 8C_T^2 + 8D_T^2) \\ & - \frac{1}{2}(C_P C_T - C_S C_T + D_P D_T - D_S D_T), \end{aligned} \tag{4.36}$$

$$D \equiv (C_A - D_V)^2 - (C_V - D_A)^2 - 4(C_T^2 + D_T^2) + C_S^2 + D_P^2. \tag{4.37}$$

It is important to note that all these calculations assume that incoming neutrinos and antineutrinos are left-handed and right-handed, respectively. Interestingly, the two distributions are related through the exchange $A \leftrightarrow C$ and that none of the parameters mix the (axial)-vector type interactions with any other. Detailed explanations on this topic can be found in ref. [133].

In this case, the SM values for the parameters A, B, C, D, for NC contributions, are as follows

$$\Big(A, B, C, D\Big)^{\rm SM} = \Big((1 - 2s_{\rm w}^2)^2, 0, 4s_{\rm w}^4, 1 - (1 - 4s_{\rm w}^2)^2\Big), \tag{4.38}$$

which lead to a cross section that has the same value for Dirac and Majorana neutrinos, as anticipated. Then, other interactions are needed in order to distinguish the Dirac and Majorana cases in this process.

4.2.3 Cross Section for Massive Neutrinos

We now generalize the previous results by incorporating finite neutrino masses and all their potential effects on the differential cross section, thereby extending the analysis further. If we consider finite neutrino masses, the current neutrino (ν_L for the weak isospin doublets electrically neutral component and ν'_R for singlets) is assumed to be the superposition of the mass-eigenstate neutrinos (N_j) with the mass m_j, that is,

$$\nu_{\ell L} = \sum_j U_{\ell j} N_{jL}, \quad \nu'_{\ell R} = \sum_j V_{\ell j} N_{jR}, \tag{4.39}$$

where $j = \{1, 2, ..., n\}$, with n the number of mass-eigenstate neutrinos, as stated in the last section.

The U matrix refers to the mixing of the active left-handed sector with massive neutrinos, while V parameterizes the mixing of the sterile right-handed neutrinos. They are not directly related, except for the condition that unitarity or a specific model can implement.

For a comprehensive discussion of left- and right-handed mixing, we refer the reader to Appendix A of Ref. [99], where the topic is explained in full detail and aligns with our notation. For a complementary perspective, the lepton mixing formalism is also reviewed in Appendix A of Ref. [136], which uses slightly different notation but presents the material with great clarity.

Thus, in the laboratory frame, the explicit cross section of elastic neutrino (antineutrino) scattering on charged leptons is

$$\begin{aligned}\frac{d\sigma}{dT}(\nu + e) = \sum_{i,f} |U_{\ell i}|^2 \frac{G_F^2 M}{2\pi} \frac{E_\nu^2}{E_\nu^2 - m_{\nu_i}^2} \Bigg\{ & A + 2B\left(1 - \frac{T}{E_\nu}\right) + C\left(1 - \frac{T}{E_\nu}\right)^2 \\ & + D\frac{MT}{4E_\nu^2} + \frac{(m_{\nu_i}^2 - m_{\nu_f}^2)}{2ME_\nu}\left[(A + 2B) + C\left(1 - \frac{T}{E_\nu}\right) + F\frac{m_{\nu_f}}{E_\nu}\right] \\ & - B\frac{m_{\nu_i}^2 T}{ME_\nu^2} + \frac{m_{\nu_f}}{E_\nu}\left[G + F\left(1 - \frac{T}{E_\nu}\right)\right] + D\frac{m_{\nu_i}^2 + m_{\nu_f}^2}{8E_\nu^2} \Bigg\},\end{aligned} \tag{4.40}$$

$$\frac{d\sigma}{dT}(\bar{\nu}+e) = \sum_{i,f} |U_{\ell i}|^2 \frac{G_F^2 M}{2\pi} \frac{E_\nu^2}{E_\nu^2 - m_{\nu_i}^2} \left\{ C + 2B\left(1 - \frac{T}{E_\nu}\right) + A\left(1 - \frac{T}{E_\nu}\right)^2 \right.$$
$$+ D\frac{MT}{4E_\nu^2} + \frac{(m_{\nu_i}^2 - m_{\nu_f}^2)}{2ME_\nu}\left[(C+2B) + A\left(1 - \frac{T}{E_\nu}\right) - G\frac{m_{\nu_f}}{E_\nu}\right]$$
$$\left. - B\frac{m_{\nu_i}^2 T}{ME_\nu^2} - \frac{m_{\nu_f}}{E_\nu}\left[F + G\left(1 - \frac{T}{E_\nu}\right)\right] + D\frac{m_{\nu_i}^2 + m_{\nu_f}^2}{8E_\nu^2} \right\}, \tag{4.41}$$

where m_{ν_i} (m_{ν_f}) is the mass of the initial (final) neutrino and we only added two new parameters F and G, that were not contributing in the massless neutrino case. These, together with the A, B, C, D parameters already appearing in eqs. (4.32) and (4.33), are given, in the massive neutrino case, by

$$A \equiv |U_{\ell f}|^2 \left[\frac{1}{4}(C_A - D_A + C_V - D_V)^2\right] + |V_{\ell f}|^2 \left[\frac{1}{8}(C_P^2 + C_S^2 + D_P^2 + D_S^2 + 8C_T^2 + 8D_T^2) + \frac{1}{2}(C_P C_T - C_S C_T + D_P D_T - D_S D_T)\right], \tag{4.42}$$

$$B \equiv -|V_{\ell f}|^2 \left[\frac{1}{8}(C_P^2 + C_S^2 + D_P^2 + D_S^2 - 8C_T^2 - 8D_T^2)\right], \tag{4.43}$$

$$C \equiv |U_{\ell f}|^2 \left[\frac{1}{4}(C_A + D_A - C_V - D_V)^2\right] + |V_{\ell f}|^2 \left[\frac{1}{8}(C_P^2 + C_S^2 + D_P^2 + D_S^2 + 8C_T^2 + 8D_T^2) - \frac{1}{2}(C_P C_T - C_S C_T + D_P D_T - D_S D_T)\right], \tag{4.44}$$

$$D \equiv |U_{\ell f}|^2 \left[(C_A - D_V)^2 - (C_V - D_A)^2\right] + |V_{\ell f}|^2 \left[-4(C_T^2 + D_T^2) + C_S^2 + D_P^2\right], \tag{4.45}$$

$$F \equiv \mathrm{Re}\left[U_{\ell f} V_{\ell f}^*\right] \frac{1}{4}[(C_S + 6C_T)(C_V - D_A) + (C_P - 6C_T)(C_A - D_V)], \tag{4.46}$$

$$G \equiv \mathrm{Re}\left[U_{\ell f} V_{\ell f}^*\right] \frac{1}{4}[(C_S - 6C_T)(C_V - D_A) - (C_P + 6C_T)(C_A - D_V)]. \tag{4.47}$$

The reason we have an overall factor of $|U_{\ell i}|^2$ in the differential cross section is because of the assumption that the incoming neutrinos or antineutrinos are left-handed or right-handed, respectively [19]; while the final neutrino could be produced in any chirality state, depending on the specific physics involved. We emphasize that this result applies to both relativistic and non-relativistic neutrino scattering, as will be discussed in more detail later.

Thus, all of these parameters can, in principle, be extracted from scattering data and used

[19] See, conversely, ref.[137].

to probe both the existence of a potential heavy neutrino sector and the fundamental nature of neutrinos, as will be discussed in the following sections. It is also remarkable that this generalization of the cross section introduces only two more parameters, F and G, which mix the vector and axial currents with the scalar, pseudoscalar and tensor ones; that is a new feature compared with the previous result [133]. In the following sections, each aspect of these earlier findings will be clarified and examined in detail.

Finally, it is useful to remark some of the symmetry properties that the cross sections have. The cross sections for neutrinos and antineutrinos scattering are related by the exchanges $A \leftrightarrow C$, $F \leftrightarrow G$, $m_{\nu_i} \leftrightarrow -m_{\nu_i}$ and $m_{\nu_f} \leftrightarrow -m_{\nu_f}$, which could be used while analyzing model-dependent scenarios. Also, in the light neutrino case, if we sum over all the possible mass-eigenstate neutrinos (using the unitarity condition) and neglect the explicit neutrino mass terms, we recover the results already obtained in ref. [133], just as a trivial check of our expressions.

One of the main goals of this computation is to incorporate the effects of neutrino masses, particularly to study their potential contributions in scenarios where new heavy sterile neutrinos have non-negligible mixing with the light, active states. The differential cross section given in Eqs. (4.40, 4.41) is general under the assumptions discussed and, in principle, accounts for the contributions of all neutrino mass eigenstates that are kinematically accessible. These contributions exhibit distinct dependencies on the neutrino masses, such as:

$$\frac{m_\nu}{E_\nu}, \quad \frac{m_\nu^2}{E_\nu^2}, \quad \frac{m_\nu^2 T}{M E_\nu^2}. \tag{4.48}$$

These structures are precisely what suppress the neutrino mass–dependent contributions relative to the terms that do not depend on neutrino masses. Nevertheless, for precision measurements, this suppression could be low enough to play a role in the energy spectrum, specifically under the assumption of a heavy neutrino sector, as we shall discuss.

At this stage, we just want to motivate the presence of these new terms that appear in the differential decay rate due to accounting for finite neutrino masses. For this purpose we will begin with a naive, but still realistic, approximation. Since we are considering that the incident neutrinos (antineutrinos) are left (right)-handed, we will now assume that they are predominantly contributed by the light mass eigenstates, meaning that we will not have a suppression due to the global $|U_{\ell i}|^2$ mixing factor and $E_\nu^2 - m_{\nu_i}^2 \approx E_\nu^2$.

Then, in order to have a sizable contribution of these new structures, we need to analyze the case of a heavy final state neutrino, where the suppression will come from its mixing factor $|U_{\ell f}|$[20].

In summary, we will now focus on a contribution with a light m_{ν_i} and a heavy m_{ν_f} with a suppressed mixing $|U_{\ell f}|^2$. In order to estimate the value of the structures shown in eq. (4.48), we used the current experimental limits given in refs. [138], [139], [140]. We can then consider different scenarios, depending on the incident neutrino energy and the mass of the final-state neutrino. The suppression of the neutrino mass–dependent factors is analyzed in Table 4.7, where we highlight the most relevant contributions according to our estimation assumptions. We emphasize that this represents a specific illustrative case intended to motivate the inclusion of these terms. As we can see, the suppression for

Neutrino flavor	m_{ν_f} (MeV)	$\lvert U_{\ell 4}\rvert^2$	Linear term suppression $\lvert U_{\ell 4}\rvert^2 m_{\nu_f}/E_\nu$		Quadratic term suppression $\lvert U_{\ell 4}\rvert^2 m_{\nu_f}^2/E_\nu^2$	
			E_ν 500 MeV	E_ν 2500 MeV	E_ν 500 MeV	E_ν 2500 MeV
$l = e$ [138]	150-375	10^{-8}	10^{-9}	10^{-10}-10^{-9}	10^{-10}-10^{-9}	10^{-10}
	375-440	10^{-9}	10^{-10}	10^{-10}	10^{-10}	10^{-11}
$l = \mu$ [139]	10	10^{-3}	10^{-5}	10^{-6}	10^{-7}	10^{-8}
	20	10^{-4}	10^{-6}	10^{-7}	10^{-7}	10^{-9}
	50	10^{-5}	10^{-6}	10^{-7}	10^{-7}	10^{-9}
	100	10^{-6}	10^{-7}	10^{-8}	10^{-8}	10^{-9}
$l = \tau$ [140]	100-200	10^{-3}	10^{-4}	10^{-4}	10^{-4}	10^{-5}
	300-400	10^{-4}	10^{-4}	10^{-5}	10^{-4}	10^{-6}-10^{-5}
	500-800	10^{-5}	10^{-5}	10^{-6}	10^{-5}	10^{-6}
	900-1100	10^{-5}	10^{-5}	10^{-6}	10^{-5}	10^{-6}

Table 4.7: Estimated suppression associated with neutrino mass-dependent terms.

electron neutrinos is really high because its mixing is tightly constrained [21]. The same happens with the muon neutrinos, which are not as restricted as the electron ones, but still too suppressed for the current experimental capabilities. Nevertheless, the limits on $|U_{\tau 4}|$ are the weakest, motivating the possibility that $|U_{\tau 4}| \gg |U_{e5}|, |U_{\mu 4}|$ and thus getting suppression effects of the order $10^{-4} - 10^{-5}$ which could produce measurable distortions in the energy spectrum, with the disadvantage that events with tau neutrinos are the rarest.

[20] In the case of new physics, the mixing may be not suppressed, but the net suppression will be then encoded in the coupling. For this rough estimation we are not discussing all these possibilities.

[21] Even in this case, the contributions associated to the gauge boson longitudinal polarizations can be neglected.

In this estimation, the linear neutrino mass terms with the presence of a heavy neutrino with a mass around $100 - 400$ MeV will be important for an incident neutrino energy of the order of $10^2 - 10^3$ MeV. It is also necessary to emphasize that these terms are always multiplied by the parameters F and G, which are identically zero in the SM case, so we need the presence of new physics couplings in order to be sensitive to those contributions and then an extra suppression factor must be taken into account while analyzing the possible distortions of the spectrum.

For the quadratic neutrino mass terms we also found interesting results. Indeed, the suppression for the considered energy range could be of order $10^{-4} - 10^{-5}$, which is a new feature compared to other analyses, see ergo [1], where the quadratic terms were really suppressed. Also, these neutrino mass terms appear multiplying the D parameter[22], which in eqs. (4.32, 4.33) (neglecting neutrino masses) is suppressed by the electron mass with a factor MT/E_ν^2. Then, depending on the recoil energy and the heavy neutrino sector, even the neutrino mass term could be of the same order as the one already obtained in ref. [133] for the D parameter.

We note that, although our results are applicable to the non-relativistic regime, the energy of the incident neutrino constrains the masses of heavy neutrinos that can be kinematically accessed. Consequently, significant heavy-neutrino effects may not appear at low energies. Nevertheless, the non-relativistic case without neutrino mass effects remains of interest, as discussed in Ref. [133].

Finally, more precise conclusions could be drawn by considering model-dependent scenarios, where the full suppression can be estimated based on the specific values of the new physics couplings. However, for our purposes, this rough estimation provides a clear indication of the potential signals of a heavy neutrino sector in this type of process.

4.2.4 Dirac vs Majorana Discussion

Our second goal is to use the information on the $A, \ldots, G$ parameters, including the two new ones that appear while considering finite neutrino masses, and explore the corresponding parameter space allowed by Dirac or Majorana neutrinos. This way, it

[22] They also appear in other parts of the spectrum, where the dependence is proportional to $(m_{\nu i}^2 - m_{\nu f}^2)$, so cancellations may occur while considering all the possible mass eigenstates, then we are not stating further conclusions about this.

may be possible to distinguish between both neutrino natures depending on the values extracted from the experiment, as examined in ref. [133] for the case with negligible neutrino masses.

Parameter	Dirac
A	$\|U_{\ell f}\|^2 \left[\frac{1}{4}(C_A - D_A + C_V - D_V)^2\right] + \|V_{\ell f}\|^2 \left[\frac{1}{8}(C_P^2 + C_S^2 + D_P^2 + D_S^2 + 8C_T^2 + 8D_T^2) + \frac{1}{2}(C_P C_T - C_S C_T + D_P D_T - D_S D_T)\right]$
B	$-\|V_{\ell f}\|^2 \left[\frac{1}{8}(C_P^2 + C_S^2 + D_P^2 + D_S^2 - 8C_T^2 - 8D_T^2)\right]$
C	$\|U_{\ell f}\|^2 \left[\frac{1}{4}(C_A + D_A - C_V - D_V)^2\right] + \|V_{\ell f}\|^2 \left[\frac{1}{8}(C_P^2 + C_S^2 + D_P^2 + D_S^2 + 8C_T^2 + 8D_T^2) - \frac{1}{2}(C_P C_T - C_S C_T + D_P D_T - D_S D_T)\right]$
D	$\|U_{\ell f}\|^2 \left[(C_A - D_V)^2 - (C_V - D_A)^2\right] + \|V_{\ell f}\|^2 \left[-4(C_T^2 + D_T^2) + C_S^2 + D_P^2\right]$
F	$\mathrm{Re}\left[U_{\ell f} V_{\ell f}^*\right] \frac{1}{4}[(C_S + 6C_T)(C_V - D_A) + (C_P - 6C_T)(C_A - D_V)]$
G	$\mathrm{Re}\left[U_{\ell f} V_{\ell f}^*\right] \frac{1}{4}[(C_S - 6C_T)(C_V - D_A) - (C_P + 6C_T)(C_A - D_V)]$
	Majorana
A	$\|U_{\ell f}\|^2 \left[\frac{1}{4}(C_A - D_A)^2\right] + \|V_{\ell f}\|^2 \left[\frac{1}{8}(C_P^2 + C_S^2 + D_P^2 + D_S^2)\right]$
B	$-\|V_{\ell f}\|^2 \left[\frac{1}{8}(C_P^2 + C_S^2 + D_P^2 + D_S^2\right]$
C	$\|U_{\ell f}\|^2 \left[\frac{1}{4}(C_A + D_A)^2\right] + \|V_{\ell f}\|^2 \left[\frac{1}{8}(C_P^2 + C_S^2 + D_P^2 + D_S^2\right]$
D	$\|U_{\ell f}\|^2 [C_A^2 - D_A^2] + \|V_{\ell f}\|^2 [C_S^2 + D_P^2]$
F	$-\mathrm{Re}\left[U_{\ell f} V_{\ell f}^*\right] \frac{1}{4}[C_S D_A - C_P C_A]$
G	$-\mathrm{Re}\left[U_{\ell f} V_{\ell f}^*\right] \frac{1}{4}[C_S D_A + C_P C_A]$

Table 4.8: Parameters for Dirac and Majorana cases. The parameters for the latter case can be obtained from the former ones applying the properties explained in the paragraph below eq. (4.28).

Applying the Majorana condition already discussed ($C_V = D_V = C_T = D_T = 0$), we can obtain the explicit forms of the parameters for both Dirac and Majorana neutrinos in the general interaction scenario, as presented in Table 5.2. This result facilitates a rapid analysis of various model-dependent scenarios, as will be illustrated.

Let us start with the SM case (for NC contributions). Using eq.(4.30) and eq.(4.31) in table 5.2, we can compute the values for all the parameters in the SM scenario, that are shown in table 4.9.

Here it is straightforward to confirm that, if neutrino interactions are characterized by the

Parameter	Dirac and Majorana
A	$\lvert U_{\ell f}\rvert^2(1-2s_{\rm w}^2)^2$
B	0
C	$\lvert U_{\ell f}\rvert^2 4s_{\rm w}^4$
D	$\lvert U_{\ell f}\rvert^2\left(1-(1-4s_{\rm w}^2)^2\right)$
F	0
G	0

Table 4.9: Parameters for Dirac and Majorana cases in the SM, which are obtained from table 5.2 using eq. (4.38).

SM, the cross section has the same value for Majorana and Dirac neutrinos, since all the parameters are equal in both cases. This is a result that still holds if we consider the effects of finite neutrino masses, which is an interesting feature, since in some other processes, specifically where both neutrinos appear in the final state, the difference between Dirac and Majorana cases is proportional to m_ν^2/E^2 in the SM scenario due to the helicity flipping interference.

Then, if only the SM interaction is involved in the $\nu e \to \nu e$ scattering, it is not possible, in principle, to distinguish the specific nature of neutrinos, even if their masses are taken into account. Nevertheless, as discussed in the last section, in the presence of a heavy sector, it could still be possible to discriminate which one is at work. Also, we can emphasize that in the SM case some parameters are identically zero; then, measuring a non-vanishing value for these parameters will imply the presence of new physics beyond the SM.

Now, we can give some other examples including the presence of new physics couplings, but for the Majorana condition in this process ($C_V = D_V = C_T = D_T = 0$) it is clear that we need to introduce some of these vector or tensor couplings in order to get a testable difference between Dirac and Majorana neutrinos.

Then, as a final example, we analyze the case of a C_T coupling beyond the SM case, which is of great interest since the C_T coefficient must vanish for Majorana neutrinos, as we just discussed. The results are shown in table 4.10.

As we can see, in this scenario, a new C_T coupling would generate parameters that will

Parameter	Dirac	Majorana
A	$\lvert U_{\ell f}\rvert^2(1-2s_{\rm w}^2)^2 + \lvert V_{\ell f}\rvert^2 C_T^2$	$\lvert U_{\ell f}\rvert^2(1-2s_{\rm w}^2)^2$
B	$\lvert V_{\ell f}\rvert^2 C_T^2$	0
C	$\lvert U_{\ell f}\rvert^2 4s_{\rm w}^4 + \lvert V_{\ell f}\rvert^2 C_T^2$	$\lvert U_{\ell f}\rvert^2 4s_{\rm w}^4$
D	$\lvert U_{\ell f}\rvert^2\,(1-(1-4s_{\rm w}^2)^2) - 4\lvert V_{\ell f}\rvert^2 C_T^2$	$\lvert U_{\ell f}\rvert^2\,(1-(1-4s_{\rm w}^2)^2)$
F	$6\,\mathrm{Re}\left[U_{\ell f}V_{\ell f}^*\right] C_T\ s_{\rm w}^2$	0
G	$3\,\mathrm{Re}\left[U_{\ell f}V_{\ell f}^*\right] C_T(1-2s_{\rm w}^2)$	0

Table 4.10: Parameters for Dirac and Majorana cases in the SM+C_T case.

differ for Dirac and Majorana neutrinos in all cases. Also, some of them must vanish identically for the Majorana case, so a non-null measurement for the B, F or G parameters will imply that neutrinos are Dirac fermions, if this model-dependent theory ($SM + C_T$) is the one describing nature.

We could continue exploring all possible new physics scenarios; however, as a final estimation, we follow the analysis of Ref. [133], examining the parameter space for Dirac and Majorana neutrinos in the general case, now adding the information of the new F and G parameters.

As discussed in previous works (see e.g. [133] and references therein), the parameters A, B, C are the most accurate measurable quantities and then the most important ones for the current experiments, followed by the D parameter, which is suppressed by the factor M/E_ν. In this general analysis we have two more measurable parameters (F, G) that would be the most inaccurate among the six quantities because of the neutrino mass suppression already estimated. Nevertheless and for completeness of this work, we study the behavior of Dirac and Majorana neutrinos through the possible values of these new parameters in a similar way as done in ref. [133].

In [133], for the relativistic case, the normalized parameters triad (A, B, C) was studied randomly generating arbitrary values of $(C_a,\ D_a)$ with $a = S, P, V, A$ and T, except that for Majorana neutrinos $C_V = D_V = C_T = D_T = 0$ were set, and then the corresponding (A, B, C) values were plotted and discussed, to see the accessible parameter space for Dirac and Majorana neutrinos. For the non-relativistic case, where the D parameter is

relevant, the four different parameters were studied similarly, in this case showing several 2-dimensional projections due to the extra parameter taken into account.

In this general case we have now six parameters, so instead of showing several projections, we prefer to analyze the parameter space for some parameter triads in such a way that the subsequent discussions become clearer and generally encompass the distinction between Dirac and Majorana neutrinos. Thus, we study the parameter space (X_1, X_2, X_3), where X_i could be any of the $A, \ldots, G$ parameters, in the same way as [133] randomly choosing values of $(C_a,\ D_a)$ in $[-1, 1]$.

We also remember, as discussed in previous works, that for any allowed value of (X_1, X_2, X_3), (rX_1, rX_2, rX_3) is also allowed for any positive r, since it just corresponds to a rescaling of $(C_a,\ D_a)$ by a factor of $\sqrt{r}$. Then, for simplicity, we normalize (X_1, X_2, X_3) to show the allowed region, as usually done. Thus, figure 4.3 shows the values of 10^5 samples generated by randomly choosing values of $(C_a,\ D_a)$ in $[-1, 1]$ for different parameter triads (X_1, X_2, X_3).

The difference between the Dirac (blue points) and Majorana (orange points) regions is evident in many of them, while other triads are not capable of distinguishing between Dirac and Majorana neutrinos on their own, since their boundaries are the same for both cases. In a similar way as the criterion proposed by Rosen, if (X_1, X_2, X_3) were measured in the region outside the orange space, then neutrinos would be Dirac particles, but if (X_1, X_2, X_3) were measured where blue and orange points overlap, then both Dirac and Majorana nature would be possible.

Indeed, we estimate the common region of Dirac and Majorana points for each plot, giving an approximate percentage of the overlapping areas (with estimated relative uncertainty of $\sim 2.5\%$). We accomplished this by assigning a surface to each case (Dirac and Majorana) and computing their area to determine the extent of overlap. For example, this implies that if the overlapping percentage is 100%, we cannot distinguish between Dirac and Majorana nature, as both cases share the same parameter space boundaries. This is just a first estimation, where the corresponding reported percentages may exhibit slight variations depending on the numerical analysis, but it is still a helpful feature for further discussions about distinguishing the corresponding neutrino nature within a specific set of parameters.

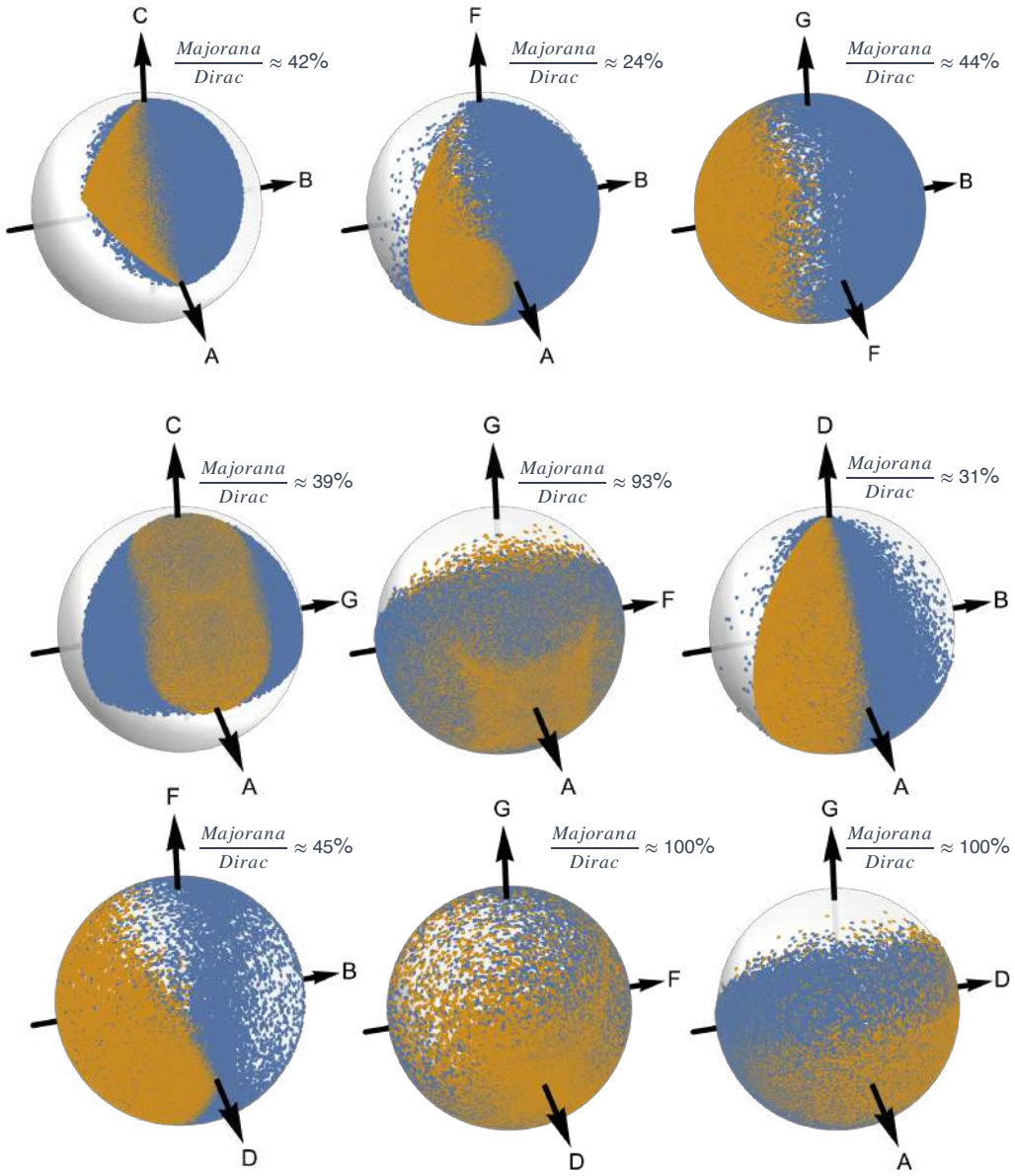

Figure 4.3: Allowed values of different normalized triads of parameters (X_1, X_2, X_3) assuming Dirac (blue points) or Majorana (orange points) neutrinos. These plots were obtained with a random generation of **N** points inside the unit spheres as explained in the main text.

The first triad (A, B, C) reproduces the result obtained in [133], where the complete discussions can be found, being the most promising way to differentiate the neutrino nature in this process. Additionally, we show eight more possible triads, which help us to illustrate some important aspects.

First, we have two possibilities: Either the Dirac and Majorana boundaries for the corresponding triads are different, and then we clearly have a distinction between blue and orange points; which holds for the (A, B, C), (A, B, F), (F, B, G), (A, G, C), (A, B, D) and (D, B, F) triads. Or, conversely, the Dirac and Majorana boundaries are the same, as in the (A, F, G), (D, F, G) and (A, D, G) cases, where we are unable to distinguish the specific neutrino nature (assuming that only the corresponding triad could be measured), as the overlapping percentages suggest.

The corresponding boundaries depend explicitly on the parameters coupling dependence. As an easy example [133] we have the B parameter, which has the following dependence for the Dirac and Majorana cases:

$$\begin{aligned} B &= -\frac{1}{8}(C_P^2 + C_S^2 + D_P^2 + D_S^2) + C_T^2 + D_T^2 \quad \text{(Dirac)}, \\ B &= -\frac{1}{8}(C_P^2 + C_S^2 + D_P^2 + D_S^2) \qquad\qquad\quad \text{(Majorana)}, \end{aligned} \tag{4.49}$$

whence is evident that $B \leq 0$ for the Majorana case, while for the Dirac case it can have either sign. This is precisely why we have a clear distinction between blue and orange points in every triad in which B appears. This analysis can be applied to any other parameter, the conclusion being less direct because of the corresponding explicit dependence.

We see now that the addition of these two new parameters F and G could give complementary information about the neutrino nature as well as of the possible heavy sector. Even if in some cases, such as the (A, F, G) or (D, F, G) triads, the accessible parameters region is not helpful to distinguish the corresponding neutrino nature; there are some others, such as the triad (A, B, F) , in which the difference could be evident, giving more information than the case of negligible neutrino masses.

For a final remark, as mentioned and justified in ref. [133], the triad (A, B, C) remains the most important, because these parameters do not have an extra suppression in the effective cross section and their extraction from experimental data is much cleaner and more precise, giving the strongest constraints. Nevertheless, the analysis of F and G is also included here for completeness and to illustrate the impact of neutrino nature on each parameter.

Altogether, this underscores the importance of searching for new neutrino interactions and the potential existence of a heavy neutrino sector, a topic of considerable interest that continues to drive exciting research in the field.

4.3 Dirac-Majorana Distinction in Four-Body Decays

Based on Ref.[3], we explored the possibility of distinguishing the neutrino nature within the SM in four-body decays, that could generate a non-suppressed observable, as recently suggested in the literature [141]. During our analysis, we identified a loophole in the derivation of the proposed method. Once corrected, this led to a highly suppressed result, consistent with previous discussions. We focused our effort on this issue and provided a detailed explanation using an alternative process to illustrate the impossibility of distinguishing the neutrino nature in this case.

It is crucial that the distinction between Dirac and Majorana neutrinos can be determined independently of their masses, provided their momenta are not integrated out. Since neutrino momenta are not directly accessible experimentally, a method is required to infer them, allowing the determination of neutrino-related variables without the need for explicit observation—a task that remains extremely challenging with current technology. Kim, Murthy and Sahoo claimed [141] that we can deduce the neutrinos momenta working in the back-to-back ($b2b$ from now on) kinematic configuration of a four-body decay with two final-state neutrinos, where the difference between Dirac and Majorana cases does survive irrespectively of the neutrino mass values, as long as neutrinos are not strictly massless. We suggest to take a look of their work [141] for a complete discussion.

Therefore, this could be a really exciting and important strategy to distinguish the specific neutrino nature. Motivated by this approach (hereafter referred to as the "KMS method"), we analyze radiative leptonic decays ($\ell^- \to \ell'^- \nu_\ell \bar{\nu}_{\ell'} \gamma$) as an independent approach in order to distinguish the Dirac or Majorana nature of neutrinos. We emphasize that the quoted KMS method of analysis considers processes with $\nu\bar{\nu}$ final states with same-flavour neutrinos, in order to apply the quantum statistical properties of Majorana neutrinos. Nevertheless, the Majorana nature of neutrinos could be implemented even with $\nu\bar{\nu}$ final states with different flavours, working in the mass basis, where the quantum statistical properties could be applied to distinguish between Dirac and Majorana nature, as we

shall discuss, see e.g. [1], [99], [101] [23]. This observation enables the study of many other processes as alternative strategies—without hadronic transitions—featuring larger branching ratios, such as the radiative leptonic decays of leptons, which we focus on here while neglecting possible non-standard interactions.

The main idea is to study the potential effects of Majorana neutrinos in the radiative leptonic decays of μ and τ leptons, under the assumption that their kinematic variables can be inferred—i.e., avoiding integration over their momenta. In such cases, we demonstrate that the distinction between Dirac and Majorana neutrinos remains at the level of the differential decay rate and explicitly depends on the neutrino kinematics. Then, given the $b2b$ configuration analysis, we will show that the D-M difference vanishes upon integration over the neutrinos variables and discuss the origin of the discrepancy with the KMS result.

4.3.1 Radiative Leptonic Decay

Since $m_\ell << M_W$, we can safely integrate out the W boson, allowing the use of a Fermi-type theory of weak interactions to describe charged lepton decays. The leading Feynman diagrams contributing to the radiative leptonic ℓ-decay are shown in figure 5.9.

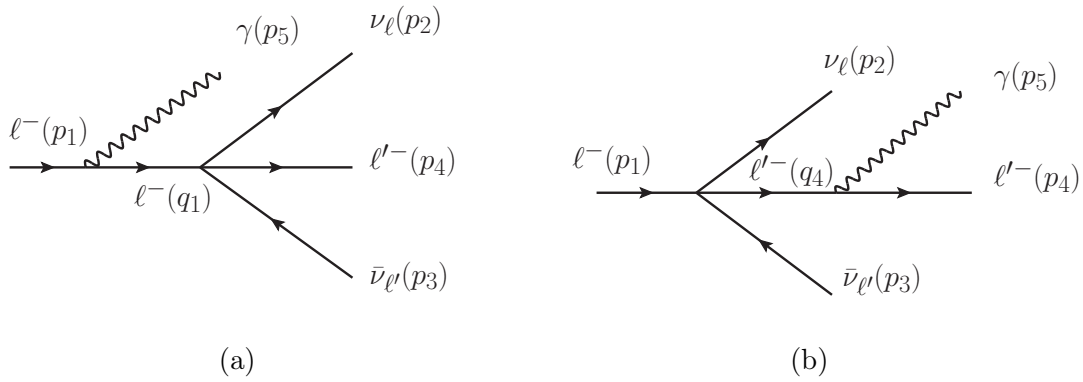

(a) (b)

Figure 4.4: Lowest order Feynman diagrams for radiative leptonic lepton-decay.

In the mass basis, using the same mixing notation, the $\ell^- \to \ell'^- \nu_\ell \bar{\nu}_{\ell'} \gamma$ decay consists of the subsets of all the n^2 separate decays of neutrino mass eigenstates allowed by phase

[23] Obviously, physics conclusions cannot depend on basis choice, although a particular one can be most convenient in a given analysis.

space, i.e., the incoherent sum of the separate modes $\ell^- \to \ell'^- \overline{N}_j N_k \gamma$ [142]:

$$d\Gamma(\ell^- \to \ell'^- \nu_\ell \bar{\nu}_{\ell'} \gamma) = \sum_{j,k} d\Gamma(\ell^- \to \ell'^- \overline{N}_j N_k \gamma)\,. \tag{4.50}$$

Again, note that $\overline{N}$ represents an antineutrino for the Dirac neutrino case, but should be identified with N for the Majorana neutrino case ($N{=}N^c{=}C\overline{N}^T$).

In the Dirac case, the corresponding amplitude for the process $\ell^- \to \ell'^- \overline{N}_j N_k \gamma$ is given by:[24]

$$\mathcal{M}^D = \mathcal{M}_{(a)} + \mathcal{M}_{(b)} \equiv \mathcal{M}(p_2, p_3), \tag{4.51}$$

where (see figure 5.9 for momenta convention)

$$\begin{aligned}
\mathcal{M}_{(a)} &= U_{\ell' j} U^*_{\ell k} \frac{eG_F}{\sqrt{2}} \left[\bar{u}_4 \gamma^\mu (1-\gamma^5) v_3\right] \bar{u}_2 \gamma_\mu (1-\gamma^5) \left(\frac{\not{q}_1 + m_1}{q_1^2 - m_1^2}\right) \gamma^\nu \epsilon^*_\nu u_1, \\
\mathcal{M}_{(b)} &= U_{\ell' j} U^*_{\ell k} \frac{eG_F}{\sqrt{2}} \bar{u}_4 \gamma^\nu \epsilon^*_\nu \left(\frac{\not{q}_4 + m_4}{q_4^2 - m_4^2}\right) \gamma_\mu (1-\gamma^5) v_3 \left[\bar{u}_2 \gamma^\mu (1-\gamma^5) u_1\right].
\end{aligned} \tag{4.52}$$

Neglecting all final lepton masses, as a good approximation, the unpolarized squared amplitude is:

$$\begin{aligned}
|\overline{\mathcal{M}^D}|^2 = |U_{\ell' j} U^*_{\ell k}|^2 \frac{64 e^2 G_F^2}{(p_4\cdot p_5)(p_1\cdot p_5)^2} \Big\{ & (p_1\cdot p_3)\Big[(p_2\cdot p_4 + p_2\cdot p_5)(p_1\cdot p_5)^2 - m_1^2 (p_2\cdot p_4)(p_4\cdot p_5) \\
& + (p_1\cdot p_4)(p_1\cdot p_5)(2(p_2\cdot p_4) + p_2\cdot p_5) - (p_1\cdot p_5)(p_4\cdot p_5)(p_1\cdot p_2 + p_2\cdot p_4)\Big] + (p_2\cdot p_4) \\
& \Big[(p_3\cdot p_4)(p_1\cdot p_5)^2 + m_1^2 (p_3\cdot p_5)(p_4\cdot p_5) + (p_1\cdot p_5)(p_3\cdot p_5)(p_4\cdot p_5 - p_1\cdot p_4)\Big]\Big\}.
\end{aligned} \tag{4.53}$$

Finally, motivated by the KMS method, we need to work in the initial charged-lepton rest frame, specifically in the $b2b$ kinematic configuration shown in figure 4.5, where the scalar

[24] Where, when computing the decay rate, we must sum incoherently over the probabilities of all the allowed $\{j,\, k\}$ channels.

products, neglecting the final lepton masses, are given by [25]:

$$\begin{aligned} p_4 \cdot p_5 &= 2E_{\ell'}^2, \quad p_2 \cdot p_3 = 2\left(\frac{m_\ell}{2} - E_{\ell'}\right)^2, \\ p_1 \cdot p_2 &= p_1 \cdot p_3 = m_\ell E_{\ell'}\left(\frac{m_\ell}{2} - E_{\ell'}\right), \\ p_1 \cdot p_4 &= p_1 \cdot p_5 = m_\ell E_{\ell'}, \\ p_3 \cdot p_4 &= p_2 \cdot p_5 = E_{\ell'}\left(\frac{m_\ell}{2} - E_{\ell'}\right)(1+\cos\theta), \\ p_3 \cdot p_5 &= p_2 \cdot p_4 = E_{\ell'}\left(\frac{m_\ell}{2} - E_{\ell'}\right)(1-\cos\theta). \end{aligned} \tag{4.54}$$

Thus, in this kinematical configuration, the process is described in terms of only two

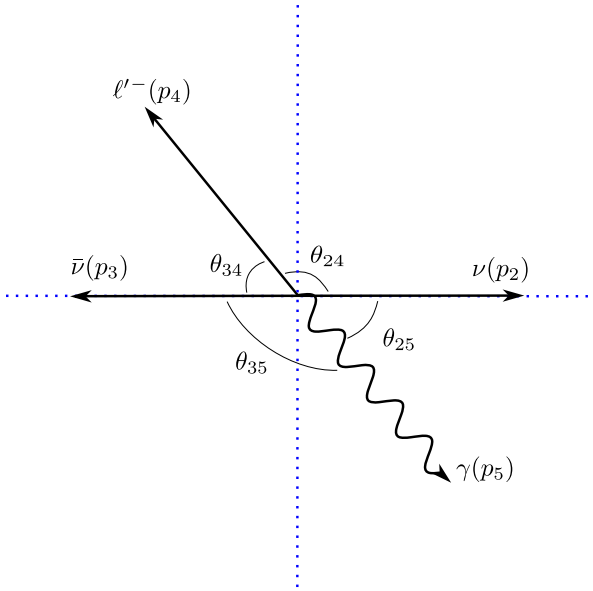

Figure 4.5: $b2b$ kinematic configuration in the initial charged-lepton rest frame.

variables, the final charged-lepton energy[26], $E_4 \equiv E_{\ell'}$, and the angle between the neutrino and final charged-lepton directions, $\theta_{24} = \theta$.

With these considerations, the final Dirac amplitude is given by:

$$|\overline{\mathcal{M}^D_{\leftrightarrow}}|^2 = |U_{\ell' j} U^*_{\ell k}|^2 \frac{8e^2 G_F^2 (m_\ell - 2E_{\ell'})^2}{m_\ell E_{\ell'}} \left(8E_{\ell'}^2 \sin^4\frac{\theta}{2} + (1+\cos\theta)m_\ell^2\right). \tag{4.55}$$

The subindex '$\leftrightarrow$' denotes the $b2b$ configuration. The $1/E_{\ell'}$-dependence reflects the infrarred behaviour of the amplitude in the soft-photon limit.

[25] The energies are related by: $E_\gamma = E_{\ell'}$ and $E_\nu = E_{\bar{\nu}} = \frac{m_\ell}{2} - E_{\ell'}$.
[26] The corresponding energy range is $0 \leq E_{\ell'} \leq \frac{m_\ell}{2}$.

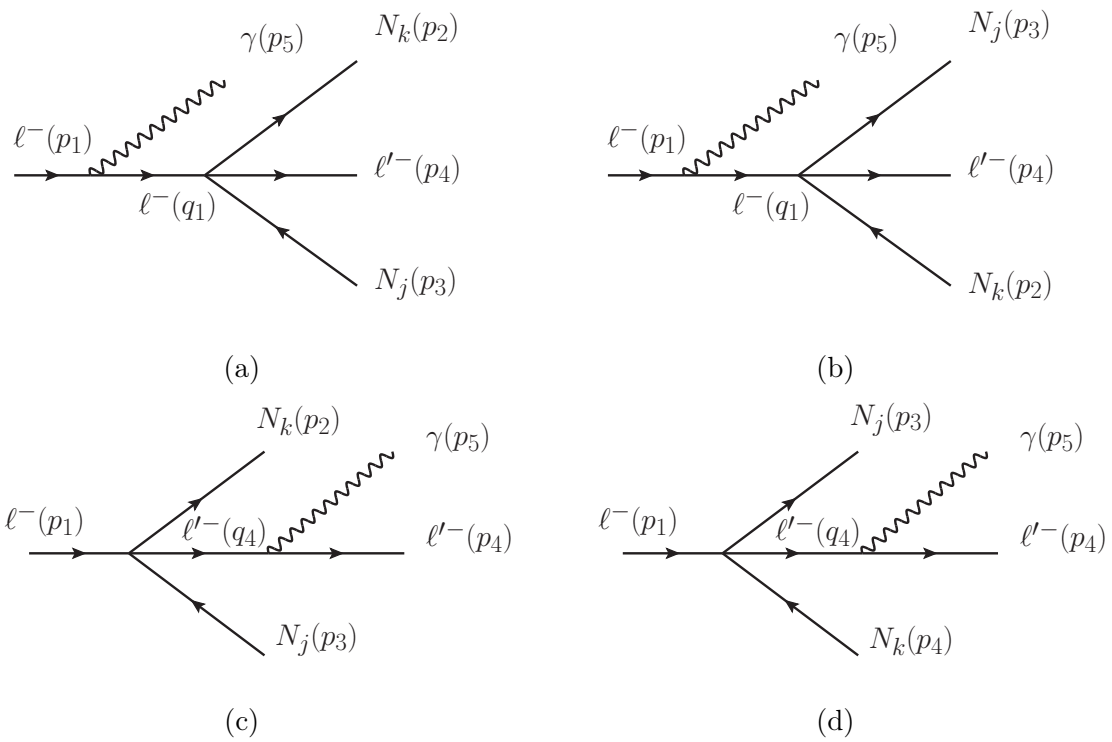

Figure 4.6: Lowest order Feynman diagrams for radiative leptonic lepton-decay in the Majorana neutrino case.

In contrast to the Dirac case, the intrinsic properties of Majorana neutrinos lead to notable modifications in the amplitude, as discussed earlier. Remember that for Majorana neutrinos the decay modes $\ell^- \to \ell'^- \overline{N}_j N_k \gamma$ and $\ell^- \to \ell'^- \overline{N}_k N_j \gamma$ yield the same final states for $k \neq j$ as well as for $k = j$ (since $\overline{N}_i = N_i$), and hence their amplitudes must be added coherently. This is a result that can be obtained rigorously in the QFT formalism.

The possible first order Feynman diagrams for the $\ell^- \to \ell'^- N_j N_k \gamma$ decay are shown in figure 4.6, leading to the total amplitude:

$$\mathcal{M}^M = \mathcal{M}_{jk}(p_2, p_3) - \mathcal{M}_{kj}(p_3, p_2)\,, \tag{4.56}$$

where the relative sign between $\mathcal{M}(p_2, p_3)$ and $\mathcal{M}(p_3, p_2)$ stems from the application of Wick's theorem in presence of Majorana fermions (see, e.g. Ref. [102]).

It can be shown that, after summing over polarizations, $Re\left(\mathcal{M}(p_2, p_3)\mathcal{M}^*(p_3, p_2)\right) \propto$

$m_\nu^2 \approx 0$ due to the smallness of neutrino masses[27]. Thus

$$|\overline{\mathcal{M}^M}|^2 = |\overline{\mathcal{M}}_{jk}(p_2, p_3)|^2 + |\overline{\mathcal{M}}_{kj}(p_3, p_2)|^2. \tag{4.57}$$

The computation, neglecting the final lepton masses, leads to the following squared amplitude for the $b2b$ kinematic configuration:

$$\begin{aligned}|\overline{\mathcal{M}^M_{\leftrightarrow}}|^2 = \frac{8e^2G_F^2(m_\ell - 2E_{\ell'})^2}{m_\ell E_{\ell'}} \Bigg\{ & |U_{\ell' j}U^*_{\ell k}|^2 \left(8E_{\ell'}^2 \sin^4\left(\frac{\theta}{2}\right) + m_\ell^2(1+\cos\theta)\right) \\ & + |U_{\ell' k}U^*_{\ell j}|^2 \left(8E_{\ell'}^2 \cos^4\left(\frac{\theta}{2}\right) + m_\ell^2(1-\cos\theta)\right)\Bigg\}\,.\end{aligned} \tag{4.58}$$

Thus, the Majorana nature of neutrinos would generate a different behavior of the amplitude compared with the Dirac neutrinos case, eq. (4.55).

4.3.2 Energy and Angular Distributions (Dirac vs Majorana)

Inspired by the KMS method, we present an independent derivation and calculate the energy and angular distributions of the $\nu - \bar{\nu}$ and $\ell' - \gamma$ systems in the $b2b$ configuration, respectively.

When we restrict ourselves to the $b2b$ scenario— which corresponds to a specific kinematic configuration of the general case, as previously discussed — we adopt the following notation for the corresponding decay rate, according to eq. (F.6) (see Appendix F for all the details):

$$\left.\frac{d\Gamma^{D,M}}{dE_\nu dE_{\bar{\nu}} d\cos\Theta_{\nu\bar{\nu}} d\cos\theta_{\ell'} d\phi}\right|_{b2b} = \frac{2E_\nu^2}{(4\pi)^6 m_\ell}\,\frac{1}{\epsilon}\sum_{j,k}|\overline{\mathcal{M}^{D,M}_{\leftrightarrow}}|^2, \tag{4.59}$$

$$\left.\frac{d\Gamma^{D,M}}{dE_{\ell'} dE_\gamma d\cos\Theta_{\ell'\gamma} d\cos\theta_\nu d\phi}\right|_{b2b} = \frac{2E_{\ell'}^2}{(4\pi)^6 m_\ell}\,\frac{1}{\epsilon}\sum_{j,k}|\overline{\mathcal{M}^{D,M}_{\leftrightarrow}}|^2, \tag{4.60}$$

where $\epsilon = 1(2)$ for Dirac (Majorana) neutrinos, showing that it is just the standard differential decay rate evaluated in the specific $b2b$ kinematics[28], and the amplitudes involved were already quoted.

Using the $|\overline{\mathcal{M}^{D/M}_{\leftrightarrow}}|^2$ previously computed, we obtain the following neutrinos differential

[27] We are considering only the contribution of the three active light neutrino mass eigenstates.
[28] Where $E_\gamma = E_{\ell'}$, $E_\nu = E_{\bar{\nu}}$ and $\Theta_{\nu\bar{\nu}} = \Theta_{\ell'\gamma} = \pi$.

decay rate:

$$d\Gamma^{D}_{\nu\nu}|_{b2b} \equiv \left.\frac{d\Gamma^{D}}{dE_\nu dE_{\bar\nu} d\cos\Theta_{\nu\bar\nu} d\cos\theta_{\ell'} d\phi}\right|_{b2b} = \frac{4\alpha G_F^2 (m_\ell - 2E_{\ell'})^4}{(4\pi)^5 m_\ell^2 E_{\ell'}} \left(8E_{\ell'}^2 \sin^4\frac{\theta}{2} + (1+\cos\theta) m_\ell^2\right),$$
$$d\Gamma^{M}_{\nu\nu}|_{b2b} \equiv \left.\frac{d\Gamma^{M}}{dE_\nu dE_{\bar\nu} d\cos\Theta_{\nu\bar\nu} d\cos\theta_{\ell'} d\phi}\right|_{b2b} = \frac{4\alpha G_F^2 (m_\ell - 2E_{\ell'})^4}{(4\pi)^5 m_\ell^2 E_{\ell'}} \left(E_{\ell'}^2 (3+\cos 2\theta) + m_\ell^2\right), \tag{4.61}$$

where we already used the unitarity relations for the mixing matrix elements considering just the three active light neutrino mass eigenstates. We can also consider the presence of a massive sector by keeping the summation explicit, where new sterile neutrinos could either be produced if kinematically allowed or affect the unitarity relation if forbidden by kinematics. Nevertheless, as discussed in Ref. [1], the possible effects are suppressed by the specific heavy–light mixing and cannot exceed the order of 10^{-4}; therefore, they should only be taken into account when such a level of precision is required.

Then the difference between Dirac and Majorana cases in the $b2b$ scenario is:

$$d\Gamma^{D}_{\nu\nu}|_{b2b} - d\Gamma^{M}_{\nu\nu}|_{b2b} = \frac{4\alpha G_F^2 (m_\ell - 2E_{\ell'})^5}{(4\pi)^5 m_\ell^2 E_{\ell'}} (m_\ell + 2E_{\ell'}) \cos\theta. \tag{4.62}$$

The difference is evident; however, the angle θ is not experimentally accessible. Therefore, we must integrate over it to obtain the final charged-lepton energy distributions for the Dirac and Majorana cases. To perform this integration over the inaccessible angle, it is sufficient to express θ, which appears on the right-hand side of the above equations, in terms of the phase-space variables $\theta_{\ell'}$ and ϕ, i.e., $\theta = \theta(\theta_{\ell'}, \phi)$.

Since θ is the angle between $\vec{p}_\nu$ and $\vec{p}_{\ell'}$, it is easy to get, as shown in eq.(G.9) that:

$$\cos\theta \equiv \hat{p}_4 \cdot \hat{p}_2 = \sin\theta_{\ell'} \sin\theta_\nu \cos\phi - \cos\theta_\nu \cos\theta_{\ell'}. \tag{4.63}$$

Now, since these neutrinos differential decay rate do not depend explicitly on θ_ν, we have the freedom to fix it to ease further computations [29] . Then, for example, we can choose the system in such a way that $\theta_\nu = 0$ and thus we get $\cos\theta = -\cos\theta_{\ell'}$, which does not have a dependence on the ϕ angle, showing explicitly the azimuthal symmetry of this specific selection. Using this dependence, where $0 \leq \theta_{\ell'} \leq \pi$ and $0 \leq \phi \leq 2\pi$ so that all

[29] The following discussion can be directly applied to eq.(4.60) for $\theta_{\ell'}$.

possible angular configurations between ℓ' and ν are accounted for, we have from eq.(4.62):

$$\begin{aligned}&\int_0^{2\pi}\int_{-1}^{1}\left(d\Gamma^D_{\nu\nu}|_{b2b}-d\Gamma^M_{\nu\nu}|_{b2b}\right)d\cos\theta_{\ell'}d\phi\\&=\int_0^{2\pi}\int_0^{\pi}\frac{-4\alpha G_F^2(m_\ell-2E_{\ell'})^5}{(4\pi)^5 m_\ell^2 E_{\ell'}}\left(m_\ell+2E_{\ell'}\right)\cos\theta_{\ell'}\sin\theta_{\ell'}d\theta_{\ell'}d\phi=0.\end{aligned}\tag{4.64}$$

Doing this, it is straightforward that the difference between Dirac and Majorana cases vanishes once the angular integration is made. We emphasize that this difference will vanish in any other selected frame, doing the angular integration properly, as derived in eq.(G.9).

Specifically, for subsequent discussions, if we work in the system where the neutrinos define the x-axis ($\theta_\nu=\pi/2$), as done in the KMS method, in such a way that $\cos\theta=\cos\phi\sin\theta_{\ell'}$, the difference between Dirac and Majorana cases after the angular integration is:

$$\begin{aligned}&\int_0^{2\pi}\int_{-1}^{1}\left(d\Gamma^D_{\nu\nu}|_{b2b}-d\Gamma^M_{\nu\nu}|_{b2b}\right)d\theta_{\ell'}d\phi\\&=\int_0^{2\pi}\int_0^{\pi}\frac{4\alpha G_F^2(m_\ell-2E_{\ell'})^5}{(4\pi)^5 m_\ell^2 E_{\ell'}}\left(m_\ell+2E_{\ell'}\right)\cos\phi\sin^2\theta_{\ell'}d\theta_{\ell'}d\phi=0.\end{aligned}\tag{4.65}$$

Once again, the difference between the Dirac and Majorana cases vanishes, consistent with the previous calculation, as the physics cannot depend on the choice of reference frame. We note that the main discrepancy with the KMS method arises from their setting $\phi=0$. This example illustrates that fixing $\phi=0$ would yield results that depend on the chosen frame, which is physically inconsistent. For this reason, along with several other arguments (see, e.g., Ref. [143]), we conclude that ϕ is not constrained by any kinematic condition and must be integrated over its full range, as will be discussed in detail later.

Actually, we can do the same computation for the $\ell'-\gamma$ decay rate (since, even if in the $b2b$ configuration we can relate $E_{\ell'}$ and E_ν, the neutrinos and electron-photon distributions are not the same in this kinematic scenario, as shown in eqs.(4.59) and (4.60)) and compute the specific energy distribution for the $\ell'-\gamma$ and $\nu-\bar{\nu}$ pairs, integrating over the inaccessible angle θ, finding that indeed both distributions are different but the Dirac and Majorana cases are, unfortunately, indistinguishable in each case.

This point is particularly important because the explanation for the impossibility of distinguishing the neutrino nature differs for each distribution. For the ℓ'-γ spectrum,

it follows directly from the Dirac–Majorana confusion theorem (DMCT), as we have already integrated over all neutrino variables and neglected neutrino mass contributions. In contrast, for the ν-$\bar{\nu}$ spectrum, one might initially expect a difference between Dirac and Majorana distributions, since information about the neutrino energies is retained. This would be true if the neutrinos energies were not equal, so the change $E_\nu \leftrightarrow E_{\bar{\nu}}$ could lead to a difference while computing the Majorana neutrino case. Regrettably, in the $b2b$ case, they are exactly the same ($E_\nu = E_{\bar{\nu}}$), so we can not distinguish between Dirac and Majorana nature from this energy variable alone. This statement is precisely the reason why the difference between Dirac and Majorana distributions can not be independent of the angular variable θ.

Then, carefully using our standard notation and considering the correct angular dependence while doing the integration, yields all results consistent with the DMCT and the above discussions, so once the inaccessible neutrino angle is integrated out from the $\ell' - \gamma$ and $\nu - \bar{\nu}$ differential decay rates, we can not distinguish between Dirac and Majorana distributions in either of them.

4.3.3 Consistency Tests

We now elaborate on our results, focusing on the primary reason for the absence of a difference between Dirac and Majorana neutrinos. This outcome, which may appear counterintuitive given the motivation provided by the KMS method, warrants a careful and detailed analysis.

We emphasize that the specific process under study is not the same as the one used in [141], and the Majorana nature affects in a distinct manner the two of them. Nevertheless, this will only influence the dynamics and not the kinematics. So, from now on, we will be focusing on the kinematic analysis, which must be the same considering all our previous assumptions.

It is straightforward to see that the difference between Dirac and Majorana cases in our approach vanishes after integrating, due to the specific angular dependence, and it can be proved that this is true in any selected system (fixing the value of θ_ν), as it must be. Particularly, working in the same system as in the KMS method, we traced back the main difference of this feature with the KMS approach and found that it primarily arises from

the ϕ variable treatment. Therefore, we want to delve further into this topic, and specify the reasons why this variable should not be fixed in the $b2b$ configuration. Additionally, we will outline the results that would be obtained if we do so in our specific process.

The KMS method suggests that $\phi = 0$ is a condition fixed by the $b2b$ kinematics. As we mentioned, the $b2b$ scenario is obtained by applying the condition $\vec{p}_2 = -\vec{p}_3$, or equivalently $\vec{p}_4 = -\vec{p}_5$. These restrictions affect three of the five phase-space kinematic independent variables as follows: $E_\nu = E_{\bar{\nu}}$ and $\Theta_{\nu\bar{\nu}} = \pi$. Consequently, the remaining two angular variables must run over all their possible configurations, meaning that we must not set ϕ to any specific value. In other words, the condition $\vec{p}_2 = -\vec{p}_3$ can be achieved for any value of ϕ, and not just for $\phi = 0$. Nevertheless, beyond these qualitative arguments, we did the quantitative derivation of this assertion in Appendix G, where it is shown explicitly that ϕ is not fixed at all by the $b2b$ restriction.

Finally, the last argument given in the KMS approach is that in the $b2b$ configuration the $\nu\bar{\nu}$ and $\ell'\gamma$ systems define a plane (since they are two independent vectors) and thus $\phi = 0$. We also clarify this statement in Appendix G, where we fully agree with the $\nu\bar{\nu}$ and $\ell'\gamma$ systems defining a plane, but show that such a plane is independent of the ϕ value, being $\phi = 0$ just an allowed specific configuration. These can be seen directly from the plane equation and applied to any selected system. Then ϕ remains an independent variable.

Also, as discussed in previous sections, the physics must not depend on the selected reference frame. We already showed that –at least in two different systems ($\theta_\nu = 0$ and $\theta_\nu = \pi/2$)– the difference between Dirac and Majorana distributions vanishes while doing the angular integration properly (not fixing $\phi = 0$), which extends to any other frame. While assuming the condition $\phi = 0$, we obtain that this difference will be non-vanishing in the system defined by $\theta_\nu = \pi/2$, whereas it will remain zero in the system where $\theta_\nu = 0$, which is clearly a physical contradiction, and again another argument against fixing ϕ in the $b2b$ kinematic configuration.

This is really important to clarify, since by imposing the condition $\phi = 0$ as a kinematic constraint, it would be possible in principle to distinguish between the Dirac and Majorana nature of neutrinos measuring the final energy distribution of the $b2b$ configuration.

Specifically, the Dirac-Majorana difference in this process will be of the form:

$$\int (d\Gamma^{D}_{\nu\nu}|_{b2b} - d\Gamma^{M}_{\nu\nu}|_{b2b})\, d\cos\theta_{\ell'} = \frac{2\alpha G_F^2}{(4\pi)^5 m_\ell^2} \frac{(m_\ell - 2E_{\ell'})^5}{E_{\ell'}} \pi \left[m_\ell + 2E_{\ell'}\right], \tag{4.66}$$

which is not suppressed by neutrino masses. It could thus be a really promising result, motivating its search in current and future experiments, being an attractive alternative process to the one studied in [141], due to its larger branching ratio (BR) [30].

Finally, focusing on this last statement, we would also like to clarify the estimation process of the BR as done in the KMS method, which could lead to confusion for the $b2b$ case. This is done in detailed in Appendix H, where we find a BR for the $b2b$ case of the following order:

$$\begin{aligned} \mathcal{BR}(\ell = \tau)_{b2b} &= (\Gamma)_{b2b}/\Gamma_\tau \approx 1.68 \times 10^{-10}, \\ \mathcal{BR}(\ell = \mu)_{b2b} &= (\Gamma)_{b2b}/\Gamma_\mu \approx 1.34 \times 10^{-10}, \end{aligned} \tag{4.67}$$

being too suppressed, as expected for such a specific kinematic configuration.

In conclusion, once the appropriate treatment of the phase-space in the $b2b$ configuration is clarified, our approach remains consistent with all the tests carried out, and allows a clearer interpretation of the results, leading to the fact that there is no difference produced by the Dirac or Majorana nature of neutrinos in $\ell \to \ell'\nu\bar{\nu}\gamma$, independently of the neutrino mass, once the inaccessible neutrino variables are integrated out. This turns out to be crucial, since its inaccurate interpretation could lead to very attractive results, even observable in current and near future experiments. Recalling our comments above eq. (4.57) and below eq. (4.61), any difference between these two cases will be heavily suppressed by squared sterile neutrino masses and mixings, likely preventing their soon observation. We remark that we were neglecting possible neutrino non-standard interactions.

[30] Unfortunately, if we consider the full angular dependence (without setting $\phi = 0$) as we just discussed, the difference between the Dirac and Majorana cases vanishes once the angular integration is performed, consistently with all the results previously obtained.

Chapter 5

Muon g-2

5.1 HEFT g-2 analysis

Based on [144], motivated by the EFT and precision physics approach, we also investigated the famous muon $g-2$ anomaly, see Appendix I. While an eventual significant discrepancy between SM prediction and measurements could be explained by various NP models, testing these contributions is extremely challenging, due to the significant hadronic uncertainties within the SM. A recent work [144] proposed a model-independent approach to test NP contributions to the muon $g-2$, bypassing low-energy hadronic uncertainties. The idea involves a simple but interesting connection between low-energy $g-2$ Feynman diagrams and high-energy scattering processes through the Higgs vev expansion in the Lagrangian. This analysis motivates the measurement of the scattering process ($\mu^+\mu^- \to H\ \gamma/Z$) to relate the corresponding Wilson coefficients to the specific NP contribution to a_μ in a future muon collider.

Since the previous discussed work, that was done within the SMEFT formalism (see section 3.2.2), involves a Higgs sector, we were particularly interested in the potential modifications that a more general analysis could induce on this process. We focused on using Higgs Effective Field Theory (HEFT) (see section 3.2.3), an EFT that treats the Higgs and Goldstone bosons separately, leading to a non-linear realization of the electroweak symmetry. This approach is more general than SMEFT, while remaining consistent with experimental data and reducing to SMEFT as a limiting case. By reproducing the analysis within the HEFT formalism, we obtained interesting results [3]. We find that, within the current HEFT analysis, there are plausible scenarios where the HEFT approach could lead to a higher sensitivity for testing the NP contributions to the muon g-2. However, a more precise knowledge of the new HEFT parameters is needed to reach definite conclusions, which motivates the search for complementary measurements.

5.1.1 SMEFT approach

Before presenting the HEFT computation, it is useful to highlight the main ideas and properties discussed in Ref. [144], which serve as motivation for our analysis. We strongly encourage the reader to consult their work for full and detailed explanations of the summary presented here.

As commented in Ref. [144], the observed muon discrepancy can be accommodated by NP effects that arise from the dimension-6 dipole operators[31]

$$\mathcal{L} = \frac{C_{eB}^{\ell}}{\Lambda^2}\left(\bar{\ell}_L \sigma^{\mu\nu} e_R\right) H B_{\mu\nu} + \frac{C_{eW}^{\ell}}{\Lambda^2}\left(\bar{\ell}_L \sigma^{\mu\nu} e_R\right) \tau^I H W^I_{\mu\nu} + \text{h.c.}, \tag{5.1}$$

where –in the unitary gauge– the Higgs doublet H reduces to its neutral component, which is $(v+h)/\sqrt{2}$, with $v = 246$ GeV. This brings the sensitivity to the muon g-2 to NP scales of order $\Lambda \lesssim 100$ TeV (in the strongly-coupled regime, characteristic of HEFT). However, directly detecting new particles at such high scales is far beyond our current capabilities. Even if those particles were discovered, it would be nearly impossible to unambiguously link them to Δa_μ on a short time scale.

The central idea is that a high-energy muon collider provides a fully model-independent way to probe NP in the muon g-2. This is because the same dipole operator that generates the primary contribution to Δa_μ also inevitably induces an NP contribution to a muon scattering process, whose cross-section measurement is equivalent to determining Δa_μ within the effective field theory framework.

In SMEFT, the relevant effective Lagrangian contributing to the muon g-2 up to one-loop order and after SSB, is

$$\mathcal{L} = \frac{C_{e\gamma}^{\ell}}{\Lambda^2}\frac{v}{\sqrt{2}}\bar{\ell}_L \sigma^{\mu\nu} e_R F_{\mu\nu} + \frac{C_{eZ}^{\ell}}{\Lambda^2}\frac{v}{\sqrt{2}}\bar{\ell}_L \sigma^{\mu\nu} e_R Z_{\mu\nu} + \text{h.c.}\,, \tag{5.2}$$

where $C_{e\gamma}^{\ell}$ and C_{eZ}^{ℓ} are Wilson coefficients, and Λ is the NP scale.

[31] We focus here only on the operators where the Higgs boson participates. ℓ is the lepton weak doublet and e the corresponding singlet, both for the three SM families. $B_{\mu\nu}$ is the $U(1)$ field-strength tensor and $W^I_{\mu\nu}$ the corresponding one for $SU(2)$, with $I = 1, 2, 3$ and $2\tau^I = \sigma^I$ the Pauli matrices.

Computing the Feynman diagrams that contribute to the g-2, one obtains

$$\Delta a_\ell \simeq \frac{4 m_\ell v}{\sqrt{2} e \Lambda^2} \left(C^\ell_{e\gamma} - \frac{3\alpha}{2\pi} \frac{\cos^2\theta_W - \sin^2\theta_W}{\sin\theta_W \cos\theta_W} C^\ell_{eZ} \log\frac{\Lambda}{m_Z} \right), \tag{5.3}$$

where θ_W is the weak mixing angle.

But –as mentioned before– also high-energy scattering processes are generated, due to the Higgs field plus vacuum expectation value expansion after electroweak symmetry breaking, as can be seen explicitly in Fig.5.1. Then, from measuring the scattering events, we would be able to test the g-2 anomaly indirectly.

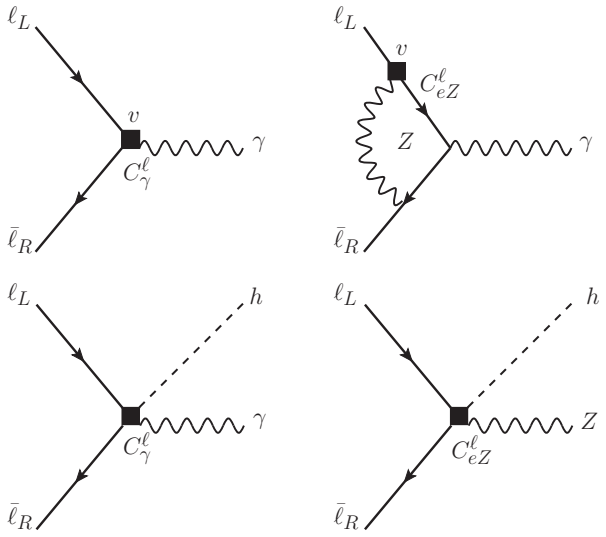

Figure 5.1: *Upper row:* Feynman diagrams contributing to $(g\text{-}2)_\ell$ in SMEFT, according to eq. (5.2). *Lower row:* Feynman diagrams of the corresponding $\ell^+\ell^- \to h + \gamma/Z$ scattering processes.

The key point is that both the g-2 contribution and the scattering process (whether mediated by the photon or the Z boson) arise from the same effective operator, sharing a common Wilson coefficient—the only free parameter in the analysis. This direct correspondence allows one to unambiguously connect the two processes and extract low-energy information through high-energy measurements.

Finally, since the SMEFT Lagrangian, and thus the specific scattering processes, depend explicitly on the Higgs field, it is interesting to wonder if anything would be modified if the analysis is carried out using a HEFT approach. This HEFT analysis is more general (see e.g. refs. [145], [146] analyzing possible imprints of HEFT in multi-Higgs processes).

For instance, new dimension-6 contributions appear, that would be really suppressed in the SMEFT case (see ref. [147] for the power counting in HEFT) and the unambiguous relation between long- and short-distance processes could be lost —due to the addition of unknown free parameters—.

5.1.2 HEFT approach

The explicit computation and main conclusions within the HEFT formalism are derived in this section, discussing the specific HEFT Lagrangian together with the $\mu^+\mu^- \to h\gamma$ and $\mu^+\mu^- \to hZ$ cross sections.

5.1.2.1 HEFT Lagrangian

Following Ref. [148], the HEFT operators with a single fermion current and up to two derivatives are contained in the following Lagrangian [32]:

$$\begin{aligned}\Delta\mathcal{L}_{2F} = &\sum_{j=1}^{8} n_j^{\mathcal{Q}}\mathcal{N}_j^{\mathcal{Q}} + \sum_{j=9}^{28}\frac{1}{\Lambda}\left(n_j^{\mathcal{Q}} + i\tilde{n}_j^{\mathcal{Q}}\right)\mathcal{N}_j^{\mathcal{Q}} + \sum_{j=29}^{36}\frac{4\pi}{\Lambda}\left(n_j^{\mathcal{Q}} + i\tilde{n}_j^{\mathcal{Q}}\right)\mathcal{N}_j^{\mathcal{Q}} \\ &+ \sum_{j=1}^{2} n_j^{\ell}\mathcal{N}_j^{\ell} + \sum_{j=3}^{11}\frac{1}{\Lambda}\left(n_j^{\ell} + i\tilde{n}_j^{\ell}\right)\mathcal{N}_j^{\ell} + \sum_{j=12}^{14}\frac{4\pi}{\Lambda}\left(n_j^{\ell} + i\tilde{n}_j^{\ell}\right)\mathcal{N}_j^{\ell} + \text{h.c.},\end{aligned} \tag{5.4}$$

where $n_j^{\mathcal{Q}}$, n_j^{ℓ}, $\tilde{n}_j^{\mathcal{Q}}$ and $\tilde{n}_j^{\ell}$ are real coefficients smaller than unity [33], and the explicit form of all the operators can be found in Ref. [148], along with enlightening explanations. In eq. (5.4) the terms with two derivatives are suppressed by the NP scale Λ, and the CP-even and -odd contributions have untilded and tilded coefficients, respectively.

Specifically, for the processes under study ($\mu^+\mu^- \to h + \gamma/Z$ and $h \to \mu^+\mu^- + \gamma/Z$), it is possible to prove that the only contributing operators are (L_L is the SM lepton doublet

[32] Higher-order HEFT Lagrangians are derived in Refs. [149], [150] and the EFT renormalization is studied in Refs. [151], [152], [153], [154].

[33] We note the explicit 4π factors in the last of term of each line in eq. (5.4), particularly in $\mathcal{N}^{\ell}_{12,13}$.

and a right-handed neutrino does not appear in L_R):

$$\begin{aligned}
\mathcal{N}_2^\ell(h) &\equiv i\bar{L}_R\gamma_\mu U^\dagger \{V^\mu, T\} U L_R \mathcal{F}, \\
\mathcal{N}_4^\ell(h) &\equiv \bar{L}_L \{V_\mu, T\} U L_R \partial^\mu \mathcal{F}, \\
\mathcal{N}_9^\ell(h) &\equiv \bar{L}_L \sigma^{\mu\nu} \{V_\mu, T\} U L_R \partial_\nu \mathcal{F}, \\
\mathcal{N}_{12}^\ell(h) &\equiv ig'\bar{L}_L \sigma^{\mu\nu} U L_R B_{\mu\nu} \mathcal{F}, \\
\mathcal{N}_{13}^\ell(h) &\equiv ig\bar{L}_L \sigma^{\mu\nu} W_{\mu\nu} U L_R \mathcal{F},
\end{aligned} \tag{5.5}$$

with (below L, R are $SU(2)_{L,R}$ transformations and f_π the scale associated to the pseudo-Goldstone electroweak bosons, V_μ and T transform in the adjoint of $SU(2)_L$ and the latter breaks custodial symmetry, so it is tightly constrained)

$$\begin{aligned}
&U = \exp^{i\sigma_a \pi^a(x)/f_\pi},\ U(x) \to L U(x) R^\dagger, \\
&V_\mu \equiv (D_\mu U)U^\dagger, \quad T \equiv U\sigma_3 U^\dagger, \\
&D_\mu U(x) \equiv \partial_\mu U(x) + igW_\mu(x)U(x) - \frac{ig'}{2}B_\mu(x)U(x)\sigma_3\,, \\
&\mathcal{F}_i(h) = 1 + 2a_i\frac{h}{v} + b_i\frac{h^2}{v^2} + ...
\end{aligned} \tag{5.6}$$

The SM is reproduced if $a_0 = 1$, $b_0 = 1$ in the leading order term $(v^2/4)\mathrm{Tr}[(D_\mu U)^\dagger(D^\mu U)]$ $\mathcal{F}_0(h)$, the Higgs potential is $V(h) = v^4\left[\frac{m_h^2}{2v^2}\left(\frac{h}{v}\right)^3 + \frac{m_h^2}{8v^2}\left(\frac{h}{v}\right)^4\right]$, and all other coefficients in operators with energy dimension larger than four vanish. A possible generalized function (with in principle unconstrained coefficients) in the Higgs potential does not play any role in this work.

The measured values of the a_0 and b_0 coefficients agree with SM predictions within uncertainties, but the current experimental accuracy of these measurements is only at the level of $\sim 10\%$. The unitarity condition for the HEFT amplitudes imposes a NP scale Λ depending on the specific deviations from SM expectations. A significant departure implies a lower Λ, potentially around the TeV range. Conversely, for minor deviations, Λ could be considerably higher, approaching arbitrarily large values in the limit where the SM is recovered. This relationship has been thoroughly explored from a geometric perspective, as elaborated in Ref. [87]. For further details, we refer the reader to Ref. [155], which discusses various processes and UV complete models, illustrating the operational

mechanics of HEFT and its implications for determining the NP scale.

Certain processes, such as multi-boson radiation in the TeV range, may affect the sensitivity of the parameters, particularly in scenarios with a low cutoff scale that enhances these contributions. However, as noted in Ref. [155], these effects can also lead to a suppression relative to the naively expected $(E/(4\pi v))^2$ factor, depending on the specific UV complete model. Given the large cutoff scale adopted in our analysis, this effect is not included in the main result of our calculation.

Then, if we use expressions (5.6) in (5.5), we obtain the following operators in the unitary gauge:

$$\begin{aligned}
\mathcal{N}_2^\ell(h) &\equiv -g_z \bar{L}_R \gamma^\mu Z_\mu L_R \mathcal{F}_2, \\
\mathcal{N}_4^\ell(h) &\equiv i g_z \bar{L}_L Z_\mu L_R \partial^\mu \mathcal{F}_4, \\
\mathcal{N}_9^\ell(h) &\equiv i g_z \bar{L}_L \sigma^{\mu\nu} Z_\mu L_R \partial_\nu \mathcal{F}_9,
\end{aligned} \tag{5.7}$$

with $g_z = e/(\sin\theta_W \cos\theta_W)$ and where only the Z_μ part of the operator contributes [83]. The remaining $\mathcal{N}_{12}^\ell$ and $\mathcal{N}_{13}^\ell$ operators are analogous to those also appearing in the SMEFT dimension-six Lagrangian case, eq. (5.1) (with a Higgs doublet instead of the $\mathcal{F}$ function, which can be different for every operator, as we emphasized with a subindex). Among these operators, only $\mathcal{N}_2^\ell$ is not suppressed by $1/\Lambda$ in eq. (5.4), enhancing relatively its contributions at low energies.

Indeed, each HEFT operator can be generated within the SMEFT framework up to a certain dimension, as discussed above. For completeness, Table 5.1 presents the set of SMEFT operators that account for the additional HEFT terms. It is also remarkable

HEFT	SMEFT (D=Dimension)
$\mathcal{N}_2^\ell$	$\mathcal{Q}_{\varphi e}$ [66] (D=6)
$\mathcal{N}_4^\ell$	$Q_{leH^3D^2}^{(1),(2),(5)}$ [156] (D=8)
$\mathcal{N}_9^\ell$	$Q_{leH^3D^2}^{(3),(4),(6)}$ [156] (D=8)
$\mathcal{N}_{12}^\ell$	$\mathcal{Q}_{eW}$ [66] (D=6)
$\mathcal{N}_{13}^\ell$	$\mathcal{Q}_{eB}$ [66] (D=6)

Table 5.1: Correspondence between the HEFT operators analyzed in this work and the operators coming from SMEFT.

that none of these new HEFT operators ($\mathcal{N}_2^\ell$, $\mathcal{N}_4^\ell$ and $\mathcal{N}_9^\ell$) contribute to the anomalous magnetic moment of the muon directly, so only their contributions to the processes $\mu^+\mu^- \to hZ$ and $h \to \mu^+\mu^- Z$ will be taken into account.

Then, the corresponding HEFT Lagrangian for this work is given by

$$\mathcal{L} = C_2^\ell \mathcal{N}_2^\ell + \frac{1}{\Lambda} C_4^\ell \mathcal{N}_4^\ell + \frac{1}{\Lambda} C_9^\ell \mathcal{N}_9^\ell + \frac{4\pi}{\Lambda} C_Z^\ell \mathcal{N}_Z^\ell + \frac{4\pi}{\Lambda} C_\gamma^\ell \mathcal{N}_\gamma^\ell, \tag{5.8}$$

where the last two operators, $\mathcal{N}_Z^\ell$ and $\mathcal{N}_\gamma^\ell$ result from the linear combination of the $\mathcal{N}_{12}^\ell$ and $\mathcal{N}_{13}^\ell$ operators rendering gauge bosons in the mass eigenstate basis, and have the following form

$$\mathcal{N}_Z^\ell(h) \equiv \bar{L}_L \sigma^{\mu\nu} L_R Z_{\mu\nu} \mathcal{F}_Z \,, \tag{5.9}$$

$$\mathcal{N}_\gamma^\ell(h) \equiv \bar{L}_L \sigma^{\mu\nu} L_R F_{\mu\nu} \mathcal{F}_\gamma \,. \tag{5.10}$$

5.1.2.2 $\mu^+\mu^- \to h\gamma$ cross section

Here we compare the results obtained in the SMEFT and HEFT approaches, driven only by the $\mathcal{N}_\gamma^\ell$ operator in eq. (5.10), since all others contribute exclusively to the Z scattering process, as we will derive in the following section.

The differential and total cross section for the $\mu^+\mu^- \to h\gamma$ process, assuming that $\sqrt{s} \gg m_h$, where $\sqrt{s}$ is the collider center-of-mass energy, are given by (θ is the photon scattering angle)

$$\begin{aligned} \frac{d\sigma_{h\gamma}^{\text{HEFT}}}{d\cos\theta} &= \frac{2\pi a_\gamma^2 |C_\gamma^\mu|^2 s \, \sin^2\theta}{v^2\Lambda^2} \,, \\ \sigma_{h\gamma}^{\text{HEFT}} &= \frac{8\pi a_\gamma^2 |C_\gamma^\mu|^2 s}{3v^2\Lambda^2} \,, \end{aligned} \tag{5.11}$$

where one recovers the SMEFT expression by taking $a_\gamma = 1$ and rescaling the HEFT Wilson coefficient:

$$C_\gamma^\mu = \frac{v \, C_{e\gamma}^\mu}{8\pi\sqrt{2}\,\Lambda} \,, \tag{5.12}$$

with $C_{e\gamma}^\mu$ the coefficient in the SMEFT Lagrangian in eq. (5.2).

It should be noted that including a_γ in the HEFT expression introduces an additional

degree of freedom, which—without further constraints—breaks the direct and unambiguous link between low- and high-energy processes. In contrast, in the SMEFT framework, where $a_\gamma = 1$ (since the Higgs is an $SU(2)_L$ doublet), the straightforward relation discussed earlier is preserved.

In order to compare the SMEFT and HEFT approaches, we follow the method used in Ref. [144], where the authors considered a cut-and-count experiment in the $b\bar{b}$ final state ($h \to b\bar{b}$), which has the highest signal yield (with branching ratios $\mathcal{B}(h \to b\bar{b}) = 0.58$ and $\mathcal{B}(Z \to b\bar{b} = 0.15)$). The significance of the signal is defined as $N_S/\sqrt{N_S + N_B}$, with $N_S(N_B)$ the number of signal (background) events. Thus, requiring at least one jet to be tagged as a b, and assuming a plausible b-tagging efficiency, $\epsilon_b = 80\%$, one gets the 95% C.L. reach on the muon anomalous magnetic moment Δa_μ, as a function of the collider center-of-mass energy, $\sqrt{s}$, from the process $\mu^+\mu^- \to h\gamma$. See Ref. [144] for all the details in the SMEFT derivation of this result.

We stress here that the SM irreducible $\mu^+\mu^- \to h\gamma$ background can be neglected for $\sqrt{s} > 1$ TeV, being the $Z\gamma$ events the main source of contamination, where the Z boson is incorrectly reconstructed as a Higgs, as commented in Ref. [144]. For this specific channel we take the central region cut $|\cos\theta| \leq 0.6$, where the significance of the signal is maximized, leading to the following signal and background total decay rates at $\sqrt{s} = 30$ TeV:

$$\sigma^{cut}_{h\gamma} \approx 0.40\,\text{ab}\left(\frac{\Delta a_\mu}{3\times 10^{-9}}\right)^2 a_\gamma^2, \qquad \sigma^{cut}_{Z\gamma} \approx 80.5\,\text{ab}, \tag{5.13}$$

where ab denotes attobarns.

After rescaling the Wilson coefficient, the only difference between the two approaches arises from the a_γ parameter appearing in the HEFT $\mathcal{F}$-function expansion. Following the discussion and limits presented in Ref. [145], the examples below analyze cases with $\frac{1}{5} < a_i \leq 5$, as a first reasonable approximation.

In fig. 5.2, we show the 95% C.L. reach from $\mu^+\mu^- \to h\gamma$ on Δa_μ as a function of the collider energy, assuming that only $\mathcal{N}^\ell_\gamma$ contributes to Δa_μ. The point where the curves and the dashed line intersect shows the specific energy needed to test the presumed NP under the assumption that it generates a contribution of 2.49×10^{-9} to Δa_μ. In the same way, the region below the dashed line is interesting under the assumption that this NP

generates only a partial contribution to the current Δa_μ, which would be equivalent to lowering the dashed line (in case the revised a_μ turns out to be smaller than in ref. [36]). The black line reproduces the SMEFT result, corresponding to $a_\gamma = 1$, and we also show the curves generated when $a_\gamma = 0.2, 0.5, 2$ and 5.

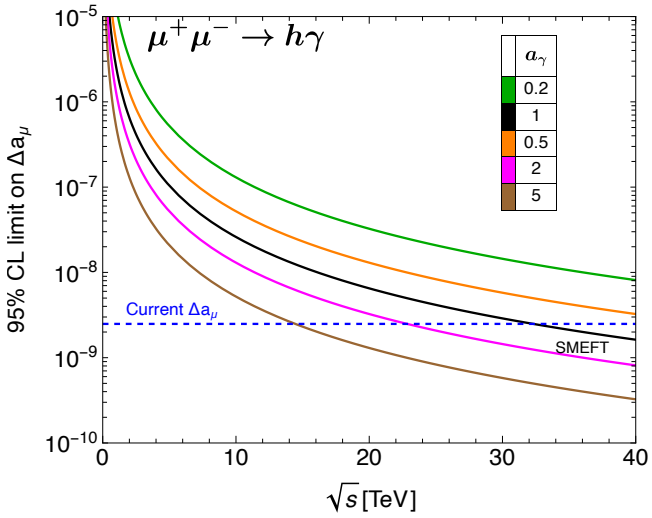

Figure 5.2: 95% C.L. reach on the muon anomalous magnetic moment Δa_μ for operator $\mathcal{N}_\gamma^\ell$ contribution with different a_γ values. In this and later figures, the black curve shows the SMEFT result, corresponding to $a_\gamma = 1$. The dashed line shown as 'Current Δa_μ' displays the 2020 White Paper prediction [36], updated after this work by [43].

Note that for values of $a_\gamma > 1$, the sensitivity to test the g_μ-2 anomaly improves with respect to that in SMEFT. For instance, if we take $a_\gamma = 5$, the 95% C.L. on Δa_μ is reached at a center-of-mass energy of ~ 14 TeV. In SMEFT, a $\sqrt{s} \sim 30$ TeV is needed to test the g-2 anomaly with the desired accuracy. This behavior was already expected, since increasing a_γ means a higher number of signal events.

We want to emphasize that for the SMEFT case, under the assumption that the NP generates a contribution of 2.49×10^{-9} to the Δa_μ, the required muon collider energy is completely fixed in order to generate the desired signal events expected from the unambiguous relation between the low- and high-energy processes. That is why only one SMEFT curve is present in Fig. 5.2. In other words, if the NP contribution to Δa_μ is assumed to really exist, a fixed number of scattering events, generated by the same NP, can be tested at a muon collider with a specific center-of-mass energy, without requiring additional assumptions.

In the HEFT analysis, the above discussion is no longer true, since having an extra degree of freedom, a_γ, modifies the relation between the different processes. Then, it could happen that even if the same NP contribution to Δa_μ is considered, we may not see enough high-energy scattering events ($|a_\gamma| < 1$) or we could get a higher event rate at smaller collider energies ($|a_\gamma| > 1$), as shown in Fig. 5.2. Consequently, the HEFT conclusion will depend on the specific a_γ value.

On the other hand, from a phenomenological perspective, a_γ is expected to be close to the SM prediction, $a_\gamma \approx 1$. Regardless of that, this analysis highlights the need for independent measurements to constrain the value of a_γ. This would ensure an unambiguous relationship between low- and high-energy processes, even within the HEFT framework, allowing for a definitive conclusion.

5.1.2.3 $\mu^+\mu^- \to hZ$ cross section

Using the HEFT Lagrangian, the differential cross sections for the process $\mu^+\mu^- \to hZ$ at $\sqrt{s} \gg m_h$ are (we first give the contributions from squaring the amplitude for each operator and then the only relevant interference):

$$\begin{aligned}
&\bullet \text{ Operator } \mathcal{N}_2^\mu : \ C_2^2 \frac{s \sin^2\theta}{512\pi m_Z^2} . \qquad \bullet \text{ Operator } \mathcal{N}_4^\mu : \ \frac{|C_4|^2}{\Lambda^2} \frac{s^2}{256\pi m_Z^2} . \\
&\bullet \text{ Operator } \mathcal{N}_9^\mu : \ \frac{|C_9|^2}{\Lambda^2} \frac{s^2 \cos^2\theta}{256\pi m_Z^2} . \qquad \bullet \text{ Operator } \mathcal{N}_Z^\mu : \ \frac{|C_Z|^2}{\Lambda^2} \frac{s \sin^2\theta}{32\pi} . \\
&\bullet \text{ Interference } \mathcal{N}_9^\mu - \mathcal{N}_Z^\mu : \ -\frac{\mathrm{Re}\,(C_9^* C_Z)}{\Lambda^2} \frac{s \cos^2\theta}{32\pi} .
\end{aligned} \tag{5.14}$$

This leads to

$$\begin{aligned}
\frac{d\sigma_{\text{HEFT}}}{d\cos\theta} &= \frac{C_2^2 s \sin^2\theta}{512\pi m_Z^2} + \frac{s}{\Lambda^2}\left[\frac{|C_Z|^2 \sin^2\theta}{32\pi} + \frac{|C_4|^2 s}{256\pi m_Z^2} + \frac{|C_9|^2 s \cos^2\theta}{256\pi m_Z^2} - \frac{\mathrm{Re}\,(C_9^* C_Z)\cos^2\theta}{32\pi}\right], \\
\sigma_{\text{HEFT}} &= \frac{C_2^2 s}{384\pi m_Z^2} + \frac{s}{24\pi\Lambda^2}\left[|C_Z|^2 + \frac{3|C_4|^2 s}{16 m_Z^2} + \frac{|C_9|^2 s}{16 m_Z^2} - \frac{\mathrm{Re}\,(C_9^* C_Z)}{2}\right],
\end{aligned} \tag{5.15}$$

where, for simplicity, we have redefined the coefficients as follows

$$C_Z \to \frac{2(4\pi) a_Z}{v} C_Z^\mu, \ C_9 \to \frac{2i a_9}{v} C_9^\mu g_z, \ C_2 \to \frac{-2 a_2}{v} C_2^\mu g_z, \ C_4 \to \frac{2i a_4}{v} C_4^\mu g_z. \tag{5.16}$$

Note that the cross section in eq. (5.15) has the expected energy dimensions after the substitution of the coefficients in eq. (5.16). Furthermore, as shown explicitly in eq. (5.15) for the new HEFT operators, due to the specific energy dependence (where $m_h \ll \sqrt{s} \ll \Lambda$) and its numerical coefficient, the $\mathcal{N}_2$ operator will have the largest contribution, followed by $\mathcal{N}_4$ and $\mathcal{N}_9$ respectively, as will be discussed in detail later.

The interference between operators $\mathcal{N}_2^\ell$-$\mathcal{N}_Z^\ell$, $\mathcal{N}_2^\ell$-$\mathcal{N}_9^\ell$ and $\mathcal{N}_2^\ell$-$\mathcal{N}_4^\ell$ are all proportional to the lepton mass and are therefore negligible in the energy range of interest ($\sqrt{s} \gg m_h$), while the interferences between operators $\mathcal{N}_4^\ell$-$\mathcal{N}_Z^\ell$ and $\mathcal{N}_4^\ell$-$\mathcal{N}_9^\ell$ are identically zero. Also, the result obtained from the operator $\mathcal{N}_Z^\ell$ alone has the same functional form as that obtained in the SMEFT case [144], both related by a rescaling of the Wilson coefficient, $C_Z = \frac{C_{eZ}^\mu}{\sqrt{2}\Lambda}$ (where C_{eZ}^μ is the coefficient in the SMEFT Lagrangian in eq. (5.2)).

We would like to stress that the calculation for the cross sections presented in this paper includes diagrams at tree level only, i.e., at leading-order (LO). For a more precise estimation of our results, one should include next-to-leading order (NLO) corrections. To address this issue, we refer to Ref. [157], which provides a complete analysis of NLO electroweak (EW) corrections and initial-state radiation (ISR) effects in multiple massive boson production processes in a future muon collider. Specifically, for the process $\mu^+\mu^- \to HZ$, they concluded that the overall effect is a decrease in the cross section of $\sim 20\%$ (with respect to the LO result) at $\sqrt{s} \sim 16$ TeV, and an even larger decrease at higher energies. It is also important to note that these results were obtained in a fully inclusive analysis. Therefore, although the general effect should apply approximately to our exclusive calculation, $\mu^+\mu^- \to HZ \to (\bar{b}b)(\bar{b}b)$, a difference in the magnitude of such effect could be expected. The previous discussion is meant to stand out the importance of the NLO corrections for the precise computation of a cross section at high energies.

However, such a detailed estimation is beyond the scope of the present study. We emphasize that our main objective—demonstrating that the HEFT framework is more suitable than SMEFT for exploring new physics related to the muon g-2 at a muon collider [144]—remains valid. As noted earlier, the current experimental precision capable of confirming how the three Goldstone bosons and the massive Higgs scalar are embedded in the SM is only at the level of $\sim 10\%$. Nevertheless, even at leading order, the results of this analysis already highlight potential differences in the 95% C.L. reach on the muon

anomalous magnetic moment Δa_μ, depending on the chosen effective approach.

Now we can give a rough estimate of the new HEFT contributions compared with the SMEFT one. Following the same cut-and-count experimental method outlined previously, together with hadronic decays of the Z ($\mathcal{B}(Z \to \text{had}) = 0.699$), one gets the 95% C.L. reach on the muon anomalous magnetic moment Δa_μ, as a function of the collider center-of-mass energy, $\sqrt{s}$, from the process $\mu^+\mu^- \to hZ$.

Since our main goal is to study the impact of the new HEFT contributions to the possible reach on the muon anomalous magnetic moment, Δa_μ, we must be careful when defining the signal and background events. As done in Ref. [144], the significance of the signal is defined as $N_S/\sqrt{N_T}$, where N_T is the total number of events generated including the possible background $N_T = N_S + N_B$. In this case, the signal events will be due to all operators that generate $\mu^+\mu^- \to hZ$ but also contribute to Δa_μ, where we can directly relate the Wilson coefficient entering the scattering process with the Δa_μ value. All other contributions, including the SM and new HEFT operators, that generate $\mu^+\mu^- \to hZ$ but do not contribute directly to Δa_μ, will be considered as background for the sought signal.

Then, as already discussed, the $\mathcal{N}_2^\ell$, $\mathcal{N}_4^\ell$ and $\mathcal{N}_9^\ell$ operators, which do not contribute to Δa_μ, must be considered as part of the "background" events in order to study the reach from $\mu^+\mu^- \to hZ$ on Δa_μ as a function of the collider energy at a 95% C.L. This is a new challenge compared to the $\mu^+\mu^- \to h\gamma$ case, as HEFT background contributions depend on unknown a_i parameters and Wilson coefficients and therefore the subtraction of these backgrounds would require knowledge of such parameters.

Finally, we assumed that only $\mathcal{N}_Z^\ell$ contributes to Δa_μ [34] and considered the SM irreducible background to be:

$$\sigma_{Zh}^{SM} \approx 122\,\text{ab}\left(\frac{10\,\text{TeV}}{\sqrt{s}}\right)^2. \tag{5.17}$$

The bound on Δa_μ (at a 95% C.L. reach), that could be extracted from the high-energy measurement, in terms of all the HEFT Wilson coefficients, after fixing m_Z, v, g_Z and

[34] This might correspond to an unnatural scenario but is nevertheless meaningful, as explained in Ref. [144].

$\Lambda \approx 100$ TeV, is roughly given by:

$$\Delta a_\mu \approx \frac{10^{-8}}{a_Z}\Bigg\{16a_9\mathrm{Im}(C_9^\mu) + 3.4\Bigg[\frac{1.1}{s^2} + 21a_9^2(\mathrm{Im}(C_9^\mu))^2 + \frac{12}{s}\Big(\frac{3.4}{s^2} + 3.7\times 10^5 a_2^2|C_2^\mu|^2 + s\big\{1.1\times 10^2 a_4^2|C_4^\mu|^2 + 37a_9^2|C_9^\mu|^2\big\}\Big)^{1/2}\Bigg]^{1/2}\Bigg\}, \tag{5.18}$$

where the energy units of each term can be traced following the s (TeV^2) powers.

From a preliminary inspection of eq. (5.18), we can anticipate several properties of the new HEFT terms. For instance, the numerical coefficient suggests that the $\mathcal{N}2$ operator could produce the largest contribution in the energy range of interest, as anticipated from eq. (5.15). Additionally, the explicit global dependence on a_Z implies that sensitivity to a small $\Delta a\mu$ can be achieved more rapidly at a given $\sqrt{s}$ when a_Z is larger, as expected. These properties will be discussed in detail in the following sections.

This can be done systematically considering the new HEFT contributions one-by-one. As a first result, we work only with the $\mathcal{N}_Z^\ell$ operator, which is the same appearing in the SMEFT case. This scenario is analogous to the comparison between SMEFT and HEFT approaches using the $\mathcal{N}_\gamma^\ell$ operator, where after the Wilson coefficient rescaling ($C_Z = \frac{C_{eZ}^\mu}{\sqrt{2}\Lambda}$), the only difference between both frameworks is now due to the "a_Z" parameter that appears in the HEFT $\mathcal{F}$-function expansion. To study its possible effects, we plot the 95% C.L. reach on Δa_μ in Fig. 5.3, considering different "a_Z" values, being $a_Z = 1$ identical to the SMEFT case, shown as the black curve. As we can see, in an optimistic scenario, we find that a value of $\Delta a_\mu = 2.49\times 10^{-9}$ can be tested at 95% C.L. at a 4-7 TeV collider due to the presence of the extra "a_Z" parameter in the HEFT case, instead of the 10 TeV required for the SMEFT analysis. However, as discussed in the last section, this cannot be used as a model-independent probe of the muon g-2 in this context without additional information about a_Z.

Now we can study the effects of the new $\mathcal{N}_2^\mu$, $\mathcal{N}_4^\mu$ and $\mathcal{N}_9^\mu$ operators one by one, together with the $\mathcal{N}_Z^\mu$ contribution, in order to compare it with the SMEFT case. For this purpose, we focus on a new single HEFT contribution at a time, setting the other Wilson coefficients to zero. After that, we plot the 95% C.L. reach on Δa_μ considering reasonable values of the corresponding "a_i" parameter and C_i^μ Wilson coefficient.

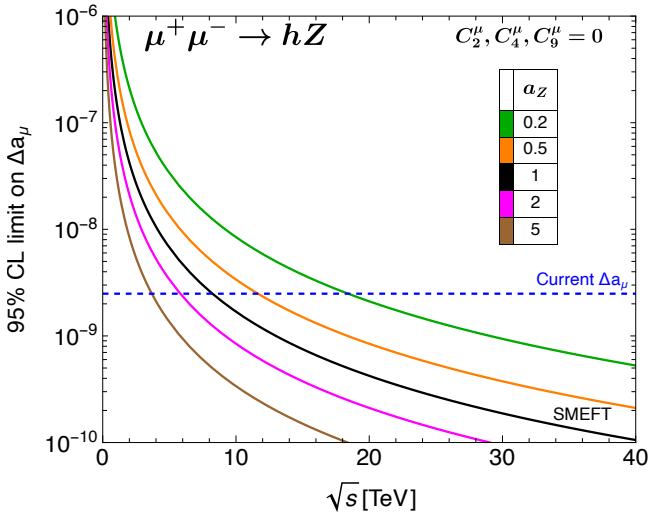

Figure 5.3: 95% C.L. reach on the muon anomalous magnetic moment Δa_μ for operator $\mathcal{N}_Z^\ell$ contribution with different a_Z values. The black curve shows the SMEFT result, corresponding to $a_Z = 1$.

Motivated by the Wilson coefficient rescaling ($C_Z^\mu = \frac{v\ C_{eZ}^\mu}{2(4\pi)\sqrt{2}\Lambda}$), an $\mathcal{O}(1)$ SMEFT Wilson coefficient will imply an $\mathcal{O}(10^{-4} - 10^{-5})$ HEFT coefficient [35] and it would be naturally expected that the other HEFT couplings will be even more suppressed since their counterparts in SMEFT appear as higher dimension operators. Then, even if it is true that the HEFT coefficients are not restricted to have these values, for a first and reasonable approach we shall study the HEFT operators effects considering their Wilson coefficients varying in the range $10^{-5} < C_i^\mu < 10^{-7}$. This assumption, again, is necessary due to the additional degrees of freedom, and precise information about C_i^μ would be crucial for a definite conclusion.

In all the following examples we try to show some limiting cases, for illustrative purposes, where in the left figure we fix the Wilson coefficient and plot the effects of the a_i and a_Z parameters considering their minimum and maximum values. In the right figure the procedure is essentially analogous, fixing $a_i = 1$ in order to see the interplay between the Wilson coefficient and a_Z for their extreme values. In this way, almost all possible cases will be contained in the intermediate region delimited by the outer curves of each graph.

For the $\mathcal{N}_2^\mu$ operator we get Fig. 5.4, being the black curve the SMEFT case. Strictly speaking, one could consider the operator $\mathcal{N}_2^\mu$ as part of the SMEFT approach, up to

[35] This agrees with the current C_2^μ upper-limit [158].

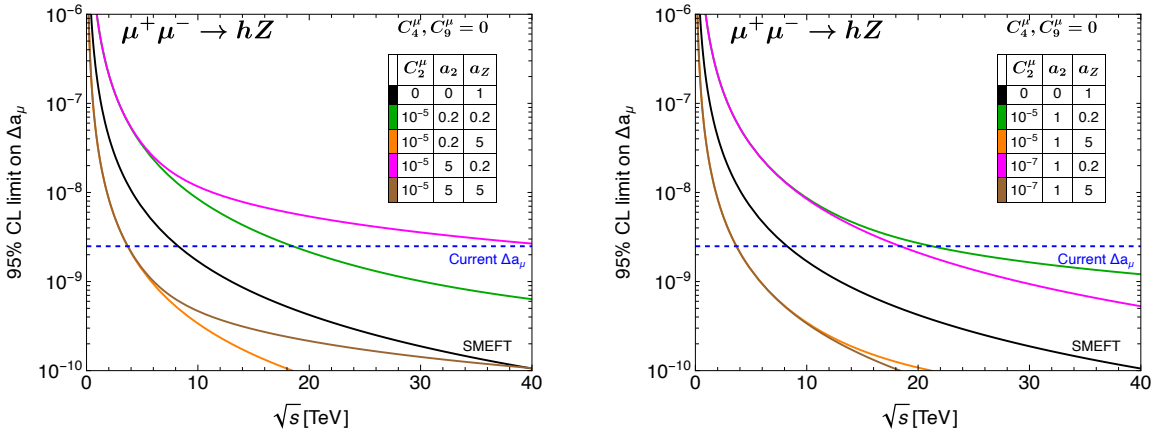

(a) a_2 effect for a fixed C_2^μ Wilson coefficient. **(b)** C_2^μ Wilson coefficient effect for a fixed a_2 value.

Figure 5.4: 95% C.L. reach on the muon anomalous magnetic moment Δa_μ with the $\mathcal{N}_2^\ell$ operator contribution. The black curve shows the SMEFT result.

dimension 6 (as shown in table 5.1). However, incorporating its contribution into the black line in Fig. 5.4 —for all reasonable values of the Wilson coefficient C_2^μ—, does not alter the intersection point between the SMEFT curve (black line) and the current Δa_μ value (dashed blue curve). Therefore, for clarity and simplicity, only a single SMEFT line (that does not include $\mathcal{N}_2^\mu$) is presented in this case, without affecting the overall conclusions.

We find that –even though the $\mathcal{N}_2^\mu$ operator would distort the SMEFT case in almost all scenarios– only a couple of them would be useful to test $\Delta a_\mu = 2.49 \times 10^{-9}$ at a smaller collider energy than that required within the SMEFT approach. Specifically, for a maximum value of a_Z, the collider energy needed could be about 4 TeV, approximately. We also see that smaller C_2^μ and a_2 values could help to increase the Δa_μ sensitivity for a given $a_Z > 1$ value.

This result can be easily understood, since a larger a_Z value together with smaller C_2^μ and a_2 contributions will generate more signal events while decreasing the background ones, respectively, achieving the desired sensitivity at a lower energy scale. If $a_Z < 1$, the signal events are reduced, and if C_2^μ or a_2 get larger, the background increases; in both cases losing sensitivity to Δa_μ, as shown in the plots. Again, the previous discussion holds only if all new HEFT degrees of freedom are well-known, allowing for an unambiguous characterization of HEFT background and signal events. We keep going with the next HEFT operator, $\mathcal{N}_4^\mu$, whose contribution is shown in Fig. 5.5, again for both cases already

explained.

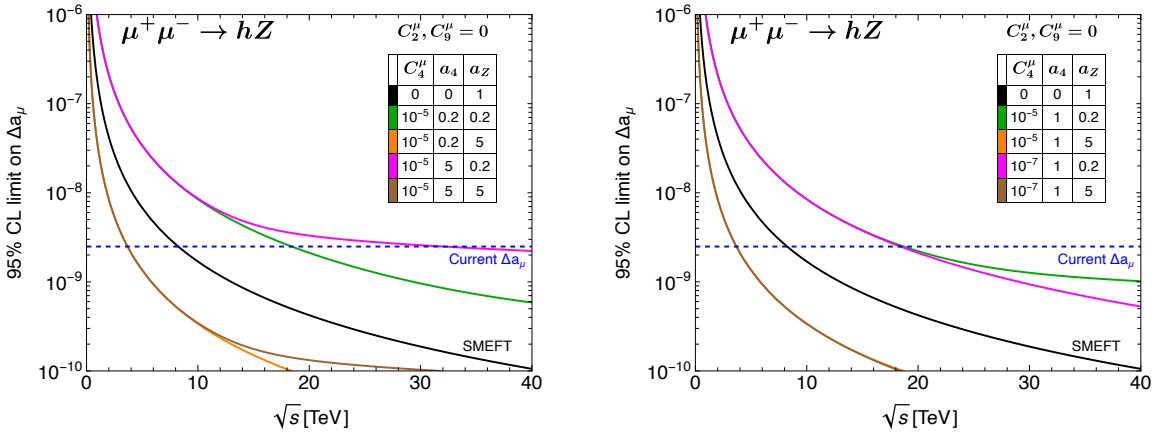

(a) a_4 effect for a fixed C_4^μ Wilson coefficient. **(b)** C_4^μ Wilson coefficient effect for a fixed a_4 value.

Figure 5.5: 95% C.L. reach on the muon anomalous magnetic moment Δa_μ for the operator $\mathcal{N}_4^\ell$ contribution. The black curve shows the SMEFT result.

The results are basically the same. As we can see, the scenarios with larger a_Z values could explore $\Delta a_\mu = 2.49 \times 10^{-9}$ at a 4 TeV collider energy, while other combinations with $a_Z < 1$ and larger $(C_4^\mu,\, a_4)$ values would lose sensitivity to Δa_μ at reduced energies. It is also interesting that there are small differences between the $\mathcal{N}_2^\ell$ and $\mathcal{N}_4^\ell$ contributions, as can be seen directly from the plots, but they do not alter the conclusions of this work. Finally, the same analysis for the last $\mathcal{N}_9^\mu$ operator contribution is displayed in Fig. 5.6, leading to identical conclusions as above. For a last discussion, we plot a set of different

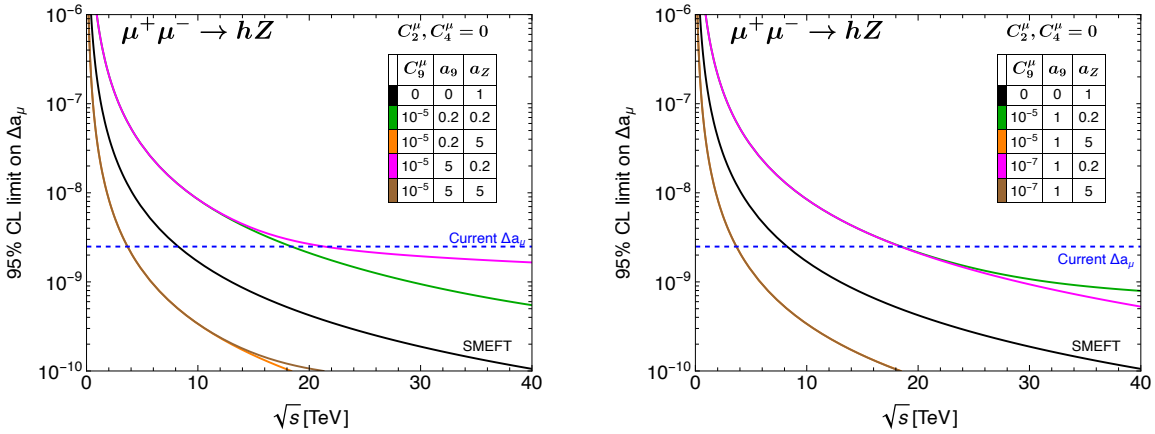

(a) a_9 effect for a fixed C_9^μ Wilson coefficient. **(b)** C_9^μ Wilson coefficient effect for a fixed a_9 value.

Figure 5.6: 95% C.L. reach on the muon anomalous magnetic moment Δa_μ for operator $\mathcal{N}_9^\ell$ contribution. The black curve shows the SMEFT result.

general cases, considering many C_i^μ and a_i values in order to analyze the modification due to the entire HEFT contribution, shown in Fig. 5.7.

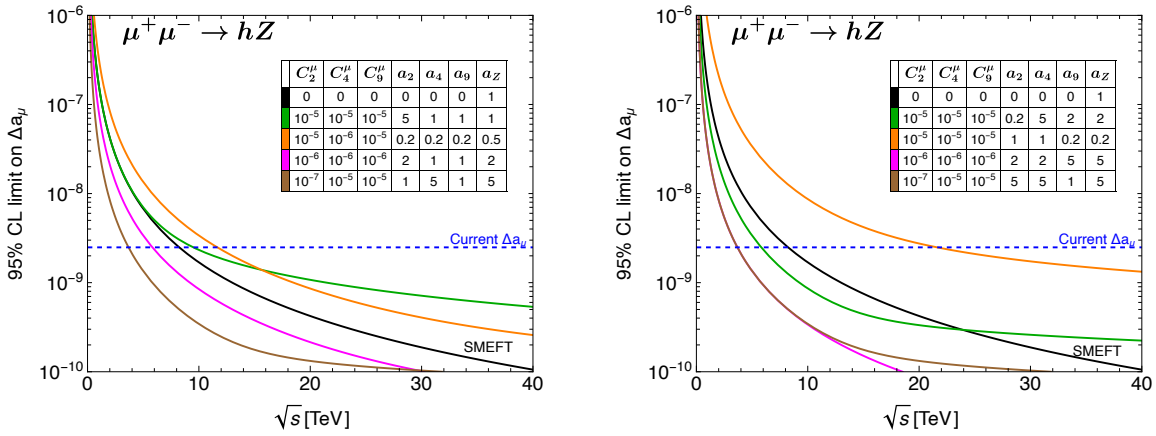

Figure 5.7: 95% C.L. reach on the muon anomalous magnetic moment Δa_μ for all dimension-6 HEFT operators contributions for different sets of C_i^μ Wilson coefficients and a_i values.

Here, it is interesting to note the different behaviors that the HEFT case could induce depending on all the coupling values. Some of them would require a higher center of mass energy to test the g_μ-2 anomaly at 95% C.L. However, there are possible scenarios where the collider energy required is smaller, as shown in Fig. 5.7, that could test the muon anomalous magnetic moment at $\sim 4-7$ TeV collider energy.

Another interesting remark is that, in some cases, one specific configuration of Wilson coefficients and a_i values could lead to a higher sensitivity to Δa_μ in a given energy region but could be worse in other energy range. This is explicitly shown in Fig. 5.7, by the green and orange curves on the left-hand side, or by the green and black ones on the right-hand side. All this shows the different possible behaviors in the general case, agreeing with all the conclusions previously given.

We stress that the results shown in Fig. 5.7 have reasonable values for the C_i^μ Wilson coefficients and a_i parameters. However, experimental data allowing us to constrain them are required, in order to develop a more precise analysis. Specifically, for the case of hZ production- where several new operators can contribute within the HEFT approach without affecting the g_μ-2.

Also, as a complementary computation, in appendix J, we analyze the related Higgs rare

decays as an alternative tool to study new physics effects from the HEFT approach, and discuss the corresponding results.

In summary, the HEFT framework provides a more general approach than SMEFT for probing new physics in the Higgs sector and can give rise to distinct phenomenological scenarios. For example, the previously mentioned discrepancy between the theoretical and experimental values of the muon g-2, which could in principle be tested via $\mu^+\mu^- \to h{+}\gamma/Z$ in SMEFT in a model-independent way, cannot serve as a model-independent probe in the HEFT context due to the presence of additional degrees of freedom.

This is due to the singlet nature of the Higgs in the HEFT, where all interactions involving the physical Higgs boson have independent couplings a_i that cannot be directly related to quantities without the Higgs. Therefore, without precise information about the new degrees of freedom, observing a deviation at high energies would not necessarily confirm a NP contribution to Δa_μ, and the absence of a deviation would not definitively rule it out.

All these discussions are specifically important for the $\mu^+\mu^- \to hZ$ process, where the NP HEFT background contributions could not be subtracted without further knowledge of the unknown parameters. Therefore, complementary measurements are crucial to determine the values of the relevant couplings. This motivates further theoretical and experimental analyses.

Finally, a more realistic study would require a more sophisticated definition of inclusive signals and backgrounds, motivating future work that includes a dedicated discussion of both LO and NLO corrections, particularly in light of potential data from a future muon collider.

5.2 HLbL Proton-Box

Based on [36], motivated by the need for high-precision a_μ calculations, we computed a hadronic contribution to the muon magnetic moment [36]. We calculated the proton-box HLbL contribution to a_μ, the first reported baryonic contribution of this type [5]. This contribution was suggested to be relatively large in some models, such as the Heavy Mass Expansion (HME) approach ($\mathcal{O}(10^{-10})$). By applying a robust formalism derived in the

[36] This observable, and the main aspects of its computation in the SM are briefly reviewed in appendix I.

literature, we computed the corresponding HLbL Master integral for the proton-box case, employing various sets and parametrizations for the required form factors. The analysis was conducted considering both data-driven and lattice form factor results, leading to a suppressed result by two orders of magnitude ($a_\mu^{\text{p-box}} = 1.82(7) \times 10^{-12}$) compared to the initial HME expectation and smaller than the forthcoming uncertainty on a_μ. The origin of this high suppression was investigated in detail and attributed to the damping of the form factors in the regions where the integral kernel peaks.

5.2.1 HLbL Master Formula

A comprehensive review of the HLbL contributions to the muon g-2 anomaly has been presented in Refs. [159], [160], [161]. In these works, the authors derived a master integral that allows the use of unitarity relations to consider individual intermediate states and evaluate their contributions to a_μ^{HLbL} using physical observables, such as on-shell form factors. These form factors can be obtained from phenomenological models, lattice calculations, or parametrizations of experimental data. This framework provides a general description of the electromagnetic tensor involved in the two-loop diagram shown in Fig. 5.8, leading to:

$$a_\mu^{\text{HLbL}} = \frac{2\alpha^3}{3\pi^2} \int_0^\infty dQ_1 \int_0^\infty dQ_2 \int_{-1}^{1} d\tau \sqrt{1-\tau^2}\, Q_1^3\, Q_2^3 \sum_{i=1}^{12} T_i(Q_1, Q_2, \tau) \bar{\Pi}_i(Q_1, Q_2, \tau), \tag{5.19}$$

where $Q_i^2 = -q_i^2$ is the squared four-momentum of the photons in the space-like region and τ is defined by the relation $Q_3^2 = Q_1^2 + Q_2^2 + 2Q_1Q_2\tau$. Moreover, T_i are the 12 independent integral kernels (explicitly shown in Appendix B of Ref.[160]) and $\bar{\Pi}_i$ corresponds to scalar functions that encode all the information of the specific HLbL intermediate-state contribution. Both can be obtained after a decomposition of the light-by-light tensor, following the recipe introduced by Bardeen-Tung-Tarrach (BTT) [162], [163]. [37] Indeed, analytical expressions for $\bar{\Pi}_i$ have been computed for different contributions, such as the pseudo-scalar poles, pseudo-scalar and fermion box-diagrams, etc. [159], [160], [161].

[37] This procedure ensures that the expressions are free of kinematic zeros and singularities, see [159], [160] for details.

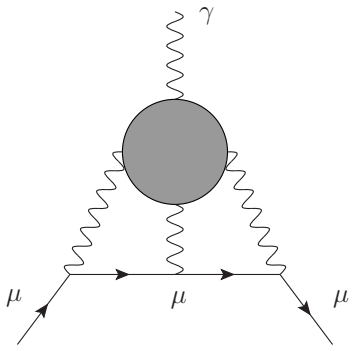

Figure 5.8: General light-by-light contribution to the muon g-2 anomaly.

The aim of this work is to first evaluate the proton-box contribution (Fig.5.9) to a_μ^{HLbL}. For this purpose, we consider the following general nucleon-photon matrix element, consistent with Lorentz and gauge invariance, as well as $\mathcal{P}$ and $\mathcal{CP}$ conservation:

$$\langle p^+(P_2)|J^\mu_{e.m.}(q)|p^+(P_1)\rangle = \bar{u}(P_2)\,\Gamma^\mu(q)u(P_1) \tag{5.20}$$

$$= \bar{u}(P_2)\left(F_1(q^2)\gamma^\mu + i\,\frac{F_2(q^2)}{2\,M_p}\sigma^{\mu\,\nu}q_\nu\right)u(P_1), \tag{5.21}$$

where $F_{1,2}$ are the proton Dirac and Pauli form factors, respectively, and $q = P_2 - P_1$.

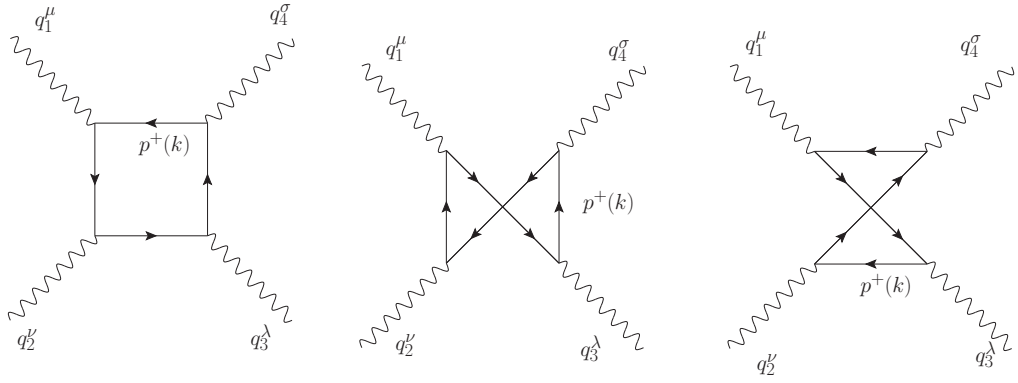

Figure 5.9: Feynman diagrams for light-by-light scattering induced by a proton-box loop (plus the corresponding diagrams with exchanged fermion fluxes inside the loop).

In this analysis, the dominant term in eq. (5.2.1) is the one proportional to $F_1(q^2)$. This arises from the additional q_ν/M_p factor in the tensor vertex, which causes the tensor coupling to be significantly suppressed in the low-momentum transfer regime (below 1 GeV). Consequently, it is a valid approximation to consider only the vector coupling.[38]

[38]This simplification is commonly applied in other processes, such as electron-proton scattering in the same momentum transfer region. Similarly, in the proton-loop contribution to HVP, incorporating a non-zero F_2 modifies the central value by only 0.02%, which remains much smaller than the current uncertainty, consistent with the results reported in Ref. [164].

Conversely, at high photon virtualities (or even above 1 GeV), the $F_2(q^2)$ behavior becomes the suppression factor. In fact, in this case, also the $F_1(q^2)$ and kernel functions are highly damped, making the contributions of this q^2 region negligible. Indeed, due to the asymptotic constrains of the form factors F_1 and F_2 from p-QCD[165], which should behave as $\sim Q^{-4}, Q^{-6}$, respectively (satisfied by construction in both parametrizations employed in this work, as we discuss later), the regime of high-transferred momentum is free of divergences and we do not expect to have any significant error coming from this approximation [39].

Therefore, as a reasonable first approximation, we will consider only the vector coupling in eq. (5.2.1) as input for the scattering amplitude calculation shown in Fig. 5.9. Under this approximation, the scalar functions required in the $a_\mu^{\rm HLbL}$ master integral take the following form:

$$\bar{\Pi}_i = F_1(Q_1^2)F_1(Q_2^2)F_1(Q_3^2)\,\frac{1}{16\pi^2}\int_0^1 dx \int_0^{1-x} dy\, I_i(Q_1, Q_2, \tau, x, y), \tag{5.22}$$

where –for completeness– we write the analytical expressions for the functions I_i required for our analysis, cf. eq. (5.19), where the $\overline{\Pi}_i$ scalar functions enter. These had been obtained in Ref.[161] for a quark box-loop in terms of two Feynman parameters, $0 \leq x \leq 1$

[39] In this sense, we have: $\Gamma^\mu(q)|_{q\to\infty} = \gamma^\mu\, A\, q^{-4} + i\, B\, \sigma^{\mu\nu}\hat{q}_\nu (2\, q^5\, M_p)^{-1}$, with $\hat{q}_\nu \equiv q_\nu/q$ a normalized four-vector and A and B being constants.

and $0 \leq y \leq 1-x$. We confirm the results in [160] [40]

$$I_1 = -\frac{16x(1-x-y)}{\Delta_{132}^2} - \frac{16xy(1-2x)(1-2y)}{\Delta_{132}\Delta_{32}}, \tag{5.23}$$

$$I_3 = \frac{32xy(1-2x)(x+y)(1-x-y)^2(q_1^2-q_2^2+q_3^2)}{\Delta_{312}^3} - \frac{32(1-x)x(x+y)(1-x-y)}{\Delta_{312}^2} - \frac{32xy(1-2x)(1-2y)}{\Delta_{312}\Delta_{12}}, \tag{5.24}$$

$$I_5 = -\frac{64xy^2(1-x-y)(1-2x)(1-y)}{\Delta_{132}^3}, \tag{5.25}$$

$$I_9 = -\frac{32x^2y^2(1-2x)(1-2y)}{\Delta_{312}^2\Delta_{12}}, \tag{5.26}$$

$$I_{10} = \frac{64xy(1-x-y)((2x-1)y^2+xy(2x-3)+x(1-x)+y)}{\Delta_{132}^3}, \tag{5.27}$$

$$I_{12} = -\frac{16xy(1-x-y)(1-2x)(1-2y)(x-y)}{\Delta_{312}\Delta_{12}}\left(\frac{1}{\Delta_{312}}+\frac{1}{\Delta_{12}}\right), \tag{5.28}$$

where $\Delta_{ijk} = m^2 - xyq_i^2 - x(1-x-y)q_j^2 - y(1-x-y)q_k^2$ and $\Delta_{ij} = m^2 - x(1-x)q_i^2 - y(1-y)q_j^2$. The rest of scalar functions, entering the master formula, can be obtained from q_i permutations, as follows:

$$\begin{aligned} &\bar{\Pi}_2 = \mathcal{C}_{23}[\bar{\Pi}_1], \quad \bar{\Pi}_4 = \mathcal{C}_{23}[\bar{\Pi}_3], \quad \bar{\Pi}_6 = \mathcal{C}_{12}[\mathcal{C}_{13}[\bar{\Pi}_5]], \\ &\bar{\Pi}_7 = \mathcal{C}_{23}[\bar{\Pi}_5], \quad \bar{\Pi}_8 = \mathcal{C}_{13}[\bar{\Pi}_9], \quad \bar{\Pi}_{11} = -\mathcal{C}_{23}[\bar{\Pi}_{12}], \end{aligned} \tag{5.29}$$

where the crossing operators C_{ij} exchange momenta and Lorentz indices of the photons i and j.

The only difference between the expression above and that reported in [161] for the quark-box loop is the inclusion of the vector form factors $F_1(Q^2)$ and the absence of the global quark factor $N_C Q_q^4$ in the Feynman parameter integrals of eq. (5.22).

A preliminary analysis reveals that the full integral kernel $\sqrt{1-\tau^2}\, Q_1^3\, Q_2^3 T_i \bar{\Pi}_i$, [41] without accounting for any form factor, primarily contributes to the overall integral at low momentum transfers (below 1 GeV), as illustrated by the density plot in Fig. 5.10 for three different τ values. Furthermore, the vector proton form factors term alone

[40] In ref. [161] the I_i functions multiply the $\hat{\Pi}_i$ functions. The relation between both bases is given in eq. (2.22) of ref. [160]. Specifically, our $I_{1,3,5,9,10,12}$ correspond, respectively, to the $I_{1,4,7,17,39,54}$ in the tilded basis.

[41] The explicit dependence of T_i and $\bar{\Pi}_i$ on Q_1, Q_2 and τ has been omitted and the Einstein sum notation is understood.

$F_1(Q_1^2)F_1(Q_2^2)F_1(Q_3^2)$, [42] acquires its maximum value within the same momenta region, as shown by the contour curves in the figure. Finally, due to the mismatch between the kernels and the maximum values of the form factors, a significant reduction in the HME approximation is expected. We will discuss this effect in more detail in the following sections.

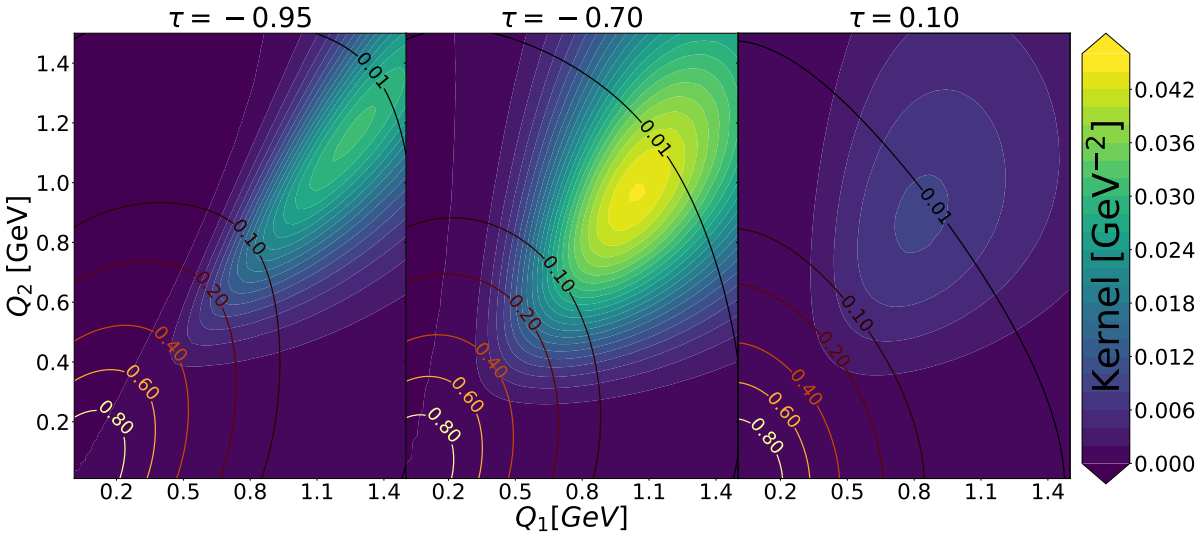

Figure 5.10: Integral kernel (density plot) versus form factors dependence (contour plot) at relevant different virtualities for the off-shell photons, as described in the text.

5.2.2 Proton Form Factors

To obtain an accurate estimate of the leading contribution of the proton-box to a_μ^{HLbL}, we numerically compute the master integral in eq. (5.19) using two different descriptions of the form factors. The first approach is data-driven [166], while the second relies on lattice QCD calculations [167]. In both cases, fitted parametrizations of the proton electric (G_E) and magnetic (G_M) form factors are used, which are related to the Dirac and Pauli form factors through:

$$G_E(Q^2) = F_1(Q^2) - \frac{Q^2}{4M_p^2} F_2(Q^2), \tag{5.30}$$

$$G_M(Q^2) = F_1(Q^2) + F_2(Q^2). \tag{5.31}$$

[42] Evaluated using the dependence on Q^2 as a z-expansion (setup 1).

5.2.2.1 Setup 1: Data-Driven Form Factors

First, we make use of the electric and magnetic form factors obtained in Ref.[166] after fitting the experimental data to a z-expansion parametrization of order 12 [168], where sum-rule constraints were applied on each form factor to warrant the asymptotic scaling $G_{E,M} \sim Q^{-4}$ and the correct normalization at null photon virtuality. [43] Both systematic and statistical uncertainties were taken into account in the computation of these form factors, which we implemented in our analysis. Consequently, the proton form factors can be expressed as:

$$G_E^{(p)}(Q^2),\ \frac{G_M^{(p)}(Q^2)}{\mu_p} = \sum_{i=0}^{12} a_i^{\{E,M\}} z^i, \tag{5.32}$$

where a_i are fitting parameters shown in table 5.2, and z is defined as follows:

$$z \equiv \frac{\sqrt{t_{\rm cut} + Q^2} - \sqrt{t_{\rm cut} - t_0}}{\sqrt{t_{\rm cut} + Q^2} + \sqrt{t_{\rm cut} - t_0}}, \tag{5.33}$$

with $t_0 = -0.7$ GeV^2, $t_{\rm cut} = 4m_\pi^2$ and the form factors normalization fixed by the proton's electric charge non-renormalization and magnetic moment in Bohr magneton units, $G_E^p(0) = 1$ and $G_M^p(0) = \mu_p = 2.793$, in turn.

	E	M
a_0^X	0.239163298067	0.264142994136
a_1^X	−1.109858574410	−1.095306122120
a_2^X	1.444380813060	1.218553781780
a_3^X	0.479569465603	0.661136493537
a_4^X	−2.286894741870	−1.405678925030
a_5^X	1.126632984980	−1.356418438880
a_6^X	1.250619843540	1.447029155340
a_7^X	−3.631020471590	4.235669735900
a_8^X	4.082217023790	−5.334045653410
a_9^X	0.504097346499	−2.916300520960
a_{10}^X	−5.085120460510	8.707403067570
a_{11}^X	3.967742543950	−5.706999943750
a_{12}^X	−0.981529071103	1.280814375890

Table 5.2: z-expansion proton form factor fitted parameters, taken from Ref.[166].

[43] Other parametrizations, as the ones reported in Refs.[169], [170], have been considered for the $a_\mu^{\rm p-box}$ numerical evaluation, being consistent with the one used in this work within less than 1σ.

5.2.2.2 Setup 2: Lattice QCD Form Factors

A second approach, which is also worth to consider, is a lattice QCD motivated computation of $a_\mu^{\mathrm{p-box}}$. In [167], the Lattice data for the form factors can be parametrized using a simple dipole approximation: [44]

$$G^{\{E,M\}}(Q^2) = G^{\{E,M\}}(0)/(1+Q^2/\Lambda)^2, \tag{5.34}$$

where Λ –which has energy squared dimension– is related to the electric and magnetic radii by $\Lambda = 12/\langle r^2_{\{E,M\}}\rangle$ and the normalization is $G_E(0) = 1$ and $G_M(0) = \mu_p$. It is important to remark that this parametrization automatically fulfills the QCD-ruled asymptotic behavior for large values of Q^2. The numerical values required in eq.(5.34) are shown in table 5.3, where the normalization at null photon virtuality is automatically fulfilled for the electric form factor by setting $G_E^p(0) \to 1$. As discussed in [167], the electric r.m.s. radius is underestimated due to the slower decay of the electric form factor. Additionally, the proton's magnetic moment is underestimated, which may result from a combination of residual finite-volume effects and multi-hadron contributions.

$\sqrt{\langle r_E^2\rangle}$[fm]	$\sqrt{\langle r_M^2\rangle}$ [fm]	μ_p
$0.742 \pm 0.013 \pm 0.023$	$0.710 \pm 0.026 \pm 0.086$	$2.43 \pm 0.09 \pm 0.04$

Table 5.3: Numerical values of eq.(5.34) according to Ref.[167]. The uncertainties stand for the statistic and systematic errors, respectively.

As we show in Fig.5.11, the z-expansion reported in [166] is in good agreement with the data set of $G_M(Q^2)$ and $G_E(Q^2)$ from [170] extracted from the world's data on elastic electron-proton scattering and calculations of two-photon exchange effects. We also compared the former fit and the one obtained from Lattice QCD results with a $N_f = 2+1+1$ ensemble, reported in Ref.[167]. Finally, due to the small deviations between the two data sets, in the $Q^2 < 1\,\mathrm{GeV}^2$ region, it seems interesting to analyze both frameworks separately during the numerical evaluation of eq.(5.19).

[44] A z-expansion was performed as well, but no significant difference was found with respect to the simple dipole approximation.

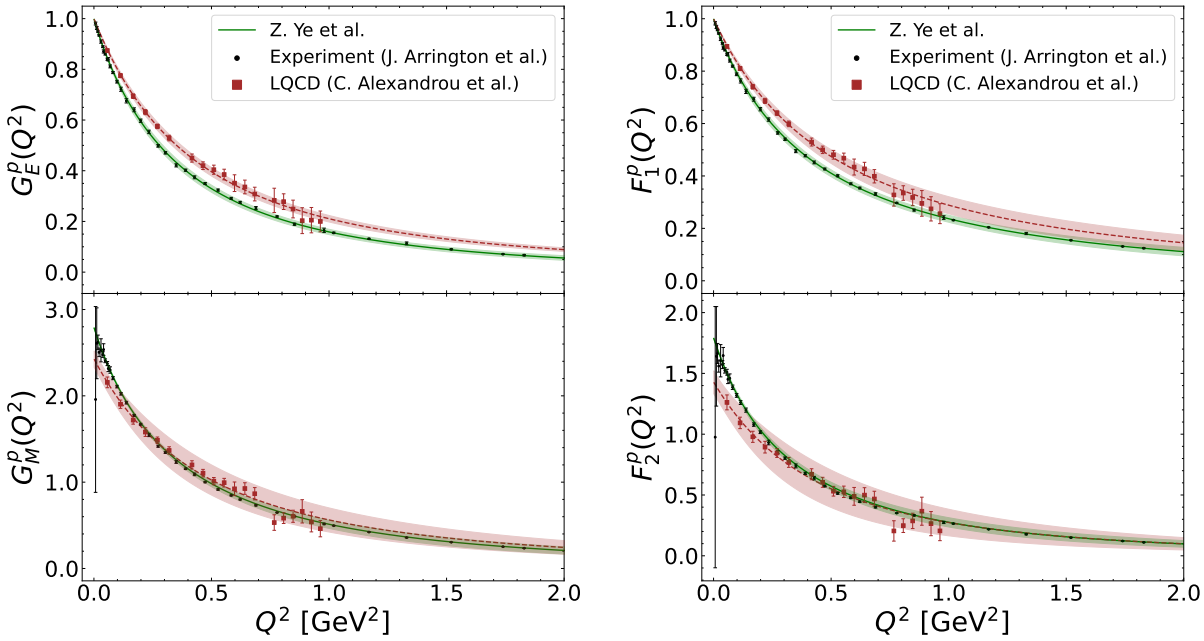

Figure 5.11: G_E and G_M (F_1 and F_2) proton form factors. In black we show the experimental points taken from Ref.[166], meanwhile, red dots correspond to the Lattice QCD results of Ref.[167].

5.2.3 Proton-Box Contribution

In order to obtain the explicit a_μ^{HLbL} contribution via the master integral, we implemented a numerical evaluation, using the VEGAS algorithm [171], [172].

As an initial consistency check of our integration method, we successfully reproduced all previously well-established results, including the π-pole, π-box, and c-loop contributions. In particular, we verified that using the quark-loop scalar functions without any form factors yields the same result as the HME approximation for the proton case, obtaining a central value of 9.4×10^{-11}, in agreement with the HME estimate of 9.7×10^{-11}.

Once the corresponding vector form factor $F_1(Q^2)$ is included in the analysis, we get the following results for the different setups described above: [45]

$$a_\mu^{\text{p-box}} = 1.82(7) \times 10^{-12} \quad \textbf{(Setup 1)}, \tag{5.35}$$

$$a_\mu^{\text{p-box}} = 2.38(16) \times 10^{-12} \quad \textbf{(Setup 2)}, \tag{5.36}$$

[45] Using a different parametrization [169] of the same data, as the setup 1, a result of $a_\mu^{\text{p-box}}$=1.79(5)×10^{-12} was found, consistent with the results using [166].

where both the systematic and statistic uncertainties were considered in order to estimate the error for each setup.

As previously discussed, the numerical suppression observed in the final result, compared to the HME approximation, can be directly attributed to the interplay between the kernel and the form factors, as illustrated in Fig. 5.10. In this context, we highlight their behavior as a function of τ in three distinct regions:

- Close to ± 1, the $\sqrt{1-\tau^2}$ factor suppresses the values of the integral kernel.
- As τ increases, Q_3 does as well, and the T_i decrease [160], causing the kernel to start diluting after its maximum value is reached, and to be almost negligible for positive values of τ.
- The maximum values of the integration kernel appear in $\tau \in [-0.85, -0.65]$, as shown in the supplementary material of the paper [5]. For this value of τ, the relevant region of the kernel and the effect of the form factors in the numerical evaluation of eq. (5.19) can be analyzed.

Indeed, the region where the integral kernel reaches its maximum contribution lies between the values of 0.1 and 0.01 of the form factors term, $F_1(Q_1^2)F_1(Q_2^2)F_1(Q_3^2)$ for all values of τ. [46] Since the HME treats the proton as a point-like particle, the integrand in eq. (5.19) is expected to be one to two orders of magnitude smaller compared to the structureless case. This mismatch between the peak positions of the kernels and the form factors provides a clear and consistent explanation for the observed numerical integration results.

In the case of setup 1, both errors were computed for $F_1^p(Q^2)$ for each value of Q^2 as discussed in [166], and these $\Delta F_1^p(Q^2)$ were used for the error propagation of eq. (5.19) considering the structure of eq. (5.22) in terms of the form factors. For the setup 2, a numerical computation of the Jacobian matrix of eq. (5.19) within this setup was performed, and it was combined to obtain both the statistical and the systematic error by assuming a maximal correlation of the magnetic form factor parameters.[47]

Even though there is an underestimation of μ_p using a lattice QCD form factor, the slower decay of G_E^p compared with the data-driven one compensates for this, and it results

[46] Despite Fig. 5.10 results are presented for just three τ values. A .mp4 file showing the same behavior for all the τ-range is added as supplementary material of [5].

[47] The uncertainty associated with the numerical integration method is subleading, of order $\mathcal{O}(10^{-15})$.

in a higher $F_1^p(Q^2)$ for the lattice QCD result, as explained in Ref.[167] and visible in Fig. 5.11. Consequently, the setup 2 result for $a_\mu^{\text{p-box}}$ is larger than the one of the first setup. Therefore, in this work, we will adopt the data-driven $a_\mu^{\text{p-box}}$ approximation as our central value, awaiting more precise lattice results anticipated in the near future.

As a summary, since the hadronic light-by-light scattering is expected to soon dominate the theory uncertainty in a_μ, a detailed analysis of its various contributions has become an important task. Specifically, the proton-box contribution to the HLbL piece of a_μ –computed as a good approximation in this work for the first time– yields an estimate of $a_\mu^{\text{p-box}} = 1.82(7)\times10^{-12}$, two orders of magnitude smaller than the forthcoming uncertainty on the a_μ measurement.

Finally, as previously discussed, achieving a more precise result would require a complete description of the scalar functions, including the contribution from the tensor vertex. Incorporating the $F_2(Q^2)$ form factor—which is expected to be subdominant compared to the vector term weighted by $F_1(Q^2)$—would improve the analysis and enable its extension to other baryons with well-characterized form factors, such as the neutron, for which the F_1 contribution vanishes.

Chapter 6

Work in progress

In this chapter, we provide a brief summary of two ongoing projects, which we anticipate will lead to published articles in the near future. Both of them are again an application of EFTs in the search of possible new physics in specific processes.

The first one consists in a detailed study of a τ decay into a charged lepton and two invisible particles $\tau \to \ell\alpha\alpha$. Experimentally, these invisible particles—denoted as α—are typically assumed to be standard model neutrinos. The corresponding energy and angular distributions, known as the Michel spectrum, were previously analyzed in Ch.4.1. However, it remains an intriguing possibility that the invisible particles could be of a different nature, such as spinless fields potentially connected to dark matter or other new physics scenarios (generally, α may not be its own antiparticle, which needs to be accounted for). This motivates a thorough investigation into how such alternative interpretations could alter the observable energy and angular distributions, offering a novel probe of physics beyond the Standard Model.

In this context, we are currently computing the relevant observables for the decay process $\tau \to \ell\alpha\alpha$, under the assumption that the invisible particles α are spinless and undetectable. The goal is to compare these results with the standard Michel distribution and analyze potential deviations or distinctive signatures that could arise. Such a comparison may provide a means to experimentally distinguish between the standard neutrino case and alternative scenarios involving new physics.

The second project involves an effective field theory analysis of the exclusive decays $\tau^- \to VP^-\nu_\tau$ decays, where V and P denote a narrow vector [48] and a pseudoscalar meson, respectively. In these processes, the presence of NP could lead to non-trivial modifications of the energy and angular distributions of the final-state particles. In principle, precise measurements of these observables can be used to constrain the corresponding NP couplings

[48] For the ρ meson one would need to analyze the corresponding $\pi\pi$ decay products, with invariant mass around M_ρ (accounting for its width), instead.

in a model-independent framework.

To this end, we are analyzing these observables, complementing the study with additional tools such as Dalitz plot distributions and global fits. Through this comprehensive approach, our ultimate objective is to derive updated constraints on the NP couplings that appear in the effective Hamiltonian, using currently available experimental data.

These two projects constitute our current research focus, and we are actively working toward their completion and eventual publication.

Chapter 7

Summary and Conclusions

The existence of several physical phenomena that remain unexplained within the Standard Model (SM) continues to motivate the search for new physics (NP). Among these, leptonic decay processes offer a particularly clean and precise testing ground for probing the internal consistency of the SM and for uncovering possible signatures of NP. Likewise, the anomalous magnetic moment of the muon (muon $g-2$) remains a compelling case for further investigation through precision tests.

In this thesis, we have employed effective field theory (EFT) frameworks to study neutrino phenomenology and to explore the implications of NP for the muon $g-2$ anomaly. A key focus has been the precise computation of hadronic light-by-light (HLbL) contributions to the muon $g-2$ within the SM. Additionally, we have identified alternative processes and potential measurements that could complement or enhance ongoing efforts in the search for NP and help elucidate fundamental questions, including the nature of neutrinos.

We have investigated the processes $\ell^- \longrightarrow \ell'^- \bar{\nu}_{\ell'} \nu_\ell$ and $\nu e \to \nu e$, constructing their matrix elements using the most general four-lepton effective interaction Hamiltonian. This allowed us to derive detailed energy and angular distributions of the final charged leptons, incorporating polarization effects and the distinctions arising from Dirac versus Majorana neutrino masses. Our analysis generalizes previous results and enables their application in model-dependent contexts, providing a framework to potentially distinguish between Dirac and Majorana neutrino scenarios.

To estimate the impact of neutrino mass–dependent contributions, we used stringent experimental constraints on invisible heavy neutrinos. Our results indicate that, in most scenarios, these contributions are several orders of magnitude below the sensitivity of current and near-future experiments. Nevertheless, there exist allowed regions in parameter space where some heavy mass ranges together with a non-negligible heavy-light mixing contributions could approach current experimental sensitivity. For instance, in the case of τ decays with a single heavy final-state neutrino in the $100-1000$ MeV range, the

linear suppression factor could be of order 10^{-4} , potentially within reach of upcoming experiments. A similar conclusion holds for tau neutrino scattering processes at neutrino energies of $100 - 1000$ MeV and a heavy neutrino mass of order $100 - 400$ MeV.

We also studied the radiative decay process $\ell^- \to \ell'^- \nu_\ell \bar{\nu}_{\ell'} \gamma$, where a back-to-back (b2b) kinematic configuration might evade constraints imposed by the DMCT. This initially suggested promising differences between the Dirac and Majorana cases, not suppressed by tiny neutrino masses. However, a thorough analysis revealed that, once the undetectable neutrino angle is integrated out, the energy and angular distributions become indistinguishable between the Dirac and Majorana cases. We provided a detailed discussion of the angular analysis and clarified why earlier interpretations may have been misleading, potentially yielding incorrect expectations about observable differences.

These results reinforce the importance of ongoing searches for new neutrino interactions and the exploration of possible heavy sectors, both of which remain at the forefront of research in this dynamic field.

Regarding the muon $g - 2$, we first analyzed the contributions from NP within the Higgs Effective Field Theory (HEFT) formalism. Unlike SMEFT, HEFT provides a more general framework for exploring NP in the Higgs sector and can give rise to qualitatively distinct phenomenological signatures. Notably, the observed deviation in the muon $g - 2$ —while potentially testable in processes such as $\mu^+\mu^- \to h\ \gamma/Z$ within SMEFT— cannot serve as a model-independent probe in the HEFT framework. This limitation arises because the Higgs in HEFT is treated as a singlet, with all interactions involving the physical Higgs characterized by independent couplings a_i, which cannot be directly related to observables that do not involve the Higgs. Consequently, deviations observed at high energies would not unambiguously confirm a NP contribution to Δa_μ, nor would their absence definitively rule it out.

Finally, we presented an estimation of the proton-box contribution to the HLbL component of a_μ. Employing various parameterizations of the proton form factors and applying the master formula with appropriate scalar functions, our data-driven approach yields a consistent result:

$$a_\mu^{\text{p-box}} = 1.82(7) \times 10^{-12}. \tag{7.1}$$

We discussed the implications of different modeling approaches and emphasized the need for further refinement. In particular, a more precise determination would require a complete description of the scalar functions, including the tensor vertex contributions. Incorporating the $F_2(Q^2)$ form factor —which, though subdominant compared to the vector term scaled by $F_1(Q^2)$, might still be important in some cases— will improve the accuracy of the analysis. This methodology could also be extended to other baryons with well-characterized form factors, such as the neutron, where the $F_1(Q^2)$ term vanishes trivially.

In summary, the results presented in this thesis contribute to a deeper understanding of neutrino properties and muon $g-2$ phenomenology, highlighting both the promise and the limitations of current theoretical tools in the ongoing search for physics beyond the Standard Model.

References

[1] J. M. Márquez, G. L. Castro, and P. Roig, "Michel parameters in the presence of massive Dirac and Majorana neutrinos," *JHEP*, vol. 11, p. 117, 2022. DOI: 10.1007/JHEP11(2022)117. arXiv: 2208.01715 [hep-ph].

[2] J. M. Márquez, P. Roig, and M. Salinas, "νE $\to$ νe scattering with massive dirac or majorana neutrinos and general interactions," *JHEP*, vol. 05, p. 227, 2024. DOI: 10.1007/JHEP05(2024)227. arXiv: 2401.14305 [hep-ph].

[3] J. M. Márquez, D. Portillo-Sánchez, and P. Roig, "Dirac-Majorana neutrinos distinction in four-body decays," *Phys. Rev. D*, vol. 109, no. 3, p. 033 005, 2024. DOI: 10.1103/PhysRevD.109.033005. arXiv: 2305.14140 [hep-ph].

[4] F. Fortuna, J. M. Márquez, and P. Roig, "HEFT approach to investigate the muon g-2 anomaly at a muon collider," *Phys. Rev. D*, vol. 111, no. 7, p. 075 012, 2025. DOI: 10.1103/PhysRevD.111.075012. arXiv: 2408.16954 [hep-ph].

[5] E. J. Estrada, J. M. Márquez, D. Portillo-Sánchez, and P. Roig, "Proton-box contribution to aμHLbL," *Phys. Rev. D*, vol. 111, no. 9, p. 093 008, 2025. DOI: 10.1103/PhysRevD.111.093008. arXiv: 2411.07115 [hep-ph].

[6] S. L. Glashow, "Partial Symmetries of Weak Interactions," *Nucl. Phys.*, vol. 22, pp. 579–588, 1961. DOI: 10.1016/0029-5582(61)90469-2.

[7] S. Weinberg, "A Model of Leptons," *Phys. Rev. Lett.*, vol. 19, pp. 1264–1266, 1967. DOI: 10.1103/PhysRevLett.19.1264.

[8] A. Salam, "Weak and Electromagnetic Interactions," *Conf. Proc. C*, vol. 680519, pp. 367–377, 1968. DOI: 10.1142/9789812795915_0034.

[9] S. Navas et al., "Review of particle physics," *Phys. Rev. D*, vol. 110, no. 3, p. 030 001, 2024. DOI: 10.1103/PhysRevD.110.030001.

[10] A. Pich, "Precision Tau Physics," *Prog. Part. Nucl. Phys.*, vol. 75, pp. 41–85, 2014. DOI: 10.1016/j.ppnp.2013.11.002. arXiv: 1310.7922 [hep-ph].

[11] A. Pich, "Precision tests of the standard model," in *25th International Meeting on Fundamental Physics*, Nov. 1997, pp. 1–30. arXiv: hep-ph/9711279.

[12] T. P. Gorringe and D. W. Hertzog, "Precision Muon Physics," *Prog. Part. Nucl. Phys.*, vol. 84, pp. 73–123, 2015. DOI: 10.1016/j.ppnp.2015.06.001. arXiv: 1506.01465 [hep-ex].

[13] W. Rodejohann, "Neutrino-less Double Beta Decay and Particle Physics," *Int. J. Mod. Phys. E*, vol. 20, pp. 1833–1930, 2011. DOI: 10.1142/S0218301311020186. arXiv: 1106.1334 [hep-ph].

[14] J. D. Vergados, H. Ejiri, and F. Simkovic, "Theory of Neutrinoless Double Beta Decay," *Rept. Prog. Phys.*, vol. 75, p. 106 301, 2012. DOI: 10.1088/0034-4885/75/10/106301. arXiv: 1205.0649 [hep-ph].

[15] M. J. Dolinski, A. W. P. Poon, and W. Rodejohann, "Neutrinoless Double-Beta Decay: Status and Prospects," *Ann. Rev. Nucl. Part. Sci.*, vol. 69, pp. 219–251, 2019. DOI: 10.1146/annurev-nucl-101918-023407. arXiv: 1902.04097 [nucl-ex].

[16] G. Hernández-Tomé, J. I. Illana, M. Masip, G. López Castro, and P. Roig, "Effects of heavy Majorana neutrinos on lepton flavor violating processes," *Phys. Rev. D*, vol. 101, no. 7, p. 075 020, 2020. DOI: 10.1103/PhysRevD.101.075020. arXiv: 1912.13327 [hep-ph].

[17] G. Hernández-Tomé, G. L. Castro, and D. Portillo-Sánchez, "ΔL=2 hyperon decays induced by majorana neutrinos and doubly charged scalars," *Phys. Rev. D*, vol. 105, no. 11, p. 113 001, 2022. DOI: 10.1103/PhysRevD.105.113001. arXiv: 2112.02227 [hep-ph].

[18] G. Hernández-Tomé, D. Portillo-Sánchez, and G. Toledo, "Resonant Majorana neutrino effects in ΔL=2 four-body hyperon decays," *Phys. Rev. D*, vol. 107, no. 5, p. 055 042, 2023. DOI: 10.1103/PhysRevD.107.055042. arXiv: 2212.03994 [hep-ph].

[19] A. Ilakovac, "Probing lepton number / flavor violation in semileptonic τ decays into two mesons," *Phys. Rev. D*, vol. 54, pp. 5653–5673, 1996. DOI: 10.1103/PhysRevD.54.5653. arXiv: hep-ph/9608218.

[20] G. Lopez Castro and N. Quintero, "Lepton number violating four-body tau lepton decays," *Phys. Rev. D*, vol. 85, p. 076 006, 2012, [Erratum: Phys.Rev.D 86, 079904 (2012)]. DOI: 10.1103/PhysRevD.85.076006. arXiv: 1203.0537 [hep-ph].

[21] C. S. Kim, G. López Castro, and D. Sahoo, "Discovering intermediate mass sterile neutrinos through $\tau^- \to \pi^-\mu^-e^+\nu$ (or $\bar{\nu}$) decay," *Phys. Rev. D*, vol. 96, no. 7, p. 075 016, 2017. DOI: 10.1103/PhysRevD.96.075016. arXiv: 1708.00802 [hep-ph].

[22] N. Quintero, G. Lopez Castro, and D. Delepine, "Lepton number violation in top quark and neutral B meson decays," *Phys. Rev. D*, vol. 84, p. 096 011, 2011, [Erratum: Phys.Rev.D 86, 079905 (2012)]. DOI: 10.1103/PhysRevD.84.096011. arXiv: 1108.6009 [hep-ph].

[23] H. Novales-Sánchez, M. Salinas, and J. J. Toscano, "About heavy neutrinos: Lepton-flavor violation in decays of charged leptons," *J. Phys. G*, vol. 45, no. 9, p. 095 004, 2018. DOI: 10.1088/1361-6471/aad53c. arXiv: 1710.08474 [hep-ph].

[24] A. J. Long, C. Lunardini, and E. Sabancilar, "Detecting non-relativistic cosmic neutrinos by capture on tritium: phenomenology and physics potential," *JCAP*, vol. 08, p. 038, 2014. DOI: 10.1088/1475-7516/2014/08/038. arXiv: 1405.7654 [hep-ph].

[25] C. Lunardini and Y. F. Perez-Gonzalez, "Dirac and Majorana neutrino signatures of primordial black holes," *JCAP*, vol. 08, p. 014, 2020. DOI: 10.1088/1475-7516/2020/08/014. arXiv: 1910.07864 [hep-ph].

[26] X. Luo, W. Rodejohann, and X.-J. Xu, "Dirac neutrinos and N_{eff}. Part II. The freeze-in case," *JCAP*, vol. 03, p. 082, 2021. DOI: 10.1088/1475-7516/2021/03/082. arXiv: 2011.13059 [hep-ph].

[27] X. Luo, W. Rodejohann, and X.-J. Xu, "Dirac neutrinos and N_{eff}," *JCAP*, vol. 06, p. 058, 2020. DOI: 10.1088/1475-7516/2020/06/058. arXiv: 2005.01629 [hep-ph].

[28] A. Baha Balantekin and B. Kayser, "On the Properties of Neutrinos," *Ann. Rev. Nucl. Part. Sci.*, vol. 68, pp. 313–338, 2018. DOI: 10.1146/annurev-nucl-101916-123044. arXiv: 1805.00922 [hep-ph].

[29] A. B. Balantekin, A. de Gouvêa, and B. Kayser, "Addressing the Majorana vs. Dirac Question with Neutrino Decays," *Phys. Lett. B*, vol. 789, pp. 488–495, 2019. DOI: 10.1016/j.physletb.2018.11.068. arXiv: 1808.10518 [hep-ph].

[30] L. Funcke, G. Raffelt, and E. Vitagliano, "Distinguishing Dirac and Majorana neutrinos by their decays via Nambu-Goldstone bosons in the gravitational-anomaly model of neutrino masses," *Phys. Rev. D*, vol. 101, no. 1, p. 015 025, 2020. DOI: 10.1103/PhysRevD.101.015025. arXiv: 1905.01264 [hep-ph].

[31] M. Sajjad Athar et al., "Status and perspectives of neutrino physics," *Prog. Part. Nucl. Phys.*, vol. 124, p. 103 947, 2022. DOI: 10.1016/j.ppnp.2022.103947. arXiv: 2111.07586 [hep-ph].

[32] B. Kayser, "Majorana neutrinos and their electromagnetic properties," *Phys. Rev. D*, vol. 26, pp. 1662–1670, 7 Oct. 1982. DOI: 10.1103/PhysRevD.26.1662. [Online]. Available: https://link.aps.org/doi/10.1103/PhysRevD.26.1662.

[33] D. P. Aguillard et al., "Measurement of the Positive Muon Anomalous Magnetic Moment to 0.20 ppm," *Phys. Rev. Lett.*, vol. 131, no. 16, p. 161 802, 2023. DOI: 10.1103/PhysRevLett.131.161802. arXiv: 2308.06230 [hep-ex].

[34] B. Abi et al., "Measurement of the Positive Muon Anomalous Magnetic Moment to 0.46 ppm," *Phys. Rev. Lett.*, vol. 126, no. 14, p. 141 801, 2021. DOI: 10.1103/PhysRevLett.126.141801. arXiv: 2104.03281 [hep-ex].

[35] G. W. Bennett et al., "Final Report of the Muon E821 Anomalous Magnetic Moment Measurement at BNL," *Phys. Rev. D*, vol. 73, p. 072 003, 2006. DOI: 10.1103/PhysRevD.73.072003. arXiv: hep-ex/0602035.

[36] T. Aoyama et al., "The anomalous magnetic moment of the muon in the Standard Model," *Phys. Rept.*, vol. 887, pp. 1–166, 2020. DOI: 10.1016/j.physrep.2020.07.006. arXiv: 2006.04822 [hep-ph].

[37] J. A. Miranda and P. Roig, "New τ-based evaluation of the hadronic contribution to the vacuum polarization piece of the muon anomalous magnetic moment," *Phys. Rev. D*, vol. 102, p. 114 017, 2020. DOI: 10.1103/PhysRevD.102.114017. arXiv: 2007.11019 [hep-ph].

[38] P. Masjuan, A. Miranda, and P. Roig, "Tau Data-Based Evaluations of the hadronic vacuum polarization contribution to the muon $g-2$," in *17th International Workshop on Tau Lepton Physics*, Jun. 2024. arXiv: 2406.00902 [hep-ph].

[39] M. Davier, A. Hoecker, A.-M. Lutz, B. Malaescu, and Z. Zhang, "Tensions in $e^+e^- \to \pi^+\pi^-(\gamma)$ measurements: the new landscape of data-driven hadronic vacuum polarization predictions for the muon $g-2$," *Eur. Phys. J. C*, vol. 84, no. 7, p. 721, 2024. DOI: 10.1140/epjc/s10052-024-12964-7. arXiv: 2312.02053 [hep-ph].

[40] S. Borsanyi et al., "Leading hadronic contribution to the muon magnetic moment from lattice QCD," *Nature*, vol. 593, no. 7857, pp. 51–55, 2021. DOI: 10.1038/s41586-021-03418-1. arXiv: 2002.12347 [hep-lat].

[41] F. V. Ignatov et al., "Measurement of the e+e-→π+π- cross section from threshold to 1.2 GeV with the CMD-3 detector," *Phys. Rev. D*, vol. 109, no. 11, p. 112 002, 2024. DOI: 10.1103/PhysRevD.109.112002. arXiv: 2302.08834 [hep-ex].

[42] F. V. Ignatov et al., "Measurement of the Pion Form Factor with CMD-3 Detector and its Implication to the Hadronic Contribution to Muon (g-2)," *Phys. Rev. Lett.*, vol. 132, no. 23, p. 231 903, 2024. DOI: 10.1103/PhysRevLett.132.231903. arXiv: 2309.12910 [hep-ex].

[43] R. Aliberti et al., "The anomalous magnetic moment of the muon in the Standard Model: an update," May 2025. arXiv: 2505.21476 [hep-ph].

[44] W. N. Cottingham and D. A. Greenwood, *An introduction to the standard model of particle physics*, http://einstein-schrodinger.com/Standard_Model.pdf, Cambridge University Press, (2007).

[45] P. Langacker, *The Standard Model and Beyond*. CRC Press, (2010).

[46] Palash B. Pal, *An Introductory course of particle physics*. CRC Press, (2015).

[47] David Griffiths, *Introduction to Elementary Particles*. John Wiley Sons, Inc., (1987).

[48] A. Pich, "The Standard Model of Electroweak Interactions," in *2010 European School of High Energy Physics*, Jan. 2012, pp. 1–50. arXiv: 1201.0537 [hep-ph].

[49] A. Djouadi, "The Higgs mechanism and the origin of mass," *AIP Conf. Proc.*, vol. 1444, no. 1, N. Mebarki, J. Mimouni, N. Belaloui, and K. Ait Moussa, Eds., pp. 45–57, 2012. DOI: 10.1063/1.4715399.

[50] P. W. Higgs, "Broken symmetries, massless particles and gauge fields," *Phys. Lett.*, vol. 12, pp. 132–133, 1964. DOI: 10.1016/0031-9163(64)91136-9.

[51] P. W. Higgs, "Broken Symmetries and the Masses of Gauge Bosons," *Phys. Rev. Lett.*, vol. 13, J. C. Taylor, Ed., pp. 508–509, 1964. DOI: 10.1103/PhysRevLett.13.508.

[52] F. Englert and R. Brout, "Broken Symmetry and the Mass of Gauge Vector Mesons," *Phys. Rev. Lett.*, vol. 13, J. C. Taylor, Ed., pp. 321–323, 1964. DOI: 10.1103/PhysRevLett.13.321.

[53] G. S. Guralnik, C. R. Hagen, and T. W. B. Kibble, "Global Conservation Laws and Massless Particles," *Phys. Rev. Lett.*, vol. 13, J. C. Taylor, Ed., pp. 585–587, 1964. DOI: 10.1103/PhysRevLett.13.585.

[54] S. Chatrchyan et al., "Observation of a New Boson at a Mass of 125 GeV with the CMS Experiment at the LHC," *Phys. Lett. B*, vol. 716, pp. 30–61, 2012. DOI: 10.1016/j.physletb.2012.08.021. arXiv: 1207.7235 [hep-ex].

[55] G. Aad et al., "Observation of a new particle in the search for the Standard Model Higgs boson with the ATLAS detector at the LHC," *Phys. Lett. B*, vol. 716, pp. 1–29, 2012. DOI: 10.1016/j.physletb.2012.08.020. arXiv: 1207.7214 [hep-ex].

[56] A. Pich, "Effective field theory: Course," in *Les Houches Summer School in Theoretical Physics, Session 68: Probing the Standard Model of Particle Interactions*, Jun. 1998, pp. 949–1049. arXiv: hep-ph/9806303.

[57] A. V. Manohar, "Effective field theories," *Lect. Notes Phys.*, vol. 479, H. Latal and W. Schweiger, Eds., pp. 311–362, 1997. DOI: 10.1007/BFb0104294. arXiv: hep-ph/9606222.

[58] E. Fermi, "An attempt of a theory of beta radiation. 1.," *Z. Phys.*, vol. 88, pp. 161–177, 1934. DOI: 10.1007/BF01351864.

[59] G. Rajasekaran, "Fermi and the Theory of Weak Interactions," *Resonance J. Sci. Educ.*, vol. 19, no. 1, pp. 18–44, 2014. DOI: 10.1007/s12045-014-0005-2. arXiv: 1403.3309 [physics.hist-ph].

[60] N. Cabibbo, "Unitary Symmetry and Leptonic Decays," *Phys. Rev. Lett.*, vol. 10, pp. 531–533, 1963. DOI: 10.1103/PhysRevLett.10.531.

[61] M. Kobayashi and T. Maskawa, "CP Violation in the Renormalizable Theory of Weak Interaction," *Prog. Theor. Phys.*, vol. 49, pp. 652–657, 1973. DOI: 10.1143/PTP.49.652.

[62] B. Pontecorvo, "Inverse beta processes and nonconservation of lepton charge," *Zh. Eksp. Teor. Fiz.*, vol. 34, p. 247, 1957.

[63] Z. Maki, M. Nakagawa, and S. Sakata, "Remarks on the unified model of elementary particles," *Prog. Theor. Phys.*, vol. 28, pp. 870–880, 1962. DOI: 10.1143/PTP.28.870.

[64] S. Weinberg, "Baryon and Lepton Nonconserving Processes," *Phys. Rev. Lett.*, vol. 43, pp. 1566–1570, 1979. DOI: 10.1103/PhysRevLett.43.1566.

[65] W. Buchmuller and D. Wyler, "Effective Lagrangian Analysis of New Interactions and Flavor Conservation," *Nucl. Phys. B*, vol. 268, pp. 621–653, 1986. DOI: 10.1016/0550-3213(86)90262-2.

[66] B. Grzadkowski, M. Iskrzynski, M. Misiak, and J. Rosiek, "Dimension-Six Terms in the Standard Model Lagrangian," *JHEP*, vol. 10, p. 085, 2010. DOI: 10.1007/JHEP10(2010)085. arXiv: 1008.4884 [hep-ph].

[67] I. Brivio and M. Trott, "The Standard Model as an Effective Field Theory," *Phys. Rept.*, vol. 793, pp. 1–98, 2019. DOI: 10.1016/j.physrep.2018.11.002. arXiv: 1706.08945 [hep-ph].

[68] G. Isidori, F. Wilsch, and D. Wyler, "The standard model effective field theory at work," *Rev. Mod. Phys.*, vol. 96, no. 1, p. 015 006, 2024. DOI: 10.1103/RevModPhys.96.015006. arXiv: 2303.16922 [hep-ph].

[69] L. F. Abbott and M. B. Wise, "The Effective Hamiltonian for Nucleon Decay," *Phys. Rev. D*, vol. 22, p. 2208, 1980. DOI: 10.1103/PhysRevD.22.2208.

[70] L. Lehman, "Extending the Standard Model Effective Field Theory with the Complete Set of Dimension-7 Operators," *Phys. Rev. D*, vol. 90, no. 12, p. 125 023, 2014. DOI: 10.1103/PhysRevD.90.125023. arXiv: 1410.4193 [hep-ph].

[71] L. Lehman and A. Martin, "Low-derivative operators of the Standard Model effective field theory via Hilbert series methods," *JHEP*, vol. 02, p. 081, 2016. DOI: 10.1007/JHEP02(2016)081. arXiv: 1510.00372 [hep-ph].

[72] B. Henning, X. Lu, T. Melia, and H. Murayama, "2, 84, 30, 993, 560, 15456, 11962, 261485, ...: Higher dimension operators in the SM EFT," *JHEP*, vol. 08, p. 016, 2017, [Erratum: JHEP 09, 019 (2019)]. DOI: 10.1007/JHEP08(2017)016. arXiv: 1512.03433 [hep-ph].

[73] G. Passarino, "Field reparametrization in effective field theories," *Eur. Phys. J. Plus*, vol. 132, no. 1, p. 16, 2017. DOI: 10.1140/epjp/i2017-11291-5. arXiv: 1610.09618 [hep-ph].

[74] D. B. Kaplan and H. Georgi, "SU(2) x U(1) Breaking by Vacuum Misalignment," *Phys. Lett. B*, vol. 136, pp. 183–186, 1984. DOI: 10.1016/0370-2693(84)91177-8.

[75] D. B. Kaplan, H. Georgi, and S. Dimopoulos, "Composite Higgs Scalars," *Phys. Lett. B*, vol. 136, pp. 187–190, 1984. DOI: 10.1016/0370-2693(84)91178-X.

[76] T. Banks, "CONSTRAINTS ON SU(2) x U(1) BREAKING BY VACUUM MISALIGNMENT," *Nucl. Phys. B*, vol. 243, pp. 125–130, 1984. DOI: 10.1016/0550-3213(84)90389-4.

[77] K. Agashe, R. Contino, and A. Pomarol, "The Minimal composite Higgs model," *Nucl. Phys. B*, vol. 719, pp. 165–187, 2005. DOI: 10.1016/j.nuclphysb.2005.04.035. arXiv: hep-ph/0412089.

[78] B. Gripaios, A. Pomarol, F. Riva, and J. Serra, "Beyond the Minimal Composite Higgs Model," *JHEP*, vol. 04, p. 070, 2009. DOI: 10.1088/1126-6708/2009/04/070. arXiv: 0902.1483 [hep-ph].

[79] T. Appelquist and C. W. Bernard, "Strongly Interacting Higgs Bosons," *Phys. Rev. D*, vol. 22, p. 200, 1980. DOI: 10.1103/PhysRevD.22.200.

[80] T. Appelquist and C. W. Bernard, "The Nonlinear σ Model in the Loop Expansion," *Phys. Rev. D*, vol. 23, p. 425, 1981. DOI: 10.1103/PhysRevD.23.425.

[81] A. C. Longhitano, "Heavy Higgs Bosons in the Weinberg-Salam Model," *Phys. Rev. D*, vol. 22, p. 1166, 1980. DOI: 10.1103/PhysRevD.22.1166.

[82] A. C. Longhitano, "Low-Energy Impact of a Heavy Higgs Boson Sector," *Nucl. Phys. B*, vol. 188, pp. 118–154, 1981. DOI: 10.1016/0550-3213(81)90109-7.

[83] F. Feruglio, "The Chiral approach to the electroweak interactions," *Int. J. Mod. Phys. A*, vol. 8, pp. 4937–4972, 1993. DOI: 10.1142/S0217751X93001946. arXiv: hep-ph/9301281.

[84] B. Grinstein and M. Trott, "A Higgs-Higgs bound state due to new physics at a TeV," *Phys. Rev. D*, vol. 76, p. 073 002, 2007. DOI: 10.1103/PhysRevD.76.073002. arXiv: 0704.1505 [hep-ph].

[85] R. Alonso, M. B. Gavela, L. Merlo, S. Rigolin, and J. Yepes, "The Effective Chiral Lagrangian for a Light Dynamical "Higgs Particle"," *Phys. Lett. B*, vol. 722, pp. 330–335, 2013, [Erratum: Phys.Lett.B 726, 926 (2013)]. DOI: 10.1016/j.physletb.2013.04.037. arXiv: 1212.3305 [hep-ph].

[86] G. Buchalla, O. Catà, and C. Krause, "Complete Electroweak Chiral Lagrangian with a Light Higgs at NLO," *Nucl. Phys. B*, vol. 880, pp. 552–573, 2014, [Erratum: Nucl.Phys.B 913, 475–478 (2016)]. DOI: 10.1016/j.nuclphysb.2014.01.018. arXiv: 1307.5017 [hep-ph].

[87] R. Alonso, E. E. Jenkins, and A. V. Manohar, "A Geometric Formulation of Higgs Effective Field Theory: Measuring the Curvature of Scalar Field Space," *Phys. Lett. B*, vol. 754, pp. 335–342, 2016. DOI: 10.1016/j.physletb.2016.01.041. arXiv: 1511.00724 [hep-ph].

[88] R. Alonso, E. E. Jenkins, and A. V. Manohar, "Geometry of the Scalar Sector," *JHEP*, vol. 08, p. 101, 2016. DOI: 10.1007/JHEP08(2016)101. arXiv: 1605.03602 [hep-ph].

[89] I. Brivio et al., "Disentangling a dynamical Higgs," *JHEP*, vol. 03, p. 024, 2014. DOI: 10.1007/JHEP03(2014)024. arXiv: 1311.1823 [hep-ph].

[90] M. B. Gavela, J. González-Fraile, M. C. González-García, L. Merlo, S. Rigolin, and J. Yepes, "CP violation with a dynamical Higgs," *JHEP*, vol. 10, p. 044, 2014. DOI: 10.1007/JHEP10(2014)044. arXiv: 1406.6367 [hep-ph].

[91] I. Brivio et al., "Non-linear Higgs portal to Dark Matter," *JHEP*, vol. 04, p. 141, 2016. DOI: 10.1007/JHEP04(2016)141. arXiv: 1511.01099 [hep-ph].

[92] H. Murayama, V. Rentala, and J. Shu, "Probing strong electroweak symmetry breaking dynamics through quantum interferometry at the LHC," *Phys. Rev. D*, vol. 92, no. 11, p. 116 002, 2015. DOI: 10.1103/PhysRevD.92.116002. arXiv: 1401.3761 [hep-ph].

[93] R. L. Delgado, A. Dobado, and F. J. Llanes-Estrada, "One-loop W_LW_L and Z_LZ_L scattering from the electroweak Chiral Lagrangian with a light Higgs-like scalar," *JHEP*, vol. 02, p. 121, 2014. DOI: 10.1007/JHEP02(2014)121. arXiv: 1311.5993 [hep-ph].

[94] I. Brivio, J. González-Fraile, M. C. González-García, and L. Merlo, "The complete heft lagrangian after the lhc run i," *The European Physical Journal C*, vol. 76, no. 7, Jul. 2016, ISSN: 1434-6052. DOI: 10.1140/epjc/s10052-016-4211-9. [Online]. Available: http://dx.doi.org/10.1140/epjc/s10052-016-4211-9.

[95] L. Michel, "Interaction between four half spin particles and the decay of the μ meson," *Proc. Phys. Soc. A*, vol. 63, T. Damour, I. Todorov, and B. Zhilinskii, Eds., pp. 514–531, 1950. DOI: 10.1088/0370-1298/63/5/311.

[96] C. Bouchiat and L. Michel, "Theory of μ-Meson Decay with the Hypothesis of Nonconservation of Parity," *Phys. Rev.*, vol. 106, T. Damour, I. Todorov, and B. Zhilinskii, Eds., pp. 170–172, 1957. DOI: 10.1103/PhysRev.106.170.

[97] W. Fetscher, H. J. Gerber, and K. F. Johnson, "Muon Decay: Complete Determination of the Interaction and Comparison with the Standard Model," *Phys. Lett. B*, vol. 173, pp. 102–106, 1986. DOI: 10.1016/0370-2693(86)91239-6.

[98] P. Langacker and D. London, "Analysis of Muon Decay With Lepton Number Nonconserving Interactions," *Phys. Rev. D*, vol. 39, p. 266, 1989. DOI: 10.1103/PhysRevD.39.266.

[99] M. Doi, T. Kotani, and H. Nishiura, "New parameterization in muon decay and type of neutrino," *Prog. Theor. Phys.*, vol. 114, pp. 845–871, 2005. DOI: 10.1143/PTP.114.845. arXiv: hep-ph/0502136.

[100] M. M. Giannini, "An improved upper limit for the (muon based) neutrino mass," Jul. 2022. arXiv: 2207.02718 [hep-ph].

[101] R. E. Shrock, "Pure Leptonic Decays With Massive Neutrinos and Arbitrary Lorentz Structure," *Phys. Lett. B*, vol. 112, pp. 382–386, 1982. DOI: 10.1016/0370-2693(82)91074-7.

[102] A. Denner, H. Eck, O. Hahn, and J. Kublbeck, "Feynman rules for fermion number violating interactions," *Nucl. Phys. B*, vol. 387, pp. 467–481, 1992. DOI: 10.1016/0550-3213(92)90169-C.

[103] M. Doi, T. Kotani, and E. Takasugi, "Double beta Decay and Majorana Neutrino," *Prog. Theor. Phys. Suppl.*, vol. 83, p. 1, 1985. DOI: 10.1143/PTPS.83.1.

[104] C. A. Gagliardi, R. E. Tribble, and N. J. Williams, "Global analysis of muon decay measurements," *Phys. Rev. D*, vol. 72, p. 073 002, 2005. DOI: 10.1103/PhysRevD.72.073002. arXiv: hep-ph/0509069.

[105] R. E. Behrends, R. J. Finkelstein, and A. Sirlin, "Radiative corrections to decay processes," *Phys. Rev.*, vol. 101, pp. 866–873, 2 Jan. 1956. DOI: 10.1103/PhysRev.101.866. [Online]. Available: https://link.aps.org/doi/10.1103/PhysRev.101.866.

[106] S. M. Berman, "Radiative corrections to muon and neutron decay," *Phys. Rev.*, vol. 112, pp. 267–270, 1958. DOI: 10.1103/PhysRev.112.267.

[107] T. Kinoshita and A. Sirlin, "Radiative corrections to fermi interactions," *Phys. Rev.*, vol. 113, pp. 1652–1660, 6 Mar. 1959. DOI: 10.1103/PhysRev.113.1652. [Online]. Available: https://link.aps.org/doi/10.1103/PhysRev.113.1652.

[108] A. Stahl, "The Michel parameter eta in tau decays," *Phys. Lett. B*, vol. 324, pp. 121–124, 1994. DOI: 10.1016/0370-2693(94)00124-3.

[109] K. Abe et al., "Measurement of the tau-neutrino helicity and the Michel parameters in polarized e+ e- collisions," *Phys. Rev. Lett.*, vol. 78, pp. 4691–4696, 1997. DOI: 10.1103/PhysRevLett.78.4691. arXiv: hep-ex/9701020.

[110] A. Heister et al., "Measurement of the Michel parameters and the nu/tau helicity in tau lepton decays," *Eur. Phys. J. C*, vol. 22, pp. 217–230, 2001. DOI: 10.1007/s100520100813.

[111] P. Abreu et al., "A Study of the Lorentz structure in tau decays," *Eur. Phys. J. C*, vol. 16, pp. 229–252, 2000. DOI: 10.1007/s100520050017. arXiv: hep-ex/0107076.

[112] K. Ackerstaff et al., "Measurement of the Michel parameters in leptonic tau decays," *Eur. Phys. J. C*, vol. 8, pp. 3–21, 1999. DOI: 10.1007/s100529901080. arXiv: hep-ex/9808016.

[113] M. Acciarri et al., "Measurement of the Michel parameters and the average tau-neutrino helicity from tau decays at LEP," *Phys. Lett. B*, vol. 438, pp. 405–416, 1998. DOI: 10.1016/S0370-2693(98)01082-X.

[114] H. Albrecht et al., "Determination of the Michel parameters rho, xi and delta in tau lepton decays with tau —> rho neutrino tags," *Phys. Lett. B*, vol. 431, pp. 179–187, 1998. DOI: 10.1016/S0370-2693(98)00565-6. arXiv: hep-ex/9711022.

[115] J. P. Alexander et al., "Determination of the Michel parameters and the tau-neutrino helicity in tau decay," *Phys. Rev. D*, vol. 56, pp. 5320–5329, 1997. DOI: 10.1103/PhysRevD.56.5320. arXiv: hep-ex/9705009.

[116] A. Hillairet et al., "Precision muon decay measurements and improved constraints on the weak interaction," *Phys. Rev. D*, vol. 85, p. 092 013, 2012. DOI: 10.1103/PhysRevD.85.092013. arXiv: 1112.3606 [hep-ex].

[117] N. Danneberg et al., "Muon decay: Measurement of the transverse polarization of the decay positrons and its implications for the Fermi coupling constant and time reversal invariance," *Phys. Rev. Lett.*, vol. 94, p. 021 802, 2005. DOI: 10.1103/PhysRevLett.94.021802.

[118] B. Balke et al., "Precise measurement of the asymmetry parameter δ in muon decay," *Phys. Rev. D*, vol. 37, pp. 587–617, 3 Feb. 1988. DOI: 10.1103/PhysRevD.37.587. [Online]. Available: https://link.aps.org/doi/10.1103/PhysRevD.37.587.

[119] I. Beltrami et al., "Muon Decay: Measurement of the Integral Asymmetry Parameter," *Phys. Lett. B*, vol. 194, pp. 326–330, 1987. DOI: 10.1016/0370-2693(87)90552-1.

[120] D. e. a. Bodrov, "First measurement of the michel parameter ξ' in the $\tau^- \to \mu^- \overline{\nu}_\mu \nu_\tau$ decay at belle," *Phys. Rev. Lett.*, vol. 131, p. 021 801, 2 Jul. 2023. DOI: 10.1103/PhysRevLett.131.021801. [Online]. Available: https://link.aps.org/doi/10.1103/PhysRevLett.131.021801.

[121] N. Shimizu et al., "Measurement of the tau Michel parameters $\bar{\eta}$ and $\xi\kappa$ in the radiative leptonic decay $\tau^- \to \ell^- \nu_\tau \bar{\nu}_\ell \gamma$," *PTEP*, vol. 2018, no. 2, p. 023C01, 2018. DOI: 10.1093/ptep/pty003. arXiv: 1709.08833 [hep-ex].

[122] A. Stahl and H. Voss, "Testing the Lorentz structure of the charged weak current in tau decays," *Z. Phys. C*, vol. 74, pp. 73–78, 1997. DOI: 10.1007/s002880050371.

[123] A. Flores-Tlalpa, G. López Castro, and P. Roig, "Five-body leptonic decays of muon and tau leptons," *JHEP*, vol. 04, p. 185, 2016. DOI: 10.1007/JHEP04(2016)185. arXiv: 1508.01822 [hep-ph].

[124] J. Sasaki, "Study of five-body leptonic decays of tau at Belle experiment," *J. Phys. Conf. Ser.*, vol. 912, no. 1, I. Bautista, E. de la Cruz Burelo, A. Fernández-Téllez, G. López-Castro, M. Rodríguez-Cahuantzi, and P. Roig, Eds., p. 012 002, 2017. DOI: 10.1088/1742-6596/912/1/012002.

[125] A. de Gouvêa and A. Kobach, "Global Constraints on a Heavy Neutrino," *Phys. Rev. D*, vol. 93, no. 3, p. 033 005, 2016. DOI: 10.1103/PhysRevD.93.033005. arXiv: 1511.00683 [hep-ph].

[126] A. Kobach and S. Dobbs, "Heavy Neutrinos and the Kinematics of Tau Decays," *Phys. Rev. D*, vol. 91, no. 5, p. 053 006, 2015. DOI: 10.1103/PhysRevD.91.053006. arXiv: 1412.4785 [hep-ph].

[127] C. S. Kim, G. López Castro, and D. Sahoo, "Constraints on a sub-eV scale sterile neutrino from nonoscillation measurements," *Phys. Rev. D*, vol. 98, no. 11, p. 115 021, 2018. DOI: 10.1103/PhysRevD.98.115021. arXiv: 1809.02265 [hep-ph].

[128] J. P. Lees et al., "Search for heavy neutral leptons using tau lepton decays at BaBaR," *Phys. Rev. D*, vol. 107, no. 5, p. 052 009, 2023. DOI: 10.1103/PhysRevD.107.052009. arXiv: 2207.09575 [hep-ex].

[129] M. Fael, L. Mercolli, and M. Passera, "W-propagator corrections to μ and τ leptonic decays," *Phys. Rev. D*, vol. 88, no. 9, p. 093 011, 2013. DOI: 10.1103/PhysRevD.88.093011. arXiv: 1310.1081 [hep-ph].

[130] D. Bodrov and P. Pakhlov, "A new method for the measurement of the Michel parameters that describe the daughter muon polarization in the $\tau \to \mu\overline{\nu}\nu$ decay," *JHEP*, vol. 10, p. 035, 2022. DOI: 10.1007/JHEP10(2022)035. arXiv: 2203.12743 [hep-ph].

[131] A. Sirlin and A. Ferroglia, "Radiative corrections in precision electroweak physics: A historical perspective," *Rev. Mod. Phys.*, vol. 85, pp. 263–297, 1 Feb. 2013. DOI: 10.1103/RevModPhys.85.263. [Online]. Available: https://link.aps.org/doi/10.1103/RevModPhys.85.263.

[132] B. Kayser, "Majorana Neutrinos and their Electromagnetic Properties," *Phys. Rev. D*, vol. 26, p. 1662, 1982. DOI: 10.1103/PhysRevD.26.1662.

[133] W. Rodejohann, X.-J. Xu, and C. E. Yaguna, "Distinguishing between Dirac and Majorana neutrinos in the presence of general interactions," *JHEP*, vol. 05, p. 024, 2017. DOI: 10.1007/JHEP05(2017)024. arXiv: 1702.05721 [hep-ph].

[134] I. Bischer and W. Rodejohann, "General neutrino interactions from an effective field theory perspective," *Nucl. Phys. B*, vol. 947, p. 114 746, 2019. DOI: 10.1016/j.nuclphysb.2019.114746. arXiv: 1905.08699 [hep-ph].

[135] M. Lindner, W. Rodejohann, and X.-J. Xu, "Coherent Neutrino-Nucleus Scattering and new Neutrino Interactions," *JHEP*, vol. 03, p. 097, 2017. DOI: 10.1007/JHEP03(2017)097. arXiv: 1612.04150 [hep-ph].

[136] A. Atre, T. Han, S. Pascoli, and B. Zhang, "The Search for Heavy Majorana Neutrinos," *JHEP*, vol. 05, p. 030, 2009. DOI: 10.1088/1126-6708/2009/05/030. arXiv: 0901.3589 [hep-ph].

[137] A. Błaut and W. Sobków, "Neutrino elastic scattering on polarized electrons as a tool for probing the neutrino nature," *Eur. Phys. J. C*, vol. 80, no. 3, p. 261, 2020. DOI: 10.1140/epjc/s10052-020-7806-0. arXiv: 1812.09828 [hep-ph].

[138] E. Cortina Gil et al., "Search for heavy neutral lepton production in K^+ decays," *Phys. Lett. B*, vol. 778, pp. 137–145, 2018. DOI: 10.1016/j.physletb.2018.01.031. arXiv: 1712.00297 [hep-ex].

[139] P. Abratenko et al., "Search for Heavy Neutral Leptons in Electron-Positron and Neutral-Pion Final States with the MicroBooNE Detector," *Phys. Rev. Lett.*, vol. 132, no. 4, p. 041 801, 2024. DOI: 10.1103/PhysRevLett.132.041801. arXiv: 2310.07660 [hep-ex].

[140] R. Barouki, G. Marocco, and S. Sarkar, "Blast from the past II: Constraints on heavy neutral leptons from the BEBC WA66 beam dump experiment," *SciPost Phys.*, vol. 13, p. 118, 2022. DOI: 10.21468/SciPostPhys.13.5.118. arXiv: 2208.00416 [hep-ph].

[141] C. S. Kim, M. V. N. Murthy, and D. Sahoo, "Inferring the nature of active neutrinos: Dirac or Majorana?" *Phys. Rev. D*, vol. 105, no. 11, p. 113 006, 2022. DOI: 10.1103/PhysRevD.105.113006. arXiv: 2106.11785 [hep-ph].

[142] R. E. Shrock, "New Tests For, and Bounds On, Neutrino Masses and Lepton Mixing," *Phys. Lett. B*, vol. 96, pp. 159–164, 1980. DOI: 10.1016/0370-2693(80)90235-X.

[143] E. Akhmedov and A. Trautner, "Can quantum statistics help distinguish Dirac from Majorana neutrinos?" *JHEP*, vol. 05, p. 156, 2024. DOI: 10.1007/JHEP05(2024)156. arXiv: 2402.05172 [hep-ph].

[144] D. Buttazzo and P. Paradisi, "Probing the muon $g-2$ anomaly with the Higgs boson at a muon collider," *Phys. Rev. D*, vol. 104, no. 7, p. 075 021, 2021. DOI: 10.1103/PhysRevD.104.075021. arXiv: 2012.02769 [hep-ph].

[145] R. Gómez-Ambrosio, F. J. Llanes-Estrada, A. Salas-Bernárdez, and J. J. Sanz-Cillero, "Distinguishing electroweak EFTs with WLWL→n×h," *Phys. Rev. D*, vol. 106, no. 5, p. 053 004, 2022. DOI: 10.1103/PhysRevD.106.053004. arXiv: 2204.01763 [hep-ph].

[146] R. L. Delgado, R. Gómez-Ambrosio, J. Martínez-Martín, A. Salas-Bernárdez, and J. J. Sanz-Cillero, "Production of two, three, and four Higgs bosons: where SMEFT and HEFT depart," *JHEP*, vol. 03, p. 037, 2024. DOI: 10.1007/JHEP03(2024)037. arXiv: 2311.04280 [hep-ph].

[147] B. M. Gavela, E. E. Jenkins, A. V. Manohar, and L. Merlo, "Analysis of General Power Counting Rules in Effective Field Theory," *Eur. Phys. J. C*, vol. 76, no. 9, p. 485, 2016. DOI: 10.1140/epjc/s10052-016-4332-1. arXiv: 1601.07551 [hep-ph].

[148] I. Brivio, J. Gonzalez-Fraile, M. C. Gonzalez-Garcia, and L. Merlo, "The complete HEFT Lagrangian after the LHC Run I," *Eur. Phys. J. C*, vol. 76, no. 7, p. 416, 2016. DOI: 10.1140/epjc/s10052-016-4211-9. arXiv: 1604.06801 [hep-ph].

[149] H. Sun, M.-L. Xiao, and J.-H. Yu, "Complete NLO operators in the Higgs effective field theory," *JHEP*, vol. 05, p. 043, 2023. DOI: 10.1007/JHEP05(2023)043. arXiv: 2206.07722 [hep-ph].

[150] H. Sun, M.-L. Xiao, and J.-H. Yu, "Complete NNLO operator bases in Higgs effective field theory," *JHEP*, vol. 04, p. 086, 2023. DOI: 10.1007/JHEP04(2023)086. arXiv: 2210.14939 [hep-ph].

[151] F.-K. Guo, P. Ruiz-Femenía, and J. J. Sanz-Cillero, "One loop renormalization of the electroweak chiral Lagrangian with a light Higgs boson," *Phys. Rev. D*, vol. 92, p. 074 005, 2015. DOI: 10.1103/PhysRevD.92.074005. arXiv: 1506.04204 [hep-ph].

[152] G. Buchalla, O. Catà, A. Celis, M. Knecht, and C. Krause, "Complete One-Loop Renormalization of the Higgs-Electroweak Chiral Lagrangian," *Nucl. Phys. B*, vol. 928, pp. 93–106, 2018. DOI: 10.1016/j.nuclphysb.2018.01.009. arXiv: 1710.06412 [hep-ph].

[153] R. Alonso, K. Kanshin, and S. Saa, "Renormalization group evolution of Higgs effective field theory," *Phys. Rev. D*, vol. 97, no. 3, p. 035 010, 2018. DOI: 10.1103/PhysRevD.97.035010. arXiv: 1710.06848 [hep-ph].

[154] M. J. Herrero and R. A. Morales, "One-loop renormalization of vector boson scattering with the electroweak chiral Lagrangian in covariant gauges," *Phys. Rev. D*, vol. 104, no. 7, p. 075 013, 2021. DOI: 10.1103/PhysRevD.104.075013. arXiv: 2107.07890 [hep-ph].

[155] R. L. Delgado, A. Dobado, M. J. Herrero, and J. J. Sanz-Cillero, "One-loop $\gamma\gamma \to W_L^+ W_L^-$ and $\gamma\gamma \to Z_L Z_L$ from the Electroweak Chiral Lagrangian with a light Higgs-like scalar," *JHEP*, vol. 07, p. 149, 2014. DOI: 10.1007/JHEP07(2014)149. arXiv: 1404.2866 [hep-ph].

[156] C. W. Murphy, "Dimension-8 operators in the Standard Model Effective Field Theory," *JHEP*, vol. 10, p. 174, 2020. DOI: 10.1007/JHEP10(2020)174. arXiv: 2005.00059 [hep-ph].

[157] P. M. Bredt, W. Kilian, J. Reuter, and P. Stienemeier, "NLO electroweak corrections to multi-boson processes at a muon collider," *JHEP*, vol. 12, p. 138, 2022. DOI: 10.1007/JHEP12(2022)138. arXiv: 2208.09438 [hep-ph].

[158] O. J. P. Éboli, M. C. González-Garcia, and M. Martines, "Electroweak Higgs effective field theory after LHC run 2," *Phys. Rev. D*, vol. 105, no. 5, p. 053 003, 2022. DOI: 10.1103/PhysRevD.105.053003. arXiv: 2112.11468 [hep-ph].

[159] G. Colangelo, M. Hoferichter, M. Procura, and P. Stoffer, "Dispersion relation for hadronic light-by-light scattering: theoretical foundations," *JHEP*, vol. 09, p. 074, 2015. DOI: 10.1007/JHEP09(2015)074. arXiv: 1506.01386 [hep-ph].

[160] G. Colangelo, M. Hoferichter, M. Procura, and P. Stoffer, "Dispersion relation for hadronic light-by-light scattering: two-pion contributions," *JHEP*, vol. 04, p. 161, 2017. DOI: 10.1007/JHEP04(2017)161. arXiv: 1702.07347 [hep-ph].

[161] G. Colangelo, F. Hagelstein, M. Hoferichter, L. Laub, and P. Stoffer, "Longitudinal short-distance constraints for the hadronic light-by-light contribution to $(g-2)_\mu$ with large-N_c Regge models," *JHEP*, vol. 03, p. 101, 2020. DOI: 10.1007/JHEP03(2020)101. arXiv: 1910.13432 [hep-ph].

[162] W. A. Bardeen and W. K. Tung, "Invariant amplitudes for photon processes," *Phys. Rev.*, vol. 173, pp. 1423–1433, 1968, [Erratum: Phys.Rev.D 4, 3229–3229 (1971)]. DOI: 10.1103/PhysRev.173.1423.

[163] R. Tarrach, "Invariant Amplitudes for Virtual Compton Scattering Off Polarized Nucleons Free from Kinematical Singularities, Zeros and Constraints," *Nuovo Cim. A*, vol. 28, p. 409, 1975. DOI: 10.1007/BF02894857.

[164] A. Keshavarzi, D. Nomura, and T. Teubner, "$g-2$ of charged leptons, $\alpha(M_Z^2)$, and the hyperfine splitting of muonium," *Phys. Rev. D*, vol. 101, no. 1, p. 014 029, 2020. DOI: 10.1103/PhysRevD.101.014029. arXiv: 1911.00367 [hep-ph].

[165] S. J. Brodsky and G. R. Farrar, "Scaling Laws at Large Transverse Momentum," *Phys. Rev. Lett.*, vol. 31, pp. 1153–1156, 1973. DOI: 10.1103/PhysRevLett.31.1153.

[166] Z. Ye, J. Arrington, R. J. Hill, and G. Lee, "Proton and Neutron Electromagnetic Form Factors and Uncertainties," *Phys. Lett. B*, vol. 777, pp. 8–15, 2018. DOI: 10.1016/j.physletb.2017.11.023. arXiv: 1707.09063 [nucl-ex].

[167] C. Alexandrou et al., "Proton and neutron electromagnetic form factors from lattice QCD," *Phys. Rev. D*, vol. 100, no. 1, p. 014 509, 2019. DOI: 10.1103/PhysRevD.100.014509. arXiv: 1812.10311 [hep-lat].

[168] R. J. Hill and G. Paz, "Model independent extraction of the proton charge radius from electron scattering," *Phys. Rev. D*, vol. 82, p. 113 005, 2010. DOI: 10.1103/PhysRevD.82.113005. arXiv: 1008.4619 [hep-ph].

[169] W. M. Alberico, S. M. Bilenky, C. Giunti, and K. M. Graczyk, "Electromagnetic form factors of the nucleon: New Fit and analysis of uncertainties," *Phys. Rev. C*, vol. 79, p. 065 204, 2009. DOI: 10.1103/PhysRevC.79.065204. arXiv: 0812.3539 [hep-ph].

[170] J. Arrington, W. Melnitchouk, and J. A. Tjon, "Global analysis of proton elastic form factor data with two-photon exchange corrections," *Phys. Rev. C*, vol. 76, p. 035 205, 2007. DOI: 10.1103/PhysRevC.76.035205. arXiv: 0707.1861 [nucl-ex].

[171] G. P. Lepage, "Adaptive multidimensional integration: VEGAS enhanced," *J. Comput. Phys.*, vol. 439, p. 110 386, 2021. DOI: 10.1016/j.jcp.2021.110386. arXiv: 2009.05112 [physics.comp-ph].

[172] G. P. Lepage, "A New Algorithm for Adaptive Multidimensional Integration," *J. Comput. Phys.*, vol. 27, p. 192, 1978. DOI: 10.1016/0021-9991(78)90004-9.

[173] Y. Fukuda et al., "Evidence for oscillation of atmospheric neutrinos," *Phys. Rev. Lett.*, vol. 81, pp. 1562–1567, 1998. DOI: 10.1103/PhysRevLett.81.1562. arXiv: hep-ex/9807003.

[174] R. N. Mohapatra and P. B. Pal, *Massive neutrinos in physics and astrophysics. Second edition.* 1998, vol. 60.

[175] B. Pontecorvo, Zh. Eksp. Teor. Fiz. 34, 247, (1957).

[176] Z. Maki, M. Nakagawa, and S. Sakata, Prog. Theor. Phys.28, 870, (1962).

[177] S.N. Gninenko, *The miniboone anomaly and heavy neutrino decay*, http://arxiv.org/abs/0902.3802v5, (2009).

[178] R. N. Mohapatra and J. W. F. Valle, Phys. Rev. D 34, 1642, (1986).

[179] J. Bernabéu, A. Santamaría, J. Vidal, A. Méndez, and J. W. F. Valle, Phys. Lett. B 187, 303, (1987).

[180] M. Malinsky, J.C. Romao, and J. W.F. Valle, , Phys. Rev. Lett. 95, 161801, (2005).

[181] T. Fukuyama and K. Tsumura, "Detecting Majorana nature of neutrinos in muon decay," Sep. 2008. arXiv: 0809.5221 [hep-ph].

[182] Anupama Atre, Tao Han, Silvia Pascoli, Bin Zhang, *The search for heavy majorana neutrinos*, http://arxiv.org/abs/0901.3589v2, (2009).

[183] A. G. Dias , C. A. de S. Pires , P. S. Rodrigues da Silva, A. Sampieri, *A simple realization of the inverse seesaw mechanism*, http://arxiv.org/abs/1206.2590v2, (2012).

[184] K. Mursula, F.Scheck, *Analysis of leptonic charged weak interactions*, Nuclear Physics B253 (1985).

[185] W. Fetscher, H.J. Gerber and K.F. Johnson, Electroweak and Strong Interactions, (Springer Verlag, 1996).

[186] A. Ferroglia, C. Greub, A. Sirlin, and Z. Zhang, "Contributions of the W-boson propagator to μ and τ leptonic decay rates," *Phys. Rev. D*, vol. 88, no. 3, p. 033 012, 2013. DOI: 10.1103/PhysRevD.88.033012. arXiv: 1307.6900 [hep-ph].

[187] M. Fael, L. Mercolli, and M. Passera, "Radiative μ and τ leptonic decays at NLO," *JHEP*, vol. 07, p. 153, 2015. DOI: 10.1007/JHEP07(2015)153. arXiv: 1506.03416 [hep-ph].

[188] W. Altmannshofer et al., "The Belle II Physics Book," *PTEP*, vol. 2019, no. 12, E. Kou and P. Urquijo, Eds., p. 123C01, 2019, [Erratum: PTEP 2020, 029201 (2020)]. DOI: 10.1093/ptep/ptz106. arXiv: 1808.10567 [hep-ex].

[189] R. D. Bolton et al., "Search for Rare Muon Decays with the Crystal Box Detector," *Phys. Rev. D*, vol. 38, p. 2077, 1988. DOI: 10.1103/PhysRevD.38.2077.

[190] L. Bartoszek et al., "Mu2e Technical Design Report," Oct. 2014. DOI: 10.2172/1172555. arXiv: 1501.05241 [physics.ins-det].

[191] D. P. Aguillard et al., "Measurement of the Positive Muon Anomalous Magnetic Moment to 127 ppb," Jun. 2025. arXiv: 2506.03069 [hep-ex].

[192] M. Abe et al., "A New Approach for Measuring the Muon Anomalous Magnetic Moment and Electric Dipole Moment," *PTEP*, vol. 2019, no. 5, p. 053C02, 2019. DOI: 10.1093/ptep/ptz030. arXiv: 1901.03047 [physics.ins-det].

[193] T. Aoyama, M. Hayakawa, T. Kinoshita, and M. Nio, "Complete Tenth-Order QED Contribution to the Muon g-2," *Phys. Rev. Lett.*, vol. 109, p. 111 808, 2012. DOI: 10.1103/PhysRevLett.109.111808. arXiv: 1205.5370 [hep-ph].

[194] S. Volkov, "Calculating the five-loop QED contribution to the electron anomalous magnetic moment: Graphs without lepton loops," *Phys. Rev. D*, vol. 100, no. 9, p. 096 004, 2019. DOI: 10.1103/PhysRevD.100.096004. arXiv: 1909.08015 [hep-ph].

[195] S. Volkov, "Calculation of the total 10th order QED contribution to the electron magnetic moment," *Phys. Rev. D*, vol. 110, no. 3, p. 036 001, 2024. DOI: 10.1103/PhysRevD.110.036001. arXiv: 2404.00649 [hep-ph].

[196] T. Aoyama, M. Hayakawa, A. Hirayama, and M. Nio, "Verification of the tenth-order QED contribution to the anomalous magnetic moment of the electron from diagrams without fermion loops," *Phys. Rev. D*, vol. 111, no. 3, p. L031902, 2025. DOI: 10.1103/PhysRevD.111.L031902. arXiv: 2412.06473 [hep-ph].

[197] R. H. Parker, C. Yu, W. Zhong, B. Estey, and H. Müller, "Measurement of the fine-structure constant as a test of the Standard Model," *Science*, vol. 360, p. 191, 2018. DOI: 10.1126/science.aap7706. arXiv: 1812.04130 [physics.atom-ph].

[198] L. Morel, Z. Yao, P. Cladé, and S. Guellati-Khélifa, "Determination of the fine-structure constant with an accuracy of 81 parts per trillion," *Nature*, vol. 588, no. 7836, pp. 61–65, 2020. DOI: 10.1038/s41586-020-2964-7.

[199] X. Fan, T. G. Myers, B. A. D. Sukra, and G. Gabrielse, "Measurement of the Electron Magnetic Moment," *Phys. Rev. Lett.*, vol. 130, no. 7, p. 071 801, 2023. DOI: 10.1103/PhysRevLett.130.071801. arXiv: 2209.13084 [physics.atom-ph].

[200] J. Lüdtke, M. Procura, and P. Stoffer, "Dispersion relations for the hadronic VVA correlator," *JHEP*, vol. 04, p. 130, 2025. DOI: 10.1007/JHEP04(2025)130. arXiv: 2410.11946 [hep-ph].

[201] A. Czarnecki, W. J. Marciano, and A. Vainshtein, "Refinements in electroweak contributions to the muon anomalous magnetic moment," *Phys. Rev. D*, vol. 67, p. 073 006, 2003, [Erratum: Phys.Rev.D 73, 119901 (2006)]. DOI: 10.1103/PhysRevD.67.073006. arXiv: hep-ph/0212229.

[202] C. Gnendiger, D. Stöckinger, and H. Stöckinger-Kim, "The electroweak contributions to $(g-2)_\mu$ after the Higgs boson mass measurement," *Phys. Rev.*

D, vol. 88, p. 053 005, 2013. DOI: 10.1103/PhysRevD.88.053005. arXiv: 1306.5546 [hep-ph].

[203] M. Hoferichter, J. Lüdtke, L. Naterop, M. Procura, and P. Stoffer, "Improved Evaluation of the Electroweak Contribution to Muon g-2," *Phys. Rev. Lett.*, vol. 134, no. 20, p. 201 801, 2025. DOI: 10.1103/PhysRevLett.134.201801. arXiv: 2503.04883 [hep-ph].

[204] L. Di Luzio, A. Keshavarzi, A. Masiero, and P. Paradisi, "Model-Independent Tests of the Hadronic Vacuum Polarization Contribution to the Muon g-2," *Phys. Rev. Lett.*, vol. 134, no. 1, p. 011 902, 2025. DOI: 10.1103/PhysRevLett.134.011902. arXiv: 2408.01123 [hep-ph].

[205] A. Kurz, T. Liu, P. Marquard, and M. Steinhauser, "Hadronic contribution to the muon anomalous magnetic moment to next-to-next-to-leading order," *Phys. Lett. B*, vol. 734, pp. 144–147, 2014. DOI: 10.1016/j.physletb.2014.05.043. arXiv: 1403.6400 [hep-ph].

[206] G. Colangelo, M. Hoferichter, A. Nyffeler, M. Passera, and P. Stoffer, "Remarks on higher-order hadronic corrections to the muon g−2," *Phys. Lett. B*, vol. 735, pp. 90–91, 2014. DOI: 10.1016/j.physletb.2014.06.012. arXiv: 1403.7512 [hep-ph].

[207] T. Blum et al., "Hadronic Light-by-Light Scattering Contribution to the Muon Anomalous Magnetic Moment from Lattice QCD," *Phys. Rev. Lett.*, vol. 124, no. 13, p. 132 002, 2020. DOI: 10.1103/PhysRevLett.124.132002. arXiv: 1911.08123 [hep-lat].

[208] E.-H. Chao, R. J. Hudspith, A. Gérardin, J. R. Green, H. B. Meyer, and K. Ottnad, "Hadronic light-by-light contribution to $(g-2)_\mu$ from lattice QCD: a complete calculation," *Eur. Phys. J. C*, vol. 81, no. 7, p. 651, 2021. DOI: 10.1140/epjc/s10052-021-09455-4. arXiv: 2104.02632 [hep-lat].

[209] E.-H. Chao, R. J. Hudspith, A. Gérardin, J. R. Green, and H. B. Meyer, "The charm-quark contribution to light-by-light scattering in the muon $(g-2)$ from lattice QCD," *Eur. Phys. J. C*, vol. 82, no. 8, p. 664, 2022. DOI: 10.1140/epjc/s10052-022-10589-2. arXiv: 2204.08844 [hep-lat].

[210] T. Blum et al., "Hadronic light-by-light contribution to the muon anomaly from lattice QCD with infinite volume QED at physical pion mass," *Phys. Rev. D*, vol. 111, no. 1, p. 014 501, 2025. DOI: 10.1103/PhysRevD.111.014501. arXiv: 2304.04423 [hep-lat].

[211] Z. Fodor, A. Gerardin, L. Lellouch, K. K. Szabo, B. C. Toth, and C. Zimmermann, "Hadronic light-by-light scattering contribution to the anomalous magnetic moment of the muon at the physical pion mass," Nov. 2024. arXiv: 2411.11719 [hep-lat].

[212] P. Masjuan and P. Sanchez-Puertas, "Pseudoscalar-pole contribution to the $(g_\mu - 2)$: a rational approach," *Phys. Rev. D*, vol. 95, no. 5, p. 054 026, 2017. DOI: 10.1103/PhysRevD.95.054026. arXiv: 1701.05829 [hep-ph].

[213] M. Hoferichter, B.-L. Hoid, B. Kubis, S. Leupold, and S. P. Schneider, "Dispersion relation for hadronic light-by-light scattering: pion pole," *JHEP*, vol. 10, p. 141, 2018. DOI: 10.1007/JHEP10(2018)141. arXiv: 1808.04823 [hep-ph].

[214] G. Eichmann, C. S. Fischer, E. Weil, and R. Williams, "Single pseudoscalar meson pole and pion box contributions to the anomalous magnetic moment of the muon," *Phys. Lett. B*, vol. 797, p. 134 855, 2019, [Erratum: Phys.Lett.B 799, 135029 (2019)]. DOI: 10.1016/j.physletb.2019.134855. arXiv: 1903.10844 [hep-ph].

[215] J. Bijnens, N. Hermansson-Truedsson, and A. Rodríguez-Sánchez, "Short-distance constraints for the HLbL contribution to the muon anomalous magnetic moment," *Phys. Lett. B*, vol. 798, p. 134 994, 2019. DOI: 10.1016/j.physletb.2019.134994. arXiv: 1908.03331 [hep-ph].

[216] J. Leutgeb and A. Rebhan, "Axial vector transition form factors in holographic QCD and their contribution to the anomalous magnetic moment of the muon," *Phys. Rev. D*, vol. 101, no. 11, p. 114 015, 2020. DOI: 10.1103/PhysRevD.101.114015. arXiv: 1912.01596 [hep-ph].

[217] L. Cappiello, O. Catà, G. D'Ambrosio, D. Greynat, and A. Iyer, "Axial-vector and pseudoscalar mesons in the hadronic light-by-light contribution to the muon $(g-2)$," *Phys. Rev. D*, vol. 102, no. 1, p. 016 009, 2020. DOI: 10.1103/PhysRevD.102.016009. arXiv: 1912.02779 [hep-ph].

[218] P. Masjuan, P. Roig, and P. Sánchez-Puertas, "The interplay of transverse degrees of freedom and axial-vector mesons with short-distance constraints in g $-$ 2," *J. Phys. G*, vol. 49, no. 1, p. 015 002, 2022. DOI: 10.1088/1361-6471/ac3892. arXiv: 2005.11761 [hep-ph].

[219] J. Bijnens, N. Hermansson-Truedsson, L. Laub, and A. Rodríguez-Sánchez, "Short-distance HLbL contributions to the muon anomalous magnetic moment beyond perturbation theory," *JHEP*, vol. 10, p. 203, 2020. DOI: 10.1007/JHEP10(2020)203. arXiv: 2008.13487 [hep-ph].

[220] J. Bijnens, N. Hermansson-Truedsson, L. Laub, and A. Rodríguez-Sánchez, "The two-loop perturbative correction to the $(g-2)_\mu$ HLbL at short distances," *JHEP*, vol. 04, p. 240, 2021. DOI: 10.1007/JHEP04(2021)240. arXiv: 2101.09169 [hep-ph].

[221] I. Danilkin, M. Hoferichter, and P. Stoffer, "A dispersive estimate of scalar contributions to hadronic light-by-light scattering," *Phys. Lett. B*, vol. 820, p. 136 502, 2021. DOI: 10.1016/j.physletb.2021.136502. arXiv: 2105.01666 [hep-ph].

[222] D. Stamen, D. Hariharan, M. Hoferichter, B. Kubis, and P. Stoffer, "Kaon electromagnetic form factors in dispersion theory," *Eur. Phys. J. C*, vol. 82, no. 5, p. 432, 2022. DOI: 10.1140/epjc/s10052-022-10348-3. arXiv: 2202.11106 [hep-ph].

[223] J. Leutgeb, J. Mager, and A. Rebhan, "Hadronic light-by-light contribution to the muon g-2 from holographic QCD with solved U(1)A problem," *Phys. Rev. D*, vol. 107, no. 5, p. 054 021, 2023. DOI: 10.1103/PhysRevD.107.054021. arXiv: 2211.16562 [hep-ph].

[224] M. Hoferichter, B. Kubis, and M. Zanke, "Axial-vector transition form factors and $e^+e^- \to f_1\pi^+\pi^-$," *JHEP*, vol. 08, p. 209, 2023. DOI: 10.1007/JHEP08(2023)209. arXiv: 2307.14413 [hep-ph].

[225] M. Hoferichter, P. Stoffer, and M. Zillinger, "An optimized basis for hadronic light-by-light scattering," *JHEP*, vol. 04, p. 092, 2024. DOI: 10.1007/JHEP04(2024)092. arXiv: 2402.14060 [hep-ph].

[226] E. J. Estrada, S. Gonzàlez-Solís, A. Guevara, and P. Roig, "Improved π^0, η, η' transition form factors in resonance chiral theory and their a_μ^{HLbL} contribution," *JHEP*, vol. 12, p. 203, 2024. DOI: 10.1007/JHEP12(2024)203. arXiv: 2409.10503 [hep-ph].

[227] O. Deineka, I. Danilkin, and M. Vanderhaeghen, "Dispersive estimate of the a0(980) contribution to (g-2)μ," *Phys. Rev. D*, vol. 111, no. 3, p. 034 009, 2025. DOI: 10.1103/PhysRevD.111.034009. arXiv: 2410.12894 [hep-ph].

[228] G. Eichmann, C. S. Fischer, T. Haeuser, and O. Regenfelder, "Axial-vector and scalar contributions to hadronic light-by-light scattering," *Eur. Phys. J. C*, vol. 85, no. 4, p. 445, 2025. DOI: 10.1140/epjc/s10052-025-14055-7. arXiv: 2411.05652 [hep-ph].

[229] J. Bijnens, N. Hermansson-Truedsson, and A. Rodríguez-Sánchez, "Constraints on the hadronic light-by-light tensor in corner kinematics for the muon g $-$ 2," *JHEP*, vol. 03, p. 094, 2025. DOI: 10.1007/JHEP03(2025)094. arXiv: 2411.09578 [hep-ph].

[230] M. Hoferichter, P. Stoffer, and M. Zillinger, "Dispersion relation for hadronic light-by-light scattering: subleading contributions," *JHEP*, vol. 02, p. 121, 2025. DOI: 10.1007/JHEP02(2025)121. arXiv: 2412.00178 [hep-ph].

[231] S. Holz, M. Hoferichter, B.-L. Hoid, and B. Kubis, "Dispersion relation for hadronic light-by-light scattering: η and η poles," *JHEP*, vol. 04, p. 147, 2025. DOI: 10.1007/JHEP04(2025)147. arXiv: 2412.16281 [hep-ph].

[232] L. Cappiello, J. Leutgeb, J. Mager, and A. Rebhan, "Tensor meson transition form factors in holographic QCD and the muon $g-2$," Jan. 2025. arXiv: 2501.09699 [hep-ph].

[233] K. Melnikov and A. Vainshtein, "Hadronic light-by-light scattering contribution to the muon anomalous magnetic moment revisited," *Phys. Rev. D*, vol. 70, p. 113 006, 2004. DOI: 10.1103/PhysRevD.70.113006. arXiv: hep-ph/0312226.

[234] P. Roig and P. Sánchez-Puertas, "Axial-vector exchange contribution to the hadronic light-by-light piece of the muon anomalous magnetic moment," *Phys. Rev. D*, vol. 101, no. 7, p. 074 019, 2020. DOI: 10.1103/PhysRevD.101.074019. arXiv: 1910.02881 [hep-ph].

[235] G. Colangelo, F. Hagelstein, M. Hoferichter, L. Laub, and P. Stoffer, "Short-distance constraints on hadronic light-by-light scattering in the anomalous magnetic moment of the muon," *Phys. Rev. D*, vol. 101, no. 5, p. 051 501, 2020. DOI: 10.1103/PhysRevD.101.051501. arXiv: 1910.11881 [hep-ph].

[236] M. Knecht, "On some short-distance properties of the fourth-rank hadronic vacuum polarization tensor and the anomalous magnetic moment of the muon," *JHEP*, vol. 08, p. 056, 2020. DOI: 10.1007/JHEP08(2020)056. arXiv: 2005.09929 [hep-ph].

[237] J. Leutgeb, J. Mager, and A. Rebhan, "Holographic QCD and the muon anomalous magnetic moment," *Eur. Phys. J. C*, vol. 81, no. 11, p. 1008, 2021. DOI: 10.1140/epjc/s10052-021-09780-8. arXiv: 2110.07458 [hep-ph].

[238] P. Colangelo, F. Giannuzzi, and S. Nicotri, "Hadronic light-by-light scattering contributions to (g-2)μ from axial-vector and tensor mesons in the holographic soft-wall model," *Phys. Rev. D*, vol. 109, no. 9, p. 094 036, 2024. DOI: 10.1103/PhysRevD.109.094036. arXiv: 2402.07579 [hep-ph].

[239] J. Mager, L. Cappiello, J. Leutgeb, and A. Rebhan, "Longitudinal short-distance constraints on hadronic light-by-light scattering and tensor meson contributions to the muon $g-2$," Jan. 2025. arXiv: 2501.19293 [hep-ph].

[240] E. J. Estrada and P. Roig, "Tensor Meson Pole contributions to the HLbL piece of a_μ^{HLbL} within RχT," Apr. 2025. arXiv: 2504.00448 [hep-ph].

[241] A. Anastasi et al., "Combination of KLOE $\sigma\big(e^+e^- \to \pi^+\pi^-\gamma(\gamma)\big)$ measurements and determination of $a_\mu^{\pi^+\pi^-}$ in the energy range $0.10 < s < 0.95$ GeV^2," *JHEP*, vol. 03, p. 173, 2018. DOI: 10.1007/JHEP03(2018)173. arXiv: 1711.03085 [hep-ex].

[242] J. P. Lees et al., "Precise Measurement of the $e^+e^- \to \pi^+\pi^-(\gamma)$ Cross Section with the Initial-State Radiation Method at BABAR," *Phys. Rev. D*, vol. 86, p. 032 013, 2012. DOI: 10.1103/PhysRevD.86.032013. arXiv: 1205.2228 [hep-ex].

[243] T. Blum et al., "Calculation of the hadronic vacuum polarization contribution to the muon anomalous magnetic moment," *Phys. Rev. Lett.*, vol. 121, no. 2, p. 022 003, 2018. DOI: 10.1103/PhysRevLett.121.022003. arXiv: 1801.07224 [hep-lat].

[244] D. Giusti, V. Lubicz, G. Martinelli, F. Sanfilippo, and S. Simula, "Electromagnetic and strong isospin-breaking corrections to the muon $g-2$ from Lattice QCD+QED,"

Phys. Rev. D, vol. 99, no. 11, p. 114 502, 2019. DOI: 10.1103/PhysRevD.99.114502. arXiv: 1901.10462 [hep-lat].

[245] C. Lehner and A. S. Meyer, "Consistency of hadronic vacuum polarization between lattice QCD and the R-ratio," *Phys. Rev. D*, vol. 101, p. 074 515, 2020. DOI: 10.1103/PhysRevD.101.074515. arXiv: 2003.04177 [hep-lat].

[246] G. Wang, T. Draper, K.-F. Liu, and Y.-B. Yang, "Muon g-2 with overlap valence fermions," *Phys. Rev. D*, vol. 107, no. 3, p. 034 513, 2023. DOI: 10.1103/PhysRevD.107.034513. arXiv: 2204.01280 [hep-lat].

[247] C. Aubin, T. Blum, M. Golterman, and S. Peris, "Muon anomalous magnetic moment with staggered fermions: Is the lattice spacing small enough?" *Phys. Rev. D*, vol. 106, no. 5, p. 054 503, 2022. DOI: 10.1103/PhysRevD.106.054503. arXiv: 2204.12256 [hep-lat].

[248] M. Cè et al., "Window observable for the hadronic vacuum polarization contribution to the muon g-2 from lattice QCD," *Phys. Rev. D*, vol. 106, no. 11, p. 114 502, 2022. DOI: 10.1103/PhysRevD.106.114502. arXiv: 2206.06582 [hep-lat].

[249] C. Alexandrou et al., "Lattice calculation of the short and intermediate time-distance hadronic vacuum polarization contributions to the muon magnetic moment using twisted-mass fermions," *Phys. Rev. D*, vol. 107, no. 7, p. 074 506, 2023. DOI: 10.1103/PhysRevD.107.074506. arXiv: 2206.15084 [hep-lat].

[250] T. Blum et al., "Update of Euclidean windows of the hadronic vacuum polarization," *Phys. Rev. D*, vol. 108, no. 5, p. 054 507, 2023. DOI: 10.1103/PhysRevD.108.054507. arXiv: 2301.08696 [hep-lat].

[251] S. Kuberski et al., "Hadronic vacuum polarization in the muon g − 2: the short-distance contribution from lattice QCD," *JHEP*, vol. 03, p. 172, 2024. DOI: 10.1007/JHEP03(2024)172. arXiv: 2401.11895 [hep-lat].

[252] A. Boccaletti et al., "High precision calculation of the hadronic vacuum polarisation contribution to the muon anomaly," Jul. 2024. arXiv: 2407.10913 [hep-lat].

[253] S. Spiegel and C. Lehner, "High-precision continuum limit study of the HVP short-distance window," *Phys. Rev. D*, vol. 111, no. 11, p. 114 517, 2025. DOI: 10.1103/mj3d-yq87. arXiv: 2410.17053 [hep-lat].

[254] T. Blum et al., "Long-Distance Window of the Hadronic Vacuum Polarization for the Muon g-2," *Phys. Rev. Lett.*, vol. 134, no. 20, p. 201 901, 2025. DOI: 10.1103/PhysRevLett.134.201901. arXiv: 2410.20590 [hep-lat].

[255] D. Djukanovic et al., "The hadronic vacuum polarization contribution to the muon g − 2 at long distances," *JHEP*, vol. 04, p. 098, 2025. DOI: 10.1007/JHEP04(2025)098. arXiv: 2411.07969 [hep-lat].

[256] C. Alexandrou et al., "Strange and charm quark contributions to the muon anomalous magnetic moment in lattice QCD with twisted-mass fermions," *Phys. Rev. D*, vol. 111, no. 5, p. 054 502, 2025. DOI: 10.1103/PhysRevD.111.054502. arXiv: 2411.08852 [hep-lat].

[257] A. Bazavov et al., "Hadronic vacuum polarization for the muon g-2 from lattice QCD: Complete short and intermediate windows," *Phys. Rev. D*, vol. 111, no. 9, p. 094 508, 2025. DOI: 10.1103/PhysRevD.111.094508. arXiv: 2411.09656 [hep-lat].

[258] A. Bazavov et al., "Hadronic vacuum polarization for the muon $g-2$ from lattice QCD: Long-distance and full light-quark connected contribution," Dec. 2024. arXiv: 2412.18491 [hep-lat].

[259] G. L. Castro, A. Miranda, and P. Roig, "Isospin breaking corrections in 2π production in tau decays and e+e- annihilation: Consequences for the muon g-2 and conserved vector current tests," *Phys. Rev. D*, vol. 111, no. 7, p. 073 004, 2025. DOI: 10.1103/PhysRevD.111.073004. arXiv: 2411.07696 [hep-ph].

[260] M. Davier, B. Malaescu, and Z. Zhang, "Data-based form factor corrections between the two-pion τ and e^+e^- spectral functions," Apr. 2025. arXiv: 2504.13789 [hep-ph].

[261] C. M. Carloni Calame, M. Passera, L. Trentadue, and G. Venanzoni, "A new approach to evaluate the leading hadronic corrections to the muon g-2," *Phys. Lett. B*, vol. 746, pp. 325–329, 2015. DOI: 10.1016/j.physletb.2015.05.020. arXiv: 1504.02228 [hep-ph].

Appendices

Appendix A

Massive Neutrinos

A1 Neutrinos in the SM

In the SM neutrinos come in three flavours, corresponding to the associated charged lepton. They belong to $SU(2)$ doublets

$$\begin{pmatrix} \nu_e \\ e \end{pmatrix}_L , \quad \begin{pmatrix} \nu_\mu \\ \mu \end{pmatrix}_L , \quad \begin{pmatrix} \nu_\tau \\ \tau \end{pmatrix}_L \tag{A.1}$$

and alike (e_R, μ_R, τ_R). There are no SU(2) neutrino singlets.

In the Standard Model, neutrinos are left-handed, and antineutrinos are right-handed. These are the only chiralities that participate in weak interactions, as explicitly shown by the interaction Lagrangians below. Neutrinos interact solely through the weak force via the charged current (CC):

$$\begin{aligned} W^- &\longrightarrow l_\alpha^- + \overline{\nu}_\alpha \\ W^+ &\longrightarrow l_\alpha^+ + \nu_\alpha, \end{aligned} \tag{A.2}$$

with the interaction Lagrangian

$$\mathcal{L}_{int}^{CC} = -\frac{g}{2\sqrt{2}} \left(\sum_\alpha \overline{\nu}_\alpha \gamma_\mu (1 - \gamma_5) l_\alpha W^\mu + \text{h.c.} \right) \tag{A.3}$$

And via the neutral current (NC):

$$Z^0 \longrightarrow \nu_\alpha + \overline{\nu}_\alpha, \tag{A.4}$$

with the interaction Lagrangian

$$\mathcal{L}_{int}^{NC} = -\frac{g}{4\cos\theta_W}\left(\sum_{\alpha}\overline{\nu}_{\alpha}\gamma_{\mu}(1-\gamma_5)\nu_{\alpha}Z^{\mu} + \text{h.c.}\right), \tag{A.5}$$

where $\alpha = e, \mu, \tau$.

In the SM, fermion masses appear in the Lagrangian as Dirac mass terms of the form $m\overline{\Psi}\Psi$. Thus, decomposing into its chiral states ($\Psi = \Psi_L + \Psi_R$):

$$\begin{aligned}\mathcal{L}_{m_D} &= m_D\overline{\Psi}\Psi = m_D(\overline{\Psi}_L + \overline{\Psi}_R)(\Psi_L + \Psi_R)\\ &= m_D(\overline{\Psi}_L\Psi_L + \overline{\Psi}_L\Psi_R + \overline{\Psi}_R\Psi_L + \overline{\Psi}_R\Psi_R),\end{aligned} \tag{A.6}$$

and using the properties of the chiral projectors: $\Psi_{L,R} = P_{L,R}\Psi$, $\overline{\Psi}_{L,R} = \overline{\Psi}P_{R,L}$ and $P_{L,R}P_{R,L} = 0$ we obtain, for the Dirac mass term

$$\mathcal{L}_{m_D} = m_D(\overline{\Psi}_L\Psi_R + \overline{\Psi}_R\Psi_L), \tag{A.7}$$

coupling the L and R chiral states of a particle. But since SM neutrinos have only a L-chiral state, i.e., there is no R-chiral states for neutrinos (N_R), this mass term is not possible, so neutrinos cannot have a Dirac mass in the SM.

The only option left, is to try to make a mass term from ν_L alone. This kind of term, known as Majorana mass term, is of the form:

$$\mathcal{L}_{m_M} = \frac{1}{2}m_M(\overline{\nu_L^C}\nu_L + \overline{\nu}_L\nu_L^C), \tag{A.8}$$

where ν^C is the charge conjugate field, defined as $\nu^C = C\overline{\nu}^T$.

This type of term violates all lepton numbers by two units. However, as we shall see in Appendix B, neutrinos can be Majorana fermions, so such a term is not forbidden. Nonetheless, this mass term is not invariant under weak isospin, and therefore it cannot appear in the Standard Model Lagrangian in its current form (see the next section).

In conclusion, the fact that no right-handed neutrinos N_R appear in the SM and that the $\overline{\nu_L^C}\nu_L$ term is forbidden by weak isospin, make the neutrinos massless within the SM. Nowadays, we know that neutrinos do have mass [173], so we need to introduced neutrino

masses beyond the SM.

A2 Massive Neutrinos

In order to account for neutrino masses, the SM framework needs to be extended. There are many extensions of the SM that try to explain the experimental results of neutrino masses, these new models usually incorporate right-handed neutrino fields and extend even more the particle content with the existence of a new Higgs triplet or other lepton $SU(2)$ singlets, etc.

Every model comes with a characteristic energy scale for the new physics, and in principle, some of these scenarios could produce observable deviations from the Standard Model predictions in current experiments, thanks to the high precision that has been achieved.

A minimal extension is the so-called νSM [174], which adds right-handed components for the three neutrinos families. The neutrino masses appear as a Dirac mass term in the Lagrangian via Yukawa couplings with the Higgs doublet, just like for all other fermions. Nevertheless, the νSM requires extremely tiny Yukawa couplings ($Y_\nu \simeq 10^{-13}$) in order to explain the observed neutrino masses. As a consequence of the mass mechanism, there is a mixing between the mass eigenstates and the flavour eigenstates, analogous to the quark sector. This mixing is described by the well-known Pontecorvo-Maki-Nakagawa-Sakata (PMNS) matrix [175], [176].

In the νSM the effects of Majorana neutrinos are suppressed by a factor of $(m_\nu/E)^2$, being E the energy scale of the process and m_ν the corresponding neutrino mass ($m_\nu \sim eV$). Thus, in this model, any experimental observation of these effects is out of scope, even with the accuracy achieved by the recent experiments. Other models include a heavy neutrino sector (N) with Majorana masses, where the processes can also be mediated by those heavy neutrinos, but the heavy-light mixing implies then a suppression of order of $(E/m_N)^2$.

In the simplest scenarios, the heavy neutrino mass can be as large as $m_N \simeq 10^{14}\ GeV$ so $(E/m_N)^2$ is really small. Even so, there are scenarios, usually known as low-scale seesaw models, that allow for arbitrary masses in the heavy neutrino sector and then unsuppressed heavy-light mixings, where precise measurements of the possible new physics

could be made, see e.g., [99], [177], [178], [179], [180], [181].

In the following sections, we will briefly describe two neutrino mass models: the type-I seesaw model, where the tiny neutrino masses arise from a very large Majorana mass of the right-handed singlet, and a low-scale variant known as the inverse seesaw model, which features an unsuppressed heavy–light neutrino mixing.

A3 Type I Seesaw Model

Based on [182], once the right-handed neutrino field (N_R) is included, no SM symmetry forbids the Majorana mass term to appear. Thus, if, in addition to the Dirac mass term, the right-handed singlets have Majorana masses, the full mass Lagrangian becomes:

$$\mathcal{L}_{D+M} = \overline{\nu}_L m_D N_R + \frac{1}{2}\overline{N_R^C} m_R N_R + \text{h.c.} \tag{A.9}$$

Where ν_L and N_R are, respectively, the weak eigenstates of the left-handed and right-handed neutrinos. Explicitly, we write $\nu_L^T = (\nu_{eL}, \nu_{\mu L}, \nu_{\tau L})$ and $N_R^T = (N_{eR}, N_{\mu R}, N_{\tau R})$. Actually, the leptonic content in the theory can include n right-handed SM singlets (n≥2 for at least two massive neutrinos), but here we choose only three, that correspond to the right-handed parts of the weak eigenstates, just to show the general idea of the type I seesaw mechanism.

Now, using the identity $\overline{\nu}_L m_D N_R = \overline{(N_R)^C} m_D^T (\nu_L)^C$, the mass term (A.9) can be written as:

$$\mathcal{L}_{D+M} = \frac{1}{2}\left[\overline{(\nu_L)} m_D (N_R) + \overline{(N_R)^C} m_D^T (\nu_L)^C + \overline{(N_R)^C} m_R (N_R)\right] + \text{h.c.} \tag{A.10}$$

$$\mathcal{L}_{D+M} = \frac{1}{2}\begin{pmatrix}\overline{(\nu_L)} & \overline{(N_R)^C}\end{pmatrix} \mathcal{M} \begin{pmatrix}(\nu_L)^C \\ (N_R)\end{pmatrix}, \tag{A.11}$$

where $\mathcal{M}$ is a symmetric 6×6 matrix defined by

$$\mathcal{M} = \begin{pmatrix} 0 & m_D \\ m_D^T & m_R \end{pmatrix}. \tag{A.12}$$

In principle, the $\mathcal{M}$ matrix can be diagonalized by an orthogonal transformation to

determine the neutrino masses. However, we employ the 6×6 unitary matrix $\mathcal{U}$ to ensure that all mass eigenvalues are positive [174]:

$$\mathcal{U}^{\dagger}\mathcal{M}\mathcal{U}^{*} = \mathcal{U}^{\dagger}\begin{pmatrix} 0 & m_D \\ m_D^T & m_R \end{pmatrix}\mathcal{U}^{*} = \begin{pmatrix} m_\nu & 0 \\ 0 & m_N \end{pmatrix} \equiv \mathcal{D}, \tag{A.13}$$

$$\mathcal{M} = \mathcal{U}\mathcal{D}\mathcal{U}^{T}. \tag{A.14}$$

Here, $\mathcal{D}$ is a diagonal matrix whose elements represent the masses of the Majorana-type neutrinos and the mass eigenvalues are of the order

$$m_\nu \approx \frac{m_D^2}{m_R}, \quad m_N \approx m_R, \tag{A.15}$$

where $m_R >> m_D$ and m_D is of the order of the mass of a charged lepton or quark.

Therefore, substituting (A.14) in (A.11) we obtain:

$$\mathcal{L}_{D+M} = \frac{1}{2}\begin{pmatrix}\overline{(\nu_L)} & \overline{(N_R)^C}\end{pmatrix}\mathcal{U}\mathcal{D}\mathcal{U}^{T}\begin{pmatrix}(\nu_L)^C \\ (N_R)\end{pmatrix} = \frac{1}{2}\begin{pmatrix}\overline{(\nu_L^m)} & \overline{(N_R^m)^C}\end{pmatrix}\mathcal{D}\begin{pmatrix}(\nu_L^m)^C \\ (N_R^m)\end{pmatrix}, \tag{A.16}$$

with the mass eigenstates ν^m and N^m.

In this scenario, the small masses of the left-handed Majorana neutrinos (ν^m) are naturally explained by the seesaw mechanism, assuming that the right-handed Majorana neutrinos (N^m) have very large masses. For instance, if the neutrino Dirac mass is $m_D \approx 10$ GeV and the heavy partner mass is $m_N \approx 10^{14}$ GeV, the resulting light neutrino mass m_ν falls in the meV range, consistent with current experimental observations.

Furthermore, the weak eigenstates of neutrinos are expressed as superpositions of the mass eigenstates Majorana neutrinos as follows:

$$\begin{pmatrix}(\nu_L) \\ (N_R)^C\end{pmatrix} = \mathcal{U}\begin{pmatrix}(\nu_L^m) \\ (N_R^m)^C\end{pmatrix}. \tag{A.17}$$

The unitary matrix can be parameterized as

$$\mathcal{U} = \begin{pmatrix} U_{3\times3} & V_{3\times3} \\ X_{3\times3} & Y_{3\times3} \end{pmatrix}, \tag{A.18}$$

then

$$\nu_{aL} = \sum_{m=1}^{3} U_{am}\nu_L^m + \sum_{m=4}^{6} V_{am}(N_R^m)^C, \tag{A.19}$$

$$N_{bR} = \sum_{m=1}^{3} X_{Bm}^*(\nu_L^m)^C + \sum_{m=4}^{6} Y_{bm}^* N_R^m. \tag{A.20}$$

Parametrically, U$U^\dagger$ and $Y^\dagger$ Y $\sim \mathcal{O}(1)$, V$V^\dagger$ and $X^\dagger$ X$\sim \mathcal{O}(m_\nu/m_N)$.
From the neutrinos mixing (A.19) and (A.20) we see that our familiar left-handed neutrinos are mostly the light Majorana neutrinos, with small masses $m_\nu \approx m_D^2/m_N$ and the right-handed neutrinos are mostly the heavy Majorana neutrinos with large masses m_N.

In conclusion, in this model the sterile right-handed Majorana neutrinos must have extremely large masses for the light neutrino masses m_ν to lie in the meV range. Under these conditions, the heavy-light mixing is negligible, leading to a strong suppression of Majorana effects. Moreover, the N^m Majorana neutrinos are too heavy to be produced on-shell. Therefore, within this framework, any deviations from the Standard Model due to Majorana neutrinos in leptonic decays or other processes are expected to be far beyond the reach of foreseeable experiments.

A4 Inverse Seesaw Model

As we discussed in the type I seesaw model, in order to have small neutrino masses the typical scale of the extra particles (such as right-handed neutrinos) is in general very high, potentially very close to the gauge coupling unification (GUT) scale, thus implying that direct experimental tests of the seesaw hypothesis might be impossible. In contrast, low-scale seesaw mechanisms, in which sterile fermions are added to the SM particle content with masses around the electroweak scale or even lower, are very attractive from a phenomenological point of view, since the new states can be produced in colliders or low-energy experiments, and their contributions to physical processes can be sizeable.

In this section, we briefly summarize the main properties of the inverse seesaw model

(ISS), based on [178], [183], which is a low-scale seesaw mechanism. The ISS requires the addition of right-handed neutrinos (N_R) and extra sterile fermions (S).

$$(\nu, N^C, S) \quad \text{with} \quad L = (+1, -1, +1), \tag{A.21}$$

where N and S are $SU(2)$ singlets.

With this lepton content, it is possible to build the general mass Lagrangian, as we did for the type I seesaw model case, and obtain the $\mathcal{M}$ matrix, analogue to (A.12), defined by

$$\mathcal{L}_{m_\nu} = \frac{1}{2} n_L^T C \mathcal{M} n_L + \text{h.c.}, \tag{A.22}$$

where $n_L = (\nu_L, (N_R)^C, S)^T$ and

$$\mathcal{M} = \begin{pmatrix} 0 & m_D & 0 \\ m_D^T & 0 & M \\ 0 & M^T & \mu \end{pmatrix}. \tag{A.23}$$

Once $\mathcal{M}$ is diagonalized, the light mass-eigenstate neutrinos (ν^m) acquire the mass eigenvalues

$$m_\nu = m_D (M^T)^{-1} \mu M^{-1} m_D^T. \tag{A.24}$$

The distinctive feature of the ISS is the presence of an additional dimensionful parameter, μ, which allows the smallness of the active neutrino masses to be achieved even for a low seesaw scale. This, in turn, permits sizeable mixings between the active and additional sterile states. These characteristics stand in clear contrast to the canonical type I seesaw.

It happens that standard neutrinos with mass at sub-eV scale are obtained for m_D at electroweak scale, M at TeV scale and μ at keV scale. Thus, m_ν can be very light even if M is far below GUT scale. In this case all the heavy neutrinos may develop masses around TeV scale and their mixing with the standard neutrinos is modulated by the ratio m_D/M, not as supressed as the one obtained from the type I seesaw model.

In conclusion, this low-scale seesaw mechanism results in non-negligible mixings and moderately heavy neutrino masses—much lower than in the type I seesaw—so that their potential contributions to physical processes could be measurable in current and future

experiments.

Appendix B

Majorana Fermions

B1 Majorana Fermions

For a Dirac fermion we already have an invariant that is quadratic in the fermion fields, the well-known operator $\overline{\Psi}\Psi$, that is identified as the mass term for such fermion field Ψ. Actually, there can be other kinds of quadratic invariants involving fermion fields. Especially we can ask whether we can make any invariant of the form $\Psi_a A_{ab} \Psi_b$, where a,b are spinor indexes and A is a constant matrix. The spinor indexes are contracted in order to obtain a Lorentz invariant and thus, this new term can be written as $\Psi^T A \Psi$ in matrix notation.

Under Lorentz transformations, a fermion field transforms as follows:

$$\Psi(x) \longrightarrow \Psi^{'}(x') = \exp\left(-\frac{i}{4}\omega^{\mu\nu}\sigma_{\mu\nu}\right)\Psi(x), \tag{B.1}$$

where

$$\sigma_{\mu\nu} = \frac{i}{2}\left[\gamma_\mu, \gamma_\nu\right], \tag{B.2}$$

and $w^{\mu\nu}$'s are the parameters of the transformation. Thus, in order for $\Psi^T A \Psi$ to be Lorentz invariant, it needs to satisfy:

$$\Psi^{'T}(x')A\Psi^{'}(x') = \Psi^T(x)A\Psi(x). \tag{B.3}$$

Using (B.1) in the left-hand side of (B.3) we have

$$\Psi^{'T}(x')A\Psi^{'}(x') = \Psi^T(x)\ \exp\left(-\frac{i}{4}\omega^{\mu\nu^T}\sigma_{\mu\nu}\right) A\ \exp\left(-\frac{i}{4}\omega^{\mu\nu}\sigma_{\mu\nu}\right)\Psi(x), \tag{B.4}$$

or, examining the first-order terms in the transformation parameters $w^{\mu\nu}$

$$\begin{aligned}\Psi'^{T}(x')A\Psi'(x') &= \Psi^{T}(x)\left(1-\frac{i}{4}\omega^{\mu\nu}\sigma^{T}_{\mu\nu}\right)A\left(1-\frac{i}{4}\omega^{\mu\nu}\sigma_{\mu\nu}\right)\Psi(x)\\ &= \Psi^{T}(x)\left(A-\frac{i}{4}\omega^{\mu\nu}(\sigma^{T}_{\mu\nu}A+A\sigma_{\mu\nu})\right)\Psi(x).\end{aligned} \tag{B.5}$$

Equation (B.5), together with (B.3), shows that invariance will be achieved if the matrix A satisfies the condition

$$\sigma^{T}_{\mu\nu}A + A\sigma_{\mu\nu} = 0, \tag{B.6}$$

i.e., if

$$\sigma^{T}_{\mu\nu} = -A\sigma_{\mu\nu}A^{-1}. \tag{B.7}$$

Finally, it is well known that, under charge conjugation C, a fermion field transforms as

$$\Psi(x) \longrightarrow \Psi^{c}(x) = \gamma_0 C\Psi^{*}(x), \tag{B.8}$$

such that the Lorentz transformation properties of $\Psi^{c}(x)$ and $\Psi(x)$ are identical.

This implies, from (B.1), that

$$\Psi'^{c}(x') = \gamma_0 C\Psi'^{*}(x') = \gamma_0\ C\ \exp\left(\frac{i}{4}\omega^{\mu\nu}\sigma^{*}_{\mu\nu}\right)\Psi(x)^{*}, \tag{B.9}$$

needs to be equal to

$$\Psi'^{c}(x') = \exp\left(-\frac{i}{4}\omega^{\mu\nu}\sigma_{\mu\nu}\right)\Psi(x)^{c} = \exp\left(-\frac{i}{4}\omega^{\mu\nu}\sigma_{\mu\nu}\right)\gamma_0 C\Psi^{*}(x). \tag{B.10}$$

Then, comparing these two equations to first order, we obtain the relation

$$\gamma_0 C\sigma^{*}_{\mu\nu} = -\sigma_{\mu\nu}\gamma_0 C, \tag{B.11}$$

or

$$\sigma^{*}_{\mu\nu} = -C^{-1}\gamma_0\sigma_{\mu\nu}\gamma_0 C = -C^{-1}\sigma^{\dagger}_{\mu\nu}C, \tag{B.12}$$

where we have used $\gamma_0\gamma_0 = 1$ and $\sigma^{\dagger}_{\mu\nu} = \gamma_0\sigma_{\mu\nu}\gamma_0$. Thus, taking the hermitian conjugate

and using the unitary nature of the C matrix that ensures $C^\dagger = C^{-1}$, we obtain

$$\sigma_{\mu\nu}^T = -C^{-1}\sigma_{\mu\nu}C. \tag{B.13}$$

Comparing (B.13) with (B.7), we find that we can choose

$$A = C^{-1}. \tag{B.14}$$

Thus, $\Psi^T C^{-1}\Psi$ is a Lorentz invariant quadratic in the fermion field. This kind of invariant was not considered before in the SM formulation, because it can annihilate two units of *charge* and would therefore defy any *charge* conservation. Here, we refer to *charge* as any internal quantum number carried by the corresponding fermion state, such as electric charge or lepton number.

It is immediately clear that for electrically charged fermions, such an invariant cannot be used due to electric charge conservation. In contrast, neutrinos are electrically neutral and carry only lepton number. Although this new invariant would violate lepton number, it is important to note that lepton number is merely an accidental symmetry of the Standard Model and can be broken if additional fields are introduced. Therefore, it is worthwhile to consider the possibility of such a term in the neutrino sector.

Now that we have constructed two kinds of mass terms $\overline{\Psi}\Psi$ and $\Psi^T C^{-1}\Psi$, the equality of both requires

$$\overline{\Psi}\Psi = e^{i\alpha}\Psi^T C^{-1}\Psi, \tag{B.15}$$

where we have introduced a phase $e^{i\alpha}$ in order for $\Psi^T C^{-1}\Psi$ to be hermitian.

Thus

$$\overline{\Psi} = e^{i\alpha}\Psi^T C^{-1}, \tag{B.16}$$

and taking the transpose

$$\gamma_0^T\Psi^* = e^{i\alpha}\left(C^{-1}\right)^T\Psi, \tag{B.17}$$

$$\gamma_0^T\Psi^* = -e^{i\alpha}C^{-1}\Psi \;\longrightarrow\; C\gamma_0^T\Psi^* = -e^{i\alpha}\Psi \;\longrightarrow\; \gamma_0 C\Psi^* = e^{i\alpha}\Psi, \tag{B.18}$$

where we have used the identities $C^T = -C$ and $C\gamma_\mu^T = -\gamma_\mu C$.

So

$$\Psi^c(x) = \gamma_0 C \Psi^*(x) = e^{i\alpha}\Psi(x). \tag{B.19}$$

A fermion field that satisfies eq. (B.19) is called a Majorana field. From the definition of the conjugate field, this implies that a Majorana fermion is its own antiparticle. Imposing the Majorana condition on the plane-wave expansion of a Dirac field, we find that it takes the form:

$$\Psi(x) = \sum_s \int \frac{d^3p}{\sqrt{(2\pi)^3 2E_p}} \left(d_s(\mathbf{p}) u_s(\mathbf{p}) e^{-ip\cdot x} + e^{-i\alpha} d_s^\dagger(\mathbf{p}) v_s(\mathbf{p}) e^{ip\cdot x} \right). \tag{B.20}$$

Thus the plane wave expansion (B.20) is the explicit form of a Majorana field and can annihilate as well as create a Majorana particle.

In this case, the u- and v-spinors satisfy the relations

$$v_s = \gamma_0 C u_s^*, \qquad u_s = \gamma_0 C v_s^*. \tag{B.21}$$

This formalism, as evident from the Majorana condition (B.19), would lead to expressions involving the C matrix, which make it representation-dependent, as we shall see in the Z decay example at the end of this appendix.

B2 Feynman Rules for Majorana Fermions

To work with C-independent expressions, we adopt a more convenient approach. We summarize the Feynman rules for Majorana fermions as presented in [102]. These rules avoid explicit use of the charge-conjugation matrix, enabling representation-independent calculations.

We consider a typical coupling term $\mathcal{L}_I = \overline{\chi}\Gamma\chi$ where each χ can be a Dirac or a Majorana fermion and Γ denotes a generic fermionic interaction including Dirac matrices, coupling constants h^i_{abc} and boson fields:

$$\overline{\chi}\Gamma\chi = h^i_{abc}\overline{\chi}_a\Gamma_i\chi_b\Phi_c, \tag{B.22}$$

where the field Φ summarizes scalar and vector fields and $\Gamma_i = 1, i\gamma_5, \gamma_\mu\gamma_5, \gamma_\mu, \sigma_{\mu\nu}$.

Finally, the charge conjugated Γ' is given by $\Gamma' = C\Gamma^T C^{-1}$ and

$$\Gamma_i' = C\Gamma_i^T C^{-1} = \eta_i \Gamma_i, \tag{B.23}$$

with

$$\eta_i = \begin{cases} 1 & \text{for } \Gamma_i = 1, i\gamma_5, \gamma_\mu\gamma_5 \\ -1 & \text{for } \Gamma_i = \gamma_\mu, \sigma_{\mu\nu} \end{cases} \tag{B.24}$$

In the case of a pure Majorana fermion vertex we obtained $\Gamma = \Gamma'$.

Let Φ be a scalar or vector field and λ, Ψ Majorana and Dirac fermions, respectively. Due to the Goldstone equivalence theorem, these rules also define how the fermion chain interacts with the massive gauge boson.

In our Feynman diagrams, fermions are denoted by solid lines. For Dirac fermions (Ψ), each line carries an arrow which indicates the fermion number flow. Majorana fermions (λ) lines do not carry arrows. The Dirac propagator is denoted by $S(p)$.

The Feynman rules are as follows:

- Draw all possible Feynman diagrams for the process.
- Fix an arbitrary orientation (fermion flow) for each fermion chain. This is shown as blue arrows.
- Start at an external leg (for closed loops at some arbitrary propagator) and write down the Dirac matrices proceeding oppositely to the chosen orientation (blue arrows) through the chain.
- For each internal propagator, external line and vertex insert the appropriate analytic expression as given in Figs. B2.1, B2.2 and B2.3 corresponding to the chosen fermion flow.
- Multiply by a factor (-1) for every closed loop.
- Multiply by the permutation parity of the spinors in the obtained analytical expression with respect to some reference order.
- As far as the determination of the combinatorial factor is concerned, Majorana fermions behave exactly like real scalar or vector fields.

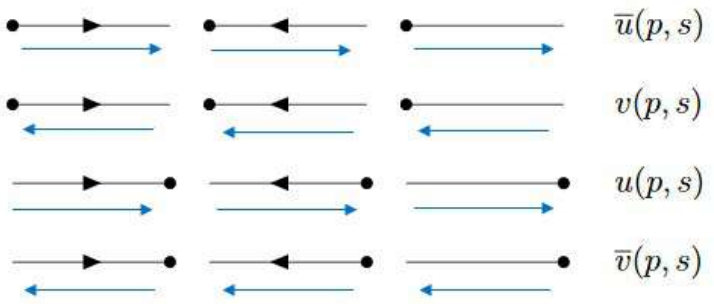

Figure B2.1: Feynman rules for external fermion lines with orientation (blue arrows). The momentum p flows from left to right.

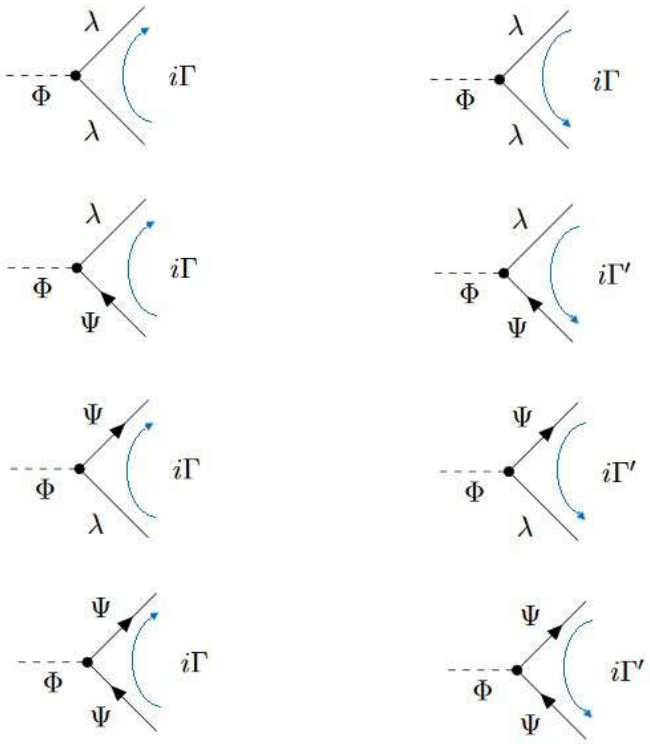

Figure B2.2: Feynman rules for fermionic vertices with orientation (blue arrows).

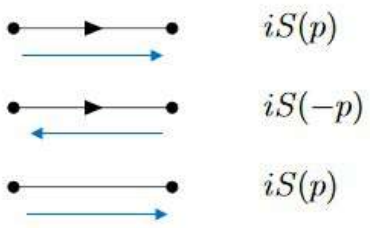

Figure B2.3: Feynman rules for fermion propagators with orientation (blue arrows). The momentum p flows from left to right.

Finally, it is important to note that the analytical expressions are independent of the

chosen orientation (fermion flow), as shown explicitly in [102].

B3 Example: Z Decay into two Majorana Neutrinos

Let us discuss first the decay of a general boson into two Majorana fermions with momenta p_1 and p_2 of the form $\phi \longrightarrow \lambda(p_1) + \lambda(p_2)$. We assume the interaction Lagrangian contains the bilinear $\overline{\Psi} F \Psi$, where F is some numerical matrix. We conclude from the explicit form of the Majorana field operator (B.20), that the amplitude will be

$$\mathcal{M} = e^{-i\alpha} \left[\overline{u}(p_1) F v(p_2) - \overline{v}(p_1) F u(p_2) \right] \mathcal{M}_0, \tag{B.25}$$

where $\mathcal{M}_0$ is a factor that comes from the field operator of the initial boson state.

The amplitude (B.25) shows explicitly the Majorana nature of the final states; since both, Ψ and $\overline{\Psi}$, can create a Majorana particle, it is possible that $\lambda(p_1)$ comes from the action of the Ψ field operator, and $\lambda(p_2)$ from $\overline{\Psi}$; but it can also be the other way around. So we have two contributions in (B.25) because of these two possibilities. If we were dealing with Dirac particles, only one of these two terms would be in the amplitude.

Now, using (B.21) in (B.25) we obtain

$$\begin{aligned} \mathcal{M} &= e^{-i\alpha} \left[\overline{u}(p_1) F v(p_2) - u^T(p_1) C^\dagger \gamma_0^\dagger \gamma_0 F \gamma_0 C v^*(p_2) \right] \mathcal{M}_0 \\ &= e^{-i\alpha} \left[\overline{u}(p_1) F v(p_2) - u^T(p_1) C^{-1} F \gamma_0 C v^*(p_2) \right] \mathcal{M}_0, \end{aligned} \tag{B.26}$$

where we have used all the properties of the C matrix described before.

Finally, since each term is ultimately a number, we can write the second one as the transpose of the matrix expression. Thus, the amplitude (B.25) can be expressed as follows

$$\mathcal{M} = e^{-i\alpha}\ \overline{u}(p_1) \left[F + C F^T C^{-1} \right] v(p_2) \mathcal{M}_0. \tag{B.27}$$

We note the explicit matrix C in (B.27), which makes it representation-dependent, as we discussed before.

For the Lorentz bilinears, we have [46]

F	1	γ_μ	$\sigma_{\mu\nu}$	$\gamma_\mu\gamma_5$	γ^5
CF^TC^{-1}	1	$-\gamma_\mu$	$-\sigma_{\mu\nu}$	$\gamma_\mu\gamma_5$	γ^5

If ϕ corresponds to the Z boson, then $F = \gamma^\mu(a - b\gamma^5)$ and $\mathcal{M}_0 = \epsilon_\mu(k)$, where $\epsilon_\mu(k)$ denotes the polarization vector for the Z boson.

Thus, the amplitude (B.27) for the Z decay into Majorana fermions is written as

$$\mathcal{M} = e^{-i\alpha}\ \overline{u}(p_1)\left[\gamma^\mu(a - b\gamma^5) + C\ (\gamma^\mu(a - b\gamma^5))^T C^{-1}\right] v(p_2)\epsilon_\mu(k). \tag{B.28}$$

But

$$C\ (\gamma^\mu(a - b\gamma^5))^T C^{-1} = aC{\gamma^\mu}^T C^{-1} - bC(\gamma^\mu\gamma^5)^T C^{-1} \tag{B.29}$$

and, as we just discussed,

$$\begin{aligned} C{\gamma^\mu}^T C^{-1} &= -\gamma^\mu \\ C(\gamma^\mu\gamma^5)^T C^{-1} &= \gamma^\mu\gamma^5. \end{aligned} \tag{B.30}$$

Considering these properties, the amplitude (B.28) is reduced to

$$\mathcal{M} = e^{-i\alpha}\ \overline{u}(p_1)\left[\gamma^\mu(a - b\gamma^5) + \gamma^\mu(-a - b\gamma^5)\right] v(p_2)\epsilon_\mu(k). \tag{B.31}$$

$$\mathcal{M} = e^{-i\alpha}\ \overline{u}(p_1)\gamma^\mu(-2b\gamma^5)v(p_2)\epsilon_\mu(k). \tag{B.32}$$

Then, the polar vector term does not contribute to the Feynman amplitude and the axial vector term gets a contribution twice bigger.

Actually, for the standard Z decay into Dirac fermions, it is well-known that [46]

$$\mathcal{M}_Z = \overline{u}(p_1)\gamma^\mu(a - b\gamma^5)v(p_2)\epsilon_\mu(k), \tag{B.33}$$

that leads to the following total decay rate

$$\Gamma_{Z_D} = \frac{M_Z}{12\pi}(a^2 + b^2), \tag{B.34}$$

where the fermion masses have been neglected.

As we can see, the amplitude for the Majorana case (B.32) is exactly the same, up to a non-physical global phase, as the one for the Dirac case (B.33), just by the change $a \to 0$ and $b \to 2b$. So the total decay rate to Majorana fermions can be obtained directly from

(B.34), taking into account the above considerations and multiplying it by a factor (1/2!) due to the indistinguishable property of the Majorana final-state particles.

Thus, for the Z decay into Majorana fermions, the total decay rate is given by

$$\Gamma_{Z_M} = \frac{1}{2}\frac{M_Z}{12\pi}(-2b)^2, \tag{B.35}$$

$$\Gamma_{Z_M} = \frac{M_Z}{6\pi}b^2. \tag{B.36}$$

Finally, if we consider the final fermion states as neutrinos, we know, from the SM, that its couplings to the Z boson is purely left-chiral, i.e., $a = b$, so the total decay rate for the Z boson into two Dirac neutrinos (B.34) reduces to

$$\Gamma_{Z_D} = \frac{M_Z}{6\pi}b^2. \tag{B.37}$$

Comparing (B.36) with (B.37) it is immediate that

$$\Gamma_{Z_D} = \Gamma_{Z_M}. \tag{B.38}$$

As we have just shown, the Dirac or Majorana nature of the neutrino does not affect the decay rate of the Z boson. In principle, for non-zero neutrino masses, there would be corrections that depend on whether the neutrino is Dirac or Majorana. However, these corrections are practically negligible, as they are proportional to the factorm_ν/M_Z, which is really tiny.

It is important to note that this result is consequence of the pure left-chiral coupling $(V - A)$ of the neutrino. Maybe, if there were any other type of coupling or new physics involved in the process, the Majorana effect would lead to a measurable difference in the total decay rate. We therefore have to look for other kind of signatures in order to distinguish between the Dirac or Majorana nature of neutrinos. A way to do that, especially important for this thesis, is the search for Majorana neutrino effects in lepton decays, due to new non-standard couplings and the existence of new high-energy physics that may be detectable in near future experiments, see e.g. [99], [181].

Finally, let us compute the amplitude for the Z decay process using the Feynman rules for Majorana fermions described above, in order to verify the consistency of both approaches.

The possible tree level Feynman diagrams for this process are shown in Fig.B3.1, where we have two distinct contributions due to the Majorana nature of the final particles.

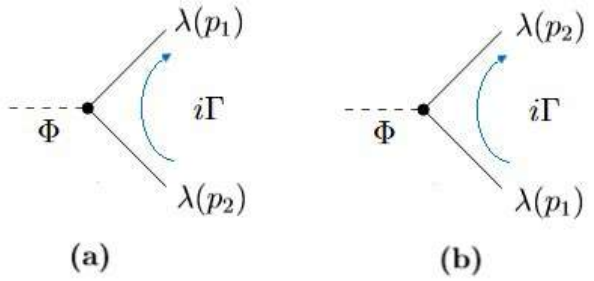

Figure B3.1: Possible Feynman diagrams for the $\phi \longrightarrow \lambda(p_1) + \lambda(p_2)$ process with a fix orientation (blue arrows).

Now, to construct the amplitude, we just insert the appropriate analytic expression as given in Figs. B2.1, B2.2 and B2.3 corresponding to the chosen fermion flow. Thus,

$$i\mathcal{M}' = i\overline{u}(p_1)\Gamma v(p_2) - i\overline{u}(p_2)\Gamma v(p_1), \tag{B.39}$$

where the minus sign is due to the permutation parity of the spinors and the reference order of the external fermions has been chosen as $(p_1; p_2)$.

If we choose the other possible orientation, as shown in Fig. B3.2 , we will have

$$i\mathcal{M}'' = -i\overline{u}(p_2)\Gamma v(p_1) + i\overline{u}(p_1)\Gamma v(p_2). \tag{B.40}$$

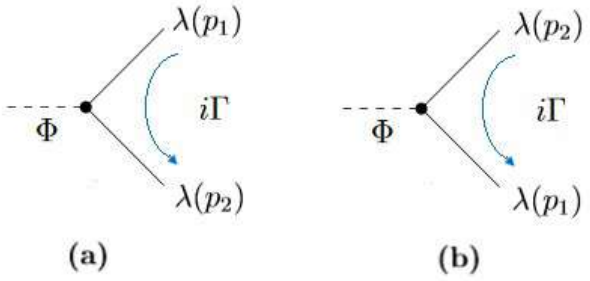

Figure B3.2: Possible Feynman diagrams for the $\phi \longrightarrow \lambda(p_1) + \lambda(p_2)$ process with a fix orientation (blue arrows).

So, as we can see immediately, $\mathcal{M}' = \mathcal{M}''$. Thus, as we discussed before, the amplitude is independent of the chosen orientation of the fermion chain.

Taking $\mathcal{M}'$ with Γ defined as (B.22), we have

$$\mathcal{M}' = \overline{u}(p_1)h_i^c\Gamma^i\phi_c v(p_2) - \overline{u}(p_2)h_i^c\Gamma^i\phi_c v(p_1), \tag{B.41}$$

where for the Z decay $h_i^c\Gamma^i\phi_c = \gamma^\mu(a - b\gamma^5)\epsilon_\mu(k)$, which in terms of the notation used at the beginning of this subsection, $h_i^c\Gamma^i\phi_c = F\mathcal{M}_0$. This leads to the following amplitude

$$\mathcal{M}' = [\overline{u}(p_1)Fv(p_2) - \overline{u}(p_2)Fv(p_1)]\mathcal{M}_0. \tag{B.42}$$

Then,

$$\begin{aligned}
\mathcal{M}' &= \left[\overline{u}(p_1)Fv(p_2) - v^T(p_2)C^\dagger\gamma_0^\dagger\gamma_0 F\gamma_0 C u^*(p_1)\right]\mathcal{M}_0 \\
&= \left[\overline{u}(p_1)Fv(p_2) - v^T(p_2)C^{-1}F\gamma_0 C u^*(p_1)\right]\mathcal{M}_0 \\
&= \left[\overline{u}(p_1)Fv(p_2) - u^\dagger(p_1)C^T\gamma_0^T F^T(C^{-1})^T v(p_2)\right]\mathcal{M}_0 \\
&= \left[\overline{u}(p_1)Fv(p_2) + \overline{u}(p_1)CF^TC^{-1}v(p_2)\right]\mathcal{M}_0,
\end{aligned} \tag{B.43}$$

where in the third line we used the fact that each term is ultimately a number, so we can write it as the transpose of the matrix expression, and we have also used all the properties of the C matrix described before.

Finally,

$$\mathcal{M}' = \overline{u}(p_1)\left[F + CF^TC^{-1}\right]v(p_2)\mathcal{M}_0. \tag{B.44}$$

Comparing (B.44) with (B.27), we see that both amplitudes are the same, up to a non-physical global phase. So either of them would lead to the same observables; ensuring the consistency of both methods.

Appendix C

Fierz Transformations

A Fierz transformation is an operation that rearranges the order of fermion fields in a four-fermion interaction Lagrangian. Two Hamiltonians related by a Fierz transformation are physically equivalent. This is particularly useful, as choosing a specific form of the Hamiltonian can simplify calculations and make the physical interpretation more intuitive.

In this appendix, we summarize the specific Fierz transformations among the most commonly used Hamiltonians in lepton decays. Our primary goal is to show the Fierz transformation relating the Hamiltonian used in [101] to the one employed in this thesis, thereby demonstrating the consistency of both approaches. For further details on Fierz identities and their derivations, we refer the reader to [45], [46].

C1 Lepton Decay Hamiltonians

Leptonic decays can be described using the most general four-fermion contact interaction Hamiltonian. This contact interaction permits the use of equivalent Hamiltonians that differ only in how the fermion fields are grouped.

As discussed in [184], the older literature preferred a *charge retention* form (CRF) with parity-odd and parity-even terms in which the charged-leptons, as the usually detected particles, were grouped together. The CRF Hamiltonian takes the following form:

$$\mathcal{H} = \frac{G_{ll'}}{\sqrt{2}} \sum_i \left\{ (\overline{f}_1 \Gamma_i f_4) \left[D_i (\overline{f}_3 \Gamma^i f_2) + D_i' (\overline{f}_3 \Gamma^i \gamma^5 f_2) \right] + \text{h.c.} \right\}, \tag{C.1}$$

with $i = S, P, A, V, T$ and the Lorentz bilinears are defined as:[49]

$$\begin{aligned} &\Gamma_S \equiv \mathbb{I}, \qquad &&\Gamma_P \equiv i\gamma^5, \qquad &&\Gamma_V \equiv \gamma^\mu, \\ &\Gamma_A \equiv \gamma^\mu \gamma^5, \qquad &&\Gamma_T \equiv \frac{1}{\sqrt{2}} \sigma^{\mu\nu}, \end{aligned} \tag{C.2}$$

with the identification $f_1 = l'$, $f_2 = \nu_{l'}$, $f_3 = \nu_l$ and $f_4 = l$.

[49] Note, in particular, the factor i in the definition of Γ_P.

This had the advantage that limits to some coupling constants could be obtained from the then existing results, but is not adapted to represent a charged boson exchange. For this purpose, one uses a *charge changing* form (CCF), where the charged leptons are grouped with their neutrinos [50] and which is adapted to charged boson exchange and results in absolute values of differences of coupling constants. This CCF Hamiltonian takes the form:

$$\mathcal{H} = \frac{G_{ll'}}{\sqrt{2}} \sum_i \left\{ \left(\overline{f}_1 \Gamma_i f_2\right) \left[C_i (\overline{f}_3 \Gamma^i f_4) + C_i^{'} (\overline{f}_3 \Gamma^i \gamma^5 f_4) \right] + \text{h.c.} \right\} \tag{C.3}$$

However, both these forms are complicated by the fact that a fully parity-violating interaction, such as e.g. the V-A interaction, is represented by four coupling constants C_V , $C_V^{'}$, C_A and $C_A^{'}$ (instead of two, because an interference is needed to violate parity).

Finally, there is the *helicity projection* form (HPF) Hamiltonian, which is the most used nowadays, where the canonical V-A interaction is particularly simple because then $g_{LL}^V = 1$ while all other coupling constants vanish [51] and the contributions from new physics are immediately identified. Its explicit form, used in this thesis, is:

$$\begin{aligned}
\mathcal{H} = \frac{G_{ll'}}{\sqrt{2}} \Bigg\{ & g_{LL}^S \left[\vec{l}\,' (1+\gamma^5) \nu_{l'} \right] \left[\bar{\nu}_l (1-\gamma^5) l \right] + g_{LL}^V \left[\vec{l}\,' \gamma^\mu (1-\gamma^5) \nu_{l'} \right] \left[\bar{\nu}_l \gamma_\mu (1-\gamma^5) l \right] \\
& + g_{RR}^S \left[\vec{l}\,' (1-\gamma^5) \nu_{l'} \right] \left[\bar{\nu}_l (1+\gamma^5) l \right] + g_{RR}^V \left[\vec{l}\,' \gamma^\mu (1+\gamma^5) \nu_{l'} \right] \left[\bar{\nu}_l \gamma_\mu (1+\gamma^5) l \right] \\
& + g_{LR}^S \left[\vec{l}\,' (1+\gamma^5) \nu_{l'} \right] \left[\bar{\nu}_l (1+\gamma^5) l \right] + g_{LR}^V \left[\vec{l}\,' \gamma^\mu (1-\gamma^5) \nu_{l'} \right] \left[\bar{\nu}_l \gamma_\mu (1+\gamma^5) l \right] \\
& + g_{LR}^T \left[\vec{l}\,' \frac{\sigma^{\mu\nu}}{\sqrt{2}} (1+\gamma^5) \nu_{l'} \right] \left[\bar{\nu}_l \frac{\sigma_{\mu\nu}}{\sqrt{2}} (1+\gamma^5) l \right] + g_{RL}^S \left[\vec{l}\,' (1-\gamma^5) \nu_{l'} \right] \left[\bar{\nu}_l (1-\gamma^5) l \right] \\
& + g_{RL}^V \left[\vec{l}\,' \gamma^\mu (1+\gamma^5) \nu_{l'} \right] \left[\bar{\nu}_l \gamma_\mu (1-\gamma^5) l \right] + g_{RL}^T \left[\vec{l}\,' \frac{\sigma^{\mu\nu}}{\sqrt{2}} (1-\gamma^5) \nu_{l'} \right] \left[\bar{\nu}_l \frac{\sigma_{\mu\nu}}{\sqrt{2}} (1-\gamma^5) l \right] \Bigg\}.
\end{aligned} \tag{C.4}$$

Thus, we can obtain the specific Fierz transformation that relates each pair of Hamiltonians.

[50] For this reason also called flavor retention form.

[51] Since the vector and axial vector strengths are the same, we can factor it out this way, recalling that parity violation requires an interference between two different contributions (like CP violation).

The Fierz transformation that relates the CRF and CCF Hamiltonians is [185]:

$$\begin{pmatrix} D_S \\ D_P \\ D_V \\ D_A \\ D_T \end{pmatrix} = \frac{1}{4}\begin{pmatrix} -1 & 1 & -4 & 4 & -6 \\ 1 & -1 & -4 & 4 & 6 \\ -1 & -1 & 2 & 2 & 0 \\ 1 & 1 & 2 & 2 & 0 \\ -1 & 1 & 0 & 0 & 2 \end{pmatrix}\begin{pmatrix} C_S \\ C_P \\ C_V \\ C_A \\ C_T \end{pmatrix}, \quad \begin{pmatrix} D'_S \\ D'_P \\ D'_V \\ D'_A \\ D'_T \end{pmatrix} = \frac{1}{4}\begin{pmatrix} -1 & 1 & 4 & -4 & -6 \\ 1 & -1 & 4 & -4 & 6 \\ 1 & 1 & 2 & 2 & 0 \\ -1 & -1 & 2 & 2 & 0 \\ -1 & 1 & 0 & 0 & 2 \end{pmatrix}, \begin{pmatrix} C'_S \\ C'_P \\ C'_V \\ C'_A \\ C'_T \end{pmatrix}. \tag{C.5}$$

In the same way, the Fierz transformation that relates the CCF and HPF Hamiltonians is [184]:

$$\left.\begin{matrix} C_S \\ C_P \end{matrix}\right\} = (g^S_{LL} + g^S_{RR}) \pm (g^S_{LR} + g^S_{RL}), \qquad \left.\begin{matrix} C'_S \\ C_{P'} \end{matrix}\right\} = -(g^S_{LL} - g^S_{RR}) \pm (g^S_{LR} - g^S_{RL}),$$

$$\left.\begin{matrix} C_V \\ C_A \end{matrix}\right\} = (g^V_{RR} + g^V_{LL}) \pm (g^V_{RL} + g^V_{LR}), \qquad \left.\begin{matrix} C_{V'} \\ C_{A'} \end{matrix}\right\} = (g^V_{RR} - g^V_{LL}) \mp (g^V_{RL} - g^V_{LR}),$$

$$\left.\begin{matrix} C_T \\ C_{T'} \end{matrix}\right\} = 2(g^T_{LR} \pm g^T_{RL}). \tag{C.6}$$

Thus, the final relation between the CRF and HPF is given by:

$$\begin{pmatrix} D_S \\ D_P \\ D_V \\ D_A \\ D_T \end{pmatrix} = \frac{1}{4}\begin{pmatrix} -1 & 1 & -4 & 4 & -6 \\ 1 & -1 & -4 & 4 & 6 \\ -1 & -1 & 2 & 2 & 0 \\ 1 & 1 & 2 & 2 & 0 \\ -1 & 1 & 0 & 0 & 2 \end{pmatrix}\begin{pmatrix} g^S_{LL} + g^S_{RR} + g^S_{LR} + g^S_{RL} \\ g^S_{LL} + g^S_{RR} - g^S_{LR} - g^S_{RL} \\ g^V_{RR} + g^V_{LL} + g^V_{RL} + g^V_{LR} \\ g^V_{RR} + g^V_{LL} - g^V_{RL} - g^V_{LR} \\ 2(g^T_{LR} + g^T_{RL}), \end{pmatrix} \tag{C.7}$$

$$\begin{pmatrix} D'_S \\ D'_P \\ D'_V \\ D'_A \\ D'_T \end{pmatrix} = \frac{1}{4}\begin{pmatrix} -1 & 1 & 4 & -4 & -6 \\ 1 & -1 & 4 & -4 & 6 \\ 1 & 1 & 2 & 2 & 0 \\ -1 & -1 & 2 & 2 & 0 \\ -1 & 1 & 0 & 0 & 2 \end{pmatrix}\begin{pmatrix} -g^S_{LL} + g^S_{RR} + g^S_{LR} - g^S_{RL} \\ -g^S_{LL} + g^S_{RR} - g^S_{LR} + g^S_{RL} \\ g^V_{RR} - g^V_{LL} - g^V_{RL} + g^V_{LR} \\ g^V_{RR} - g^V_{LL} + g^V_{RL} - g^V_{LR} \\ 2(g^T_{LR} - g^T_{RL}) \end{pmatrix}. \tag{C.8}$$

Finally, it is important to note that the CRF Hamiltonian used in [101] differs from (C.1)

in the definition of Γ_P. In Shrock's paper $\Gamma_P = \gamma^5$, this change will induce a minus sign in the definition of the constants C_P and $C_P^{'}$ previously introduced. Thus, the Fierz transformation between the Shrocks's Hamiltonian (using his couplings conventions) and the Hamiltonian used in this thesis is:

$$\begin{pmatrix} g_S \\ g_P \\ g_V \\ g_A \\ g_T \end{pmatrix} = \frac{1}{4} \begin{pmatrix} -1 & 1 & -4 & 4 & -6 \\ -1 & 1 & 4 & -4 & -6 \\ -1 & -1 & 2 & 2 & 0 \\ 1 & 1 & 2 & 2 & 0 \\ -1 & 1 & 0 & 0 & 2 \end{pmatrix} \begin{pmatrix} g_{LL}^S + g_{RR}^S + g_{LR}^S + g_{RL}^S \\ g_{LL}^S + g_{RR}^S - g_{LR}^S - g_{RL}^S \\ g_{RR}^V + g_{LL}^V + g_{RL}^V + g_{LR}^V \\ g_{RR}^V + g_{LL}^V - g_{RL}^V - g_{LR}^V \\ 2\big(g_{LR}^T + g_{RL}^T\big), \end{pmatrix} \tag{C.9}$$

$$\begin{pmatrix} g_S^{'} \\ g_P^{'} \\ g_V^{'} \\ g_A^{'} \\ g_T^{'} \end{pmatrix} = \frac{1}{4} \begin{pmatrix} -1 & 1 & 4 & -4 & -6 \\ -1 & 1 & -4 & 4 & -6 \\ 1 & 1 & 2 & 2 & 0 \\ -1 & -1 & 2 & 2 & 0 \\ -1 & 1 & 0 & 0 & 2 \end{pmatrix} \begin{pmatrix} -g_{LL}^S + g_{RR}^S + g_{LR}^S - g_{RL}^S \\ -g_{LL}^S + g_{RR}^S - g_{LR}^S + g_{RL}^S \\ g_{RR}^V - g_{LL}^V - g_{RL}^V + g_{LR}^V \\ g_{RR}^V - g_{LL}^V + g_{RL}^V - g_{LR}^V \\ 2\big(g_{LR}^T - g_{RL}^T\big). \end{pmatrix} \tag{C.10}$$

After some work of simplification, the specific relations between constants are:

$$\begin{aligned}
g_S &= -\frac{1}{2}g_{LR}^S - \frac{1}{2}g_{RL}^S - 2g_{RL}^V - 2g_{LR}^V - 3g_{LR}^T - 3g_{RL}^T, \\
g_S^{'} &= -\frac{1}{2}g_{LR}^S + \frac{1}{2}g_{RL}^S - 2g_{RL}^V + 2g_{LR}^V - 3g_{LR}^T + 3g_{RL}^T, \\
g_P &= -\frac{1}{2}g_{LR}^S - \frac{1}{2}g_{RL}^S + 2g_{RL}^V + 2g_{LR}^V - 3g_{LR}^T - 3g_{RL}^T, \\
g_P^{'} &= -\frac{1}{2}g_{LR}^S + \frac{1}{2}g_{RL}^S + 2g_{RL}^V - 2g_{LR}^V - 3g_{LR}^T + 3g_{RL}^T, \\
g_V &= g_{RR}^V + g_{LL}^V - \frac{1}{2}g_{LL}^S - \frac{1}{2}g_{RR}^S, \\
g_V^{'} &= g_{RR}^V - g_{LL}^V - \frac{1}{2}g_{LL}^S + \frac{1}{2}g_{RR}^S, \\
g_A &= g_{RR}^V + g_{LL}^V + \frac{1}{2}g_{LL}^S + \frac{1}{2}g_{RR}^S, \\
g_A^{'} &= g_{RR}^V - g_{LL}^V + \frac{1}{2}g_{LL}^S - \frac{1}{2}g_{RR}^S, \\
g_T &= -\frac{1}{2}g_{LR}^S - \frac{1}{2}g_{RL}^S + g_{LR}^T + g_{RL}^T, \\
g_T^{'} &= -\frac{1}{2}g_{LR}^S + \frac{1}{2}g_{RL}^S + g_{LR}^T - g_{RL}^T.
\end{aligned} \tag{C.11}$$

Appendix D

Generalized Michel Functions

D1 Generalized Michel Functions

The corresponding functions are defined as:

$$F_{IS}(x) = x(1-x)(I)_{jk} + \frac{2}{9}(\rho)_{jk}\left(4x^2 - 3x - x_0^2\right) + (\eta)_{jk}x_0(1-x),$$

$$F_{AS}(x) = \frac{(\xi)_{jk}}{3}\sqrt{x^2 - x_0^2}\left(1 - x + \frac{2}{3}(\delta)_{jk}\left(4x - 4 + \sqrt{1-x_0^2}\right)\right),$$

$$F'_{IS}(x) = \frac{1}{4}\frac{m_j}{m_\ell}\,\mathrm{Re}\left[(\kappa_L^+)_{jk}\left(x\left(1+\sqrt{1-x_0^2}\right) - x_0^2\right) - (\kappa_R^+)_{kj}\left(x_0(1-x) + x_0\sqrt{1-x_0^2}\right)\right],$$

$$F'_{AS}(x) = \frac{1}{4}\frac{m_j}{m_\ell}\sqrt{x^2 - x_0^2}\,\mathrm{Re}\left[(\kappa_R^-)_{kj}x_0 + (\lambda_L^-)_{jk}\left(1+\sqrt{1-x_0^2}\right)\right],$$

$$F''_{IS}(x) = -\frac{1}{2}\frac{m_j m_k}{m_\ell^2}\left(1+\sqrt{1-x_0^2}\right)\mathrm{Re}\left(x(C^+)_{jk} + x_0(H^+)_{jk}\right),$$

$$F''_{AS}(x) = \frac{1}{2}\frac{m_j m_k}{m_\ell^2}\left(1+\sqrt{1-x_0^2}\right)\sqrt{x^2-x_0^2}\,\mathrm{Re}(C^-)_{jk},$$

$$F_{T_1}(x) = \frac{1}{12}\Bigg[-2\left((\xi'')_{jk} + 12\left((\rho)_{jk} - \frac{3}{4}(I)_{jk}\right)\right)(1-x)x_0 - 3(\eta)_{jk}\left(x^2 - x_0^2\right) + (\eta'')_{jk}$$
$$\left(-3x^2 + 4x - x_0^2\right)\Bigg],$$

$$F_{T_2}(x) = \frac{1}{3}\sqrt{x^2-x_0^2}\left[3\left(\frac{\alpha'}{\mathcal{A}}\right)_{jk}(1-x) + 2\left(\frac{\beta'}{\mathcal{A}}\right)_{jk}\sqrt{1-x_0^2}\right],$$

$$F_{IP}(x) = \frac{1}{54}\sqrt{x^2-x_0^2}\left[9(\xi')_{jk}\left(-2x + 2 + \sqrt{1-x_0^2}\right) + 4(\xi)_{jk}\left((\delta)_{jk} - \frac{3}{4}\right)\left(4x - 4 + \sqrt{1-x_0^2}\right)\right],$$

$$F_{AP}(x) = \frac{1}{6}\left[(\xi'')_{jk}\left(2x^2 - x - x_0^2\right) + 4\left((\rho)_{jk} - \frac{3}{4}(I)_{jk}\right)\left(4x^2 - 3x - x_0^2\right) + 2(\eta'')_{jk}(1-x)x_0\right],$$

$$F'_{T_1}(x) = \frac{1}{4}\frac{m_j}{m_\ell}\,\mathrm{Re}\left[(\lambda_L^+)_{jk}\left(x_0(1-x) + x_0\sqrt{1-x_0^2}\right) - (\lambda_R^+)_{kj}\left(x\left(1+\sqrt{1-x_0^2}\right) - x_0^2\right)\right],$$

$$F'_{T_2}(x) = \frac{1}{4}\frac{m_j}{m_\ell}\sqrt{x^2-x_0^2}\,\mathrm{Im}\left[(\lambda_R^-)_{kj}\left(1+\sqrt{1-x_0^2}\right) + (\lambda_L^-)_{jk}x_0\right],$$

$$F'_{IP}(x) = \frac{1}{4}\frac{m_j}{m_\ell}\sqrt{x^2-x_0^2}\,\mathrm{Re}\left[(\lambda_R^-)_{kj}x_0 + (\kappa_L^-)_{jk}\left(1+\sqrt{1-x_0^2}\right)\right],$$

$$F'_{AP}(x) = \frac{1}{4}\frac{m_j}{m_\ell}\,\mathrm{Re}\left[(\lambda_L^+)_{jk}\left(x\left(1+\sqrt{1-x_0^2}\right) - x_0^2\right) - (\lambda_R^+)_{kj}\left(x_0(1-x) + x_0\sqrt{1-x_0^2}\right)\right],$$

$$F''_{T_1}(x) = \frac{1}{2}\frac{m_j m_k}{m_\ell^2}\left(1+\sqrt{1-x_0^2}\right)\mathrm{Re}\left(x_0(C'^+)_{jk} - 2x(J^+)_{jk}\right),$$

$$F''_{T_2}(x) = -\frac{m_j m_k}{m_\ell^2}\left(1+\sqrt{1-x_0^2}\right)\mathrm{Im}(J^+)_{jk}\sqrt{x^2-x_0^2},$$

$$F''_{IP}(x) = -\frac{1}{2}\frac{m_j m_k}{m_\ell^2}\left(1+\sqrt{1-x_0^2}\right)\mathrm{Re}(C'^{-})_{jk}\sqrt{x^2-x_0^2},$$
$$F''_{AP}(x) = \frac{1}{2}\frac{m_j m_k}{m_\ell^2}\left(1+\sqrt{1-x_0^2}\right)\mathrm{Re}\left(x(C'^{+})_{jk} - 2x_0(J^+)_{jk}\right), \tag{D.1}$$

where the parameters are bilinear combinations of the coupling constants g^n_{lm}, given by

$$\begin{aligned}
(I)_{jk} &= \frac{1}{4}(|(f^S_{RR})_{jk}|^2 + |(f^S_{RL})_{jk}|^2 + |(f^S_{LR})_{jk}|^2 + |(f^S_{LL})_{jk}|^2) + 3(|(f^T_{LR})_{jk}|^2 + |(f^T_{RL})_{jk}|^2) + (|(f^V_{RR})_{jk}|^2 \\
&\quad + |(f^V_{RL})_{jk}|^2 + |(f^V_{LR})_{jk}|^2 + |(f^V_{LL})_{jk}|^2) + \frac{\epsilon}{8}\,\mathrm{Re}\Big[12(f^T_{LR})_{jk}(f^S_{LR})^*_{kj} + 12(f^T_{LR})_{jk}(f^T_{LR})^*_{kj} \\
&\quad + 8(f^V_{RL})_{jk}(f^V_{RL})^*_{kj} - (f^S_{LR})_{jk}(f^S_{LR})^*_{kj} + 8(f^S_{LL})_{jk}(f^V_{LL})^*_{kj} + (L\leftrightarrow R)\Big], \\
(\rho)_{jk} &= \frac{3}{4}(|(f^V_{LL})_{jk}|^2 + \frac{1}{4}|(f^S_{LL})_{jk}|^2) + \frac{3}{16}|(f^S_{LR})_{jk} - 2(f^T_{LR})_{jk}|^2 + (R\leftrightarrow L) + \epsilon\frac{3}{16}\,\mathrm{Re}\Big[-(f^S_{LR})_{jk} \\
&\quad (f^S_{LR})^*_{kj} + 4(f^S_{LR})_{jk}(f^T_{LR})^*_{kj} + 4(f^S_{LL})_{jk}(f^V_{LL})^*_{kj} - 4(f^T_{LR})_{jk}(f^T_{LR})^*_{kj} + (L\leftrightarrow R)\Big], \\
(\xi)_{jk} &= 3\big(|(f^V_{LR})_{jk}|^2 + \frac{1}{16}|(f^S_{LR})_{jk} + 6(f^T_{LR})_{jk}|^2\big) + |(f^V_{LL})_{jk}|^2 + \frac{1}{4}|(f^S_{LL})_{jk}|^2 - \frac{7}{16}|(f^S_{LR})_{jk} - 2(f^T_{LR})_{jk}|^2 \\
&\quad - (R\leftrightarrow L) + \epsilon\,\mathrm{Re}\Big[-(f^S_{RR})_{jk}(f^V_{RR})^*_{kj} + \frac{17}{2}(f^T_{LR})_{jk}(f^T_{LR})^*_{kj} + \frac{1}{2}(f^S_{LR})_{jk}(f^T_{LR})^*_{kj} + 3(f^V_{LR})_{jk} \\
&\quad (f^V_{LR})^*_{kj} + \frac{5}{8}(f^S_{LR})_{jk}(f^S_{LR})^*_{kj} - (L\leftrightarrow R)\Big], \\
(\xi\delta)_{jk} &= \frac{3}{4}(|(f^V_{LL})_{jk}|^2 + \frac{1}{4}|(f^S_{LL})_{jk}|^2) - \frac{3}{16}|(f^S_{LR})_{jk} - 2(f^T_{LR})_{jk}|^2 - (R\leftrightarrow L) + \epsilon\frac{3}{4}\,\mathrm{Re}\Big[-(f^S_{RR})_{jk} \\
&\quad (f^V_{RR})^*_{kj} + (f^T_{LR})_{jk}(f^T_{LR})^*_{kj} - (f^S_{LR})_{jk}(f^T_{LR})^*_{kj} + \frac{1}{4}(f^S_{LR})_{jk}(f^S_{LR})^*_{kj} - (L\leftrightarrow R)\Big], \\
(\eta)_{jk} &= \frac{1}{2}\,\mathrm{Re}[(f^V_{LL})_{jk}(f^S_{RR})^*_{jk} + (f^V_{RR})_{jk}(f^S_{LL})^*_{jk} + (f^V_{LR})_{jk}((f^S_{RL})^*_{jk} + 6(f^T_{RL})^*_{jk}) + (f^V_{RL})_{jk}((f^S_{LR})^*_{jk} \\
&\quad + 6(f^T_{LR})^*_{jk})] + \frac{\epsilon}{8}\,\mathrm{Re}\Big[4(f^S_{LR})_{jk}(f^V_{RL})^*_{kj} + 24(f^T_{LR})_{jk}(f^V_{RL})^*_{kj} + (f^S_{LL})_{jk}(f^S_{RR})^*_{kj} + 4(f^V_{LL})_{jk} \\
&\quad (f^V_{RR})^*_{kj} + (L\leftrightarrow R)\Big], \\
(\xi')_{jk} &= -\frac{1}{4}\big(|(f^S_{RR})_{jk}|^2 + 4|(f^V_{RR})_{jk}|^2 - |(f^S_{LR})_{jk}|^2 - 4|(f^V_{LR})_{jk}|^2 - 12|(f^T_{LR})_{jk}|^2\big) - (R\leftrightarrow L) \\
&\quad + \epsilon\,\mathrm{Re}\Big[(f^S_{LL})_{jk}(f^V_{LL})^*_{kj} + \frac{3}{2}(f^S_{LR})_{jk}(f^T_{LR})^*_{kj} + \frac{3}{2}(f^T_{LR})_{jk}(f^T_{LR})^*_{kj} + (f^V_{LR})_{jk}(f^V_{LR})^*_{kj} \\
&\quad - \frac{1}{8}(f^S_{LR})_{jk}(f^S_{LR})^*_{kj} - (L\leftrightarrow R)\Big], \\
(\xi'')_{jk} &= \frac{1}{4}\Big(|(f^S_{RR})_{jk}|^2 + 4|(f^V_{RR})_{jk}|^2 - |(f^S_{LR})_{jk}|^2 + 12|(f^V_{LR})_{jk}|^2 + 20|(f^T_{LR})_{jk}|^2 + 16\,\mathrm{Re}((f^S_{LR})_{jk} \\
&\quad (f^T_{LR})^*_{jk})\Big) + (R\leftrightarrow L) + \epsilon\,\mathrm{Re}\Big[\frac{1}{2}(f^S_{LR})_{jk}(f^T_{LR})^*_{kj} + \frac{17}{2}(f^T_{LR})_{jk}(f^T_{LR})^*_{kj} + (f^S_{LL})_{jk}(f^V_{LL})^*_{kj} \\
&\quad + \frac{5}{8}(f^S_{RL})_{jk}(f^S_{RL})^*_{kj} + 3(f^V_{RL})_{jk}(f^V_{RL})^*_{kj} + (L\leftrightarrow R)\Big], \\
(\eta'')_{jk} &= \frac{1}{2}\,\mathrm{Re}\left(3(f^V_{LR})_{jk}((f^S_{RL})^*_{jk} + 6(f^T_{RL})^*_{jk}) - (f^V_{LL})_{jk}(f^S_{RR})^*_{jk}\right) + (R\leftrightarrow L) + \frac{\epsilon}{2}\,\mathrm{Re}\Big[3(f^S_{LR})_{jk}(f^V_{RL})^*_{kj} \\
&\quad + 18(f^T_{LR})_{jk}(f^V_{RL})^*_{kj} - \frac{1}{4}(f^S_{LL})_{jk}(f^S_{RR})^*_{kj} - (f^V_{LL})_{jk}(f^V_{RR})^*_{kj} + (L\leftrightarrow R)\Big]\Big],
\end{aligned}$$

$$
\begin{aligned}
\left(\frac{\alpha'}{\mathcal{A}}\right)_{jk} &= \frac{1}{2}\,\mathrm{Im}\left((f^V_{LR})_{jk}((f^S_{RL})^*_{jk}+6(f^T_{RL})^*_{jk})\right)-(R\leftrightarrow L)+\epsilon\,\mathrm{Im}\Big[\frac{1}{2}(f^V_{RL})^*_{jk}((f^S_{LR})_{kj}+6(f^T_{LR})_{kj})\\
&\quad-(L\leftrightarrow R)\Big],\\
\left(\frac{\beta'}{\mathcal{A}}\right)_{jk} &= -\frac{1}{4}\,\mathrm{Im}\left((f^V_{LL})_{jk}(f^S_{RR})^*_{jk}\right)-(R\leftrightarrow L)+\epsilon\,\mathrm{Im}\Big[-\frac{1}{2}(f^V_{LL})_{jk}(f^V_{RR})^*_{kj}-\frac{1}{8}(f^S_{LL})_{jk}(f^S_{RR})^*_{kj}\Big],\\
(\kappa^{\pm}_N)_{jk} &= (f^S_{NN})_{kj}(f^S_{LR})^*_{kj}-2(f^V_{NN})_{kj}(f^V_{LR})^*_{kj}-(f^S_{NN})_{jk}(f^V_{LR})^*_{jk}-(f^V_{NN})_{jk}((f^S_{LR})^*_{jk}-6(f^T_{LR})^*_{jk})\\
&\quad\pm(R\leftrightarrow L)+\epsilon\Big[-2(f^V_{NN})_{kj}(f^V_{LR})^*_{jk}-\frac{1}{2}(f^S_{NN})_{kj}(f^S_{LR})^*_{jk}+3(f^S_{NN})_{kj}(f^T_{LR})^*_{jk}+2(f^V_{NN})_{jk}\\
&\quad(f^S_{LR})^*_{kj}-(f^S_{NN})_{jk}(f^V_{LR})^*_{kj}\pm(L\leftrightarrow R)\Big],\\
(\lambda^{\pm}_N)_{jk} &= -(f^S_{NN})_{jk}(f^V_{LR})^*_{jk}+(f^V_{NN})_{jk}((f^S_{LR})^*_{jk}+2(f^T_{LR})^*_{jk})+2(f^S_{NN})_{kj}(f^T_{LR})^*_{kj}-2(f^V_{NN})_{kj}(f^V_{LR})^*_{kj}\\
&\quad\pm(R\leftrightarrow L)+\epsilon\Big[-2(f^V_{NN})_{kj}(f^V_{LR})^*_{jk}+\frac{1}{2}(f^S_{NN})_{kj}(f^S_{LR})^*_{jk}+(f^S_{NN})_{kj}(f^T_{LR})^*_{jk}+4(f^V_{NN})_{jk}\\
&\quad(f^T_{LR})^*_{kj}-(f^S_{NN})_{jk}(f^V_{LR})^*_{kj}\pm(L\leftrightarrow R)\Big],\\
(C^{\pm})_{jk} &= (f^S_{LL})_{jk}(f^V_{LL})^*_{jk}+(f^V_{RL})^*_{jk}((f^S_{RL})_{jk}+6(f^T_{RL})_{jk})\pm(R\leftrightarrow L)+\epsilon\Big[(f^V_{LL})_{jk}(f^V_{LL})^*_{kj}+\frac{1}{4}(f^S_{LL})_{jk}\\
&\quad(f^S_{LL})^*_{kj}+(f^S_{RL})_{jk}(f^V_{RL})^*_{kj}+6(f^V_{RL})_{jk}(f^T_{RL})^*_{kj}\pm(L\leftrightarrow R)\Big],\\
(C'^{\pm})_{jk} &= (f^S_{LL})_{jk}(f^V_{LL})^*_{jk}-(f^V_{RL})^*_{jk}((f^S_{RL})_{jk}+6(f^T_{RL})_{jk})\pm(R\leftrightarrow L)+\epsilon\Big[\frac{1}{4}(f^S_{LL})_{jk}(f^S_{LL})^*_{kj}\\
&\quad+(f^V_{LL})_{jk}(f^V_{LL})^*_{kj}-(f^S_{RL})_{jk}(f^V_{RL})^*_{kj}-6(f^V_{RL})_{jk}(f^T_{RL})^*_{kj}\pm(L\leftrightarrow R)\Big],\\
(J^{+})_{jk} &= (f^S_{LR})_{jk}(f^T_{RL})^*_{jk}+(f^T_{LR})_{jk}(f^S_{RL})^*_{jk}+2(f^V_{LR})_{jk}(f^V_{RL})^*_{jk}+4(f^T_{LR})_{jk}(f^T_{RL})^*_{jk}+\epsilon\Big[\frac{1}{4}(f^S_{LR})_{kj}\\
&\quad(f^S_{RL})^*_{jk}+\frac{1}{2}(f^S_{LR})_{kj}(f^T_{RL})^*_{jk}+\frac{1}{2}(f^T_{LR})_{kj}(f^S_{RL})^*_{jk}+5(f^T_{LR})_{kj}(f^T_{RL})^*_{jk}+2(f^V_{LR})_{jk}(f^V_{RL})^*_{kj}\Big],\\
(H^{+})_{jk} &= (f^S_{LL})_{jk}(f^S_{RR})^*_{jk}+4(f^V_{LL})_{jk}(f^V_{RR})^*_{jk}+(f^S_{LR})_{jk}(f^S_{RL})^*_{jk}+12(f^T_{LR})_{jk}(f^T_{RL})^*_{jk}\\
&\quad+4(f^V_{LR})_{jk}(f^V_{RL})^*_{jk}+\epsilon\Big[2(f^V_{LL})_{jk}(f^S_{RR})^*_{kj}-\frac{1}{4}(f^S_{LR})_{jk}(f^S_{RL})^*_{kj}+3(f^T_{LR})_{jk}(f^S_{RL})^*_{kj}+3(f^T_{LR})_{jk}\\
&\quad(f^T_{RL})^*_{kj}+2(f^V_{LR})_{jk}(f^V_{RL})^*_{kj}+(L\leftrightarrow R)\Big],
\end{aligned}
\tag{D.2}
$$

together with the normalization $1=(I)_{jk}\equiv\frac{\mathcal{A}}{16}$, where we defined the constants $(f^n_{lm})_{jk}$ as:

$$
\begin{aligned}
(f^S_{LL})_{jk} &\equiv g^S_{LL}V_{\ell' j}V^*_{\ell k}, & (f^S_{RR})_{jk} &\equiv g^S_{RR}U_{\ell' j}U^*_{\ell k},\\
(f^V_{LL})_{jk} &\equiv g^V_{LL}U_{\ell' j}U^*_{\ell k}, & (f^V_{RR})_{jk} &\equiv g^V_{RR}V_{\ell' j}V^*_{\ell k},\\
(f^S_{LR})_{jk} &\equiv g^S_{LR}V_{\ell' j}U^*_{\ell k}, & (f^S_{RL})_{jk} &\equiv g^S_{RL}U_{\ell' j}V^*_{\ell k},\\
(f^V_{LR})_{jk} &\equiv g^V_{LR}U_{\ell' j}V^*_{\ell k}, & (f^V_{RL})_{jk} &\equiv g^V_{RL}V_{\ell' j}U^*_{\ell k},\\
(f^T_{LR})_{jk} &\equiv g^T_{LR}V_{\ell' j}U^*_{\ell k}, & (f^T_{RL})_{jk} &\equiv g^T_{RL}U_{\ell' j}V^*_{\ell k},
\end{aligned}
\tag{D.3}
$$

The blue square brackets above are enclosing the Majorana contributions, which vanish for null flag parameter, $\epsilon = 0$.

Appendix E

W-Boson Propagator Corrections

E1 W-boson propagator corrections to the Michel parameters

As previously discussed, the most recent corrections from the W-boson propagator to the total and differential decay rates of polarized muons and tau leptons, as well as their numerical impact, have been calculated in [129] and [186]. Here, we adopt these results and compare them to the standard Michel distribution to extract the W-boson propagator corrections for each specific Michel parameter.

The energy-angle distribution of the final charged lepton in the decays of a polarized μ^- or τ^- at rest is [129]:

$$\begin{aligned}\frac{d^2\Gamma}{dx\,d\cos\theta} =& \frac{G_F^2 M^5}{192\pi^3}\frac{x\beta}{1+\delta_W(M,m)}\Big\{3x-2x^2+r^2(3x-4)+f(x)+r_W^2\big[2x^2\\ &-x^3-2r^2(1+x-x^2+r^2)\big]-\cos\theta\; x\beta\big[2x-1-3r^2+g(x)\\ &+r_W^2\;x(x-2r^2)\big]+\mathcal{O}(r_W^4)\Big\}.\end{aligned} \tag{E.1}$$

The functions $f(x)$ and $g(x)$ are the QED radiative corrections given, up to $\mathcal{O}(\alpha)$, by [107]:

$$\frac{2\pi}{\alpha}f(x) = (6-4x)R(x)+(6-6x)\ln x+\frac{1-x}{3x^2}\Big[(5+17x-34x^2)(w+\ln x)-22x+34x^2\Big], \tag{E.2}$$

$$\begin{aligned}\frac{-2\pi}{\alpha}g(x) =& (2-4x)R(x)+(2-6x)\ln x-\frac{1-x}{3x^2}\Big[(1+x+34x^2)(w+\ln x)+3\\ &-7x-32x^2+\frac{4(1-x)^2}{x}\ln(1-x)\Big],\end{aligned} \tag{E.3}$$

where

$$R(x) = 2\sum_{n=1}^{\infty}\frac{x^n}{n^2}-\frac{1}{3}\pi^2-2+w\left[\frac{3}{2}+2\ln\frac{1-x}{x}\right]-\ln x(2\ln x-1)+\left(3\ln x-1-\frac{1}{x}\right)\ln(1-x), \tag{E.4}$$

and $w = \ln(M/m)$.

The terms proportional to r_W^2 are induced by the W-boson propagator, where $r_W = M/M_W$. Also $\beta = \frac{|\vec{p_m}|}{E_m} = \sqrt{1-4r^2/x^2}$, where $r = m/M$.

Focusing only on the leading W-boson propagator contributions, we obtain:

$$\frac{d^2\Gamma}{dx d\cos\theta} = \frac{G_F^2 M^5}{192\pi^3} \frac{x}{1+3/5(M/M_W)^2} \Big\{ 3x - 2x^2 + r_W^2\big[2x^2 - x^3\big] - \cos\theta\; x\big[2x - 1 + r_W^2\; x^2\big] \Big\}. \tag{E.5}$$

So that the Michel parameter, defined in terms of the energy spectrum (neglecting the x_0 dependence):

$$\frac{d\Gamma_{l\to l'}}{dx d\cos\theta} = \frac{G_{ll'}^2 M^5}{192\pi^3} x \left\{ 6x(1-x) + \frac{4}{3}\rho\left(4x^2 - 3x\right) - 2\xi x\cos\theta\left(1 - x + \frac{2}{3}\delta(4x-3)\right)\right\}, \tag{E.6}$$

is given by:

$$\bullet\; \rho \to \rho_{eff} = \frac{3}{4} + \frac{3}{2}\left(\frac{M}{M_W}\right)^2, \tag{E.7}$$

where $G_{ll'}^2 = G_F^2/(1+\delta_W(m_l, m_{l'}))$ and the remaining parameters have no further modification.

Finally, to the best of our knowledge, the W-boson corrections for decays with a polarized final-state charged lepton have not been computed previously. Here, we present their expressions at first order in r_W, neglecting the x_0 dependence.

The final-lepton polarization contribution of the differential decay rate is then:

$$\begin{aligned}\frac{d\Gamma_{l\to l'}}{dx d\cos\theta} = \frac{G_{ll'}^2 M^5}{64\pi^3} x \Big\{ &- \left[\frac{1}{6}x(-2x+3) + r_W^2\frac{1}{6}x(2x-x^2)\right]\cos\phi \\ &+ \frac{1}{6}\left[(2x^2 - x) + r_W^2 x^3\right]\cos\theta\cos\phi\Big\}.\end{aligned} \tag{E.8}$$

So that the Michel parameters, defined in terms of the energy spectrum (neglecting the

x_0 dependence):

$$\begin{aligned}\frac{d\Gamma_{l\to l'}}{dx d\cos\theta} &= \frac{G_{ll'}^2 M^5}{64\pi^3} x\left\{-F_{IP}\cos\phi + F_{AP}\cos\theta\cos\phi\right\} \\ &= \frac{G_{ll'}^2 M^5}{64\pi^3} x\Bigg\{ -\frac{1}{54}x\left[9\xi'(3-2x) + 4\xi(\delta-\frac{3}{4})(4x-3)\right]\cos\phi \\ &+ \frac{1}{6}\left[\xi''(2x^2-x) + 4(\rho-\frac{3}{4})(4x^2-3x)\right]\cos\theta\cos\phi\Bigg\},\end{aligned} \tag{E.9}$$

are given by:

$$\begin{aligned}&\bullet\ \xi^{'} \to \xi^{'}_{eff} = 1 + \left(\frac{M}{M_W}\right)^2 \\ &\bullet\ \xi\left(\delta - \frac{3}{4}\right) \to \xi\left(\delta-\frac{3}{4}\right)_{eff} = 0 + \frac{9}{4}\left(\frac{M}{M_W}\right)^2\end{aligned} \tag{E.10}$$

and the remaining have no modification.

However, it is interesting to emphasize that even if the ρ, ξ and $\xi\delta$ parameters appear in both, the initial and final lepton polarization contribution, they are modified in an independent way in each of those contributions. Then, we can not simple redefine each Michel parameter with an effective and global modification, since we need to specify where they appear in the differential decay rate.

To minimize the number of parameters in our expressions, we opt not to introduce new effective parameters. Instead, we account separately for the W-boson propagator corrections and the QED contributions [129] to the differential decay rate.

Appendix F

Four-body Phase Space Notation

F1 4-body Phase Space

In order to avoid confusion, we define our differential rate notation for the process $\ell(p_1) \to \bar{\nu}(p_2)\nu(p_3)\ell'(p_4)\gamma(p_5)$. Upon defining the following five independent variables of the system, in the typical frame used in a four-body decay process (as can be seen in Fig. 4 of ref.[141]), we have:

- $s_{\nu\bar{\nu}} \equiv (p_2 + p_3)^2$ and $s_{\ell'\gamma} \equiv (p_4 + p_5)^2$, the invariant masses of the $\nu - \bar{\nu}$ and $\ell' - \gamma$ systems, respectively.
- θ_ν ($\theta_{\ell'}$), the polar angle between the three-momentum of $\bar{\nu}$ (ℓ'), in the center-of-momentum frame of the $\bar{\nu} - \nu$ ($\ell' - \gamma$) pair, and the flight direction of the $\nu - \bar{\nu}$ ($\ell' - \gamma$) system in the rest frame of ℓ.
- ϕ, the azimuthal angle described between the two planes defined by the $\nu - \bar{\nu}$ and $\ell' - \gamma$ systems, in the rest frame of ℓ.

We can write the differential decay width as

$$\frac{d\Gamma}{ds_{\nu\bar{\nu}} ds_{\ell'\gamma} d\cos\theta_\nu d\cos\theta_{\ell'} d\phi} = \frac{X\beta_\nu\beta_{\ell'}}{(4\pi)^6 m_\ell \sqrt{s_{\nu\bar{\nu}} s_{\ell'\gamma}}} |\overline{\mathcal{M}}|^2, \tag{F.1}$$

with

$$X \equiv \frac{\sqrt{\lambda(m_\ell^2, s_{\nu\bar{\nu}}, s_{\ell'\gamma})}}{2m_\ell}, \quad \beta_\nu \equiv \sqrt{\frac{\lambda(s_{\nu\bar{\nu}}, m_\nu^2, m_{\bar{\nu}}^2)}{4s_{\nu\bar{\nu}}}}, \quad \beta_{\ell'} \equiv \sqrt{\frac{\lambda(s_{\ell'\gamma}, m_{\ell'}^2, 0)}{4s_{\ell'\gamma}}}, \tag{F.2}$$

where X is the magnitude of three-momentum of $\nu - \bar{\nu}$ or $\ell' - \gamma$ system in the rest frame of ℓ, while β_ν ($\beta_{\ell'}$) refers to the magnitude of three-momentum of the ν (ℓ') in the center-of-momentum frame of the $\nu\bar{\nu}$ ($\ell'\gamma$) pair.

It is convenient to rewrite the differential width in terms of E_ν and $E_{\bar{\nu}}$ in order to obtain

the energy spectrum of the neutrinos. Thus, we can do the variables change:

$$ds_{\nu\bar{\nu}}ds_{\ell'\gamma}d\cos\theta_\nu = -\frac{4m_\ell\sqrt{s_{\nu\bar{\nu}}}}{X\beta_\nu}\sqrt{(E_\nu^2-m_\nu^2)(E_{\bar{\nu}}^2-m_{\bar{\nu}}^2)}dE_\nu dE_{\bar{\nu}}d\cos\Theta_{\nu\bar{\nu}}, \tag{F.3}$$

where $\Theta_{\nu\bar{\nu}}$ is the angle between the three-momenta of both neutrinos, in the rest frame of ℓ. We can also obtain the energy spectrum for the final charged lepton and the photon with the following change of variables:

$$ds_{\nu\bar{\nu}}ds_{\ell'\gamma}d\cos\theta_{\ell'} = -\frac{4m_\ell\sqrt{s_{\ell'\gamma}}}{X\beta_{\ell'}}E_\gamma\sqrt{(E_{\ell'}^2-m_{\ell'}^2)}dE_{\ell'}dE_\gamma d\cos\Theta_{\ell'\gamma}, \tag{F.4}$$

where $\Theta_{\ell'\gamma}$ is the angle between ℓ' and γ, in the rest frame of ℓ.

Finally, neglecting all the final-state masses, as a good approximation, we get for the neutrinos differential decay distribution:

$$\frac{d\Gamma^{D,M}}{dE_\nu dE_{\bar{\nu}}d\cos\Theta_{\nu\bar{\nu}}d\cos\theta_{\ell'}d\phi} = \frac{2}{m_\ell(4\pi)^6}\frac{E_\nu E_{\bar{\nu}}E_{\ell'}}{E_\gamma}\frac{1}{\epsilon}\sum_{j,k}|\overline{\mathcal{M}^{D,M}}|^2, \tag{F.5}$$

where $\epsilon = 1(2)$ for Dirac (Majorana) neutrinos. Here $E_{\ell'}$ and E_γ must be written in terms of $E_{\bar{\nu}}$ and E_ν, according to the energy-momentum conservation law. Note also that we are taking into account all the possible neutrino mass final states and the sum extends over all energetically allowed neutrino pairs. The 1/2 factor that appears in the Majorana case has two different origins. For the $k = j$ case, it is due to the presence of indistinguishable fermions in the final state; while for $k \neq j$, it arises because of double counting, since the sum $\sum_{j,k}$ is not restricted to $j \leq k$.

Meanwhile, for the differential decay distribution involving the charged lepton and photon energies we obtain:

$$\frac{d\Gamma^{D,M}}{dE_{\ell'}dE_\gamma d\cos\Theta_{\ell'\gamma}d\cos\theta_\nu d\phi} = \frac{2}{m_\ell(4\pi)^6}\frac{E_\nu E_{\ell'}E_\gamma}{E_{\bar{\nu}}}\frac{1}{\epsilon}\sum_{j,k}|\overline{\mathcal{M}^{D,M}}|^2, \tag{F.6}$$

where $E_{\bar{\nu}}$ and E_ν must be written in terms of $E_{\ell'}$ and E_γ according to the energy-momentum conservation law. These, in principle, are two different spectra and will be so in any specific kinematic configuration.

Appendix G

Back-to-back kinematics

G1 Back-to-back configuration

It is convenient to describe our phase space variables in the rest frame of the decaying particle to avoid any confusion. First, we are going to denote p_i' as the momentum of the $i-$particle in the corresponding center of mass frame for the relevant particle pair ($\nu - \bar{\nu}$ or $\ell' - \gamma$) and p_i the corresponding momentum in the rest frame of the decaying particle. Now, following Fig.[4] of ref.[141], both momenta, p_i' and p_i, are related by a Lorentz boost in the $\hat{z}$ direction. We define our boost in the $\hat{z}$ direction for the 4-momentum p_ν' and $p_{\bar{\nu}}'$ as follows:

$$\Lambda^{\mu}{}_{\nu} = \begin{pmatrix} \sqrt{1+\frac{X^2}{s_{\nu\bar{\nu}}}} & 0 & 0 & \frac{X}{\sqrt{s_{\nu\bar{\nu}}}} \\ 0 & 1 & 0 & 0 \\ 0 & 0 & 1 & 0 \\ \frac{X}{\sqrt{s_{\nu\bar{\nu}}}} & 0 & 0 & \sqrt{1+\frac{X^2}{s_{\nu\bar{\nu}}}} \end{pmatrix}. \tag{G.1}$$

For p_4' and p_5' we use the Lorentz transformation:

$$\Lambda'^{\mu}{}_{\nu} = \begin{pmatrix} \sqrt{1+\frac{X^2}{s_{\ell'\gamma}}} & 0 & 0 & -\frac{X}{\sqrt{s_{\ell'\gamma}}} \\ 0 & 1 & 0 & 0 \\ 0 & 0 & 1 & 0 \\ -\frac{X}{\sqrt{s_{\ell'\gamma}}} & 0 & 0 & \sqrt{1+\frac{X^2}{s_{\ell'\gamma}}} \end{pmatrix}, \tag{G.2}$$

where we use the definition of X, $s_{\nu\bar{\nu}}$ and $s_{\ell'\gamma}$ from the previous appendix. In general, we can write the corresponding 4-momentum in the rest frame of ℓ as follows:

$$p_2 = \begin{pmatrix} \sqrt{1+\frac{X^2}{s_{\nu\bar{\nu}}}} & 0 & 0 & \frac{X}{\sqrt{s_{\nu\bar{\nu}}}} \\ 0 & 1 & 0 & 0 \\ 0 & 0 & 1 & 0 \\ \frac{X}{\sqrt{s_{\nu\bar{\nu}}}} & 0 & 0 & \sqrt{1+\frac{X^2}{s_{\nu\bar{\nu}}}} \end{pmatrix} \begin{pmatrix} \frac{\sqrt{s_{\nu\bar{\nu}}}}{2} \\ \beta_\nu \sin\theta_\nu \cos\phi \\ \beta_\nu \sin\theta_\nu \sin\phi \\ \beta_\nu \cos\theta_\nu \end{pmatrix} = \begin{pmatrix} \frac{\sqrt{s_{\nu\bar{\nu}}+X^2}}{2} + \frac{X}{\sqrt{s_{\nu\bar{\nu}}}}\beta_\nu \cos\theta_\nu \\ \beta_\nu \sin\theta_\nu \cos\phi \\ \beta_\nu \sin\theta_\nu \sin\phi \\ \frac{X}{2} + \sqrt{1+\frac{X^2}{s_{\nu\bar{\nu}}}}\beta_\nu \cos\theta_\nu \end{pmatrix}, \tag{G.3}$$

$$p_3 = \begin{pmatrix} \sqrt{1+\frac{X^2}{s_{\nu\bar{\nu}}}} & 0 & 0 & \frac{X}{\sqrt{s_{\nu\bar{\nu}}}} \\ 0 & 1 & 0 & 0 \\ 0 & 0 & 1 & 0 \\ \frac{X}{\sqrt{s_{\nu\bar{\nu}}}} & 0 & 0 & \sqrt{1+\frac{X^2}{s_{\nu\bar{\nu}}}} \end{pmatrix} \begin{pmatrix} \frac{\sqrt{s_{\nu\bar{\nu}}}}{2} \\ -\beta_\nu \sin\theta_\nu \cos\phi \\ -\beta_\nu \sin\theta_\nu \sin\phi \\ -\beta_\nu \cos\theta_\nu \end{pmatrix} = \begin{pmatrix} \frac{\sqrt{s_{\nu\bar{\nu}}+X^2}}{2} - \frac{X}{\sqrt{s_{\nu\bar{\nu}}}}\beta_\nu \cos\theta_\nu \\ -\beta_\nu \sin\theta_\nu \cos\phi \\ -\beta_\nu \sin\theta_\nu \sin\phi \\ \frac{X}{2} - \sqrt{1+\frac{X^2}{s_{\nu\bar{\nu}}}}\beta_\nu \cos\theta_\nu \end{pmatrix}. \tag{G.4}$$

$$p_4 = \begin{pmatrix} \sqrt{1+\frac{X^2}{s_{\ell'\gamma}}} & 0 & 0 & -\frac{X}{\sqrt{s_{\ell'\gamma}}} \\ 0 & 1 & 0 & 0 \\ 0 & 0 & 1 & 0 \\ -\frac{X}{\sqrt{s_{\ell'\gamma}}} & 0 & 0 & \sqrt{1+\frac{X^2}{s_{\ell'\gamma}}} \end{pmatrix} \begin{pmatrix} \frac{\sqrt{s_{\ell'\gamma}}}{2} \\ \beta_{\ell'} \sin\theta_{\ell'} \\ 0 \\ -\beta_{\ell'} \cos\theta_{\ell'} \end{pmatrix} = \begin{pmatrix} \frac{\sqrt{s_{\ell'\gamma}+X^2}}{2} - \frac{X}{\sqrt{s_{\ell'\gamma}}}\beta_{\ell'} \cos\theta_{\ell'} \\ \beta_{\ell'} \sin\theta_{\ell'} \\ 0 \\ -\frac{X}{2} - \sqrt{1+\frac{X^2}{s_{\ell'\gamma}}}\beta_{\ell'} \cos\theta_{\ell'} \end{pmatrix}, \tag{G.5}$$

$$p_5 = \begin{pmatrix} \sqrt{1+\frac{X^2}{s_{\ell'\gamma}}} & 0 & 0 & -\frac{X}{\sqrt{s_{\ell'\gamma}}} \\ 0 & 1 & 0 & 0 \\ 0 & 0 & 1 & 0 \\ -\frac{X}{\sqrt{s_{\ell'\gamma}}} & 0 & 0 & \sqrt{1+\frac{X^2}{s_{\ell'\gamma}}} \end{pmatrix} \begin{pmatrix} \frac{\sqrt{s_{\ell'\gamma}}}{2} \\ -\beta_{\ell'} \sin\theta_{\ell'} \\ 0 \\ \beta_{\ell'} \cos\theta_{\ell'} \end{pmatrix} = \begin{pmatrix} \frac{\sqrt{s_{\ell'\gamma}+X^2}}{2} + \frac{X}{\sqrt{s_{\ell'\gamma}}}\beta_{\ell'} \cos\theta_{\ell'} \\ -\beta_{\ell'} \sin\theta_{\ell'} \\ 0 \\ -\frac{X}{2} + \sqrt{1+\frac{X^2}{s_{\ell'\gamma}}}\beta_{\ell'} \cos\theta_{\ell'} \end{pmatrix}. \tag{G.6}$$

Finally, we can apply the $b2b$ constraint $\vec{p}_2 = -\vec{p}_3$ or equivalently, due to energy momentum conservation, $\vec{p}_4 = -\vec{p}_5$. In this kinematic scenario it is easy to show that $X = 0$, which is consistent with the fact that, in the $b2b$ configuration, the boosts in eqs.(G.1,G.2) are exactly the identity matrix, i.e., the center of mass frame of the $\nu - \bar{\nu}$ and $\ell' - \gamma$ systems coincides with the decaying lepton rest frame. Then, in the $b2b$ case the three-momentum of the final states can be written as follows

$$\vec{p}_2 = \begin{pmatrix} \beta_\nu \sin\theta_\nu \cos\phi \\ \beta_\nu \sin\theta_\nu \sin\phi \\ \beta_\nu \cos\theta_\nu \end{pmatrix}, \qquad \vec{p}_3 = \begin{pmatrix} -\beta_\nu \sin\theta_\nu \cos\phi \\ -\beta_\nu \sin\theta_\nu \sin\phi \\ -\beta_\nu \cos\theta_\nu \end{pmatrix}, \tag{G.7}$$

$$\vec{p}_4 = \begin{pmatrix} \beta_{\ell'} \sin\theta_{\ell'} \\ 0 \\ -\beta_{\ell'} \cos\theta_{\ell'} \end{pmatrix}, \qquad \vec{p}_5 = \begin{pmatrix} -\beta_{\ell'} \sin\theta_{\ell'} \\ 0 \\ \beta_{\ell'} \cos\theta_{\ell'} \end{pmatrix}. \tag{G.8}$$

Here, it is essential to emphasize that the above equations fulfill the $b2b$ constraint ($\vec{p}_2 = -\vec{p}_3$ and $\vec{p}_4 = -\vec{p}_5$) for all possible values of $(\theta_{\ell'}, \theta_\nu, \phi)$ and not only when $\phi = 0$. Thus, we showed cleverly that $\phi = 0$ is not a constraint imposed by the $b2b$ kinematics, as suggested in [141], and it needs to be integrated over its full range.

Another important result arises from the definition of the angle θ appearing in the amplitude, which corresponds to the angle between the neutrino and the charged lepton. From this definition, one can straightforwardly express θ in terms of the angles $\theta_{\ell'}$, θ_ν, and ϕ for the $b2b$ configuration. Using the expressions for the three-momenta in the $b2b$ case, we obtain:

$$\cos\theta \equiv \hat{p}_2 \cdot \hat{p}_4 = \sin\theta_{\ell'} \sin\theta_\nu \cos\phi - \cos\theta_\nu \cos\theta_{\ell'}, \tag{G.9}$$

that shows the specific dependence of θ on θ_ν, $\theta_{\ell'}$ and ϕ. Other relations resulting from $\vec{p}_2 = -\vec{p}_3$ and $\vec{p}_4 = -\vec{p}_5$ (neglecting the mass of the final-state particles) are

$$\begin{aligned} &s_{\nu\nu} = 4E_\nu^2, \quad s_{\ell'\gamma} = (m_\ell - 2E_\nu)^2, \\ &\beta_{\ell'} = \frac{m_\ell}{2} - E_\nu, \quad \beta_\nu = E_\nu, \\ &\Theta_{\nu\bar{\nu}} = \pi, \quad \Theta_{\ell'\gamma} = \pi, \end{aligned} \tag{G.10}$$

taking $E_1 = E_2 = E_\nu$.

Finally, since in this b2b configuration the $\vec{p}_2(-\vec{p}_3)$ and $\vec{p}_4(-\vec{p}_5)$ are two independent vectors, they can always span a plane, i.e. they can always form a basis of a two-dimensional space. This argument is used in the KMS method to claim that $\phi = 0$. For completeness, we work on this subject below and demonstrate that, even it is certainly true that these two vectors span a plane, this condition does not fix $\phi = 0$, as we just showed before.

How can we describe that plane?

Since in the ℓ rest frame, these vectors start from the origin of the coordinate system $(x_0, y_0, z_0) = (0, 0, 0)$, then the plane spanned by the vectors $\vec{p}_2$ and $\vec{p}_4$ is given by the

well-known equation:

$$(x, y, z) = \lambda \vec{p}_2 + \nu \vec{p}_4, \tag{G.11}$$

where λ and ν are just the parameters of the plane-equation ($-\infty < \lambda, \nu < +\infty$).

The following computation can be performed in any chosen reference frame; however, for this discussion we continue to work in the system where $\theta_\nu = \pi/2$, as in the KMS method. In this frame, the plane equation can be written in its general form, which, after straightforward simplification, yields:

$$(\cos\theta_{\ell'} \sin\phi)x - (\cos\theta_{\ell'} \cos\phi)y + (\sin\theta_{\ell'} \sin\phi)z = 0. \tag{G.12}$$

It is thus evident that the b2b condition is satisfied for each value of ϕ and the corresponding plane spanned by the vectors $\vec{p}_2$ and $\vec{p}_4$ is given by eq.(G.12). This reaffirms that $\phi = 0$ is not a condition fixed by the b2b scenario, and instead ϕ remains as an independent variable that must be integrated over its full range.

To illustrate this plane condition, we show in Fig. G1.1 various examples with different ϕ and θ_ν:

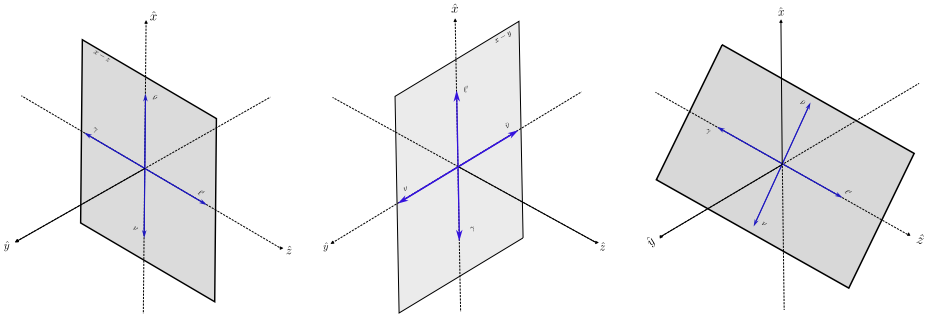

(a) $\phi = 0$ (b) $\theta_\nu = \pi/2$ (c) $\theta_{\ell'} = 0$, $\phi = -\pi/4$

Figure G1.1: Planes defined from ($\vec{p}_2$,$\vec{p}_4$) in the b2b for different values of ϕ, $\theta_{\ell'}$.

• Diagram (a): For $\phi = 0$ we get $y = 0$, which means that the plane is precisely the $x - z$ plane, which is in agreement with the KMS method, but is not the only option allowed by the kinematics.

• Diagram (b): For $\theta_{\ell'} = \pi/2$ we get $z = 0$, which means that the plane is precisely the $x - y$ one, a configuration completely allowed by the kinematics.

One can similarly consider all other possible configurations, such as diagram (c), etc. All of them are consistent with the $b2b$ constraints and with the fact that the two independent final-state vectors span a plane, confirming once again that $\phi = 0$ is merely an allowed configuration rather than a condition imposed by the $b2b$ kinematics.

Appendix H

Four-body branching ratio

H1 Branching ratio computation for the $b2b$ configuration

First, we compute the branching ratio for this $b2b$ kinematic scenario using a seemingly straightforward approach, which—without the proper considerations—can lead to erroneous conclusions. We will then discuss this issue in detail and explain the correct procedure to estimate this observable.

For a first consistency test, the total $\mathrm{BR}(\ell \to \ell' \nu \bar{\nu} \gamma)$ for the general kinematic configuration was computed, being in perfect agreement with those reported by [187], giving us a corroboration that our procedure was correct.

Now, as a first attempt, one might be tempted to estimate the $b2b$ BR by integrating over all the energy and angular configurations of the differential decay rates evaluated in this kinematic case. Essentially, for the case $\phi = 0$, integrating over the remaining energy dependence of eqs. (**??**, **??**):

$$\mathcal{B}_{\leftrightarrow}^{\{D,M\}} \equiv \frac{1}{\Gamma_\ell} \int \left(d\Gamma_{\nu\nu}^{D,M}|_{b2b} \right) dE_\nu dE_{\bar{\nu}} d\cos\theta_{\ell'} \,. \tag{H.1}$$

Doing this, and cutting off photons below an energy threshold of 10 MeV in the decaying-lepton rest frame, given by the experimental resolution at Belle [121] (achievable at Belle-II [188]) [52], we obtain:

$$\begin{aligned} \mathcal{B}_{\leftrightarrow}^{D}(\ell = \tau) &= \Gamma_{\leftrightarrow}^{D}/\Gamma_\tau \approx 4.3 \times 10^{-4}, \\ \mathcal{B}_{\leftrightarrow}^{M}(\ell = \tau) &= \Gamma_{\leftrightarrow}^{M}/\Gamma_\tau \approx 2.4 \times 10^{-4}, \end{aligned} \tag{H.2}$$

$$\begin{aligned} \mathcal{B}_{\leftrightarrow}^{D}(\ell = \mu) &= \Gamma_{\leftrightarrow}^{D}/\Gamma_\mu \approx 1.9 \times 10^{-4}, \\ \mathcal{B}_{\leftrightarrow}^{M}(\ell = \mu) &= \Gamma_{\leftrightarrow}^{M}/\Gamma_\mu \approx 1.1 \times 10^{-4}, \end{aligned} \tag{H.3}$$

[52] This threshold was 7 MeV at the Crystal Box experiment, in the search for $\mu \to e\gamma\gamma$ [189].

which, in principle, is a result that could motivate even more its search and reflect the advantages of this specific process ($\ell \to \ell'\nu\bar{\nu}\gamma$), since we do not have to deal with hadronic form factors and the computed BR is much larger than the ones estimated in [141] for B decays ($\mathcal{B}_{\leftrightarrow} \approx 10^{-12}$) and related processes.

Nevertheless, the estimated BRs in eqs. (H.2, H.3) appear problematic. First, they differ between the Dirac and Majorana cases—an artifact of having set $\phi = 0$—which contradicts the DMCT theorem, since the neutrino variables must be integrated over when calculating the branching ratios. This issue can be easily resolved by considering the full range of variation of ϕ.

The main problem is very notorious: Since the total BR($\ell \to \ell'\nu\bar{\nu}\gamma$) is of the order $\mathcal{O}(10^{-2})$, it is hard to believe that a specific kinematic configuration, such as the $b2b$, is only two orders of magnitude more suppressed than the general case. Then, for a complete discussion of this problem we will comment on the specific reason why this BR estimation is wrong, and also do the right computation for this case, which can be applied for any other specific kinematic configuration in which one (or more) of the continuous phase space variables is(are) fixed to specific value(s).

The width of a N-body decay can be seen as the hypervolume of the phase space weighted by the dynamic condition (squared amplitude) of the specific process. This hypervolume is determined by the specific range of all the continuous phase space independent variables, which is specified by the minimum and maximum values they could take according to energy-momentum conservation. If one (or more) of these variables take(s) a fixed value in an specific kinematic configuration, an integration over a zero-range variable has to be done in order to compute the theoretical BR, leading to a vanishing contribution for this specific case.

In other words, once a continuous phase-space variable is fixed, the phase-space hypervolume is reduced to a phase-space hypersurface. Consequently, the theoretical estimation of the BR for that specific configuration is effectively zero. This aligns with the intuitive notion that the probability of observing a single, unique configuration among infinitely many continuous possibilities is null.

This does not mean that the differential decay rate is zero in that case. Actually, we

can compute without further problems any differential distribution as long as the fixed variables are not integrated. Then, the main problem of the estimated BR is that we integrated over the already evaluated differential decay rate, leading to a number that does not have a probability interpretation, since for the correct theoretical BR computation, we first need the differential decay rate for the general case and then to integrate over all phase-space variables, which range will be fixed by the specific kinematic scenario and the energy-momentum conservation.

In particular, our notation first introduced in eqs.(4.59), was precisely motivated to avoid this possible confusion. It provides evidence that, once the decay rate is already evaluated in a specific kinematic scenario, we can not integrate over the kinematic variables fixed by the $b2b$ condition and interpret the result as a probability, specifically as the BR of the $b2b$ case, that could lead to a (much) larger value than the real one.

Finally, since the experimental resolution is finite, no variable can be strictly fixed in practice. Therefore, it is well-defined to estimate a non-zero BR for the $b2b$ configuration by considering a small range of variation around the theoretically fixed variables, corresponding to the experimental resolution.

Then, to estimate the real BR for the experimental $b2b$ case, without fixing ϕ and using a proper method for this estimation, we have to do the following: First we integrate over the remaining neutrino's variables (θ_ν and ϕ) in eq.(F.6), which are not fixed by any kinematic condition, leading to a decay rate that depends only on the electron and photon energy, together with the angle between them $\left(\frac{d\Gamma}{dE_{\ell'}dE_\gamma d\cos\Theta_{\ell'\gamma}}\right)$, in the general kinematic case.

Then, using this differential decay rate, we can apply the experimental energy and angular resolution[53] to integrate over the "pseudo" $b2b$ case, i.e. an infinitesimal phase-space region that will be indistinguishable from the theoretical $b2b$ case by the experiment, as shown in figure H1.1, where the energy of the final charged-lepton and the photon are equal, up to the energy resolution ($E_{\ell'} - \Delta E \leq E_\gamma \leq E_{\ell'} + \Delta E$), and the angle between them is π, up to the angular resolution ($\pi - \Delta\theta \leq \theta_{\ell'\gamma} \leq \pi$).

Since we are not evaluating the differential decay rate at a specific kinematic configuration, we can safely interpret this result as an occurrence probability. Moreover, because

[53]We use ΔE=0.01$E_{\ell'}$, $\Delta\theta$=10mrad and ΔE=0.04$E_{\ell'}$, $\Delta\theta$=13mrad for the muon and tau experimental resolution respectively, as reported by Mu2e [190] and Belle-II [188] experiments.

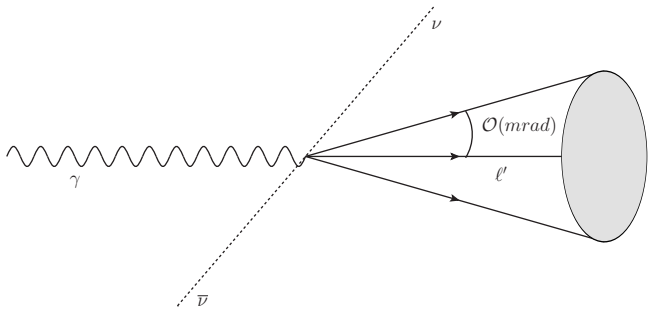

Figure H1.1: Experimental $b2b$ configuration in the initial charged-lepton rest frame.

the integration region includes the theoretical $b2b$ configuration, the corresponding BR obtained from the integration will necessarily be larger than that of the theoretical $b2b$ case alone.

Doing this, cutting off photons below an energy threshold of 10 MeV in the decaying-lepton rest frame, we estimate the following BR for the experimental $b2b$ case as follows:

$$(\Gamma)_{b2b} = \int_{E_{\ell'}^{min}}^{E_{\ell'}^{max}} \int_{E_{\ell'}-\Delta E}^{E_{\ell'}+\Delta E} \int_{\pi-\Delta\theta}^{\pi} \frac{d\Gamma}{dE_{\ell'}dE_{\gamma}d\cos\Theta_{\ell'\gamma}} dE_{\ell'}dE_{\gamma}d\cos\Theta_{\ell'\gamma}, \tag{H.4}$$

getting the results:

$$\begin{aligned} \mathcal{BR}(\ell=\tau)_{b2b} &= (\Gamma)_{b2b}/\Gamma_{\tau} \approx 1.68\times10^{-10}, \\ \mathcal{BR}(\ell=\mu)_{b2b} &= (\Gamma)_{b2b}/\Gamma_{\mu} \approx 1.34\times10^{-10}. \end{aligned} \tag{H.5}$$

As we can see, these branching ratios are many orders of magnitude smaller than those obtained using the KMS method in (H.2) and (H.3). Furthermore, the calculated BR is identical for Dirac and Majorana neutrinos, in agreement with the DMCT theorem, and fully consistent with our previous discussions.

Appendix I

Muon g-2 in the SM

I1 Anomalous magnetic moment of the muon

The anomalous magnetic moment of the muon is a privileged precision measurement, which sets stringent constraints on new physics. In early times, and together with the Lamb shift, its electron analog was instrumental to build our understanding of quantum field theories at the loop level. Almost 80 years later, it continues to be at the forefront in the understanding of matter at the most fundamental level.

The anomalous magnetic moment of a charged lepton is defined as $a_\ell = (g_\ell - 2)/2$, measuring a purely quantum effect, as the gyromagnetic factor, g, is exactly 2 according to the Dirac equation. Notwithstanding, it gets corrected by quantum effects, being the leading contribution given a photon loop, first calculated by Schwinger, giving the result $a_\ell = \alpha/(2\pi) + \mathcal{O}(\alpha^2)$, universal for all lepton flavors, which sets the size of the effect as $\sim 1 \times 10^{-3}$, a result that has not yet been tested for tau leptons, due to their fast decays.

The situation is much better for electrons and muons. Although a_e is measured more precisely than a_μ, the sensitivity to new physics typically scales as that of the weak contributions, $a_\ell^{\text{NP,weak}} \sim m_\ell^2/\Lambda^2$, as a function of the characteristic scale, Λ. Taking both facts into account, although a_e is measured with an amazing uncertainty of 12×10^{-14} [9], the error on the world average for a_μ, 15×10^{-11} [33], [34], [35], [191], makes the muon approximately 40 times more sensitive to NP effects than the electron. Theoretical uncertainty on the SM prediction for a_e is negligible, which is not the case –unfortunately– for a_μ. As we will see, this weakens a bit the possible reach on NP of a_μ (that is still ~ 20 times better than the electron), which calls for refined SM calculations in the coming years.

The accuracy of the a_μ measurement is driven by the last result published by the FNAL collaboration [191], yielding

$$a_\mu^{\text{exp, 2025}} = 116592071.5(14.5) \times 10^{-11}\,, \tag{I.1}$$

which has reduced the uncertainty of the BNL result [35] by a factor ~ 4. A slight improvement of this precision is expected from the results of the dedicated J-PARC experiment [192] at the beginning of the next decade.

The principle of these measurements rests on an intense proton beam hitting a target and producing numerous pions, which later on decay mostly to (highly-polarized) muons, that are stored magnetically in a ring (the BNL one was recycled for the FNAL experiment). Thanks to their relativistic nature, one can measure precisely the e (momentum and spin) of their Michel decays. Since the muons are subject to an extremely uniform magnetic field with cyclotron frequency ω_c, the muons would describe circular orbits with spin and momentum perfectly aligned, rotating at this frequency, if g were exactly 2. On the contrary, the difference $g-2$ is directly proportional to the anomalous precesion frequency by which the spin rotates mildly faster than the momentum. Through a terribly precise knowledge of the applied magnetic field (with numerous minute corrections to warrant its homogeneity), a_μ is directly determined from this oscillation phase, fit to the decay pattern of millions of muon decays every hundred ns.

In contrast, the theoretical accuracy of the SM prediction has decreased from 43×10^{-11} the White Paper 1 (WP20) [36] to 62×10^{-11} in its second edition (WP25) [43]. Let us briefly review how this happened.

Changes in the five-loop QED prediction were minor, with the uncertainty at the level of 0.2×10^{-11}, contributed quite evenly by the estimated six-loop result and by the experiment used to set the value of α. This resulted in [193], [194], [195], [196], [197], [198], [199]

$$a_\mu^{\mathrm{QED,\,WP25}} = 116584718.8(2) \times 10^{-11}\,, \tag{I.2}$$

0.1×10^{-11} smaller than in WP20, that was the uncertainty quoted for this piece in 2020.

The electroweak contribution is computed to two loops. Its WP25 value [200], [201], [202], [203],

$$a_\mu^{\mathrm{EW,\,WP25}} = 154.4(4) \times 10^{-11}\,, \tag{I.3}$$

has reduced the uncertainty by 60% with respect to the WP20 result, $153.6(1.0) \times 10^{-11}$, which is compatible with the current number. This reduction of the error is mostly thanks to better control of hadronic EW uncertainties, with the remaining error basically shared

by second-generation quark contributions in a(n anomalous) triangle connected to $\gamma\gamma Z$ bosons and by unknown three-loop corrections.

At the current precision, the uncertainty of $a_\mu^{\rm SM}$ comes completely from hadronic contributions, which correspond to QCD corrections evaluated with at least a relevant energy scale in the non-perturbative domain of the strong interactions. These correspond to the hadronic vacuum polarization (HVP) and hadronic light-by-light (HLBL) contributions, starting at orders $\mathcal{O}(\alpha^2, \alpha^3)$, respectively. In $a_\mu^{\rm HVP}$, the exchanged photon in the Schwinger diagram is attached to a quark-antiquark loop. In $a_\mu^{\rm HLBL}$ the four photon legs are connected to an intermediate quark loop, with three of them attached to muon lines and the other one being the external (real) photon. For WP20, the error associated to the HVP basically doubled the one for HLBL, 40 and 18 in 10^{-11} units. Recent developments have reduced the latter to 10 units, while the HVP uncertainty quoted in the WP25 has increased to 61.

We will continue with $a_\mu^{\rm HLBL,\,LO}$, see section 5.2, and then finally discuss $a_\mu^{\rm HVP,\,LO}$ and the compatibility between the SM prediction [54] and the measurements.

For WP20 lattice QCD results were not competitive with the data-driven determinations of $a_\mu^{\rm HLBL}$, with uncertainties of 35 and 19×10^{-11}, in turn. Lattice evaluations have improved dramatically since then, reaching a present uncertainty of only 9.0 units [207], [208], [209], [210], [211], commensurate with the phenomenological one, of 8.8×10^{-11} [159], [160], [200], [212], [213], [214], [215], [216], [217], [218], [219], [220], [221], [222], [223], [224], [225], [226], [227], [228], [229], [230], [231], [232]. However, they are in moderate tension (1.5σ),

$$a_\mu^{\rm HLBL\,LO,\,lattice} = 122.5(9.0) \times 10^{-11}, \tag{I.4}$$

$$a_\mu^{\rm HLBL\,LO,\,phenomenology} = 103.3(8.8) \times 10^{-11}, \tag{I.5}$$

which makes their combined error slightly larger than the individual ones [43],

$$a_\mu^{\rm HLBL\,LO,\,WP25} = 112.6(9.6) \times 10^{-11}\,. \tag{I.6}$$

On the data-driven side, progress has focused mainly in the understanding of how short-

[54] To obtain $a_\mu^{\rm SM}$ one also needs to add the subleading pieces, which amount to $a_\mu^{\rm HVP,\,NLO} = -99.6(1.3)$ [164], [204], $a_\mu^{\rm HVP,\,NNLO} = 12.4(1)$ [205], and $a_\mu^{\rm HLBL,\,NLO} = 2.6(6)$ [206], everything in 10^{-11} units.

distance QCD restrictions on the HLBL tensor apply, as well as in the related contributions from higher-mass states [161], [200], [215], [216], [217], [218], [219], [220], [223], [224], [225], [228], [229], [230], [232], [233], [234], [235], [236], [237], [238], [239], [240]. Further improvements along these directions are expected to reduce the discrepancy among the lattice, (I.4), and phenomenological predictions, (I.5), and thus the error of their combination, eq. (I.6).

The WP20 result for $a_\mu^{\rm HVP}$ was based on the data-driven evaluations using $\sigma(e^+e^- \to$ hadrons), yielding

$$a_\mu^{\rm HVP\,LO,WP20} = 6931(40) \times 10^{-11}\,, \tag{I.7}$$

which was however challenged by two results appearing by that time, the BMW lattice QCD collaboration obtained [40]

$$a_\mu^{\rm HVP\,LO,BMW20} = 7072(55) \times 10^{-11}\,, \tag{I.8}$$

and the tau-based determination was [37]

$$a_\mu^{\rm HVP\,LO,MR20} = 7057(41) \times 10^{-11}\,. \tag{I.9}$$

Both were not used to get the WP20 SM prediction. On the one hand, there was not another lattice evaluation with similar precision to scrutinize systematic BMW errors. On the other, tau data was considered not competitive with the e^+e^- measurements.

The picture changed drastically with the publication of the CMD-3 $e^+e^- \to \pi^+\pi^-$ data [41], [42]. If taken as the only input for the leading $\pi\pi$ contribution to $a_\mu^{\rm HVP}$, CMD-3 would yield $a_\mu^{\rm HVP\,LO,CMD3-23} = 713(4)\times 10^{-10}$, even larger than the predictions above. This exacerbated the old KLOE [241]-BaBar [242] tension to the level of discrepancy (particularly between KLOE and CMD-3), in which the different datasets could no longer be combined to obtain $a_\mu^{{\rm HVP},e^+e^-{\rm -based}}$. Meanwhile, lattice QCD evaluations with comparable precision to the BMW result were achieved by different groups, and showed a nice agreement, that allowed their combination, to get [40], [243], [244], [245], [246], [247], [248], [249], [250], [251], [252], [253], [254], [255], [256], [257], [258]

$$a_\mu^{\rm HVP\,LO,WP25} = 7132(61) \times 10^{-11}\,. \tag{I.10}$$

A τ-based number, $7045(62) \times 10^{-11}$, based on refs. [39], [259], was quoted in WP25 (see also ref. [260]), but not combined with the lattice determination [55]. With eq. (I.10) as input, the WP25 quotes

$$a_\mu^{\mathrm{SM,\,WP25}} = 116592033(62) \times 10^{-11}\,. \tag{I.11}$$

On the experimental side, successive results from the FNAL experiment [33], [34], [191] have only become more precise, keeping fine compatibility among them. As a result, the 5.1σ discrepancy that was obtained from the WP20 number and the FNAL runs 1-3 measurements, is now reduced, using the WP25 SM prediction, (I.11), and the world average for a_μ^{exp}, (I.1), to a very nice compatibility, $\Delta a_\mu = a_\mu^{\mathrm{exp}} - a_\mu^{\mathrm{SM}} = 39(64) \times 10^{-11}$, setting stringent constraints on NP contributing to a_μ.

[55] This may change in the future, depending on the assessment of the understanding of the required isospin-breaking corrections. Also e^+e^- data could be used again if their current inconsistency is solved. Finally, the precise measurement of μe scattering at the MUonE experiment [261] will provide a complementary (space-like) determination of $a_\mu^{\mathrm{HVP,LO}}$ that can be useful to refine the SM prediction.

Appendix J

Rare Higgs Decays

J1 Higgs decays $h \to \mu^+\mu^- + \gamma/Z$

In this appendix we take advantage of the fact that, due to the large number of produced Higgses[56], it is possible to study some rare decays, such as $h(p) \to \mu^+(p_1)\mu^-(p_2)\gamma/Z(p_3)$, which are produced by the same operators we previously analysed in 5.1.

Taking into account the HEFT and SM tree-level amplitude, the contribution to the decay $h \to \mu^+\mu^-\gamma$ is exactly the same as the SMEFT case, since no other HEFT operator contributes, upon the global a_γ parameter that could increase the total BR at most by a factor five. Considering $a_\gamma = 5$, leads to a maximum value of $\mathrm{BR}(h \to \mu^+\mu^-\gamma)_{\mathrm{NP}} \approx 4 \times 10^{-9}$.

Meanwhile, for the decay $h \to \mu^+\mu^- Z$, we can study the effect that the NP under consideration could have, where all the HEFT operators contribute. In this case, the differential decay rate contributions are (invariant masses are defined in eq. (J.11)):

- Leading term in the SM:

$$\frac{d\Gamma}{dm_{13}^2 dm_{23}^2} = \frac{g_Z^2 m_Z^2 (8\sin^4\theta_W - 4\sin^2\theta_W + 1)}{256\pi^3 m_h^3 v^2 (m_{13}^2 + m_{23}^2 - m_h^2)^2} \Big(m_h^2 m_Z^2 + 2m_Z^4 - 2m_Z^2(m_{13}^2 + m_{23}^2) + m_{13}^2 m_{23}^2 \Big) . \tag{J.1}$$

- Operator $\mathcal{N}_Z^\mu$:

$$\frac{d\Gamma}{dm_{13}^2 dm_{23}^2} = -\frac{C_Z^2}{\Lambda^2} \frac{(m_h^2 m_Z^2 - m_Z^4 + m_Z^2(m_{23}^2 + m_{13}^2) - 2m_{13}^2 m_{23}^2)}{32\pi^3 m_h^3} . \tag{J.2}$$

- Operator $\mathcal{N}_2^\mu$ (this one does not bear a suppression factor $\propto 1/\Lambda$, making it the largest

[56] A total of $\mathcal{O}(10^8)$ Higgs bosons for a $\sqrt{30}$ TeV Muon Collider with 90 ab^{-1} of integrated luminosity.

purely new physics effect, although much smaller than the SM-$\mathcal{N}_2^\mu$ interference):

$$\frac{d\Gamma}{dm_{13}^2 dm_{23}^2} = \frac{C_2^2}{256\pi^3 m_h^3 m_Z^2}\Big(m_h^2 m_Z^2 + 2m_Z^4 - 2m_Z^2(m_{13}^2 + m_{23}^2) + m_{13}^2 m_{23}^2\Big)\,. \quad \text{(J.3)}$$

- Operator $\mathcal{N}_4^\mu$:

$$\frac{d\Gamma}{dm_{13}^2 dm_{23}^2} = \frac{C_4^2}{\Lambda^2}\frac{\big(m_h^2 + m_Z^2 - m_{13}^2 - m_{23}^2\big)\big((m_{13}^2 + m_{23}^2)^2 - 4m_h^2 m_Z^2\big)}{512\pi^3 m_h^3 m_Z^2}\,. \quad \text{(J.4)}$$

- Operator $\mathcal{N}_9^\mu$:

$$\begin{aligned}\frac{d\Gamma}{dm_{13}^2 dm_{23}^2} =& \frac{C_9^2}{\Lambda^2}\frac{1}{512\pi^3 m_h^3 m_Z^2}\Big(4m_h^4 m_Z^2 + m_h^2\big(-4m_Z^4 - 4m_Z^2(m_{13}^2 + m_{23}^2) \\ &+ (m_{23}^2 - m_{13}^2)^2\big) + m_Z^2(m_{13}^4 + 6m_{13}^2 m_{23}^2 + m_{23}^4) - (m_{23}^2 - m_{13}^2)^2 \\ &(m_{13}^2 + m_{23}^2)\Big)\,. \end{aligned} \quad \text{(J.5)}$$

- Interference $\mathcal{N}_Z^\mu - \text{SM}$ (numerically suppressed, both by the muon mass and because $4\sin^2\theta_W \sim 1$):

$$\begin{aligned}\frac{d\Gamma}{dm_{13}^2 dm_{23}^2} =& -\frac{\text{Re}(C_Z)}{\Lambda}\frac{g_Z m_\mu}{64\pi^3 m_h^3}\frac{(4\sin^2\theta_W - 1)}{v\, m_{13}^2 m_{23}^2(m_{13}^2 + m_{23}^2 - m_h^2)}\Big(m_h^4\big(m_Z^2(m_{13}^2 + m_{23}^2) \\ &- m_{13}^2 m_{23}^2\big) + m_h^2\big(m_{13}^2 m_{23}^2(m_{13}^2 + m_{23}^2) - m_Z^2(m_{13}^4 + 3m_{13}^2 m_{23}^2 + m_{23}^4)\big) \\ &+ 2m_Z^2 m_{13}^2 m_{23}^2\big(2(m_{13}^2 + m_{23}^2) - 3m_Z^2\big)\Big)\,. \end{aligned} \quad \text{(J.6)}$$

- Interference $\mathcal{N}_Z^\mu - \mathcal{N}_9^\mu$ (this is the only non-vanishing interference which is purely beyond the SM [57], and thus suppressed):

$$\frac{d\Gamma}{dm_{13}^2 dm_{23}^2} = -\frac{C_9 C_Z^* + C_Z C_9^*}{128\pi^3\Lambda^2 m_h^3}\Big(m_h^2(4m_Z^2 - m_{13}^2 - m_{23}^2) - m_Z^2(m_{13}^2 + m_{23}^2) + (m_{23}^2 - m_{13}^2)^2\Big)\,. \quad \text{(J.7)}$$

- Interference $\mathcal{N}_2^\mu - \text{SM}$ (there is no parametric suppression $\propto 1/\Lambda$ in this term, which

[57] We do not consider purely beyond the SM interferences that are additionally suppressed by the muon mass.

is potentially the largest new physics effect):

$$\frac{d\Gamma}{dm_{13}^2 dm_{23}^2} = \frac{-C_2 g_Z \sin^2\theta_W}{64\pi^3 m_h^3 v(m_h^2 - m_{13}^2 - m_{23}^2)}(m_h^2 m_Z^2 + 2m_Z^4 - 2m_Z^2(m_{13}^2 + m_{23}^2) + m_{13}^2 m_{23}^2)\,. \tag{J.8}$$

- Interference $\mathcal{N}_4^\mu$ − SM (suppressed by the muon mass)

$$\begin{aligned}\frac{d\Gamma}{dm_{13}^2 dm_{23}^2} = \frac{-g_Z m_\mu \,\mathrm{Im}(C_4)}{256\pi^3\Lambda^2 m_h^3 m_Z^2 v m_{13}^2 m_{23}^2}\Big(& m_h^4 m_Z^2(m_{13}^2 + m_{23}^2) - m_Z^2 m_{13}^2 m_{23}^2(m_{13}^2 + m_{23}^2) \\ & + m_h^2\big\{m_Z^4(m_{13}^2 + m_{23}^2) - m_Z^2(m_{23}^2 - m_{13}^2)^2 - m_{13}^2 m_{23}^2(m_{13}^2 + m_{23}^2)\big\}\Big)\,.\end{aligned} \tag{J.9}$$

- Interference $\mathcal{N}_9^\mu$ − SM (again suppressed, because of m_μ and $4\sin^2\theta_W \sim 1$):

$$\begin{aligned}\frac{d\Gamma}{dm_{13}^2 dm_{23}^2} = \frac{g_Z m_\mu(4\sin^2\theta_W - 1)\mathrm{Re}(C_9)}{256\pi^3\Lambda m_h^3 v m_{13}^2 m_{23}^2(m_{13}^2 + m_{23}^2 - m_h^2)} \times \Big(& m_h^6(m_{13}^2 + m_{23}^2) \\ & - m_h^4(m_{13}^2 + m_{23}^2)\big(m_Z^2 + 2(m_{13}^2 + m_{23}^2)\big) + m_h^2\Big\{m_Z^2(m_{13}^4 - 6m_{13}^2 m_{23}^2 + m_{23}^4) \\ & + (m_{13}^2 + m_{23}^2)\big(m_{13}^4 + 4m_{13}^2 m_{23}^2 + m_{23}^4\big)\Big\} - 3m_{13}^2 m_{23}^2(m_{13}^2 + m_{23}^2) \\ & (-2m_Z^2 + m_{13}^2 + m_{23}^2)\Big)\,.\end{aligned} \tag{J.10}$$

We only took into account the leading order contributions, at most proportional to the lepton mass or quadratic in the HEFT coefficients. Also the substitution of the coefficients in eq. (5.16) has to be done. The Mandelstam variables were defined as follows

$$\begin{aligned} m_{13}^2 &\equiv (p_{\mu^-} + p_Z)^2 = (p_h - p_{\mu^+})^2, \\ m_{23}^2 &\equiv (p_{\mu^+} + p_Z)^2 = (p_h - p_{\mu^-})^2. \end{aligned} \tag{J.11}$$

Once integrated, considering $\Lambda \approx 100$ TeV, the estimated values of every contribution to the BR($h \to \mu^+\mu^- Z$) are shown in table J1.1, where we first report the values without fixing the HEFT coefficients and then show the numerical results from taking $|C_i^\mu| = 10^{-4}$ and $a_i = 1$, which is an optimistic approach where a large value of the Wilson coefficient is selected.

As can be seen from table J1.1, all the NP contributions are highly suppressed and

Operator	$BR(h \to \mu^+\mu^- Z)$	$BR(h \to \mu^+\mu^- Z)$ $\lvert C_i^\mu\rvert = 10^{-4},\ a_i = 1$
SM (Leading term)	7.66×10^{-4}	7.66×10^{-4}
$\mathcal{N}_2^\mu$−SM	$-2.52 \times 10^{-3}\ C_2^\mu a_2$	-2.52×10^{-7}
$\mathcal{N}_Z^\mu$−SM	-5.95×10^{-11}	-5.95×10^{-11}
$\mathcal{N}_2^\mu$	$5.29 \times 10^{-3}\lvert C_2^\mu\rvert^2 a_2^2$	5.29×10^{-11}
$\mathcal{N}_Z^\mu$	9.02×10^{-13}	9.02×10^{-13}
$\mathcal{N}_9^\mu$−SM	$-7.56 \times 10^{-9}\ \mathrm{Im}(C_9^\mu)a_9$	-7.56×10^{-13}
$\mathcal{N}_4^\mu$−SM	$6.93 \times 10^{-9}\,\mathrm{Re}(C_4^\mu)a_4$	6.93×10^{-13}
$\mathcal{N}_Z^\mu - \mathcal{N}_9^\mu$	$2.08 \times 10^{-10}\,\mathrm{Im}(C_9^\mu)a_9$	2.08×10^{-14}
$\mathcal{N}_9^\mu$	$1.22 \times 10^{-8}\lvert C_9^\mu\rvert^2 a_9^2$	1.22×10^{-16}
$\mathcal{N}_4^\mu$	$2.15 \times 10^{-10}\lvert C_4^\mu\rvert^2 a_4^2$	2.15×10^{-18}

Table J1.1: Estimated BR($h \to \mu^+\mu^- Z$) contributions within the HEFT approach.

many orders of magnitude below the SM leading term [58], even for the most optimistic HEFT-coupling cases. Thus, the main conclusion given in [144] for the SMEFT case still holds here, being that the current muon g-2 anomaly cannot be tested at a muon collider through this decay process [59].

These results were somewhat expected, since the main advantage of the NP scattering process is that it grows with energy and thus can become dominant over the SM cross-section at a very high-energy collider, in contrast with the decay process, fixed at the Higgs mass scale.

Then, the HEFT contribution in the $h \to \mu^+\mu^- + \gamma/Z$ channel is still too small to be observed, being the scattering process the most promising scenario to test the g-2 NP contribution in a model-independent way, highlighting the potential of a muon collider in high-energy physics.

[58] All of them are consistent with our previous explanations on their particular suppressions.

[59] The interference $\mathcal{N}_2^\mu$−SM term could be accessible only if high statistics were achieved in a future muon-collider and all relevant radiative corrections for the SM contribution to that order were known.